Winter 12-15-2017

Coupling of Oxidation-Reduction Reactions of Chromium, Iron and Manganese: Implications for the Fate and Mobility of Chromium in Aquatic Environments

Chao Pan
Washington University in St. Louis

WASHINGTON UNIVERSITY IN ST. LOUIS

School of Engineering & Applied Science
Department of Energy, Environmental & Chemical Engineering

Dissertation Examination Committee:

Daniel E. Giammar, Chair

Jeffrey G. Catalano
John D. Fortner
Young-Shin Jun
Jay Turner

Coupling of Oxidation-Reduction Reactions of Chromium, Iron and Manganese: Implications for the Fate and Mobility of Chromium in Aquatic Environments

by

Chao Pan

A dissertation presented to the
The Graduate School
of Washington University in
partial fulfillment of the
requirements for the degree
of Doctor of Philosophy

December 2017
St. Louis, Missouri

Table of Contents

List of Figures

List of Tables

Acknowledgements

I would like to express my deepest thanks to my advisor, Professor Daniel Giammar for his guidance during my Ph.D. study. His rich experience and enthusiasm on academics impressed me profoundly and motivated to continue moving forward on the road of research. I have greatly benefited from his professional advice and excellent mentorship. He has been supporting me both technically and personally, training me to think independently and to think as scientist. Much of this work within and beyond this thesis would be impossible without his supports, encouragements and guidance.

I would like to acknowledge my thesis committee for their suggestions and inputs along the course of this research. Dr. Jeffrey Catalano is co-PI of the research project I have been mainly working on during my Ph.D. study. He provides me helps with X-ray absorption and X-ray diffraction, as well as numerous valuable advice and enlightening discussions. I would like to give my sincere appreciation to Dr. John Fortner, Dr. Young-Shin Jun, and Dr. Jay Turner for providing insight suggestions to my research.

I also want to acknowledge the collaborators on my Ph.D. project. Dr. Lynsay Troyer in Jeff's group, who helps me a lot with X-ray absorption analysis and data interpretation, as well as valuable suggestion on my research. I benefited a lot from valuable discussions with Dr. Peng Liao, who can always inspire me new ideas on the project. I also thank Dr. Huan Liu for his help with X-ray photoelectron spectroscopy and Dr. Wenlu Li for the help with Transmission Electron Microscopy analysis.

Special thanks to former and current Aquatic Chemistry Lab members, including Dr. Zimeng Wang, Dr. Lin Wang, Dr. Vrajesh Mehta, Dr. Wei Xiong, Dr. Zezhen Pan, Dr. Richel Wells, Yeunook Bae, Anshuman Satpathy, and all the visiting students.

Research funding from the National Science Foundation is gratefully acknowledged.

Finally, I'm deeply thankful to my parents, who strongly supported me and provided me continuous love and understanding as I pursued this degree in the United States.

Chao Pan

Washington University in St. Louis

December, 2017

ABSTRACT OF THE DISSERTATION

Coupling of Oxidation-Reduction Reactions of Chromium, Iron and Manganese: Implications for the Fate and Mobility of Chromium in Aquatic Environments

by

Chao Pan

Doctor of Philosophy in Energy, Environmental & Chemical Engineering

Washington University in St. Louis, 2017

Professor Daniel Giammar, Chair

Both within the United States and internationally, hexavalent chromium (Cr(VI)) is a contaminant of concern in drinking water supplies. The U.S. Environmental Protection Agency is considering a Cr(VI)-specific standard. Thus improved technologies for Cr(VI) removal in drinking water are needed. Iron electrocoagulation for Cr(VI) removal was examined at conditions directly relevant to drinking water treatment, and humic acid (HA) affects the performance of electrocoagulation in multiple ways. The success of the chromium treatment or remediation also relies on the stability of the Cr(III)-containing solids with respect to reoxidation under groundwater conditions. Manganese is ubiquitous in aquatic and terrestrial environments, and the redox cycling of manganese may significantly impact the fate and transport of chromium. Coupling of redox reactions of chromium, iron and manganese involves multiple interaction pathways that occur in the aqueous phase as well as at solid-water interfaces. A mechanistic and quantitative understanding of these processes is needed to establish input parameters for kinetic and transport models and to enable decision-making for chromium treatment strategies.

Iron electrocoagulation (EC) is a technology that can successfully achieve low concentrations of Cr(VI) in treated drinking water. In our research we have applied iron electrocoagulation (EC) with iron serving as the sacrificial anode to treat simulated drinking water solutions. Experiments have evaluated the effects of pH, dissolved oxygen, and common anions on Cr(VI) removal during batch EC treatment. In addition, the presence of humic acid (HA) inhibited the rate of Cr(VI) removal in electrocoagulation, with slower Cr(VI) removal at higher pH. This is due to dissolved oxygen competing with Cr(VI) for the oxidation of Fe(II) released from the anode. As determined using dynamic light scattering and wet chemistry experiments, the presence of HA resulted in the formation of Cr(III)-Fe(III)-HA colloids during electrocoagulation, which is difficult to remove in following water treatment steps of sedimentation and granular media filtration. Characterization of the solids by X-ray diffraction indicates that the iron oxides produced are lepidocrocite at pH 8, with more ferrihydrite in the presence of HA.

Building on previous knowledge of MnO_2 as an oxidant for Cr-containing solids, we systematically evaluated the rates and products of the oxidation of Cr(III) in iron oxides by MnO_2. We found that Cr(III) dissolution from $Cr_xFe_{1-x}(OH)_3$ greatly influenced the Cr(VI) production rates. A multi-chamber reactor was used to assess the role of solid-solid mixing in $Cr_xFe_{1-x}(OH)_3$-MnO_2 interactions. A dialysis membrane divided the reactor into two chambers, eliminating the possibility of direct contact of the solids in each chamber but allowing dissolved species to diffuse across the membrane. The Cr(VI) production rate was much lower in multi-chamber experiments ($Cr_xFe_{1-x}(OH)_3||MnO_2$) than in completely mixed batch experiments under the same condition, indicating that the redox interaction is greatly accelerated by mixing of the two solids. The model was first established to predict Cr(VI) release in $Cr(OH)_3||MnO_2$

multichamber experiments, as dissolved Cr(III) concentration in equilibrium with $Cr(OH)_3$ is higher at low pH and it's easy to observe the behavior of Cr(VI) dynamics with more Cr(VI) generation. While solid phase Mn(IV) is well known oxidants of Cr(III)-containing solids, the localized oxidation of adsorbed Mn(II) by dissolved oxygen can also promote the oxidation of Cr(III) contained within $Cr_xFe_{1-x}(OH)_3$. The promotional effects was likely due to Mn redox cycling in which oxidized forms of Mn species were generated as oxidants of $Cr_xFe_{1-x}(OH)_3$ that were more potent than O_2.

Chapter 1. Introduction

1.1 Background

1.1.1 Chromium(VI) as a contaminant and drinking water regulation

Chromium(VI), also referred to as hexavalent chromium, is a toxic contaminant that has been observed in private and public water supplies. Cr(VI) is recognized to be much more toxic than chromium(III), and is found to be toxic to bacteria, plants, animals and people. Cr(III), on the other hand, is less toxic than Cr(VI) and is nearly insoluble at neutral pH (Figure 1.1).[1] Cr(III) is listed as an essential element, as micronutrient, to maintain good health and helps in maintaining the normal metabolism of glucose, cholesterol, and fat in human bodies.[2] It is toxic only at high concentration.

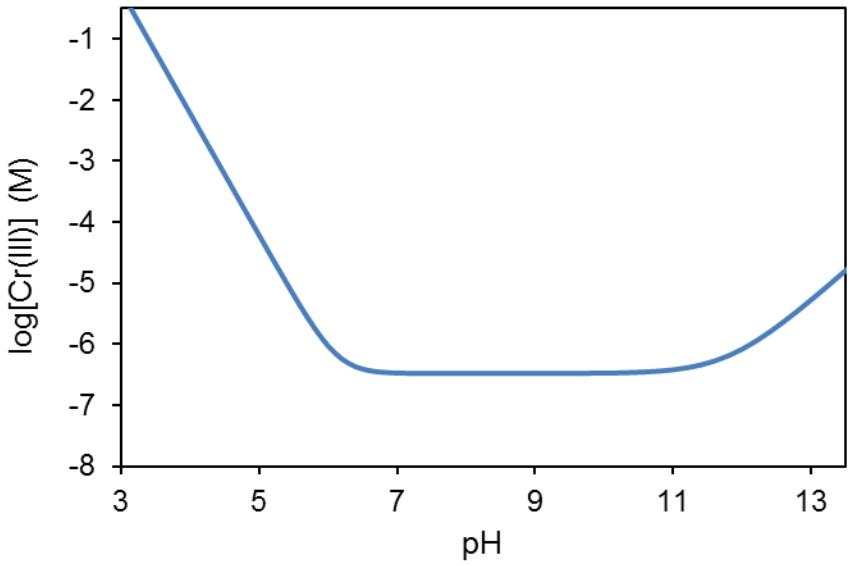

Figure 1.1 Cr(III) solubility as a function of pH

In parallel to the widespread public attention, drinking water regulators have been examining potential regulations for Cr(VI).[3] The current national primary drinking water standard is 100 μg/L for total Cr,[4] which includes both Cr(VI) and the much more prevalent and significantly less toxic Cr(III). However, the U.S. EPA is considering a Cr(VI)-specific standard and utilities have recently been required to monitor for Cr(VI) as an unregulated contaminant.

1.1.2 Methods for chromium(VI) removal

Physical and chemical processes involving iron can be used to remove Cr(VI) from solution. Cr(VI) can adsorb to iron oxides including amorphous iron oxides,[5] goethite,[6] hematite,[7] ferrihydrite[8] and to iron–oxide–coated sands.[9] Adsorption of Cr(VI) involves complexation of Cr(VI) with hydroxyl functional groups on the solid surface. Adsorption is strongly pH-dependent with maximum sorption at slightly acidic pH and often negligible adsorption in the pH range of 8-9 associated with many natural waters.[5, 7, 10-12] Cr(VI) adsorption to iron oxides can also decrease with increasing ionic strength,[13] and common ions in natural water such as SO_4^{2-} and H_4SiO_4 can inhibit adsorption.[11] SO_4^{2-} competes with CrO_4^{2-} for adsorption sites on iron oxides,[5] while H_4SiO_4 could polymerize to physically block access to adsorption sites within internal pores of the solid.[14] Because Cr(VI) adsorption to Fe(III) oxides and oxyhydroxides is highly dependent on the water chemistry and can be negligible at the conditions of many water supplies, Cr(VI) removal by coagulation using Fe(III) salts (e.g., ferric chloride) can be poor even with high coagulant doses.[15]

Several Cr(VI) remediation techniques involve its reduction to Cr(III) through the use of reducing agents, among which Fe(II) is a particularly promising reductant. For in-situ remediation of groundwater, zero-valent iron has shown to effectively remove dissolved Cr(VI)

in permeable reactive barriers both in the laboratory[16, 17] and in field tests.[18] However, the rate of reaction is slower at neutral and mildly alkaline conditions due to passivation.[19] Sulfur dioxide, sodium sulfite, sodium bisulfate, humic and fulvic acids also act as efficient reductants for Cr(VI) at very acidic pH.[20-22]

Using reduction and coagulation with Fe(II), Cr(VI) can be removed to low concentrations in drinking water.[15, 23-25] The rates of Cr(VI) reduction by Fe(II) are highly pH dependent, decreasing over the pH range 1.5-4.5 and increasing from 5 to 8.7.[26] When Fe(II) was 39.2 μM, the half life of 0.95 μM Cr(VI) was more than 150 minutes at pH 5.8 while less than 10 minutes at pH 6.6. The removal mechanism of Cr(VI) in ferrous iron coagulation involves reduction of Cr(VI) to Cr(III) coupled with the oxidation of Fe(II) to Fe(III) (eq 1.1, written based on the dominant species at pH 7) and the subsequent adsorption to or co-precipitation of Cr(III) with an Fe(III) (oxy)hydroxide (eq 1.2). In addition to adsorbing to the iron oxides produced, Cr(III) could be structurally incorporated in the iron oxide by co-precipitation to form a Fe(III)-Cr(III) (oxy)hydroxide solid solution.[27]

$$CrO_4^{2-} + 3Fe^{2+} + 3H_2O + H^+ = CrOH^{2+} + 3Fe(OH)_2^+ \quad (1.1)$$

$$xCrOH^{2+} + (1-x)Fe(OH)_2^+ + (1+x)H_2O = Cr_xFe_{1-x}(OH)_{3(s)} + (1+x)H^+ \quad (1.2)$$

1.1.3 Iron-electrocoagulation for Cr(VI) removal

While Fe(II) can be introduced to water for Cr(VI) removal by chemical addition, iron-based electrocoagulation (EC) can also generate Fe(II) for effective Cr(VI) removal from water. EC is based on applying an electric voltage to a sacrificial Fe(0) anode to generate Fe(II) in situ (eq 1.3).[28] H^+ generated during Fe(II) oxidation process (eq 1.5) could be reduced on the cathode (eq 1.4), stabilizing pH in the alkaline range.[29] The generated Fe(II) can be subsequently

oxidized by dissolved oxygen to Fe(III), which can then precipitate as Fe(III) (oxy)hydroxides depending on the pH. Research over the past decades has proven the ability of electrocoagulation to remove a wide range of pollutants in systems with simple design and operation [30, 31]. EC has been most widely studied as a technology for arsenic removal from drinking water sources at various conditions.[32-35] For chromium , most EC research has focused on applications to industrial wastewater treatment.[36, 37] When Cr(VI) is present, it could be directly reduced by Fe(II) to less soluble Cr(III) in a pathway in which the Cr(VI) competes with DO for oxidation of the Fe(II) (eq 1.1).

Anode:

$$Fe = Fe^{2+} + 2e^{-} \quad (1.3)$$

Cathode:

$$2H^{+} + 2e^{-} = H_{2\,(g)} \quad (1.4)$$

$$4Fe^{2+} + O_{2(g)} + 6H_2O = 4FeO(OH)_{(s)} + 8H^{+} \quad (1.5)$$

1.1.4 The interaction between natural organic matter and metals

Natural organic matter (NOM) is regarded as a group of chemically heterogeneous organic molecules that exist in almost all aquatic environments and can profoundly impact the biogeochemical cycling of metals and the colloidal stability of metal-bearing nanoparticles.[38-40] NOM is an important complexing agent for metal ions. For many metals the speciation is predominantly controlled by interaction with ligands/active sites of NOM.[41, 42] In most cases, complexation of trace metals with organic matter decreases their bioavailability and toxicity but facilitate metal transport in aqueous systems.[43] Natural organic matter may constitute an important sink for chromium in the environment, due to the strong interaction with

chromium(III), and to its ability to reduce chromium(VI) to chromium(III).[44] NOM can also stabilize ferrihydrite, thus preventing the transformation to more crystalline Fe phases under oxic conditions.[45, 46]

1.1.5 Cr(III) oxidation by manganese oxide in groundwater or soils

Manganese oxides (Mn(III/IV)-oxide), which are primarily formed by biologically catalyzed reactions with oxygen,[47-49] are common in natural environments. Biogenic manganese oxides are usually poorly crystalline minerals with high average Mn oxidation states (from 3.7 to 4.0) and high specific surface areas.[50] Birnessite is a manganese oxide with a layered structure that commonly forms surface coatings on weathered mineral grains.[51] Manganese oxides are strong oxidants that provide a major geochemical pathway for Cr(VI) occurrence from Cr(III) in groundwater, soils or subseafloor environments.[52-54] The oxidation of Cr(III) to Cr(VI) significantly increases its mobility and toxicity.

Under moderate pH conditions, Mn(III,IV) (hydr)oxides, which are prevalent in the environment, appear to be the only potent naturally occurring oxidants of Cr(III).[55-58] Oxidation of Cr(III) to Cr(VI) by Mn oxides in an aqueous system is complex and several factors have been credited with influencing the extent and rates of the processes involved. Adsorption mechanisms of Cr(III) on Mn oxides, mechanisms of electron transfer, and desorption and readsorption of produced Cr(VI) and Mn(II) have been reported as controlling factors for the kinetics and the oxidation capacity of Mn oxides.[56, 59-61] In addition, pH, initial Cr(III) concentration, and the ratio of surface area of Mn oxide to solution volume also determine the kinetics and oxidation capacity.[56, 60]

1.2 Research Objectives

Objective 1: Evaluate the performance of electrocoagulation for Cr(VI) removal

Objective 1.1: Determine the effects of water chemistry on the rate and extent of Cr(VI) removal from iron electrocoagulation and develop a modeling tool to predict Cr(VI) removal.

Objective 1.2: Elucidate the effect of humic acid (HA) on the performance of electrocoagulation for Cr(VI) removal.

Objective 2: Explore the stability of $Cr_xFe_{1-x}(OH)_3$ coupled with Mn redox cycling

Objective 2.1: Determine the rates and mechanisms of $Cr_xFe_{1-x}(OH)_3$ oxidation by MnO_2.

Objective 2.2: Develop a model for predicting Cr(VI) generation from Cr(III)-containing solids oxidation by MnO_2 in systems with and without convective mixing of solutes.

Objective 2.3: Test the role of Mn(II) in $Cr_xFe_{1-x}(OH)_3$ oxidation by oxygen.

1.3 Overview of Dissertation

This study includes two related main tasks that address the specific research objectives (Figure 1.2).

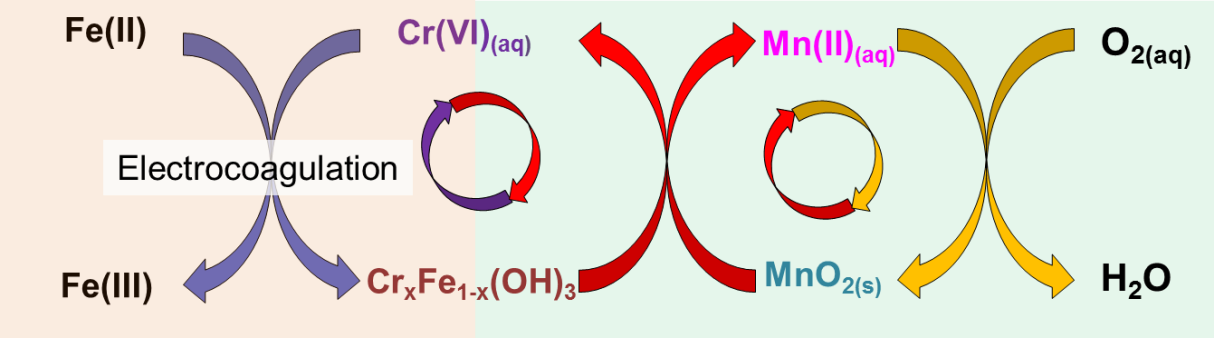

Figure 1.2 Overview of two research tasks to investigate chromium in aquatic environments

Task 1: Study the rate and extent of Cr(VI) removal from iron electrocoagulation and establish a model to predict Cr(VI) removal

Subtask 1.1 was investigation of the effect of water chemistry on Cr(VI) removal from electrocoagulation and establishing a model to predict the dynamics of Cr(VI) in EC. It is addressed in Chapter 2. I examined iron electrocoagulation for Cr(VI) removal in a laboratory-scale batch reactor. Experiments evaluated the effects of pH, oxygen level, and common groundwater solutes on Cr(VI) removal, and experiments were also performed with a simulated groundwater source of drinking water. X-ray absorption near edge structure (XANES) spectra was used to probe the oxidation state of chromium in the solids produced by electrocoagulation. A model was developed to describe the Cr(VI) and Fe(II) dynamics in iron electrocoagulation at pH 6, pH 8, oxic and anoxic conditions, which is potentially applicable to a broad range of water chemistry conditions.

Subtask 1.2 was to explore the effect of humic acid on Cr(VI) removal and characterize the solids product in EC. It is addressed in Chapter 3. Experiments examined the dynamics of Cr(VI) in electrocoagulation in the presence of humic acid over a wide range of conditions, from pH 6 to pH 9, at oxic and anoxic conditions. We used dynamic light scattering (DLS) to measure the particle size and zeta potential of suspensions. The colloidal conditions in EC are directly related with the mobility and fate of Cr(III) and HA. X-ray diffraction (XRD) and extended X-ray absorption fine structure spectroscopy (EXAFS) provided useful information help to identify the iron minerology in EC that the presence of humic acid could favor ferrihydrite formation.

Task 2: Examine the Cr(VI) production rates coupled with Mn redox cycling and establish a model to describe the process

Subtask 2.1was to determine the Cr(VI) product rates from $Cr_xFe_{1-x}(OH)_3$ oxidation by *δ*-MnO_2. It is addressed in Chapter 4. The Cr(VI) production from $Cr_xFe_{1-x}(OH)_3$ oxidation by δ-MnO_2 were examined as a function of pH and Fe/Cr ratios in solids. The Cr(VI) production rates were correlated with the corresponding dissolved Cr(III) concentration in equilibrium with $Cr_xFe_{1-x}(OH)_3$, which indicates the important role of Cr(III) dissolution in oxidation. A multichamber reactor was used to assess the role of solid-solid contact in $Cr_xFe_{1-x}(OH)_3$-MnO_2 interactions, which eliminates the contact of the two solids while still allowing aqueous species transport across a permeable membrane.

Subtask 2.2 was investigation of the interaction between Cr(III)-containing solids and δ-MnO_2 on Cr(VI) generation. It is addressed in Chapter 5, which focused on studying the $Cr(OH)_3$ oxidation. Experiments using multichamber reactors and mixed batch reactors indicated that mixing of solid suspensions is important in Cr(VI) generation, especially at the conditions when Cr(III) solubility is low. A kinetic and transport model was developed to describe the oxidation rate of $Cr(OH)_3$ oxidation by MnO_2 in multichamber reactor, which could also be applied to predict Cr(VI) release in completely mixed batch reactor.

Subtask 2.3 is to evaluate the role of Mn(II) in $Cr_xFe_{1-x}(OH)_3$ oxidation by dissolved oxygen. It is addressed in Chapter 6, examined the oxidation of $Cr_xFe_{1-x}(OH)_3$ in the presence of Mn(II) at oxic conditions. Both Cr(VI) generation and Mn(II) decline were measured in the system. The effects of pH and oxygen were studied .

Chapter 7 summarizes the results of the present work. Important accomplishments are highlighted, and areas for future investigation are identified.

Chapter 2. Cr(VI) Removal from Drinking Water by Iron Electrocoagulation

This chapter was published in Pan, C.; Troyer, L.D.; Catalano, J.G.; Giammar, D.E., Dynamics of chromium (VI) removal from drinking water by iron electrocoagulation. Environ Sci Technol 2016, 50, (24), 13502-13510.[62]

Abstract

The potential for new U.S. regulations for Cr(VI) in drinking water have spurred strong interests in improving technologies for Cr(VI) removal. This study examined iron electrocoagulation for Cr(VI) removal at conditions directly relevant to drinking water treatment. Cr(VI) is chemically reduced to less soluble Cr(III) species by the Fe(II) produced from an iron anode, and XANES spectra indicate that the Cr is entirely Cr(III) in solid-phases produced in electrocoagulation. The dynamics of Cr(VI) removal in electrocoagulation at pH 6 and pH 8 at both oxic and anoxic conditions can be described by a new model that incorporates Fe(II) release from the anode and heterogeneous and homogeneous reduction of Cr(VI) by Fe(II). Heterogeneous Cr(VI) reduction by adsorbed Fe(II) was critical to interpreting Cr(VI) removal at pH 6, and the Fe- and Cr-containing EC product was found to catalyze the redox reaction. Dissolved oxygen (DO) did not observably inhibit Cr(VI) removal because Fe(II) reacts with DO more slowly than it does with Cr(VI), and Cr(VI) removal was faster at higher pH. Even in the presence of common groundwater solutes, iron electrocoagulation lowered Cr(VI) concentrations to levels well below California's 10 μg/L.

2.1 Introduction

Both within the United States and internationally, hexavalent chromium [Cr(VI)] is a contaminant of concern in drinking water supplies.[63, 64] Cr(VI) has both natural and anthropogenic sources. Transformations of Cr(III) to Cr(VI) can be mediated by constituents that are naturally present (e.g., MnO_2 solids)in aquifers or are purposefully added to water (e.g., chlorine disinfectants).[65, 66] Water monitoring data collected in California in 2003 indicates that 3% of 6229 drinking water sources surveyed had a Cr(VI) concentration higher than 10 μg/L, and 33% had Cr(VI) concentration above the detection limit of 1 μg/L.[64] The current U.S. drinking water standard for total chromium is 100 μg/L, which includes Cr(VI) as well as less soluble and significantly less toxic trivalent chromium [Cr(III)];[67] however, in June 2014 California started regulating Cr(VI) with a maximum contaminant level (MCL) of 10 μg/L.[68] The U.S. Environmental Protection Agency is also considering a Cr(VI)-specific standard, and utilities were recently required to monitor for Cr(VI) as an unregulated contaminant.[3] If a standard for Cr(VI) of 10 μg/L or less is selected for the federal value, then many utilities that comply with the current standard will become out of compliance unless new treatment technologies are implemented or new water sources are acquired.[64, 69, 70]

Physical and chemical processes involving chromium and iron can be used to remove Cr(VI) from solution. Although Cr(VI) can adsorb to iron oxides,[5-8] adsorption decreases with increasing pH and can be negligible at the pH conditions of many water supplies. Consequently Cr(VI) removal by coagulation using Fe(III) salts (e.g., ferric chloride) can be poor even with high coagulant doses.[15]

Using reduction and coagulation with Fe(II), Cr(VI) can be removed to low concentrations in drinking water.[15, 23-25] The rates of Cr(VI) reduction by Fe(II) are highly pH dependent, decreasing with increasing pH over the range of 1.5-4.5 and then increasing from pH 5 to 8.7.[26] The removal of Cr(VI) in this process involves reduction of Cr(VI) to Cr(III) coupled with the oxidation of Fe(II) to Fe(III) (reaction 1, written based on the dominant dissolved species at pH 7) and the subsequent association of Cr(III) with the Fe(III) (oxy)hydroxide solids. These solids can be removed by filtration, sedimentation, or other downstream particle removal processes.[71] The Cr(III) can adsorb to the iron oxides produced, or it could be structurally incorporated into the iron oxide to form a Fe(III)-Cr(III) (oxy)hydroxide solid solution (reaction 2).[27]

$$CrO_4^{2-} + 3Fe^{2+} + 3H_2O + H^+ = CrOH^{2+} + 3Fe(OH)_2^+ \quad (2.1)$$

$$x\ CrOH^{2+} + (1-x)\ Fe(OH)_2^+ + (1+x)\ H_2O = Cr_xFe_{1-x}(OH)_{3(s)} + (1+x)\ H^+ \quad (2.2)$$

While Fe(II) can be introduced to water for Cr(VI) removal by chemical addition, iron-based electrocoagulation (EC) can also generate Fe(II) for effective Cr(VI) removal from water. EC involves applying an electric voltage to an iron anode to generate Fe(II) in situ.[28] The Fe(II) generated can be oxidized by Cr(VI) or by dissolved oxygen to Fe(III), which can then precipitate as Fe(III) (oxy)hydroxides depending on the pH and the electrolyte composition[72] (reaction 3 shown for the production of lepidocrocite, γ-FeOOH).

$$4Fe^{2+} + O_2 + 6H_2O = 4FeOOH_{(s)} + 8H^+ \quad (2.3)$$

Fe(III) oxide surfaces can serve as heterogeneous catalysts for the reduction of Cr(VI) by Fe(II).[73]

Electrocoagulation can remove a wide range of pollutants in systems with simple design and operation.[30, 31] EC has been most widely studied as a drinking water treatment technology for

removing arsenic.[32-35, 74] To our knowledge iron EC had not previously been studied for Cr(VI) removal at Cr(VI) concentrations, pH values, and solution compositions most relevant to drinking water treatment. Previous EC research on chromium removal has focused on applications to industrial wastewater treatment with much higher chromium concentrations, as high as several hundred mg/L, and those studies did not systematically evaluate the effects of dissolved oxygen and pH on Cr(VI) removal.[75-77] For the application of EC to arsenic removal from drinking water, Li et al established a highly constrained dynamic model of As(III) oxidation in the EC system over a broad range of operating conditions for a simulated groundwater. The model verified the role of Fe(IV) in As(III) oxidation mechanism in EC and is helpful to predict As(III,V) removal as well as the minimal iron dosage needed for the adequate treatment. There was a need to develop a model for the dynamics of the Cr(VI) removal process that could identify the rate-limiting step and predict the Cr(VI) removal as a function of water chemistry.

The objective of this study was to identify the mechanisms and quantify the rates of Cr(VI) removal from drinking water by EC over a range of relevant water chemistry conditions. Batch experiments were used to investigate the effects of pH, DO, and the presence of common solutes on Cr(VI) removal. Solid phases were characterized with respect to their mineralogy and the oxidation state of associated Cr. To examine the roles of homogeneous and heterogeneous reduction of Cr(VI) by Fe(II) in the removal process, a model for the dynamics of Cr and Fe in at batch iron EC reactor was developed.

2.2 Materials and Methods

2.2.1 Materials

Chemicals used were analytical reagents of high purity. Ultrapure water (resistivity >18.2 MΩ-cm) was used for the experiments. Glass volumetric flasks and 1-L polypropylene reaction vessels were cleaned with 10% HCl and rinsed several times with ultrapure water before use. A Cr(VI) stock solution (0.1 g/L, 1.923 mM) was prepared from $K_2Cr_2O_7$. Control of ionic strength was achieved by additions from a 1 M $NaNO_3$ stock solution. At pH 6, 1 mM MES (2-(N-morpholino) ethane sulfonic acid) (Fisher Scientific) was used, and 5 mM HEPES (4-(2-hydroxyethyl)-1-piperazineethanesulfonic acid) (≥99.5%, Sigma-Aldrich) was used at pH 7 and 8. The pH buffers and their concentrations were chosen to minimize the possible formation of Fe(III) and Cr(III) complexes with the buffers. At pH 4 and pH 5, no buffers were added and a syringe pump dosed 0.1 M trace metal grade nitric acid to maintain a constant pH during EC experiments. Silica, sulfate and phosphate were added from stock solutions of 0.1 M Na_2SiO_3, 0.5 M Na_2SO_4, and 0.1 M NaH_2PO_4/Na_2HPO_4 (molar ratio 6.8:93.2 for pH 8). In addition to experiments with simple compositions, Cr(VI) removal was also evaluated using a challenge water. Based on the large body of research on Cr(VI) removal performed in Glendale, California, a simulated Glendale groundwater (SGG) was prepared by addition of reagents to meet a published composition (Table S2.1 of the Supporting Information).[24]

2.2.2 Electrocoagulation batch experiments

The electrocoagulation reactor consisted of a 1-L polypropylene beaker with two 1.75-cm diameter iron rods immersed in solution. The reactor was filled with ultrapure water and aliquots

of sodium nitrate, pH buffer and Cr(VI) stock solutions to a total initial volume of 1 L. The Cr(VI) stock solution was added to provide an initial Cr(VI) concentration of 500 μg/L (9.62 μM). Sodium nitrate was added until the conductivity of the solution achieved 460 μS/cm, which corresponds to an ionic strength around 5 mM. Na^+ and NO_3^- do not interfere with the chemistry of Cr(VI) removal and only controlled the ionic strength. Because the different pH buffer concentrations provided different ionic strengths, the amount of sodium nitrate added depended on the pH of the experiment and was used to ensure that all pH values were studied with the same solution conductivity. The solution was continuously and completely mixed by a magnetic stir bar at a speed of 600 rpm. For oxic experiments air was vigorously bubbled through the solution at a flow rate of 0.94 L/min. Before each experiment, the two iron rods were abraded with sandpaper and thoroughly rinsed. The iron rods were inserted into solution and placed 2 cm apart. An electric potential of 4 V was applied to the rods with a direct current power supply, and the current was held constant at 37 mA (around 0.99 mA/cm^2) by raising the beaker to maintain the same depth of immersion of the iron rods (8 cm) when portions of the solution were removed for sampling.

Separate control experiments were performed to examine Cr(VI) removal by chemical addition of Fe(II) and the potential for Cr(VI) adsorption to iron oxides formed from chemical coagulation and electrocoagulation. Chemical coagulation was performed by continuous addition of Fe(II) from an $FeSO_4$ solution with a syringe pump to maintain the rate that it is released from the anode in electrocoagulation. Adsorption experiments were performed by first preparing iron oxide solids and then adding Cr(VI) to those suspensions over a range of pH values. Solids for adsorption were prepared in the absence of Cr(VI) by (a) electrocoagulation, (b) continuous

addition of $FeSO_4$, and (c) one time addition of $Fe(NO_3)_3$. Details of chemical dosage and adsorption experiments for Cr(VI) removal are provided in the supporting information.

Anoxic experiments were performed in an anaerobic chamber (Coy Laboratory Products Inc., MI) with less than 1 ppmv of O_2 in the gas phase as controlled by circulating the chamber atmosphere of 98% N_2/2% H_2 over a heated Pd catalyst. A secondary low temperature oxygen trap was introduced to achieve strictly anoxic conditions in the electrocoagulation reactor. The oxygen trap consisted of a sequence of two 200-mL suspensions of 93.2 mM Fe(III) as ferric hydroxide and 0.9 mM $FeCl_2$ at pH 8.1; at these conditions dissolved O_2 is rapidly consumed by reaction with the Fe(II).[78] An aquarium pump was used to pass air inside the anaerobic chamber through the secondary oxygen trap and then into the electrocoagulation reactor. The efficacy of the trap was tested by evaluating the stability of an Fe(II) solution at pH 8. The rate of ferrous iron oxidation was much slower with the secondary oxygen trap (Figure S2.1), and the reaction of Fe(II) with any residual DO remaining after the passage through the secondary trap can be neglected in the interpretation of the EC experiment results.

For each sampling event, a volume of suspension was drawn from the reactor using a 15 mL syringe. The first 3 mL were dispensed as an unfiltered suspension to a test tube, acidified to 2% HNO_3 to dissolve any suspended solids, and analyzed for total iron and chromium concentrations. The rest of the suspension in the syringe was filtered through a 0.22 μm polyethersulfone (PES) membrane, and the filtrate was saved for analysis of dissolved iron, chromium, Cr(VI), and Fe(II) concentrations. All the samples for ICP-MS measurements (including total and dissolved chromium and iron) were preserved with 2% HNO_3.

2.2.3 Analytical methods

The samples for measuring Fe(II) or Cr(VI) were filtered once they were collected and then measured immediately by either ferrozine or diphenylcarbazide methods. Cr(VI) concentrations in the samples were determined by measuring the absorbance at 540 nm using a UV-vis spectrophotometer with 1-cm path length cuvettes (PerkinElmer-Lambda XLS) after reaction with diphenylcarbazide.[79] Our detection limit for Cr(VI) by this method was 5μg/L (0.096 μM). Dissolved Fe(II) concentrations were determined spectrophotometrically by the ferrozine method at a wavelength of 562 nm.[80] The method detection limit for Fe(II) was 0.3 mg/L (5.4 μM). Total dissolved iron and total dissolved chromium (Cr(VI) and Cr(III) together) concentrations were measured by inductively coupled plasma mass spectrometry (ICP-MS) (Perkin Elmer ELAN DRC II) analysis of filtered samples. The instrument detection limits for Cr and Fe were 0.2 μg/L (0.0039 μM) and 0.1 mg/L (1.8 μM), respectively. Dissolved Fe(II) concentrations were found to be equal to dissolved iron concentrations in the experiments because Fe(III) has a very low solubility over the pH range studied; consequently, dissolved Fe(III) can be neglected in all conditions investigated.

Solids for characterization were collected from suspensions after 45 minutes of electrocoagulation or chemical coagulation with and without chromium. The suspensions were concentrated by centrifugation and then freeze-dried. The specific surface areas (SSA) of selected solid samples were measured by BET N_2-adsorption with a surface area analyzer (NOVA 2000e, Quantachrome Instruments). X-ray powder diffraction (XRD) patterns of solid samples were collected using Cu Kα radiation (Bruker d8 Advance X-ray diffractometer).

Cr K-edge X-ray absorption near-edge structure (XANES) spectra were collected on samples from electrocoagulation reactors at pH 6 and pH 8 after 10 minutes and 45 minutes of

reactor operation. Samples with added Si and P were collected after 10 minutes of electrocoagulation. Samples were vacuum-filtered onto mixed cellulose ester membranes (0.22 μm) and then sandwiched as wet pastes between Kapton film and sealed with Kapton tape. XANES spectra were collected at beamline 4-1 at Stanford Synchrotron Radiation Lightsource (SSRL) using a Si (220) double-crystal monochromator with a harmonic rejection mirror. Fluorescence-yield spectra were collected using a 30-element energy-dispersive solid-state Ge detector. Reference spectra were also collected on a potassium chromate salt ($K_2Cr_2O_7$) and a $Cr(OH)_3$ solid that was synthesized by adjusting the pH of Cr(III) solution to 7 using NaOH. Background subtraction and linear combination fitting of XANES spectra were performed using the Athena[81] interface to IFEFFIT.[82]

2.3 Results and Discussion

2.3.1 Overview of chromium removal in Electrocoagulation

Before systematically exploring the influence of water chemistry on Cr(VI) removal by electrocoagulation, we will present the results of the operation of the reactor at a single condition (oxic at pH 8.0). The initially clear and colorless solution became a turbid orange suspension typical of Fe(III) (oxy)hydroxides after 15 minutes. XRD showed that the dominant iron oxide formed during electrocoagulation at this condition was lepidocrocite; at pH 6 a mixture of ferrihydrite and lepidocrocite formed (Figure S2.2). Solids produced in other EC research include magnetite, lepidocrocite, ferrihydrite, and green rust.[72, 83, 84] At conditions similar to ours (pH 7.5-10 in 5 mM NaCl with a low current density of 5 mA/cm^2), Dubrawski et al. also identified lepidocrocite as the product of EC.[84] They noted that lepidocrocite is a well-known product of Fe(II) oxidation by DO in the absence of strongly adsorbing ions.

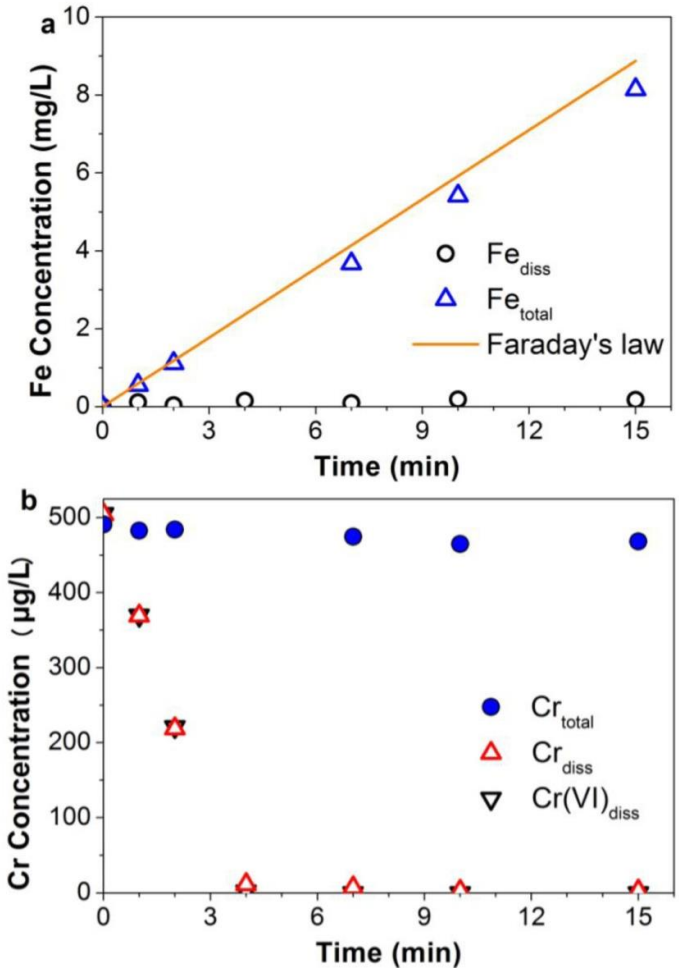

Figure 2.1. Performance of Cr(VI) removal by iron electrocoagulation at pH 8.0 in an aerated reactor. $[Cr(VI)]_0$ = 500 μg/L, 5 mM HEPES for pH 8.0, U = 4 V, I = 37 mA, and conductivity = 460 μS/cm. The performance is tracked with respect to (a) measured concentrations of total (Fe_{total}) and dissolved (Fe_{diss}) iron together with the predicted total iron concentration based on Faraday's law and (b) total (Cr_{total}) and dissolved (Cr_{diss}) chromium concentrations. Because dissolved Cr and dissolved Cr(VI) were essentially identical, the points for those values plot on top of one another.

In EC, the total iron concentration increases linearly because of the constant electrical current passed through the solution by the electrodes (Figure 2.1a); the values of the total iron concentrations were consistent with predictions based on Faraday's law (eq. S2.6 in the

supporting information) with the assumption that Fe(II) is generated at the anode. Control experiments without electric current (data not shown) indicated that iron dissolution from the anode was negligible compared with iron generated during EC. The Fe(II) released from the anode can be oxidized rapidly by either Cr(VI) or dissolved oxygen at pH 8 (Figure 2.1a). However, the rapid removal of Cr(VI) at pH 8 demonstrated that Cr(VI) is a strong competitor with DO for oxidizing Fe(II) (Figure 2.1b).

Table 2.1. The residual dissolved Cr during EC in comparison to predicted values at different pH

pH	4	5	6	7	8
Reaction time-oxic (min)	30	25	20	15	10
Measured Cr_{diss} (oxic) (μg/L)[1]	62.5	2.4	1.2	3.1	2.6
Mole ratio of Fe(III)/Cr(III) in solid (oxic)	6.8	7.3	3.3	2.8	3.7
Reaction time-anoxic (min)			7		10
Measured Cr_{diss} (anoxic) (μg/L)[2]			2.3		3.0
$Cr(III)_{diss}$ by $Cr(OH)_{3(s)}$ (μg/L)[3]	78022	517	14	0.8	1.6
$Cr(III)_{diss}$ by $(Cr_xFe_{1-x})(OH)_{3(s)}$ (μg/L)[4]	107	0.95	0.04	-	-

[1] The dissolved Cr concentration measured by ICP-MS at the end of reaction time in oxic conditions;

[2] The dissolved Cr concentration measured by ICP-MS at the end of reaction time in anoxic conditions;

[3] The estimated Cr(III) solubility controlled by $Cr(OH)_{3(s)}$, calculation is based on equilibrium constants given by [85];

[4] The estimated Cr(III) solubility controlled by $(Cr_xFe_{1-x})(OH)_{3(s)}$ co-precipitation, the concentration of dissolved Cr(III) at pH 7 and pH 8 is too low to give values, calculation is based on equilibrium constants given by a published reference.[86]

The total chromium concentration remained constant during EC (Figure 2.1b) because chromium remained in the suspension of the batch reactor and was not removed by reaction on the electrodes or the reactor walls. The total chromium includes both dissolved and suspended solids that had precipitated, and thus contains both Cr(III) and Cr(VI). For this experimental condition the dissolved Cr(VI) concentration was identical to the total dissolved Cr concentration (Figure 2.1b), indicating that the dissolved Cr(III) concentration was negligible, consistent with the expected low solubility of Cr(III) at pH 8 (Figure S2.6). The dissolved chromium dropped below the California primary drinking water standard of 10 µg/L (Table 2.1) within 10 minutes.

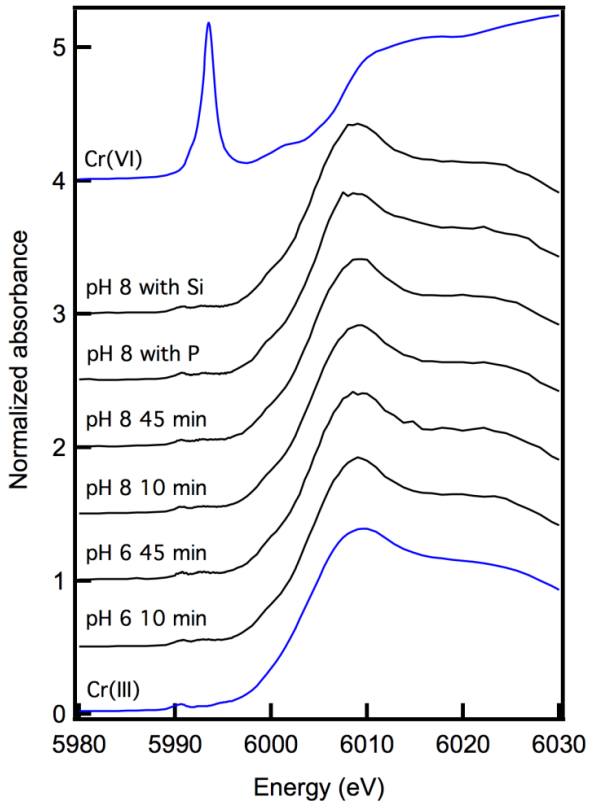

Figure 2.2. Cr K-edge XANES spectra of samples (black) from electrocoagulation reactors at pH 6 and 8 after 10 or 45 minutes of electrocoagulation. Samples at pH 8 were also reacted for 10 minutes with P and Si. Reference spectra of potassium chromate (Cr(VI)) and chromium hydroxide (Cr(III)) are shown in blue.

XANES analysis of the solids demonstrated that the rapid removal of Cr(VI) during electrocoagulation was caused by reduction of Cr(VI) to less soluble Cr(III). At both 10 minutes and 45 minutes, only Cr(III) was detected in the solids based on Cr K-edge XANES spectra (Figure 2.2). Batch adsorption experiments in which Cr(VI) was contacted with preformed solids produced by electrocoagulation found a low affinity of Cr(VI) for the solids (Figure S2.3), indicating that Cr(VI) adsorption is not a dominant mechanism for Cr(VI) removal in EC and that the reduction to Cr(III) is critical to successful treatment. In chemical coagulation experiments with continuous Fe(II) addition at rates identical to the rate of Fe(II) generation in electrocoagulation, Cr(VI) removal versus time was very similar to that for electrocoagulation (Figure S4). This further confirmed that Cr(VI) was reduced by Fe(II) generated from EC.

2.3.2 Influence of DO on rates and mechanisms

DO competes with Cr(VI) for the oxidation of Fe(II) and can potentially influence the rate and extent of Cr(VI) removal in electrocoagulation. The pH values of 6 and 8 were chosen to investigate the influence of DO on Cr(VI) removal during electrocoagulation because the rate of DO reaction is about 2800 times faster at pH 8 than at pH 6 (the Fe(II) oxidation rate by DO at pH 6 and pH 8 is provided in supporting information). The reaction rates are such that Fe(II) oxidation by DO at pH 6 is on a timescale that is very long relative to that of the treatment time, while the rate at pH 8 is sufficiently fast that it is essentially instantaneous relative to the treatment time. At pH 6, DO oxidized Fe(II) very slowly in comparison to the oxidation of Fe(II) by Cr(VI), as indicated by the by the fact that the Fe(II) concentration is only slightly lower at oxic than anoxic conditions (Figure 2.3a). Consequently, rates and extents of Cr(VI) removal at oxic and anoxic conditions were not that different at pH 6 (Figure 2.3b). Similar to our observations with EC, Schlautman and Han found that DO had only a minor influence on Cr(VI)

reduction by chemical addition of Fe(II) below pH 6.[87] At pH 8 even though Fe(II) was rapidly oxidized by DO in aerated experiments (Figure 2.3c) and held at low concentrations, Cr(VI) was still removed at a comparable rate in anoxic experiments to that in oxic experiments because of the very fast reduction of Cr(VI) by Fe(II). For the anoxic conditions, the stoichiometry of Cr(VI) reduction by Fe(II) is clear. The dissolved Fe(II) stayed low at pH 8 until the Cr(VI) was essentially all reduced (Figure 2.3c), and then dissolved Fe(II) started increasing parallel to the total iron (line of Faraday's law, eqn S2.6). At the time of essentially complete Cr(VI) removal, the difference between total and dissolved Fe indicated that about 2 mg/L (36 μM) of Fe(II) had been consumed by reduction of 500 μg/L (9.6 μM) of Cr(VI), which approaches the expected molar stoichiometry of 3:1 for oxidation of Fe(II) by Cr(VI).

A quantitative model for the dynamics of Cr(VI) reduction in electrocoagulation was developed based on detailed studies of Cr(VI)/Fe(II) and Fe(II)/O_2 systems. The rates of change of Cr(VI) (eqn. 2.4) and Fe(II) (eqn. 2.5) during electrocoagulation can be written as

$$-\frac{d[Cr(VI)]}{dt}=k_{homo}*[Cr(VI)]_{diss}*[Fe(II)]_{diss}+k'_{hetero}*[Fe(III)]_s*[Cr(VI)]_{diss}*[Fe(II)]_{diss} \quad (2.4)$$

$$-\frac{d[Fe(II)]}{dt}=3k_{homo}*[Cr(VI)]_{diss}*[Fe(II)]_{diss}+3k'_{hetero}*[Fe(III)]_s*[Cr(VI)]_{diss}*[Fe(II)]_{diss}-k_2+k_{O_2}*[Fe(II)]_{diss} \quad (2.5)$$

The definitions and values of the rate constants are summarized in Table 2.2. Eqn. 2.4 includes terms to account for both homogeneous and heterogeneous reduction of Cr(VI). In eqn. 2.5, the four terms are included to track the fate of Fe(II) as it is affected by (i) homogeneous and (ii) heterogeneous reaction of Fe(II) with Cr(VI), (iii) Fe(II) production from the anode according to Faraday's law, and (iv) Fe(II) oxidation by dissolved oxygen. $Fe(III)_s$ is the

concentration of Fe(III)-containing solid on which heterogeneous Cr(VI) reduction by Fe(II) can occur with $[Fe(III)]_s = [Fe(II)]_T - [Fe(III)]_{diss}$. The model is based on two assumptions. First, the adsorbed concentrations of both Cr(VI) and Fe(II) are negligible compared with dissolved concentrations at pH 6 and pH 8. Second, the ratio of the concentration of any adsorbed Fe(II) adsorbed (albeit small) to its dissolved concentrations remains constant during the reaction. Detailed explanations for the choices and validities of these assumptions are given in the supporting information. Based on the first assumption, we use the total Cr(VI) and Fe(II) to simulate the dissolved Cr(VI) and Fe(II) concentration in experiments. The ordinary differential equations (ODEs) in the model were solved by the ode45 solver in Matlab 7.0. The parameters in Equations 2.4 and 2.5 were determined independently in control experiments focused on specific processes (i.e., not electrocoagulation experiments) and then included in the model for examination of EC performance for Cr(VI) removal. Detailed discussion of the determination of the parameters is included in the supporting information.

Cr(VI) could be successfully modeled at pH 8 without including any terms for heterogeneous Cr(VI) reduction (i.e. $k'_{hetero}=0$ in Table 2.2) because Fe(II) generation in EC was the rate-limiting step for Cr(VI) removal (Figure 2.3c&d). The total Cr(VI) predicted by the model agrees well with the measured dissolved Cr(VI) at both oxic and anoxic conditions (Figure 2.3d), which is consistent with the assumption that Cr(VI) adsorption was negligible in the EC process. Fe(II) is generated from the anode, and it is immediately oxidized by Cr(VI) at pH 8 even when not considering the heterogeneous reaction (Figure 2.3c). The predicted total Fe(II) concentration was somewhat higher than the measured dissolved Fe(II) concentrations at pH 8, and this difference could be the result of adsorption of some of the Fe(II) to the solids produced during EC. Previous studies have found that Fe(II) can adsorb onto iron (hydr)oxides

that include lepidocrocite, goethite, magnetite and ferrihydrite, and the extent of adsorption increases with increasing pH.[88-90] The rate of Cr(VI) removal was comparable at oxic and anoxic conditions, indicating that Fe(II) reacts with Cr(VI) much faster than with dissolved oxygen. The proportion of overall Fe(II) oxidation due to Cr(VI), f_{Cr}, is given as

$$f_{cr}=\frac{3\left(k_{homo}+k'_{hetero}\cdot[Fe(III)]_s\right)\cdot[Cr(VI)]_{diss}}{k_{O_2}+3\left(k_{homo}+k'_{hetero}\cdot[Fe(III)]_s\right)\cdot[Cr(VI)]_{diss}} \quad (2.6)$$

At pH 8 with an initial Cr(VI) concentration of 500 μg/L, f_{Cr} is 0.99.

At pH 6 heterogeneous reduction of Cr(VI) was involved in the overall Cr(VI) removal process. Efforts to model the data using only homogeneous reduction were not successful (Figure S2.10 of the supporting information). The model for Cr(VI) removal predicted both dissolved Cr(VI) and dissolved Fe(II) well when all terms in equations 2.4 and 2.5 were included, including a heterogeneous reaction at pH 6 for Cr(VI) reduction by Fe(II) on the surface of freshly produced Fe(III) solids. Control experiments done in support of the model development showed that the heterogeneous Cr(VI) reduction rate was linearly correlated with the amount of Fe(III) generated, indicating that Cr(VI) reduction in EC is an autocatalytic reaction on surface sites of $Fe_xCr_{1-x}(OH)_3$ (Figure S2.11 of the supporting information). Although Buerge and Hug verified that both lepidocrocite and goethite could catalyze Cr(VI) reduction by Fe(II),[73] our experiment is the first verification that Cr(VI) was auto catalytically reduced on $Fe_xCr_{1-x}(OH)_3$ in iron based EC by modeling methods. At pH 6, DO did not affect Cr(VI) removal and Fe(II) was almost entirely oxidized by Cr(VI). The proportion of overall Fe(II) oxidation due to Cr(VI) (eq 2.7) f_{Cr} was 1.0.

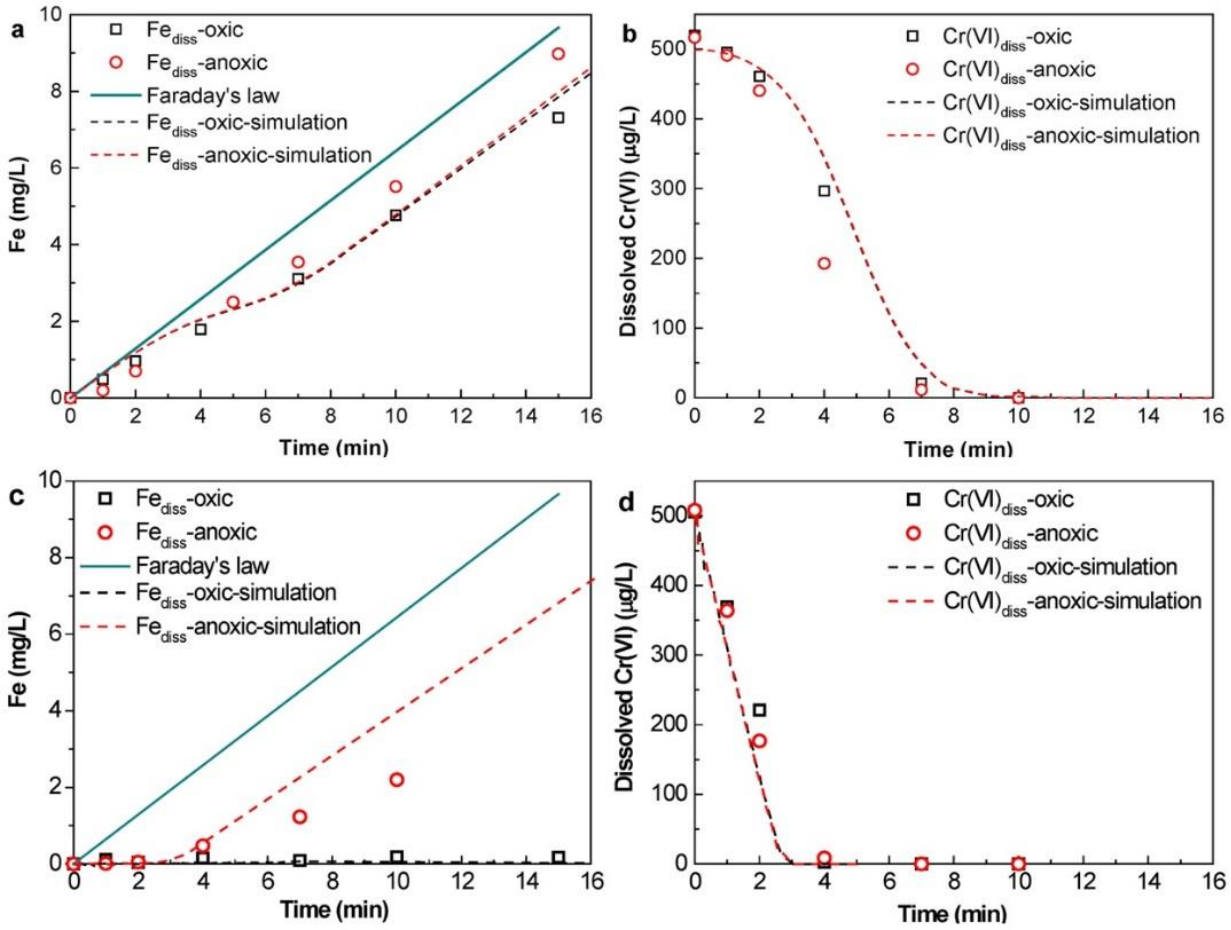

Figure 2.3. The effect of dissolved oxygen on (a) dissolved Fe(II) and (b) dissolved Cr(VI) at pH 6 and (c) dissolved Fe(II) and (d) dissolved Cr(VI) at pH 8 during electrocoagulation with$[Cr(VI)]_0$ = 500 µg/L, U = 4 V, I = 37 mA, and conductivity = 460 µS/cm. At pH 6 the pH was buffered with 1 mM MES and at pH 8 5mM HEPES was used. The points are the experimental data and the dashed lines are the output of a model based on equations 2.4 and 2.5. The solid line in panels a and c is the estimated total iron in the reactor based on release from the anode as calculated by Faraday's law.

Table 2.2. Rate constants used for modeling dissolved Cr(VI) and Fe(II) during electrocoagulation

rate constant	definition	value		dimensions	methods of determination
		pH 6	pH 8		
k_{homo}	homogeneous rate constant for reduction of Cr(VI) by Fe(II)	35	51500	$M^{-1} s^{-1}$	control experiments in SI
k'_{hetero}	Heterogeneous rate constant for Cr(VI) reduction by adsorbed Fe(II)	1.1×10^{7}	0	$M^{-2} \cdot s^{-1}$	derivation in SI using control experiments
k_2	Fe(II) generation rate in EC	1.92×10^{-7}	1.92×10^{-7}	$M \cdot s^{-1}$	Faraday's law with I=37 mA (Eq. S2.6)
k_{O_2} [1]	Fe(II) oxidation rate by O_2	3.85×10^{-6}	1.05×10^{-2}	s^{-1}	Derivation from published eqn[61]

[1] The rate constant is a pseudo first order rate constant calculated for a dissolved oxygen concentration in equilibrium with air and according to the exact Fe(II) speciation of experiments at pH 6 and 8 for calculation of the rate constant from equations in the cited reference.

2.3.3 Influence of pH

To examine the influence of pH on EC performance, experiments were conducted over a range of pH values from 4 to 8. The total iron release rate agreed well with Faraday's law for all pH values (data not shown), but the trend in dissolved Fe(II) was dramatically influenced by pH (Figure 2.4a). Less than 20% of the Fe(II) was oxidized within 15 minutes at the three lowest pH values studied (4, 5, and 6), while at pH 7 approximately 50% of Fe(II) was oxidized at 15 minutes due to the increased rate of oxidation by DO. At pH 8 essentially no iron remained as dissolved Fe(II). The large increase in the rate of Fe(II) oxidation with increasing pH is consistent with the literature.[91, 92] Because of the slow oxidation of Fe(II) by DO at pH 4 to 6, most of the Fe(II) oxidation observed in those experiments was through reaction with Cr(VI). According to the reaction stoichiometry between Cr(VI) and Fe(II) (reaction 1), 1.62 mg/L Fe(II)

(28.93 μM) would be consumed by the reduction of 500 μg/L Cr(VI) (9.62 μM). At pH 4, 5, and 6, Cr(VI) reduction is essentially complete after 20, 15, and 10 minutes respectively (Figure 2.4b), and at these times the differences between the total and dissolved iron concentrations is about 2 mg/L (Figure 2.4a), which is close to the stoichiometric value of 1.62 mg/L that would be consumed by reaction with Cr(VI).

The rate of Cr(VI) removal in EC increased with increasing pH from 4 to 7 and all the EC experiments with influence of different pH for Cr(VI) measurements were duplicated with error bars representing standard deviation (Figure 2.4b). The variation associated with different pH values was much larger than the variation between duplicate experiments. The pH-dependence of Cr(VI) reduction is consistent with several reports in the literature of an increasing rate constant for the reduction of Cr(VI) by Fe(II) with increasing pH above pH 4.5 (Figure S2.5).[26, 93, 94] At pH 8 the rate of Cr(VI) removal was slightly lower than at pH 7, although the dissolved Cr(VI) concentration still decreased to below 5 μg/L within 4 minutes. The deviation of the pH 8 results from the general trend of Cr(VI) removal versus pH was probably because DO more substantially competed with Cr(VI) for oxidation of Fe(II) at pH 8. This is the first clear quantification of the rate of Cr(VI) removal in EC at different pH. Previous studies of Cr(VI) removal by EC usually did not control pH and they only reported the removal efficiency after certain times with different initial pH.[76, 95, 96]

While Cr(VI) removal was rapid at all pH conditions studied, the final total dissolved Cr concentration [Cr(VI) and Cr(III)] was strongly dependent on pH (Table 2.1). Even when the dissolved Cr(VI) concentration decreases to below the drinking water standard, we may still need to consider trace amounts of soluble Cr(III) in filtered water because Cr(III) species could be reoxidized to Cr(VI) when they are exposed to chlorine and chloramine disinfectants in

downstream treatment processes.[97, 98] Thus, removal of both Cr(III) and Cr(VI) is important to a successful chromium treatment technology. From pH 5 to 8, the dissolved chromium could be successfully removed to below 5 µg/L within 25 minutes. However, at pH 4, the dissolved chromium was 63 µg/L after 30 minutes even when the dissolved Cr(VI) was below its detection limit of 5 µg/L; we do note that pH 4 is outside of the range of most drinking water treatment processes (Table 2.1). Similar to our results, Golder found increasing removal of Cr(III) with increasing pH from EC.[99]

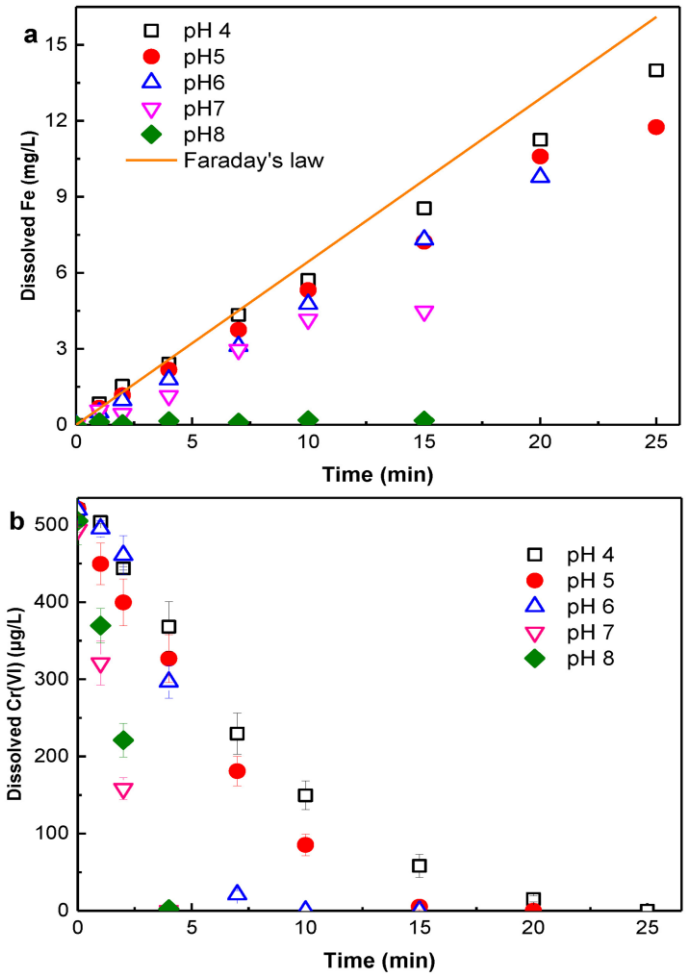

Figure 2.4. The effect of pH on a) dissolved iron and b) dissolved Cr(VI) in electrocoagulation in aerated experiments with $[Cr(VI)]_0$=500 µg/L, 1mM MES for pH=6, 5mM HEPES for pH 7.0 and 8.0, U=4 V, I=37 mA, and conductivity=460 µS/cm.

The dissolved Cr concentration at the end of the experiments can be compared with the predicted solubility of the relevant Cr(III)-containing solids (Table 2.1). Although $Cr(OH)_{3(s)}$ has a low solubility at neutral pH, the measured final Cr concentrations at pH 4-6 were much lower than the solubility of $Cr(OH)_{3(s)}$. The lower solubility is probably the result of precipitation of $(Cr_xFe_{1-x})(OH)_{3(s)}$ as a solid solution of $Cr(OH)_{3(s)}$and $Fe(OH)_{3(s)}$ that has a lower equilibrium dissolved Cr concentration than that of pure $Cr(OH)_{3(s)}$ (Table 2.1). Formation of a solid solution lowers the aqueous concentration of the minor component.[100] The dissolved Cr concentration in equilibrium with $(Cr_xFe_{1-x})(OH)_{3(s)}$ decreases with decreasing mole fraction of Cr(III) in the solid solution.[10, 27] While the dissolved Cr concentrations at pH 4 to 6 are lower than the predicted solubility of pure $Cr(OH)_{3(s)}$, they are still above the predicted solubility of $(Cr_xFe_{1-x})(OH)_{3(s)}$, which may be due to suspensions not having reached a final equilibrium state in the 30 minute reaction time of the experiments. It is also possible that at oxic conditions that some Cr(III) was removed by adsorption of Cr(III) to Fe(III) or mixed Fe(III)/Cr(III) solids. At anoxic conditions and early stages of oxic experiments, the high ratio of Cr to Fe in the solids (1:3 for anoxic conditions) indicates that there is not enough iron in the solids to provide sufficient surface area for Cr(III) adsorption.

2.3.4 Influence of sulfate, silica and phosphate

The presence of silica did not significantly influence Cr(VI) removal during EC at pH 8 (Figure 2.5). Earlier work on As(V) removal by EC found that silica had no significant effect on As removal, although silica prevented the formation of lepidocrocite and led to generation of poorly crystalline ferrihydrite.[33] Although sulfate could potentially compete for adsorption sites with chromium,[101, 102] it did not affect the performance of EC on chromium removal. This supports our conclusion that adsorption does not play a large role in Cr(VI) removal during EC.

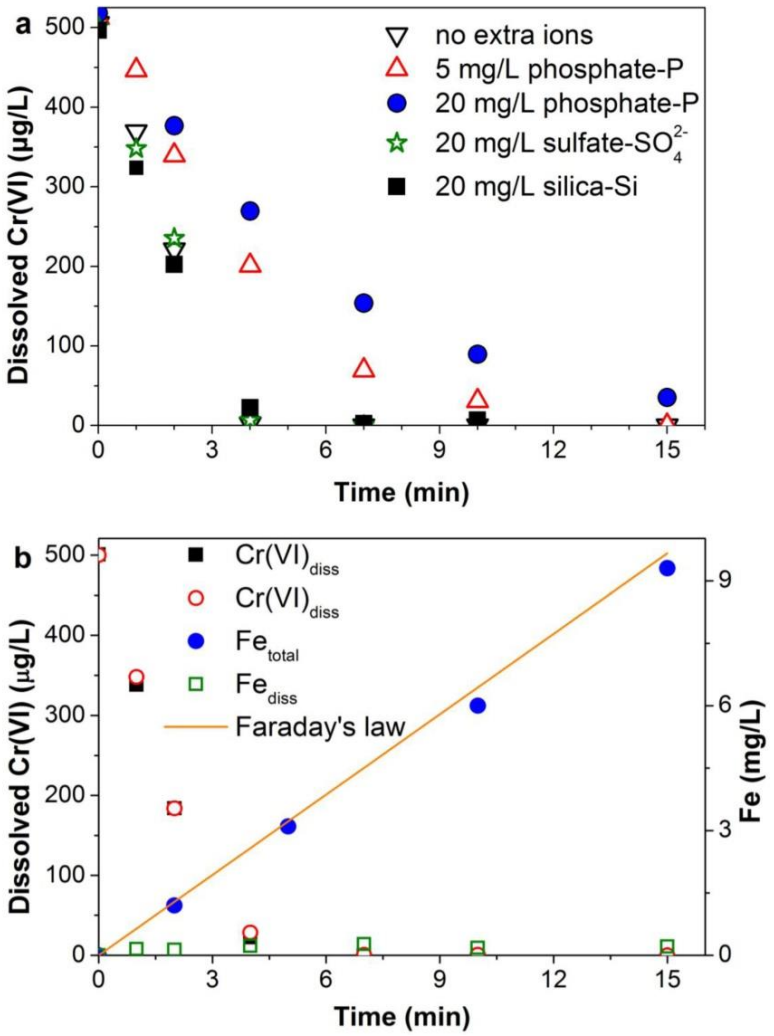

Figure 2.5. The influence of other water constituents on the removal of Cr(VI) during iron electrocoagulation was investigated in aerated experiments with $[Cr(VI)]_0$=500 µg/L, U=4 V, and I=37 mA that evaluated (a)the effects of sulfate, silica and phosphate on Cr(VI) removal with 5mM HEPES at pH 8.0 and conductivity=460 µS/cm and (b) Cr(VI) removal during electrocoagulation in simulated Glendale groundwater (pH 7.4 and conductivity= 885 µS/cm).

Phosphate inhibited Cr(VI) removal in EC (Figure 2.5). Without phosphate, Cr(VI) decreased to below detection within 4 minutes, but 15 and 20 minutes were needed when the solution contained 5 mg/L (0.16 mM) or 20 mg/L (0.65 mM) phosphate, respectively. Phosphate was observed to inhibit As removal in EC because phosphate competed with As species for the

surface sites on lepidocrocite. Because adsorption is not the dominant mechanism for Cr(VI) removal in EC, phosphate probably influences the Cr(VI) removal process by enhancing the rate of aqueous Fe(II) oxidation by DO[103] and making Fe(II) less available for Cr(VI) reduction**.** Also, both filtered Cr(III) and Fe(III) concentrations increased with the presence of phosphate in EC which might be due to phosphate forming dissolved complexes or colloids with Fe(III) and Cr(III) (Figure. S2.13).

Simulated Glendale groundwater (SGG) was used as a challenge water for Cr(VI). The SGG had high concentrations of calcium, sulfate, silica, and chloride with an initial pH of 7.4. Cr(VI) could be removed from an initial concentration of 500 μg/L in this water to below the detection limit within 7 minutes (Figure 2.5b). The dissolved chromium concentration was similar to the dissolved Cr(VI) concentration, indicating that Cr(III) was insoluble for the SGG water condition. After 10 minutes of EC treatment, the dissolved chromium was below 1 μg/L.

2.4 Environmental Implication

Electrocoagulation is an alternative to chemical coagulation that uses metal electrodes and electricity instead of chemical addition to deliver coagulants to water. With iron electrocoagulation, the iron anode releases soluble Fe(II) to reduce Cr(VI) to less mobile and less toxic Cr(III). The Cr(III) is associated with the Fe(III) oxide particles, which can then be removed by conventional processes (e.g., sedimentation followed by granular media filtration). Electrocoagulation avoids the need for chemical handling and can be attractive in settings with better access to electricity than to chemical supplies. Because the coagulant is continuously supplied in electrocoagulation, its dosing can be carefully controlled by changing the current, which can result in minimization of sludge production. This study demonstrates that, at

conditions relevant to drinking water treatment, electrocoagulation can efficiently remove Cr(VI) to a low concentration below current state and federal regulatory limits, and even below potentially more strict new Cr(VI)-specific regulations. At pH 8 the iron oxides that contained chromium had visible settled out of suspension within 30 minutes after stirring was stopped, indicating the EC could be applied without posing a large burden on downstream particle removal processes in drinking water treatment applications. At pH 6, although final dissolved Cr concentration is low, low amounts of suspended solids in the solution due to slow Fe(II) oxidation needs longer time settling and filtration was a better choice for removing Chromium. The stability of Cr(III) in the solids produced means that dissolved Cr(III) is not available to be reoxidized to Cr(VI) by downstream water treatment process. The newly established model of Cr(VI) reduction dynamics in electrocoagulation is essential for developing a reaction-based interpretation of the process. At pH 8 Fe(II) generation in EC is the rate-limiting step, and consequently homogeneous reduction of Cr(VI) by Fe(II) could fit the data well. In contrast, at pH 6 both homogeneous and heterogeneous reduction are important, and the solid products of the reaction accelerate the reduction in an autocatalytic process.

In electrocoagulation, formation of Cr(III)-Fe(III) oxides makes Cr(III) stable with respect to re-release from desorption, but the residual solids need to be protected from reoxidation by manganese oxides when discharged to natural environments. Future research can focus on the stability of the Cr(III)-Fe(III) oxides in natural environments. In addition to its use in drinking water treatment, electrocoagulation could be used to treat Cr(VI)-rich brines produced during regeneration of anion exchange resins used for Cr(VI) removal.

Acknowledgements

This research was supported by the U.S. National Science Foundation (CBET 1335613). Chao Pan acknowledges financial support from school of Engineering Applied Science in Washington University in St. Louis for a first year PhD fellowship. Zimeng Wang contributed to the initial and preliminary experiments of this project and Jenil Dedhia provided laboratory assistance. We appreciate the comments of three anonymous reviewers that helped us improve the presentation and interpretation of our study. Use of the Stanford Synchrotron Radiation Lightsource, SLAC National Accelerator Laboratory, is supported by the U.S. Department of Energy, Office of Science, Office of Basic Energy Sciences under Contract No. DE-AC02-76SF00515.

Supporting Information

Additional information regarding the SGG composition, control experiments, XRD pattern of solids generated from EC, equilibrium solubility calculations, model development and phosphate impact is included.

Table S2.1. Water composition of simulated Glendale groundwater [24]

constituent	Target concentration[a]	Laboratory concentration[b]
alkalinity	215mg/L as $CaCO_3$	215mg/L as $CaCO_3$
chloride	68 mg/L	68 mg/L
conductivity	840 µS/cm	885 µS/cm
hardness	332 mg/L as $CaCO_3$	326 mg/L as $CaCO_3$
nitrate	5.3 mg/L as N	5.3 mg/L as N
pH	7.4 pH unit	7.4 pH unit
phosphate	0.25 mg/L as PO_4	0.25 mg/L asPO_4
silicate	27 mg/L as SiO_2	27 mg/L as SiO_2
sulfate	87 mg/L as SO_4	220 mg/L as SO_4

[a] Target concentration based on reported composition.

[b] Actual concentration achieved in the laboratory in simulated Glendale groundwater. The sulfate concentration is higher than target concentration to account for the charge balance.

Fe(II) oxidation rate with varying degrees of oxygen removal

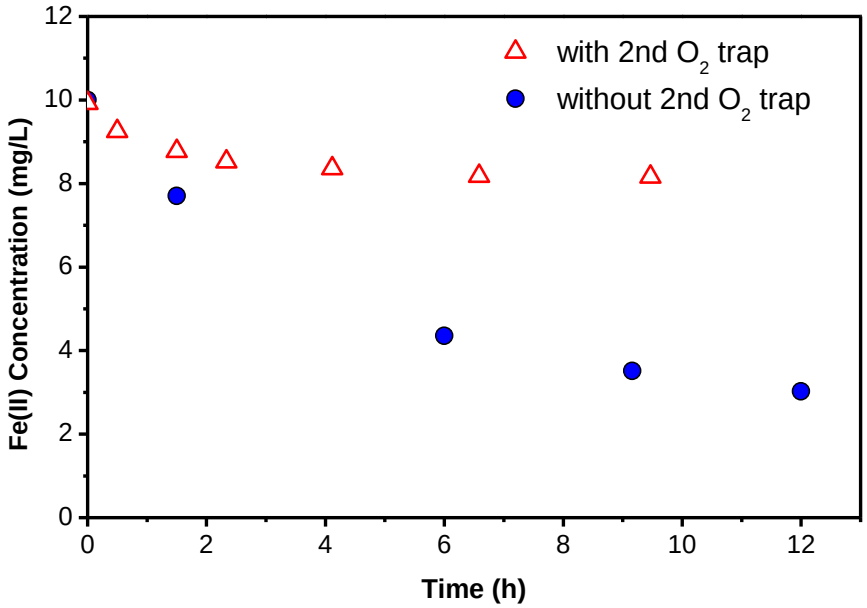

Figure S2.1. Change in Fe(II) concentration from a solution with 10 mg/L Fe(II) as a result of oxidation at pH 8 with 5mM HEPES in an anaerobic chamber (atmosphere of 98% N_2 / 2% H_2) with or without a secondary O_2 trap.

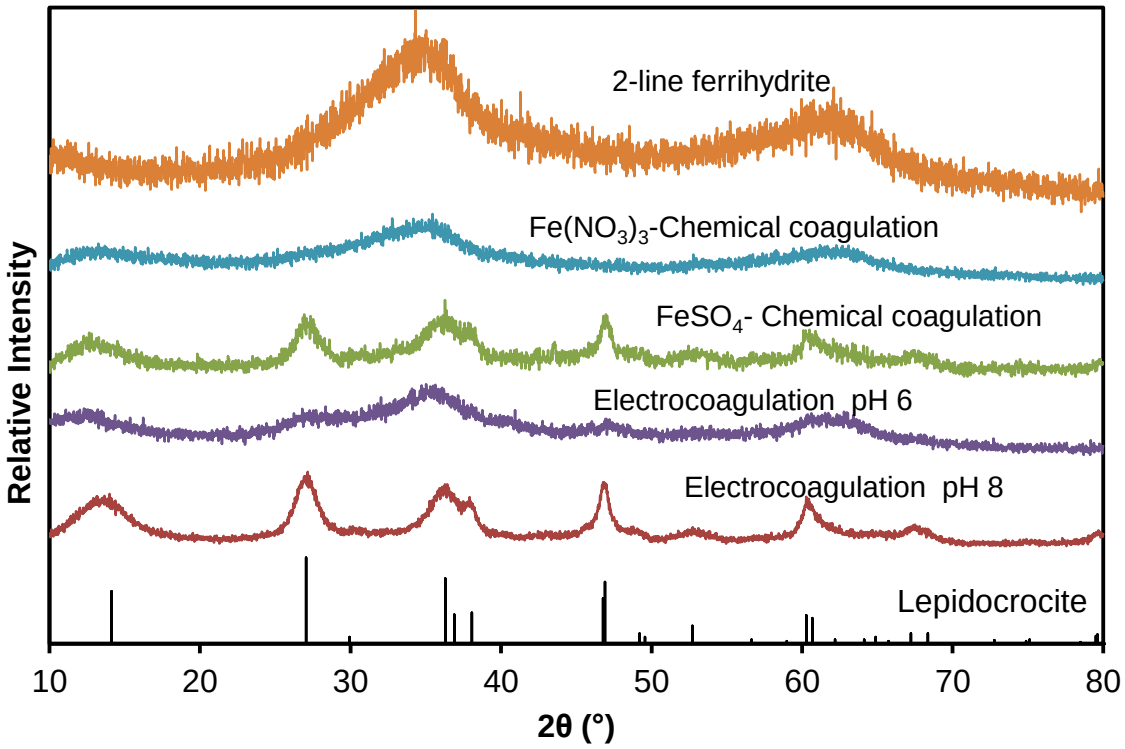

Figure S2.2. X-ray diffraction patterns of solids generated during electrocoagulation and chemical coagulation at pH 8. The reference pattern for lepidocrocite (044-1445 from the International Crystal Diffraction Database) is included for comparison. The pattern labeled $FeSO_4$-Chemical coagulation is the iron oxide generated by continuous addition of $FeSO_4$. The pattern labeled $Fe(NO_3)_3$-Chemical coagulation is for the iron oxide generated by a one-time addition of $Fe(NO_3)_3$.

Cr(VI) adsorption onto iron oxides

Because Cr(VI) adsorption to the Fe(III) oxides produced during electrocoagulation may be a part of the overall removal process, the equilibrium adsorption of Cr(VI) to iron (oxy)hydroxides generated in electrocoagulation and chemical coagulation was evaluated in batch experiments. To generate sufficient solids for adsorption tests, EC was performed for 45 minutes with 37 mA current at pH 8 and 0.94 L/min air bubbling with 5mM HEPES and 5 mM sodium nitrate. This 45-minute reaction time generated a 1 L of iron (oxy)hydroxide suspension with 29 mg/L (0.52 mM) iron. Cr(VI) adsorption was also examined for iron oxides generated from chemical addition of iron from either ferric nitrate or ferrous sulfate. For adsorption experiments to iron oxides produced using $Fe(NO_3)_3$, a 1 L solution was first prepared with 5 mM HEPES and 5 mM $NaNO_3$. Then 209 mg $Fe(NO_3)_3 \cdot 9H_2O$ was dissolved into the 1 L solution to give a total iron concentration of 29 mg/L, which is the same as the suspensions produced by electrocoagulation. The solution was rapidly stirred to ensure complete mixing of the suspension, and the pH was adjusted to 8 with NaOH. For generation of iron oxides from oxidation of Fe(II) in $FeSO_4$, 10 mM $FeSO_4$ was continuously added to a 1 L solution with 5 mM HEPES and 5 mM $NaNO_3$ at a rate of 0.644 mg/L·min as Fe for 45 minutes with 0.94 L/min air bubbling. Both EC and $FeSO_4$-based chemical coagulation solutions were bubbled for an additional 30 minutes after the period of Fe(II) addition to promote complete oxidation of Fe(II).

The 1 L suspension generated by EC or chemical coagulation was then divided into ten 100 mL volumes for use in Cr(VI) adsorption tests. In each test 0.5 mL of 0.1g/L Cr(VI) stock solution was added to the 100 mL suspension to yield an initial dissolved Cr(VI) concentration of 500 μg/L (9.62 μM). The solution pH was adjusted to a desired value by addition of diluted

NaOH or HNO_3 solution. The suspensions were stirred for 2 hours before filtration and analysis. The final pH was measured and used as the equilibrium pH.

For the iron oxides generated from EC, less than 25% of the Cr(VI) was adsorbed across the entire pH range studied, and no adsorption was observed at pH 8. The low degree of Cr(VI) adsorption to the solids from EC demonstrates that adsorption is not an important mechanism for Cr(VI) removal during EC. The adsorption capacities of Cr(VI) on iron (oxy)hydroxides generated in chemical coagulation were also investigated. Similar to the pH adsorption edge for Cr(VI) on iron oxides from EC, the iron oxide generated by $FeSO_4$-based chemical coagulation adsorbed very little of the Cr(VI). The maximum adsorption percentage (at pH 5.6) was only 11.8 %. The low extent of adsorption of Cr(VI) on these two iron oxides might be due to a lack of specific adsorption sites on lepidocrocite for Cr(VI). However, when starting with Fe(III) from a one-time dose of $Fe(NO_3)_3$ at pH 8 the solid produced was two-line ferryhydrite (FigureS2.2). In contrast to Cr(VI) adsorption to lepidocrocite, the ferrihydrite almost completely adsorbed the Cr(VI) at pH 5 in an experiment with an initial dissolved Cr(VI) concentration of 500 μg/L, although even this solid adsorbed almost no Cr(VI) at pH 8 or higher (Figure S2.3). The iron oxide from EC has a specific surface area of 169 m^2/g while that from $Fe(NO_3)_3$-based CC has a specific surface area of 299 m^2/g. Assuming a widely used site density of 2.31 sites/nm^2 of the iron oxides,[104] then the total surface site concentration of iron oxides from EC and $Fe(NO_3)_3$-based chemical coagulation are 43.6 μM and 74.3 μM, respectively, which are both much higher than the concentration of Cr(VI) of500 μg/L (9.6 μM). Consequently the differences in specific surface areas of the two materials are probably not the cause of the different extents of adsorption. Consistent with our observations, in previous work, ferrihydrite

was reported to be very reactive for Cr(VI) adsorption at low pH [105] while lepidocrocite had less affinity for adsorbing Cr(VI).[73]

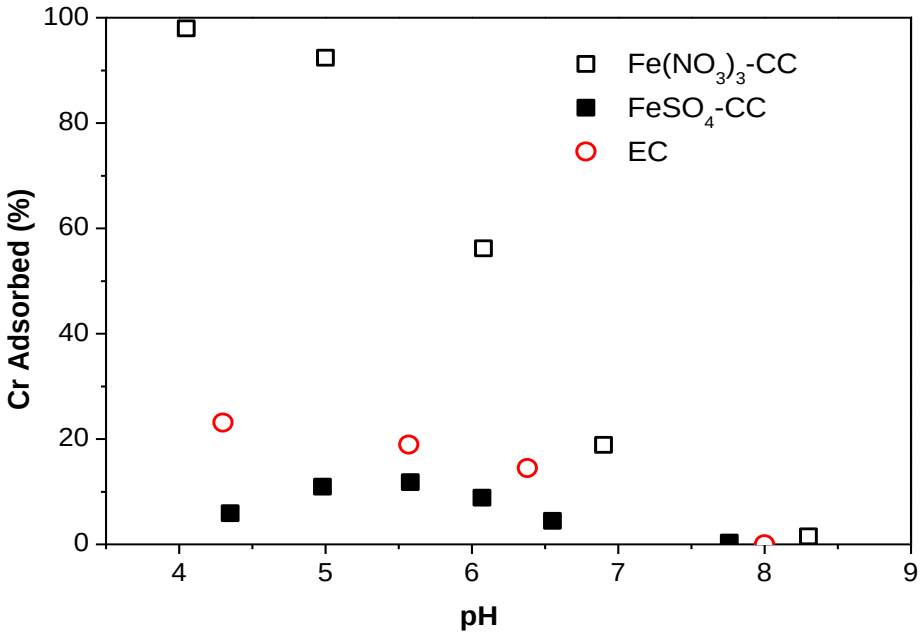

Figure S2.3. Percent of Cr(VI) that is adsorbed as a function of pH for $Cr(VI)_0$ = 500 µg/L and Fe_{total} = 29 mg/L. Adsorption edges are shown for Cr(VI) adsorption to iron oxides produced from three different approaches: chemical coagulation with a one-time dose of $Fe(NO_3)_3$, chemical coagulation with continuous $FeSO_4$ addition, and electrocoagulation.

Comparison of chemical coagulation (CC) and electrocoagulation

For Fe(II)-based chemical coagulation, a 10 mM $FeSO_4$ stock solution was continuously added to a 1 L volume of solution in the reactor with a syringe pump and NaOH was also added to neutralize acidic Fe(II) solution and maintain a stable pH. The rate of Fe(II) addition was fixed to be the same as in the EC experiments (0.644 mg Fe/L ·min). Other than the method of adding the Fe(II), the procedures for the chemical coagulation experiments were the same as those for electrocoagulation.

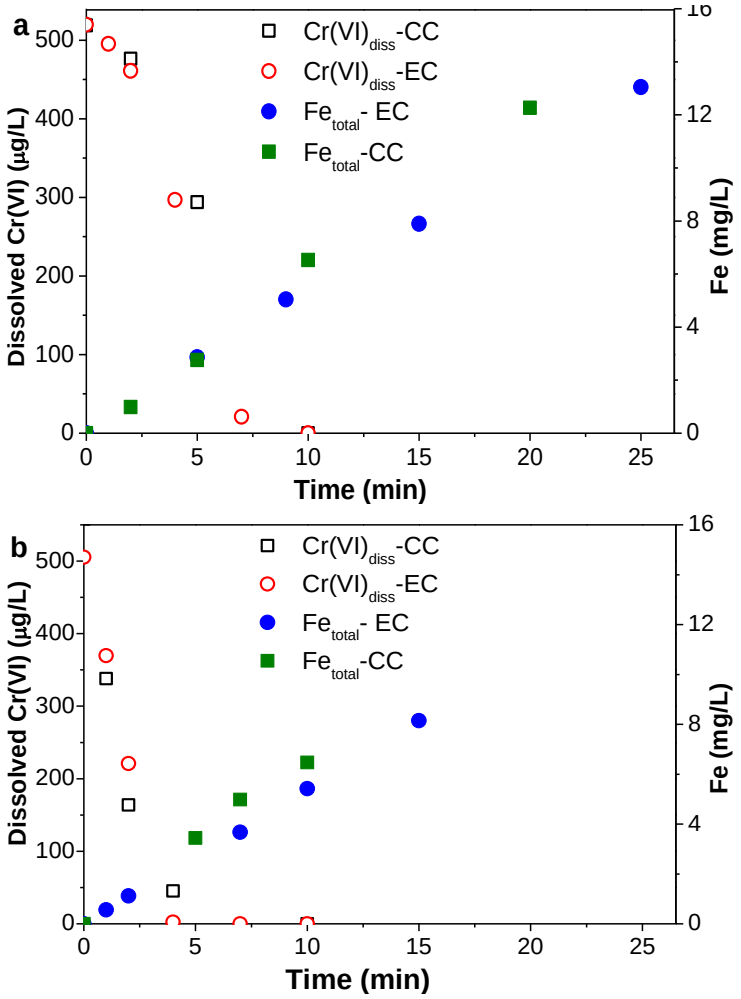

Figure S2.4. Comparison of electrocoagulation (EC) and chemical coagulation (CC) with $FeSO_4$ for removing Cr(VI) at (a) pH 6 and (b) pH 8. The experiments were performed with $[Cr(VI)]_0$ = 500 µg/L and conductivity = 460 µS/cm in aerated solutions. For EC, iron was generated using

iron electrodes with U = 4 V and I = 37 mA, and for CC, Fe(II) was provided by constant addition of a 10 mM $FeSO_4$ solution at 1.15 mL/min from a syringe pump.

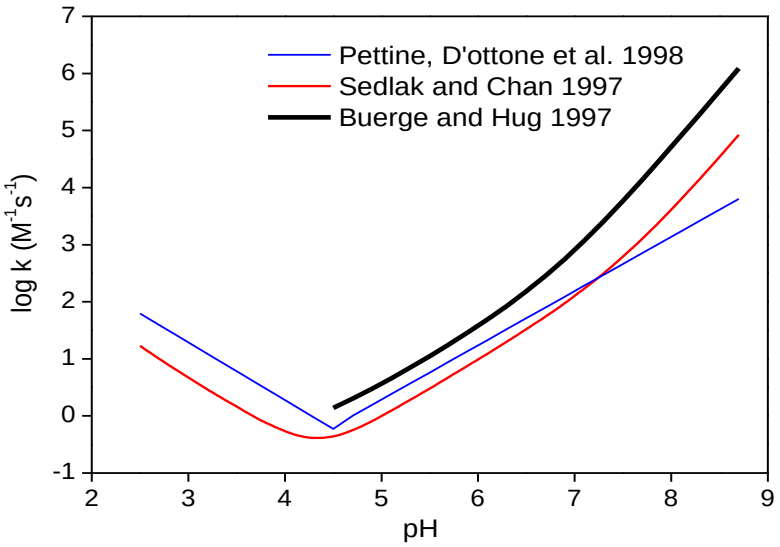

Figure S2.5. The second order rate constant for Cr(VI) reduction by Fe(II) reported in previous studies.

Cr(III) solubility versus pH

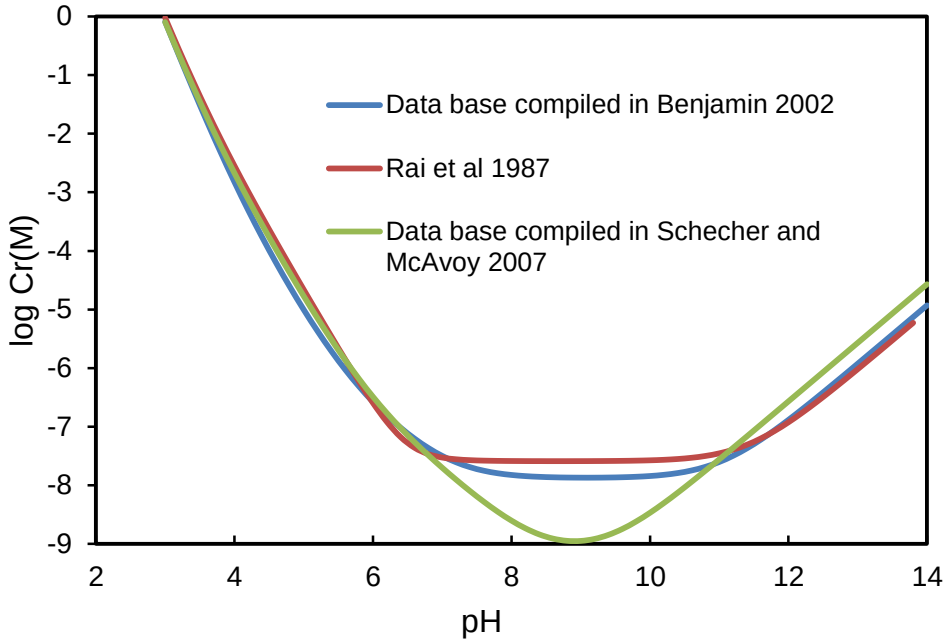

Figure S2.6. Calculated dissolved Cr(III) concentration in equilibrium with $Cr(OH)_{3(s)}$as a function of pH as determined using stability and hydrolysis constants from three different sources.

Table S2.2. Chromium(III) solubility and hydrolysis constants for calculation in Figure S2.5

Reaction	Stability Constants (data base compiled by Benjamin 2002[85])	Stability Constants (Rai et al 1987[106])	Stability Constants (data base compiled by Schecher and McAvoy 2007[107])
$Cr(OH)_{3(s)}+3H^{+}= Cr^{3+}+3H_2O$	Log K= 8.87	Log K= 9.64	Log K= 8.819
$Cr^{3+}+H_2O = Cr(OH)^{2+}+H^{+}$	Log*β_1= -4.00	Log*β_1= -3.55	Log*β_1= -3.657
$Cr^{3+}+2H_2O = Cr(OH)_2^{+}+2H^{+}$	Log*β_2= -9.62	Log*β_2= -10.59	Log*β_2= -9.569
$Cr^{3+}+3H_2O = Cr(OH)_{3(aq)}+3H^{+}$	Log*β_3= -16.75	Log*β_3= -16.46	Log*β_3= -17.991
$Cr^{3+}+4H_2O = Cr(OH)_4^{-}+4H^{+}$	Log*β_4= -27.77	Log*β_4= -27.9	Log*β_4= -27.388

Development of Model of Cr(VI) removal in electrocoagulation

1 Electrocoagulation considering homogeneous reaction at pH 8

A chemical dynamic model of Cr(VI) reduction and Fe(II) oxidation in electrocoagulation was developed based on previous detailed studies of Cr(VI)/Fe(II) and Fe(II)/O_2 systems. Assumptions are made that the adsorbed concentrations of both Cr(VI) and Fe(II) are negligible compared with dissolved species at pH 6 and pH 8. For both Cr(VI) and Fe(II), the dissolved concentrations are used to represent total concentration. Second, we assume that the ratio of the concentration of any adsorbed Fe(II) (albeit small) to its dissolved concentration remains constant during the reaction, which will be applied in later heterogeneous reaction discussion for EC at pH 6. This second assumption is valid provided that adsorption/desorption reactions are fast compared to the redox reactions[73] and that the surface sites of the solids are not close to saturation. The two assumptions are based on the following experimental observations:

1) Cr(VI) has a low affinity for the EC product at pH 6. The similarity between the filtered and the unfiltered Cr(VI) concentration indicates that Cr(VI) associated with Fe(III) solids during reaction of Cr(VI) in the EC experiments is negligible. XANES data also show that no Cr(VI) was in the solid phase following the EC experiments. Adsorption experiments showed that there was no adsorption of Cr(VI) on iron hydroxide produced from EC at pH 8 and only 15% of Cr(VI) adsorbed to iron hydroxide solids that were first generated for 45 minutes at Cr-free conditions in the EC reactor at pH 6before being contacted with Cr(VI) (Figure S2.3).
2) Control experiments showed that little Fe(II) adsorbed onto the Fe(III)-Cr(III) hydroxide solids produced from EC (data not shown) at pH 6, which might be due to a positively

charged EC product at pH 6. Positive surface charges were confirmed by zeta potential analysis.

When only considering the homogeneous reaction of Cr(VI) reduction by Fe(II), the expressions for Cr(VI) concentration and Fe(II) concentration in electrocoagulation are:

$$-\frac{d\,[Fe(II)]}{dt}=3*k_1*[Cr(VI)]*[Fe(II)]-k_2+k_{O_2}*[Fe(II)] \quad (S2.1)$$

$$-\frac{d\,[Cr(VI)]}{dt}=k_1*[Cr(VI)]*[Fe(II)] \quad (S2.2)$$

k_1 is the rate constant of Cr(VI) reduction by Fe(II), at pH =8 a value of $k_1=5.15*10^4\ M^{-1}\ s^{-1}$ is taken from previous studies.[8]

The Fe(II) generation rate in EC is $k_2=\frac{I}{z*F}$ according to Faraday's law (equation S2.3).

$$Fe_{total}=\frac{M_{Fe}\cdot I\cdot t}{Z\cdot F} \quad (S2.3)$$

Faraday's law can be used to describe the relationship between current (I) in amperes (1A=1C/s) and the amount of iron released to the solution (Fe_{total}), where M_{Fe} is the atomic weight of iron (55.85 g/mol), t is time (in seconds), z is the number of electrons transferred per iron released (z = 2 for release of Fe(II)), and F is Faraday's constant (96,485 C/mol).

The pseudo first order rate constant for Fe(II) oxidation rate by O_2 in water in equilibrium with air is k_{O_2}, $k_{O_2}=1.05\times10^{-2}\ s^{-1}$ at pH 8 and $k_{O_2}=3.85\times10^{-6}\ s^{-1}$ at pH 6, which is derived from the equation in King's paper [9] and then calculated for our conditions. The Fe(II) oxidation rates is affected by both pH and the carbonate concentration in solution.

This model with just homogeneous reduction can effectively simulate the experimental data of dissolved concentration at pH 8 as shown in the main manuscript (Figure 2.5d).

2 Electrocoagulation modeling at pH 6

2.1 Control experiments to study individual processes at anoxic conditions

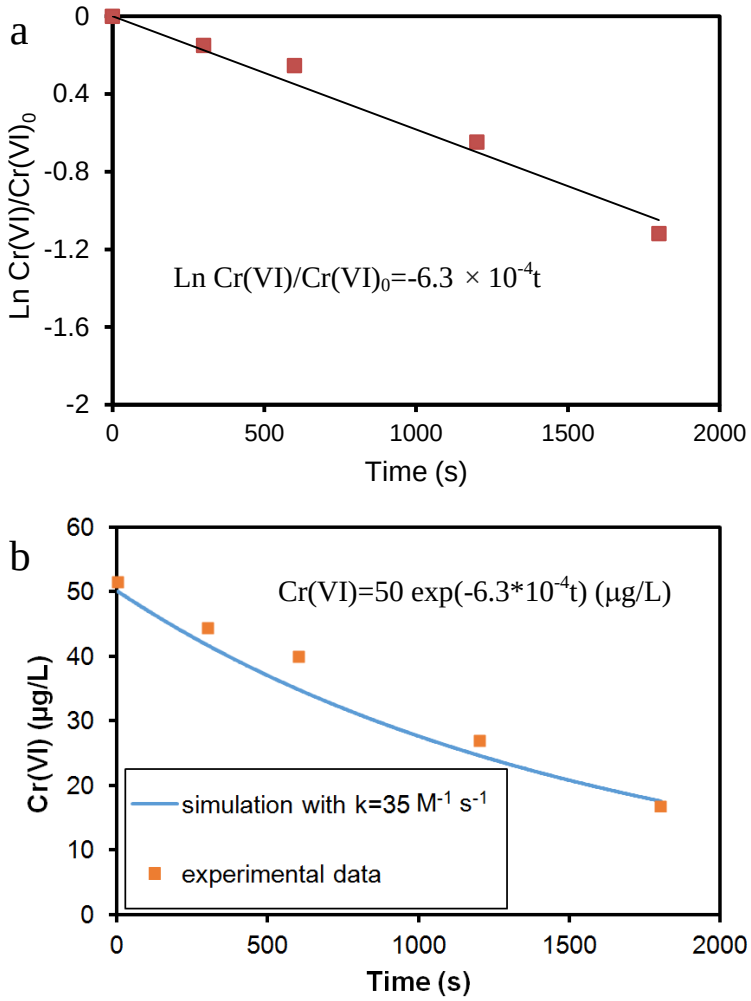

Figure S2.7. (a) 50 µg/L Cr(VI) reduced by 1000 µg/L Fe(II) at pH 6 with 4mM MES under anoxic condition (b) Experimental data with simulation result derived from equation S2.1

The rate constant for reduction of Cr(VI) by dissolved Fe(II) at pH 6 at anoxic conditions was determined in simple batch experiments with addition of known amounts of Cr(VI) and Fe(II).

$$\frac{dCr(VI)}{dt} = -k_1 * Cr(VI) * Fe(II) \qquad (S2.4)$$

The first experiments performed at pH 6 were at conditions selected to minimize contributions from any heterogeneous reduction and to enable interpretation of the reaction based on pseudo first order reaction kinetics. This experiment was performed with a low initial Cr(VI) concentration of 50 µg/L that would minimize $Cr_xFe_{1-x}(OH)_3$ generation that could otherwise lead to extensive heterogeneous Cr(VI) reduction in parallel to homogeneous reduction. With Fe(II) in great excess of Cr(VI), Cr(VI) removal could be interpreted using pseudo first kinetics (Figure S2.7a). A pseudo first order reaction rate constant of $6.3 \cdot 10^{-4}$ s^{-1} was determined, and then a second order reaction rate constant k_1 of 35 $M^{-1}s^{-1}$could be determined. This value is then used as the rate constant for homogenous reduction (k_{homo}) in the later model development (discussed further below). The second order rate constant is in the range of 29-47 $M^{-1}s^{-1}$ reported in previous study.[8] The dissolved and total Cr(VI) concentration is quite similar (data not shown). For both Cr(VI) and Fe(II), the dissolved concentrations are used to represent total concentration and this assumption will be discussed later.

The reduction was also investigated at higher Cr(VI) concentration for examining the possible autocatalytic effect of heterogeneous reaction occurring in parallel with the homogeneous reaction once some Fe(III)/Cr(III) solid has been produced. In the first experiment to study this, the amounts of Cr(VI) and Fe(II) added could lead to complete consumption of each following stoichiometric reaction. Figure S2.8 shows results of reaction of 500 µg/L (9.62 µmol/L) Cr(VI) with 1615 µg/L Fe(II) (28.84 µmol/L) ([Fe]: $[Cr]_{molar}$ = 3) at pH 6. Equation S2.4 can be integrated to the linear expressions for this special case of $[Fe(II)]_0 = 3[Cr(VI)]_0$ and at a stoichiometric progress of the reaction:

$$\frac{1}{[Cr(VI)]} = \frac{1}{[Cr(VI)]_0} + 3k_1 t \qquad \text{(S2.5)}$$

$$\frac{1}{[Fe(II)]} = \frac{1}{[Fe(II)]_0} + k_1 t \qquad (S2.6)$$

When the data were plotted according to Equation S2.5 (Figure S2.8), the slope of the data kept increasing, indicating that $k_1$was increasing with reaction time. If the reaction followed a simple second order reaction, then the data in Figure S2.8 would have plotted as a straight line according to equation S2.5 with a constant value of k_1. The concave up trend suggests an autocatalytic effect in the system at a high concentration of chromium. Such a marked autocatalytic effect for Cr(VI) reduction by a stoichiometric amount of Fe(II) was not observed in a previous study;[8] however the experiments in that study were conducted at pH 5 instead of pH 6, and the initial concentrations were higher (20 µM Cr(VI) instead of 9.62 µM).

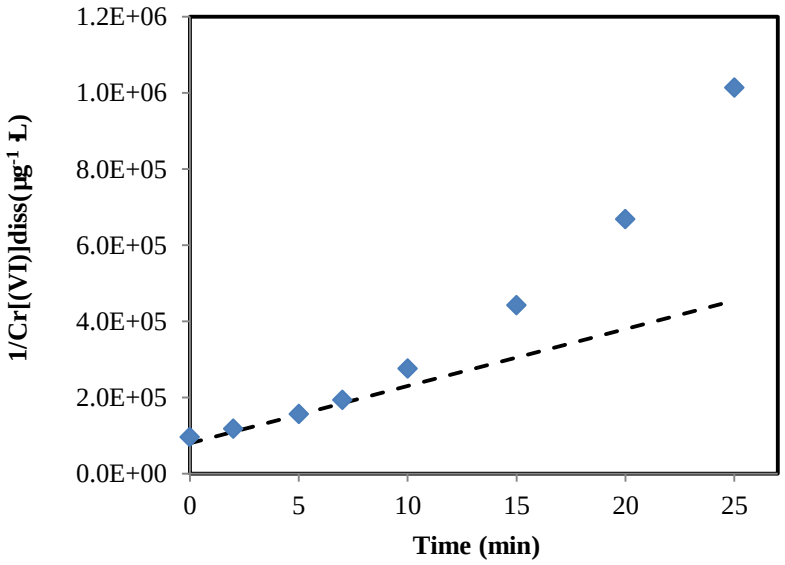

Figure S2.8. Second-order plot of $1/[Cr(VI)]_{diss}$ vs time and stoichiometric concentrations of 3[Cr(VI)]=[Fe(II)] ($[Cr(VI)]_0$=500 µg/L) at pH 6. The dashed line is an extension of the initial slope of $1/Cr(VI)_{diss}$ versus time, and the deviation of the data from this line indicates that the actual slope (which is related to the rate of the reaction) increases with increasing time.

Experiments on the reduction of 500 μg/L Cr(VI) by different concentrations of Fe(II) were performed to estimate the heterogeneous rate constant in the reaction. In Figure S2.9, Log Cr(VI) decreased linearly during the reaction process regardless of the concentration of Fe(II), which indicates that Cr(VI) reduction is pseudo first order for all of those doses, with a pseudo first order rate constant k_{obs} ($k_{obs} = k_1 \cdot [Fe(II)]$). As Fe(II) is consumed during the reaction, the rate constant for Cr(VI) reduction by Fe(II) kept increasing, especially for solutions without excess Fe(II). In Figure S2.9c, we find that $k_{obs}/[Fe(II)]_0$ increases with increasing Fe(II) initial concentration, and a suitable k_1 can be chosen for use in the model of the dynamics of Fe(II) and Cr(VI) during electrocoagulation based on the average Fe(II) concentration during the electrocoagulation experiment. According to the time at which Cr(VI) had decreased from 500 μg/L to below detection limit in EC and the corresponding Fe(II) amount, we choose the rate constant extracted from 500 μg/L Cr(VI) reduction by 3300 μg/L Fe(II) to apply as the heterogeneous rate constant in the electrocoagulation kinetic calculations described later. This value is $k'_{hetero} = 1.1 \times 10^7\ M^{-2} \cdot s^{-1}$.

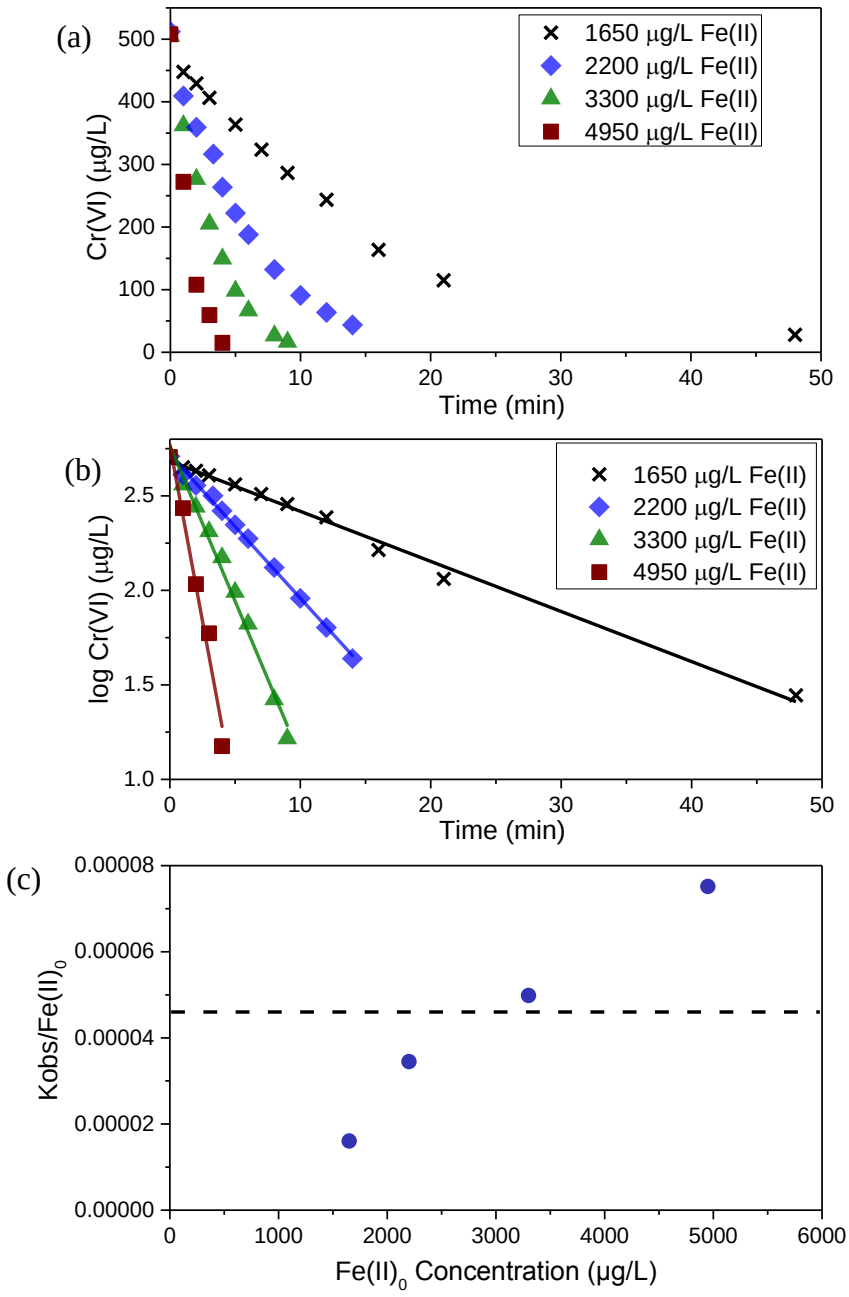

Figure S2.9. Examination of the kinetics of reduction of 500 µg/L Cr(VI) by different initial concentrations of Fe(II) at pH 6 with 4 mM MES shown with (a) a linear scale and (b) a logarithmic scale indicating a different pseudo first ordre rate constant in each case. Panel c is the value of the $k_{obs}/Fe(II)_0$ versus the initial Fe(II) concentration; if the reaction were homogeneous and second order, then $k_{obs}/[Fe(II)]_0$ would be constant and would plot as a horizontal line (e.g., like the dashed line shown).

2.2 Electrocoagulation modeling at pH 6

Figure S2.10 provides the calculated Cr(VI) and Fe(II) concentrations at pH 6 when only considering the homogeneous reduction of Cr(VI) by Fe(II). The rate constant for Cr(VI) reduction by Fe(II)determined above from control experiments is $k_1 = k_{homo} = 35 M^{-1}s^{-1}$.

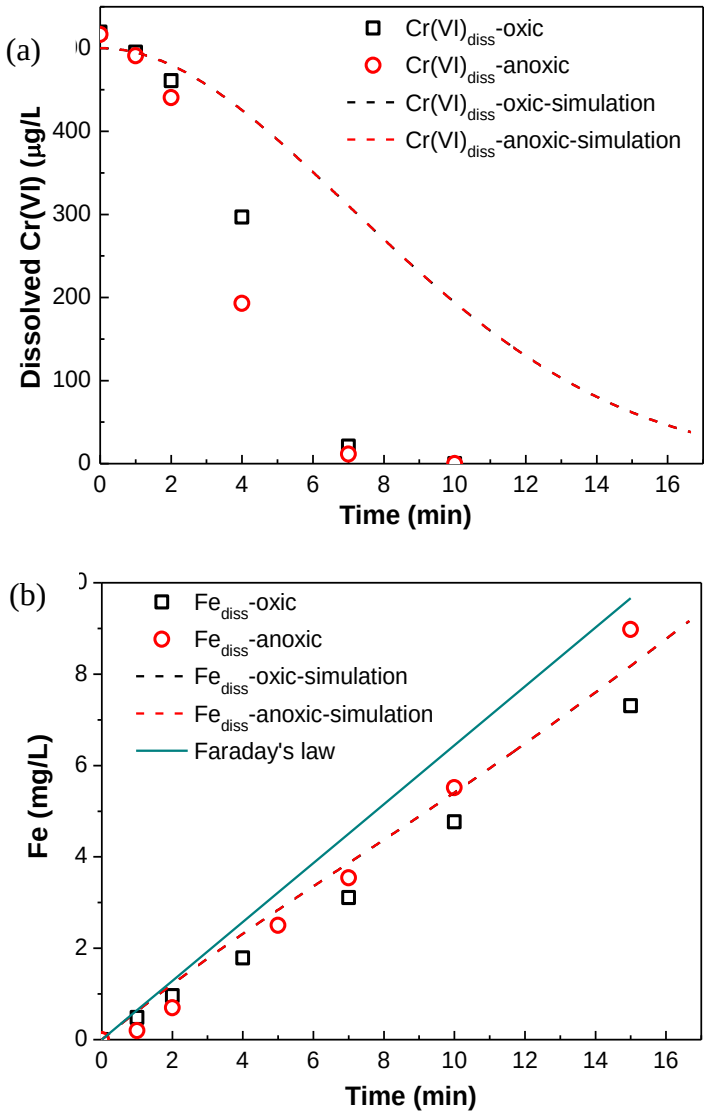

Figure S2.10. The homogeneous rate constant applied in EC at both oxic and anoxic conditions at pH 6 (a) Cr(VI) concentration (b) Fe(II) concentration

In Figure S2.10, the actual Cr(VI) decrease during electrocoagulation is much faster than predicted at pH 6 assuming only homogeneous reduction, which implies the occurrence of heterogeneous reduction of Cr(VI) by Fe(II) on the Fe(III)-containing solids. The incorporation of a heterogeneous reaction at pH 6 into the model is clearly necessary.

Based on the second assumption that adsorption/desorption reactions are fast and that the surface sites of the solids are not close to saturation for dissolved Fe(II), the rate of Cr(VI) reduction by Fe(II) (equation S2.2) can be rewritten as:

$$-\frac{d\,[Cr(VI)]}{dt}=k_1*[Cr(VI)]*[Fe(II)]=k_{dd}*[Cr(VI)]_{diss}*[Fe(II)]_{diss}+k_{ad}*[Cr(VI)]_{ads}*[Fe(II)]_{diss}$$

$$+k_{da}*[Cr(VI)]_{diss}*[Fe(II)]_{ads}+k_{aa}*[Cr(VI)]_{ads}*[Fe(II)]_{ads} \qquad (S2.7)$$

where the subscripts diss and ads mean dissolved and adsorbed species, respectively, and the subscripts on the rate constants of "a" and "d" indicate which species are interacting in which particular combination of possible reactions.

The Cr(VI) reduction rate in equation S2.7 can be simplified to equation S2.8 under the assumption that any minor fraction of adsorbed Cr(VI) does not strongly affect the kinetics ($[Cr(VI)]_{ads} = 0$). This assumption is consistent with those used in a previous study.[73]

$$-\frac{d[Cr(VI)]}{dt}=k_{homo}*[Cr(VI)]_{diss}*[Fe(II)]_{diss}+k_{hetero}*[Cr(VI)]_{diss}*[Fe(II)]_{diss} \qquad (S2.8)$$

Here $k_{homo} = k_{dd}$ and is used to represent the homogeneous rate constant of Cr(VI) reduction by dissolved Fe(II); $k_{hetero} = k_{da}*Fe_{ads}/Fe_{diss}$ and represents the rate constant for heterogeneous reduction of Cr(VI) by adsorbed Fe(II).

For the same reason, the Fe(II) concentration in electrocoagulation can be simplified to equation S2.9 as:

$$-\frac{d[Fe(II)]}{dt}=3k_{homo}*[Cr(VI)]_{diss}*[Fe(II)]_{diss}+3k_{hetero}*[Cr(VI)]_{diss}*[Fe(II)]_{diss}+k_{O_2}*[Fe(II)]_{diss} \quad (S2.9)$$

Fe(II) coordinated with surface hydroxyl groups of amorphous iron(III) hydroxides, which are precipitating during the electrocoagulation, could lead to enhanced Cr(VI) reduction rates.

Furthermore, we tried two approaches for including a value to represent the amount of solid present and the associated value of k_{hetero} for use in the model:

Approach 1: iron oxide surface sites are constant during EC process and are not a rate-limiting factor in overall Cr(VI) reduction). (k_{hetero} is constant in equation S2.8 and S2.9)

$$-\frac{d[Cr(VI)]}{dt}=k_{homo}*[Cr(VI)]_{diss}*[Fe(II)]_{diss}+k_{hetero}*[Cr(VI)]_{diss}*[Fe(II)]_{diss} \quad (S2.10)$$

Approach 2: iron oxide surface sites increase with time and are proportional to the amount of Fe(III) generated.

$$-\frac{d[Cr(VI)]}{dt}=k_{homo}*[Cr(VI)]_{diss}*[Fe(II)]_{diss} + k'_{hetero}([Fe(II)]_T-[Fe(II)]_{diss})*[Cr(VI)]_{diss}*[Fe(II)]_{diss} \quad (S2.11)$$

$[Fe(II)]_T$ is the total iron concentration in EC at time t.

For Approach 1, Figure S2.11 shows that although the model fit the control experiment data very well, the model could not simulate the EC process when using the same k_{hetero} value as in the control experiments. Further, there was a lag time in Cr(VI) removal in the EC experiments that could not be accounted for using Approach 1.

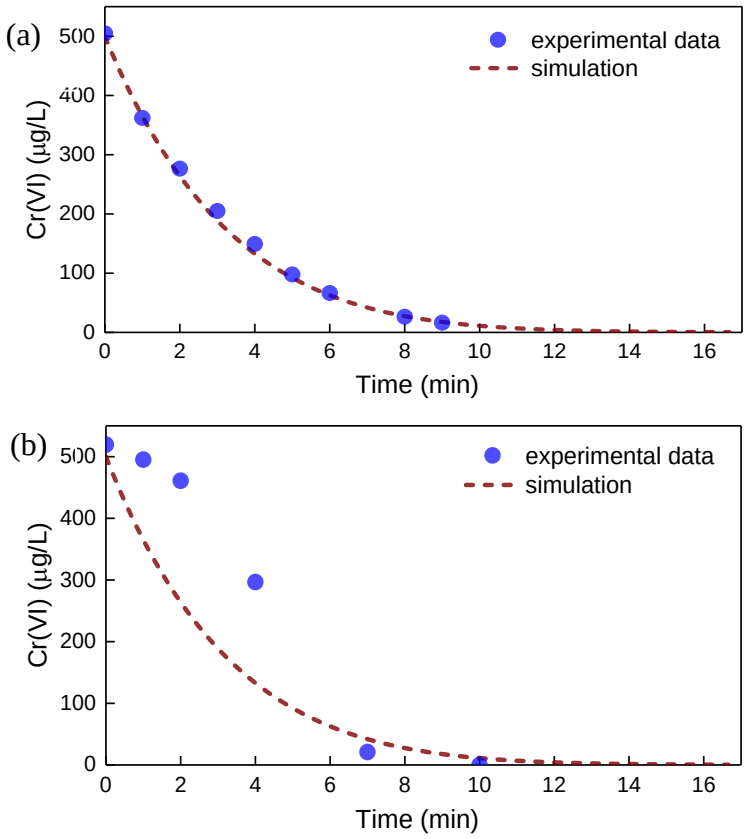

Figure S2.11. Data and output of a model with constant surface sites applied to both (a) 500 µg/L Cr(VI) reduced by 3300 µg/L Fe(II) and (b) EC at pH 6

For Approach2, we assumed that the Fe(III) solids provide surface sites for heterogeneous reaction and the availability of solid surface sites are the limiting factor for the heterogeneous reaction. Although the model does not fit the data from the control experiments (Figure S2.12a)as well as it they did when using Approach 1, the EC process can be fitted much better by the modeling with k'_{hetero} = 1.1x10^{7} M^{-2}·s^{-1}, the rate constant from the control experiment.

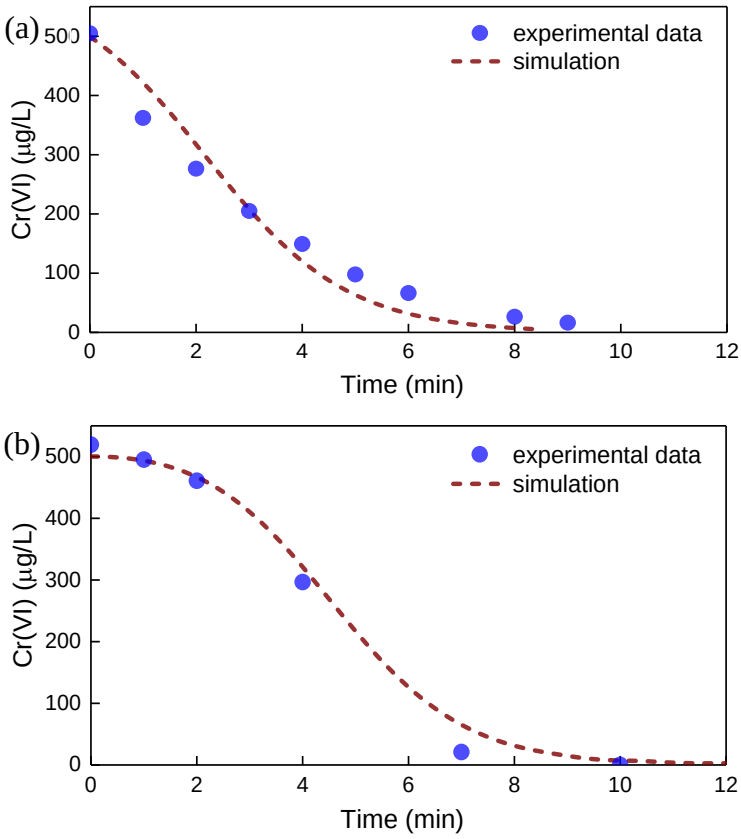

Figure S2.12. Data and a model simulation with surface sites depending on Fe(III) applied to both (a) 500 µg/L Cr(VI) reduced by 3300 µg/L Fe(II) and (b) EC at pH 6

The influence of phosphate on EC

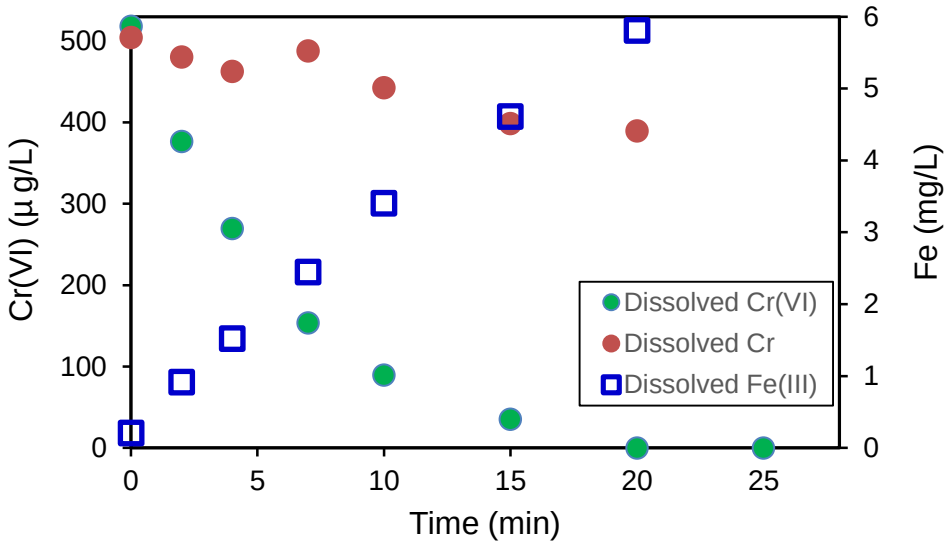

Figure S2.13. Dissolved Chromium and iron concentration in electrocoagulation with 20 mg/L phosphate-P in aerated experiments. $[Cr(VI)]_0$=500 µg/L, U=4 V, I=37 mA, pH=8.0 with 5mM HEPES and conductivity=460 µS/cm.

Chapter 3. Effect of Humic Acid on the Removal of Chromium(VI) and the Production of Solids in Iron Electrocoagulation

This chapter was published in Pan, C.; Troyer, L. D.; Liao, P.; Catalano, J. G.; Li, W.; Giammar, D. E., Effect of Humic Acid on the Removal of Chromium (VI) and the Production of Solids in Iron Electrocoagulation. Environ Sci Technol 2017, 51, (11), 6308-6318.[108]

Abstract

Iron-based electrocoagulation can be highly effective for Cr(VI) removal from water supplies. However, the presence of humic acid (HA) inhibited the rate of Cr(VI) removal in electrocoagulation, with the greatest decreases in Cr(VI) removal rate at higher pH. This inhibition was probably due to the formation of Fe(II) complexes with HA that are more rapidly oxidized than uncomplexed Fe(II) by dissolved oxygen, making less Fe(II) available for reduction of Cr(VI). Close association of Fe(III), Cr(III) and HA in the solid products formed during electrocoagulation influenced the fate of both Cr(III) and HA. At pH 8, the solid products were colloids (1-200 nm) with Cr(III) and HA concentrations in the filtered fraction being quite high, while at pH 6 these concentrations were low due to aggregation of small particles. X-ray diffraction and X-ray absorption fine structure spectroscopy indicated that the iron oxides produced were a mixture of lepidocrocite and ferrihydrite, with the proportion of ferrihydrite increasing in the presence of HA. Cr(VI) was completely reduced to Cr(III) in electrocoagulation, and the coordination environment of the Cr(III) in the solids was similar regardless of the humic acid loading, pH and dissolved oxygen level.

3.1 Introduction

Hexavalent chromium [Cr(VI)] is a toxic and carcinogenic metal found in groundwater and surface waters as a result of human activities and natural processes. A common Cr(VI) treatment technique involves Cr(VI) reduction to Cr(III) by Fe(II) and the subsequent association of Cr(III) with the produced Fe(III) (oxy)hydroxide solids.[24, 109] The Cr(III) can either adsorb to or be structurally incorporated into the iron oxide by co-precipitation to form a Fe(III)-Cr(III) (oxy)hydroxide solid solution.[110] Iron-based electrocoagulation (EC), where Fe(II) is produced from the iron anode, can lower the Cr(VI) concentrations to levels well below the 10 μg/L drinking water standard recently established in California.[62] In our recent work on electrocoagulation, the dynamics of Cr(VI) removal could be described by a model that incorporates Fe(II) release from the anode and heterogeneous and homogeneous reduction of Cr(VI) by Fe(II). The Fe- and Cr-containing EC product was found to catalyze that Cr(VI) reduction by adsorbed Fe(II). Iron-electrocoagulation is also known to destabilize and remove natural organic matter (NOM, chiefly humic substances) by charge neutralization and sweep flocculation.[111, 112] However, the influence of NOM on the extent and rate of Cr(VI) removal and the structure of the iron- and chromium-containing solids was not determined in the previous work.

Iron undergoes significant interactions with humic substances in the dissolved and particulate phases. Humic substances are complex organic macromolecules that are ubiquitous in water, soil and sediments.[113] The concentration of humic substances in groundwater can be as high as 70 mg/L as dissolved organic carbon (DOC), whereas the DOC concentration in surface waters can be as high as 100 mg/L with an average concentration of 5 mg/L.[114-116] Humic substances can be in soluble (defined as diameter less than 1 nm) or colloidal forms (1 to 200

nm)[117] depending on solution conditions. Anionic functional groups, primarily carboxylic and phenolic groups, of humic substances introduce negative charges and have a strong affinity for positively charged mineral surfaces or metal cations.[115, 118-120] NOM can become associated with iron oxides by adsorbing to already existing Fe oxides,[121, 122] but it can also become associated with iron oxides during the initial formation of iron oxides. The precipitation of Fe(III) phases and immediate adsorption of NOM to the newly formed hydrous oxides and precipitation of NOM by monomeric or polymeric Fe species are parallel processes that have been referred to as co-precipitation.[123, 124] Co-precipitation of NOM with Fe is common in environments where Fe hydrolysis occurs due to changes in pH or redox potential.[125] Lalonde et al. estimated that around 21.5 percent of organic carbon is co-precipitated or adsorbed to reactive iron-oxide phases in sediments across a wide range of depositional environments. Simple adsorption of organic matter on reactive iron oxide surfaces accounts for little uptake compared with co-precipitation and/or chelation of organic compounds with iron oxides.[119] In addition to the stabilization of NOM by association with iron oxides,[111, 112] co-precipitation is also known to alter the particle size and structural order of the newly formed oxyhydroxides.[126, 127] Eusterhues et al. found that even a small amount of NOM significantly affects crystal growth, leading to smaller ferrihydrite crystals, increased lattice spacing, and greater distortion of Fe(III) octahedra.

Besides interacting with metal oxides, humic substances also bind soluble metal ions, which is important for the speciation, transport and toxicity of these trace metals.[128-130] Cr(III) binds to Suwannee River fulvic acid (SRFA) as a monomeric Cr(III)-SRFA complex at pH<5, but it binds as polynuclear Cr(III)-SRFA at higher pH.[129] However, fewer studies have examined the chemistry of HA in systems containing both Cr(III) and Fe(III).[131, 132]

Dissolved organic matter can affect the rate of Fe(II) oxidation by dissolved oxygen.[133-136] A variety of iron(II)-binding ligands and humic acids were found to decrease the rate of iron(II) oxidation.[134] However, it has been noted that back reduction of Fe(III) species by catechol-type ligands may have decreased their observed oxidation rate.[137] In contrast, Liang, et al. [138] found that DOM can accelerate the iron(II) oxidation rate under some conditions. This study and another postulated that in the presence of DOM, net oxidation is the result of two competing pathways, DOM-iron(II) complexation followed by oxidation of the complex and oxidation of inorganic iron(II) species.[138, 139] In addition to the influence of complexed HA on Fe(II) oxidation, HA could also directly influence Cr(VI) reduction by Fe(II) at suboxic conditions. Cr(VI) reduction by Fe(II) was reported to be accelerated with the presence of different organic ligands including, and the acceleration extent is dependent on pH.[140-142]

The objectives of this study were to evaluate the effect of HA on the process of Cr(VI) removal by Fe-electrocoagulation, including its influence on the dynamics of Cr(VI) reduction, the colloidal stability of solids produced from electrocoagulation, and the coordination environments of chromium and iron in these solid products. We chose humic acid as a representative NOM to evaluate its effects on Cr(VI) removal by electrocoagulation. Humic acid might affect the process by inhibiting or accelerating the rates of Fe(II) oxidation by dissolved oxygen and Cr(VI) reduction by Fe(II), reducing Cr(VI) with specific ligands, competitively adsorbing onto reactive sites of iron oxides, adjusting or even reversing the electrostatic charge of mineral surfaces, and forming colloids composed of HA, Fe(III), and Cr(III).

3.2 Materials and Methods

3.2.1 Materials

Chemicals used were analytical reagents of high purity. Ultrapure water (resistivity >18.2 MΩ-cm) was used for the experiments. Glass volumetric flasks and 1-L polypropylene reaction vessels were cleaned with 10% HCl and rinsed several times with ultrapure water before use. A Cr(VI) stock solution (0.1 g/L, 1.923 mM) was prepared from $K_2Cr_2O_7$. Control of ionic strength was achieved by additions from a 1 M $NaNO_3$ stock solution. At pH 6, 1 mM MES (2-(N-morpholino) ethane sulfonic acid) (Fisher Scientific) was used, 2 mM HEPES (4-(2-hydroxyethyl)-1-piperazineethanesulfonic acid) (≥99.5%, Sigma-Aldrich) was used at pH 7 and 8, and 2 mM CHES (N-Cyclohexyl-2-aminoethanesulfonic acid) (≥99.5%, Sigma-Aldrich) was used for experiments at pH 9. The pH buffers and their concentrations were chosen to minimize the possible formation of Fe(III) and Cr(III) complexes with the buffers.[143, 144] MES, HEPES and CHES are widely used for their minimal influences on metal complexation.[94, 145-148] Commercial humic acid was chosen as a model for colloidal humic substances (Sigma-Aldrich). Sigma-Aldrich humic acid displays similar redox properties (midpoint potential and electron accepting capacity) as those of soil-derived humic acids[149], and it has been used in numerous other studies.[132, 150, 151] The stock solution of HA was filtered through a 0.45 μm polyethersulfone (PES) membrane (Millipore) under vacuum and stored in the dark at 4 ℃ before use.

3.2.2 Electrocoagulation batch experiments

The electrocoagulation reactor and procedure were the same as described in detail in our previous work.[62] Briefly, the electrocoagulation reactor consisted two iron rods immersed in a 1

L solution with 2 mg/L (38.5 μM) intial Cr(VI) and 5mM buffers. Sodium nitrate was added until the conductivity of the solution achieved 460 μS/cm. An electric potential of 4 V was applied to the rods with a direct current power supply, and the current was held constant at 37 mA. Anoxic experiments were performed in an anaerobic chamber (Coy Laboratory Products Inc., MI) with a secondary low temperature oxygen trap to achieve strictly anoxic conditions in the electrocoagulation reactor[62, 152]. All the EC experiments for Cr(VI) removal with different concentrations of HA were performed in duplicate with error bars representing standard deviation, as shown in Figure 3.1.

For each sampling event, a volume of suspension was drawn from the reactor. The suspensions for analyzing total iron and chromium were acidified directly after collection. The rest of the suspension in the syringe was filtered through a 0.22 μm polyethersulfone (PES) membrane, and the filtrate was saved for analysis of dissolved iron, chromium, Cr(VI), Fe(II) and humic acid concentrations. The aliquots for Cr(VI), Fe(II) and HA were not acidified and measured immediately after being collected. Only the separate aliquots for ICP-MS measurements were preserved with 2% HNO_3.

3.2.3 Analytical methods

Cr(VI) concentrations in the samples were determined with the diphenylcarbazide (DPC) method by measuring the absorbance at 540 nm using a spectrophotometer (PerkinElmer-Lambda XLS).[153] Total dissolved Fe(II) concentrations were determined spectrophotometrically by the ferrozine method at a wavelength of 562 nm.[154] Total dissolved iron and total dissolved chromium (Cr(VI) and Cr(III) together) concentrations were measured by inductively coupled plasma mass spectrometry (ICP-MS) (PerkinElmer ELAN DRC II) analysis of filtered samples. In experiments without humic acid, dissolved Fe(II) concentrations were found to be equal to

dissolved iron concentrations because Fe(III) has a very low solubility from the range of pH 6 to pH 9 that was studied. The organic carbon concentration of the humic acid stock solution was determined by a total organic carbon analyzer (TOC-L, Shidmadzu Scientific Instrument, Inc., MD). DOC concentrations of filtered samples were measured spectrophotometrically at 254 nm using a 1 cm quartz cell. To eliminate interference from Fe(III) in absorbance measurements for DOC determination, 0.05 ml 5% hydroxylamine hydrochloride was added to each 1 ml sample and the absorbance was recorded until no further change occurred, indicating that all the Fe(III) had been reduced to non-interfering Fe(II).[155]

Soluble (<10 kDa), colloidal (10 kDa - 0.22 μm) and particulate (>0.22 μm) Cr, Fe and HA were fractionated from samples by 10 kDa ultrafiltration and 0.22 μm filtration. Colloids in this study were defined as particles ranging from 10 kDa (roughly equal to 1-3 nm) to 0.22 μm (the initial filtration). Specifically, the colloidal samples were operationally isolated by the pore size of separating devices, i.e. filtered water samples (filtrates) were separated into permeates (<10 kDa, soluble phase) and retentates (10 kDa - 0.22 μm, concentrated colloidal phase) by ultrafiltration membranes (MF-Millipore) with nominal molecular weight cut-offs of 10 kDa.

The particle size distributions and zeta potential of electrocoagulation products were measured through dynamic light scattering (DLS) analysis using (ZetaSizer Nano, Malvern Instruments, UK). For each sampling event, the suspension was taken from the electrocoagulation reactor and measured by DLS within 5 minutes. TEM samples were prepared by dropping approximately 30 μL of electrocoagulation suspension quickly onto 200 mesh carbon-coated copper grids (Ted Pella, Inc.) followed by immediate evaporation of the remaining water at room temperature under vacuum. TEM micrographs were taken with a transmission electron microscope under 120 kV (FEI Spirit G2). Solids for X-ray powder diffraction (XRD)

were collected from suspensions after 30 minutes of electrocoagulation reaction. The suspensions were concentrated by centrifugation and then freeze-dried. XRD patterns of solid samples were collected using Cu Kα radiation (Bruker d8 Advance X-ray diffractometer).

Fe and Cr K-edge X-ray absorption fine structure (XAFS) spectra were collected on samples from electrocoagulation reactors after 30 minutes of reaction. Samples were vacuum-filtered onto mixed cellulose ester membranes (0.22 μm) and then sandwiched as wet pastes between Kapton film and sealed with Kapton tape. XANES spectra were collected at the Advanced Photon Source on beamlines 5-BM-D and 20-BM-B. 5-BM-D and 20-BM-B both employ a water-cooled Si (111) double crystal monochromator; harmonic rejection is achieved through detuning the monochromator by 10 to 30% and beamline-specific mirror configurations.[156, 157] Fluorescence-yield spectra were collected with a 4-element energy-dispersive silicon drift detector at beamline 5-BM-D and were collected with a 13-element solid state Ge energy-dispersive detector at beamline 20-BM-B. Fe reference compounds included lepidocrocite and 2-line ferrihydrite. Two-line ferrihydrite was synthesized by dissolving $Fe(NO_3)_3 \cdot 9H_2O$ in DI water and adding NaOH to bring the pH to 7. The suspension was then dialyzed to remove dissolved sodium and nitrate and the cleaned suspension was freeze-dried.[158] Lepidocrocite was synthesized using previously-described procedures.[158] Cr reference compounds of Fe(III)-Cr(III) co-precipitates were synthesized by first combining Fe(III) chloride and Cr(III) chloride stock solutions in varying ratios with a total concentration of 60 μM Fe and Cr with 10 mM NaCl as a background electrolyte. The solutions were then adjusted to pH 7 using NaOH and stirred for 2 days before being prepared by vacuum-filtration in the same way as the samples. Fe and Cr spectra were processed in the Athena[159] interface to IFEFFIT.[160] Athena was also used for linear combination fitting of Fe extended X-ray absorption fine

structure (EXAFS) spectra. Structural models of Cr EXAFS spectra were refined in SixPACK[161] using backscattering phase and amplitude functions generated from FEFF 7.02.[162, 163]

3.2.4 Modeling the dynamics of Cr(VI) removal

Reaction kinetics considering Fe(II) generation in EC, Cr(VI) reduction by Fe(II), Fe(II) oxidation by dissolved oxygen (DO), and acceleration of Fe(II) oxidation by DO caused by HA were applied to simulate the dynamics of dissolved Cr(VI) and Fe(II) during electrocoagulation. The rates of change of Cr(VI) (eq 3.1) and Fe(II) (eq 3.2) during electrocoagulation can be written as

$$-\frac{d[Cr(VI)]}{dt}=k_{homo}*[Cr(VI)]_{diss}*[Fe(II)]_{diss}+k'_{hetero}*[Fe(III)]_s*[Cr(VI)]_{diss}*[Fe(II)]_{diss} \quad (3.1)$$

$$-\frac{d[Fe(II)]}{dt}=3k_{homo}*[Cr(VI)]_{diss}*[Fe(II)]_{diss}+3k'_{hetero}*[Fe(III)]_s*[Cr(VI)]_{diss}*[Fe(II)]_{diss} -k_2+f*k_{O_2}*[Fe(II)]_{diss} \quad (3.2)$$

The definitions and values of the rate constants are summarized in Table S3.1. The development and initial parameterization of the model were described in our recent work on experiments in the absence of humic acid.[62] Briefly, equation 3.1 includes both homogeneous and heterogeneous reduction of Cr(VI). In equation 3.2, the four terms are included to track the fate of Fe(II) as it is affected by (i) homogeneous and (ii) heterogeneous reaction of Fe(II) with Cr(VI), (iii) Fe(II) production from the anode according to Faraday's law, and (iv) Fe(II) oxidation by dissolved oxygen. The terms of heterogeneous reactions are simplified under the assumption that any minor fraction of adsorbed Cr(VI) does not strongly affect the kinetics and that adsorbed Fe(II) is proportional to the dissolved Fe(II). In the presence of HA, the rate of Fe(II) oxidation by DO would increase and enhancing factors were used to represent the increasing extent. The enhancing factor of Fe(II) oxidation with different HA concentration (f)

was an adjustable parameter that was used to fit the model output to the experimental data. Because the rest of the model had been previously developed from independently determined parameters, the enhancing factor was the only fitting parameter in the present study.

3.3 Results and Discussion

3.3.1 Effect of humic acid on Cr(VI) removal rate in electrocoagulation

Without the presence of oxygen, HA had no effect on the rate of Cr(VI) removal from pH 6 to pH 9 (Figure 3.1). Although HA was previously reported to accelerate Cr(VI) reduction by Fe(II),[140] this was not observed from pH 7 to pH 9 even without oxygen. The lack of an observable effect of HA at anoxic conditions suggests that Fe(II) generation from the anode in electrocoagulation was the rate-limiting step for Cr(VI) removal[62] and the reduction of Cr(VI) by Fe(II) either with or without HA was much faster than Fe(II) production.

With oxygen present, HA inhibited Cr(VI) removal at the higher pH conditions studied (Figure 3.1). Humic acid has a high density of carboxylate functional groups that complex with both Fe(II) and Fe(III).[164] The strong complex with Fe(III) could drive down the free Fe(III) concentration and lower the reduction potential of the Fe(III)/Fe(II) half reaction, thus Fe(II) could be more easily oxidized by dissolved oxygen.[165, 166] In addition, the complexation of Fe(II) by carboxylate functional groups increases the rate of Fe(II) oxidation by O_2 compared to uncomplexed Fe(II).[135] Thus Cr(VI) reduction by Fe(II) was inhibited as oxygen became a strong competitor with Cr(VI) to oxidize Fe(II)-HA complexes. The greater inhibition of Cr(VI) removal by HA at higher pH during electrocoagulation might be due to the pH dependence of the rate of the complexed Fe(II) oxidation by O_2. Figure S3.1 shows the influence of HA on the evolution of dissolved Fe(II) in electrocoagulation at oxic conditions without the presence of

chromium. The enhancement of Fe(II) oxidation was not observed at pH 6 in electrocoagulation (Figure S3.1a) and the Fe(II) concentration with or without HA was similar to total iron (represented by Faraday's law, equation S3.1 in supporting information). The Fe(II) oxidation by dissolved oxygen was too slow at pH 6 and could be negligible within the short time of electrocoagulation. At a higher pH of 7, it is easier to see the trend of Fe(II) oxidation acceleration in electrocoagulation (Figure S3.1b). At pH 8 no accelerating effect of HA on Fe(II) oxidation can be discerned because the rate was very fast even in the absence of HA (Figure S3.1c). Fe(II) was immediately oxidized once generated in electrocoagulation even without HA. This pH-dependence of the HA-enhanced oxidation of Fe(II) by O_2 might be due to a greater abundance of deprotonated carboxyl groups that could complex Fe(II) better at higher pH.

We applied the model for the dynamics of Fe(II) and Cr(VI) during electrocoagulation at both oxic and anoxic conditions (eq 3.1 and eq 3.2). For the processes with HA present, we increased the Fe(II) oxidation rate constant by changing the value of the enhancing factor f in the term of Fe(II) oxidation by DO (eq 3.2). The enhancing factors for Fe(II) oxidation, f, are summarized in Table S3.2. The enhancing factors necessary to fit the evolution of Cr(VI) during electrocoagulation increased with increasing pH and humic acid concentrations. At pH 7 it is hard to precisely determine the enhancing factors of different HA concentration as experimentally there is a slight enhancement of Fe(II) oxidation (Figure S3.1b) and inhibition of Cr(VI) removal (Figure 3.1), and at pH 6 there is no experimental evidence for even a slight enhancing factor of Fe(II) oxidation by HA. In modeling the behavior at both pH 6 and 7, the enhancing factor could be set to 1 (i.e. no enhancement) and acceptable fits were achieved. Including any factor greater than 1 at pH 7 would actually have resulted in poorer fits.

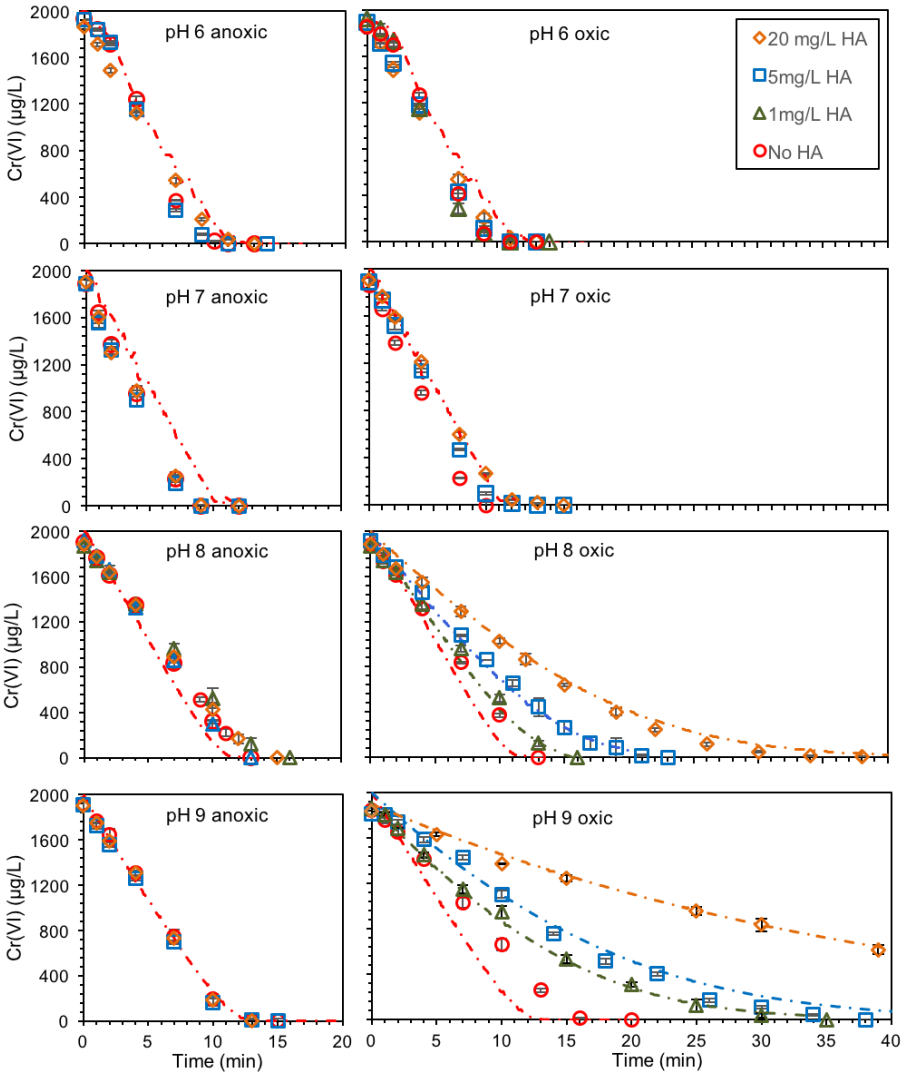

Figure 3.1 The influence of humic acid on Cr(VI) removal from pH 6 to pH 9 at oxic and anoxic conditions. The dashed lines correspond to simulations done according to the humic acid concentration present (Cr(VI) concentration derived from eq 3.1). Humic acid concentrations are expressed as mg C/L. Conditions: $[Cr(VI)]_0$ = 2 mg/L, U = 4 V, I = 37 mA, 2 mM MES for pH 6.0, 5 mM HEPES for pH 7.0 and 8.0, 5 mM CHES for pH 9, and conductivity = 460 µS/cm.

The evolution of the Fe(II) concentration during electrocoagulation calculated by the model is shown in Figure S3.2. According to the model output, HA would not influence the macroscopically observable Fe(II) concentration evolution even at oxic conditions from pH 6 to

pH 9. This is because any HA enhancement of Fe(II) oxidation by dissolved oxygen is not apparent at pH 6, is very limited at pH 7, and is not observable at pH 8 and above because all Fe(II) is immediately oxidized once generated even without HA. In the model equations, it is assumed that all the Cr(VI) in EC solids is reduced to Cr(III) even in the presence of humic acid. This is consistent with the XANES spectroscopy results discussed below.

3.3.2 Effect of HA on the formation of colloidal particles in electrocoagulation

The overall performance of iron electrocoagulation and its integration with other unit operations in water treatment will depend on the coagulation of the particles produced in addition to the Cr(VI) removal just discussed. Humic acid enhanced coagulation-flocculation at pH 6 while it inhibited coagulation-flocculation at pH 8. Without HA, Fe-Cr solid particles produced from electrocoagulation are positively charged below pH 6.5 as determined from zeta potential measurement (pH_{pzc}= 6.5 in Figure S3.3). This pH dependence of surface charge is comparable to that reported by Wan et al., where the lepidocrocite produced in electrocoagulation had an isoelectric pH of about 7.0.[33] As a result, solid particles generated during electrocoagulation with no HA present had zeta potentials that were positive at pH 6 (Figure 3.2c) and negative at pH 8 (Figure 3.2d). Particle size measured by DLS provides information on the changes in the state of colloidal systems. Without HA at pH 6, electrostatically repulsive interactions predominantly reduced the collision efficiency of particles due to their positive charge. Iron oxide solids were colloids for the first 10 minutes and then aggregated into larger particles as more iron oxide particles were generated (Figure 3.2a). The humic acid influences the surface charge properties of electrocoagulation products, which govern particle-particle interactions. Since the produced amount of iron oxide is low at the beginning of EC process, the negatively charged HA adsorbs and thus neutralizes the positive charges on the iron oxide surface at pH 6 and gives the initial

solids formed a net negative charge. In this process, the heteroaggregation between the HA and iron oxides was promoted due to favorable electrostatic attractions between oppositely charged particles.[167] With more output of positively charged iron oxides generated from EC, the surface charge of particles became less negative than 30 mV within 5 minutes, and eventually the surface charge was reversed at 15 minutes. The charge neutralization and reversal led to an unstable particle system in which aggregation occurred. As seen in Figure 3.2a for the case of 5 mg/L HA at pH 6, the aggregate size already exceeded 1 μm after 5 minutes. DLS does not give information on very large particles so we only showed the data up to five minutes.

Particles with zeta potentials more positive than +30 mV or more negative than −30 mV are normally considered stable.[168] Figure 3.2d shows the surface charge of EC products at pH 8 in the absence and presence of HA. Iron oxides generated in EC without HA are only slightly negatively charged at pH 8, and thus aggregation to larger particles occurs easily. The particle size increased from 0 to 1000 nm in less than 1 minute. In the presence of 5 mg/L HA at pH 8, the surface charge of solid particles generated during electrocoagulation is always negative (ca. -40 mV). Under this condition, the particle size is stable, ranging from 163 to 244 nm during the whole EC process. The stabilization of colloidal particles by HA at pH 8 (Figure 3.2b) can be ascribed to the enhanced electrosteric stabilization effect from adsorbed HA,[122] which increases the dispersion of the particles.

The stability of the particles in electrocoagulation greatly influences the fate of Cr(III). All Fe(II) and Cr(VI) are soluble as no Cr(VI) or Fe(II) were detected in large particles or colloids. All Cr(III), Fe(III) and HA were present in either colloids or larger suspended particles because of their negligible concentration detected in soluble filtrates after 10 kDa membrane ultrafiltration. Thus the colloidal concentrations of Cr(III), Fe(III) and HA are the same as their

concentrations in the samples filtered with 0.22 μm membranes, which are recorded in Figure S3.4. Figure 3.3 summarizes the fractions of the total amounts of Cr(III), Fe(III) and HA that are present as colloids following electrocoagulation. In the first five minutes at pH 6, when EC products with HA are small colloidal particles from DLS, the colloidal fractions of Cr(III), Fe(III) and HA concentrations are close to 1. However after 5 minutes, the Cr(III), Fe(III) and HA aggregated and became larger particles. At pH 8, the negatively charged HA prevents the aggregation of particles, and the Cr(III), Fe(III) and HA were colloids at pH 8 over the entire duration of electrocoagulation. The consistent colloidal behaviors among Cr(III), Fe(III), and HA indicate their close associations during electrocoagulation.

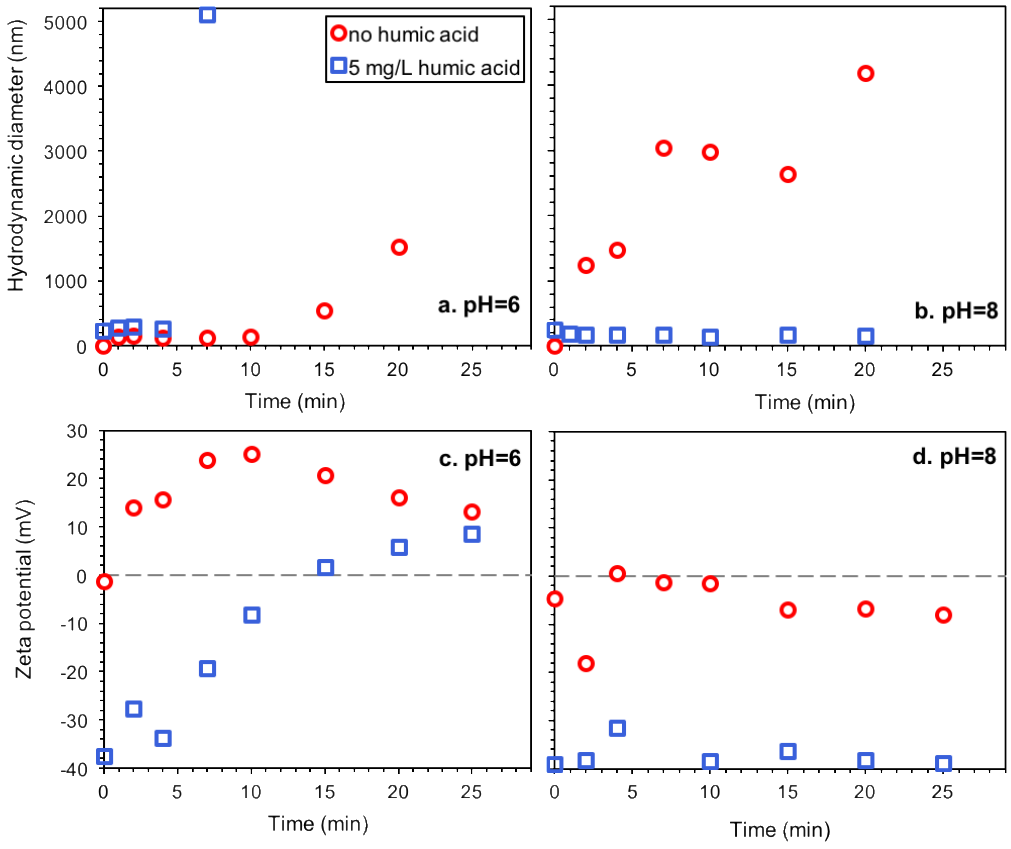

Figure 3.2. The hydrodynamic diameter and electrophoretic mobility of particles produced during electrocoagulation with (blue squares) and without (red circles) 5 mg/L HA at pH 6 and pH 8; $Cr(VI)_0$ = 2 mg/L, U = 4V, I = 0.037 A.

HA removal during electrocoagulation process is also important as NOM has been identified as a precursor to harmful disinfection by-product (DBP) from upon contact with chlorine disinfectants.[169-172] It can be seen in Figure 3.3 that HA is present in stable colloids during electrocoagulation at high pH. However HA could still be aggregated in EC with optimized operation conditions, e.g. increasing anodic Fe(II) dosage rate or dosage time. Many studies in recent years have reported that iron-electrocoagulation operations can be effective at removing natural organic matter.[111, 112, 173] The presence of divalent cations (Ca^{2+} and Mg^{2+}) might also introduce HA aggregation and subsequent removal by filtration.[174, 175]

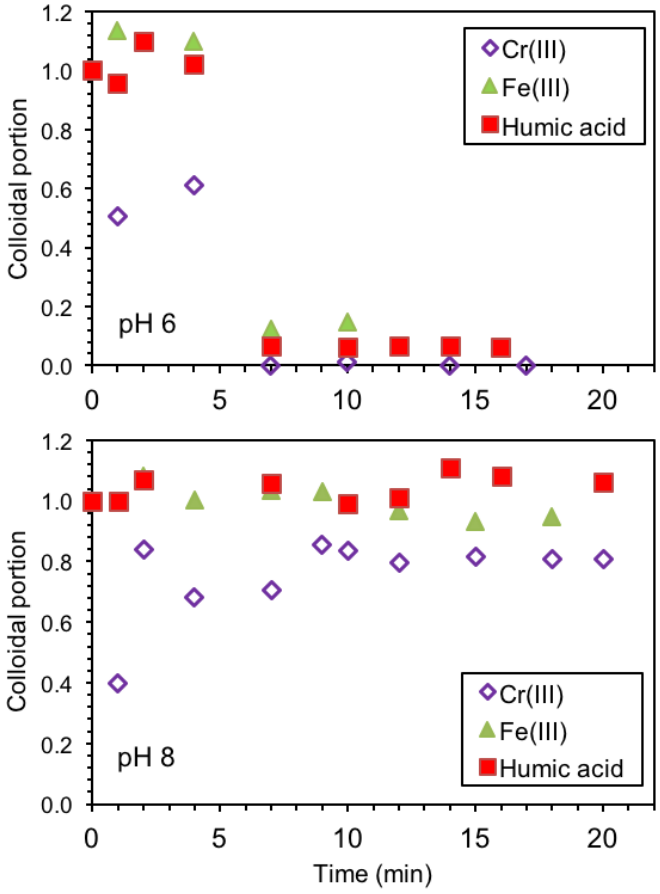

Figure 3.3 Colloid conditions of solids produced during electrocoagulation at pH 6 and pH 8. The colloidal portion is the concentration of colloidal Cr(III), Fe(III) and HA divided by the concentration of total Cr(III), Fe(III) and HA, respectively.

3.3.3 Characterization of precipitates produced during electrocoagulation

XRD measurements (Figure 3.4) show that both pH and the presence of HA affect the mineralogy of iron oxides produced during electrocoagulation. The patterns suggest that ferrihydrite dominates at pH 6, with nanocrystalline lepidocrocite also likely present, whereas lepidocrocite dominates at pH 8. The addition of HA has little apparent effect on the mineralogy at pH 6 but leads to a decrease in lepidocrocite coherent domain size (as indicated by the broadening of the XRD reflections) at pH 8. The higher concentrations of HA used may also increase the production of ferrihydrite at pH 8.

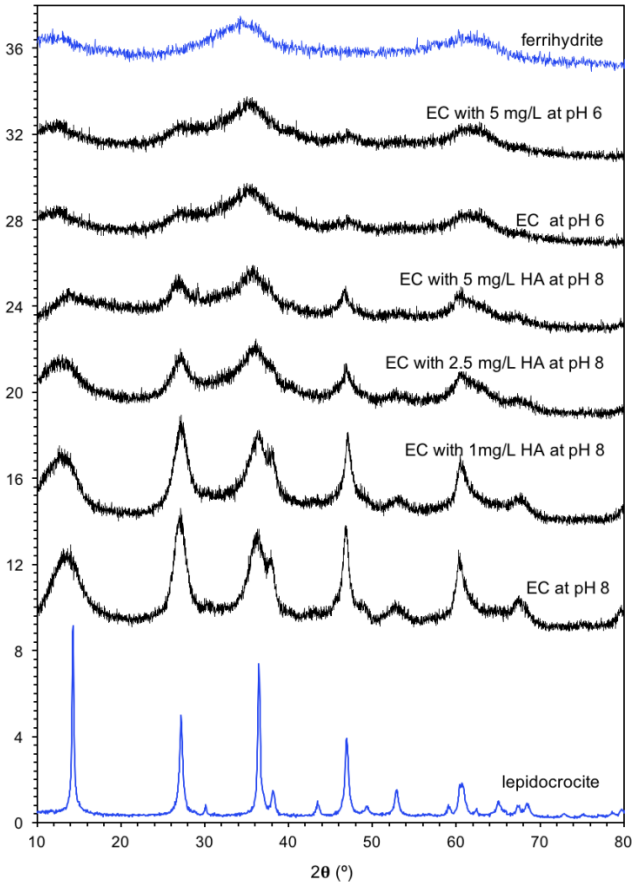

Figure 3.4. The XRD pattern of iron oxides produced during electrocoagulation without chromium present at various conditions. For reference the patterns of pure lepidocrocite and 2-line ferrihydrite are included in XRD plots.

EXAFS spectroscopy (Figure 3.5) was used to quantify the iron mineralogy produced via electrocoagulation with and without HA and Cr(VI) because such quantification of nanocrystalline phases is not possible via XRD. All spectra were modeled via linear combination fitting using the spectra of lepidocrocite and ferrihydrite, the phases identified as being dominant components in XRD. Fitting confirms that in the absence of HA lepidocrocite is the sole mineral product of electrocoagulation at pH 8 but that ferrihydrite dominates at pH 6, with a minor lepidocrocite component present (Table 3.1). The addition of HA, Cr(VI), or both species favors an increased formation of ferrihydrite at pH 8. In contrast, at pH 6 neither HA nor Cr(VI) appreciably affects the ratio of ferrihydrite to lepidocrocite, with the former dominating under all conditions studied.

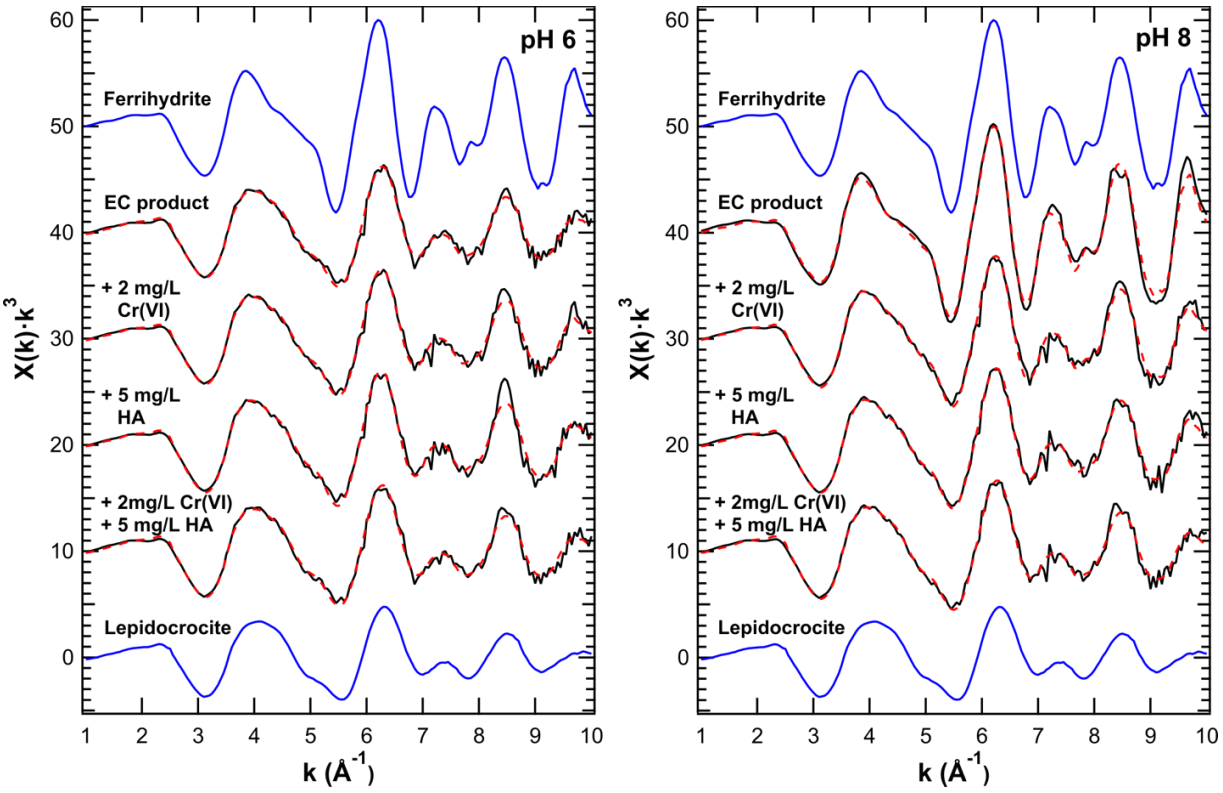

Figure 3.5. The Fe K-edge EXAFS spectra of iron oxides produced during electrocoagulation in the presence and absence of chromium at various conditions. For reference the patterns of pure lepidocrocite and 2-line ferrihydrite are included in EXAFS plots.

Table 3.1. Fe K-edge EXAFS linear combination fitting results for solids generated in the electrocoagulation reactor.

Cr (mg/L)	HA (mg/L)	pH	Percent Component		Component Sum
			Lepidocrocite	2-line Ferrihydrite	
-	-	6	20±1	80±2	1.10
2	-	6	27±2	73±3	1.09
-	5	6	31±2	69±3	1.12
2	5	6	17±1	83±2	1.13
-	-	8	100	0	1.00
2	-	8	48±2	52±3	1.10
-	5	8	37±2	63±3	1.11
2	5	8	23±1	77±3	1.15

The influence of HA and Cr(VI) on the Fe(III) solids produced at pH 8 likely results from their effect on Fe(III) nucleation and polymerization. Complexation of Fe by HA may favor smaller particle sizes and inhibit aggregation, which is supported by the hydrodynamic diameter measurements described above. Cr(VI) reduction by Fe(II) can lead to Cr(III)-Fe(III) coprecipitates[176] and the initial nuclei formed presumably favor ferrihydrite over lepidocrocite.

The TEM images of Fe/Cr oxide precipitates formed from electrocoagulation shown in Figure 3.6 further confirm the role of HA in affecting the properties of EC solids. At pH 8 without humic acid, the precipitate exhibits a "hedgehog-like" morphology that is similar to lepidocrocite-rich precipitates formed at the condition of Fe(II) oxidation by DO.[177] However, for the solids produced by electrocoagulation in the presence of 5 mg/L humic acid, the hedgehog-like morphology disappeared and the precipitates consist of smaller particles with a smoother surface aggregated into flocs, in line with previous results for amorphous Fe(III)-HA precipitates.[178] The TEM analyses further demonstrate the electrosteric stabilization effect from HA at pH 8. To further examine how HA affected the morphology of precipitated iron oxides, experiments with adsorption of 5 mg/L HA onto pre-formed electrocoagulation products at pH 8 created in the absence of HA were conducted, and the TEM images are shown in Figures 3.6c.

The “hedgehog-like” morphology is clear when HA adsorbs to pre-formed solids, distinct from iron oxides that are simultaneously precipitated in the presence of HA. Although the EXAFS shows that lepidocrocite still accounts for 23% of the solids generated after EC with 5mg/L HA at pH 8, the “hedge-like” morphology was not visible in TEM images of this solids, which is probably because the particles were too small or the lepidocrocite in these particular samples did not have that morphology. At pH 6 without HA, we still could observe the “hedgehog-like” morphology although it is less pronounced than at pH 8, consistent with the XRD and EXAFS spectroscopy results showing more ferrihydrite formation at pH 6. With 5 mg/L HA, the precipitates show greater aggregation but still contain features suggesting that some lepidocrocite is present (Figure 3.6e).[177, 179]

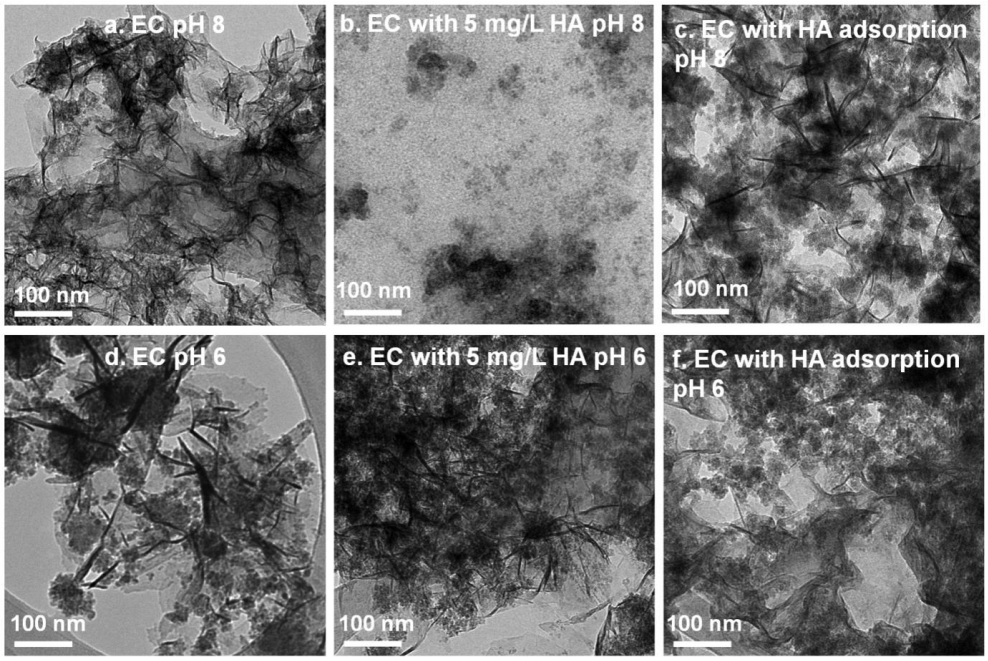

Figure 3.6. Transmission electron micrographs of solids produced by electrocoagulation at oxic conditions (a) at pH 8, (b) with 5 mg/L HA at pH 8, (c) at pH 8 and with post-electrocoagulation HA addition, (d) at pH 6, (e) with 5 mg/L HA at pH 6, (f) at pH 6 with post-electrocoagulation HA addition. Electrocoagulation with post HA addition was conducted by first producing solids in electrocoagulation and then adding HA two hours later. Scale bar is 100 nm.

XAFS spectroscopy was also used to characterize the speciation of Cr in the solids produced by electrocoagulation treatment of Cr(VI) solutions. XANES spectra show that these solids contain solely Cr(III), as indicated by the lack of a large, single pre-edge feature at ~5991 eV (Figure S3.5). All solids have similar XANES and EXAFS spectra (Figure 3.7), indicating that Cr speciation is largely unaffected by conditions in the electrocoagulation reactor. Comparison of the XANES and EXAFS spectra to those of Fe-Cr coprecipitates that have Fe:Cr ratios of 3:1 and 1:3 shows that the EC products closely resemble the 3:1 coprecipitates (Figure S3.6) . This is consistent with prior work that found that the products of Cr(VI) reduction by Fe(II) have an Fe:Cr ratio of 3:1 due to the reaction stoichiometry.[176, 180]

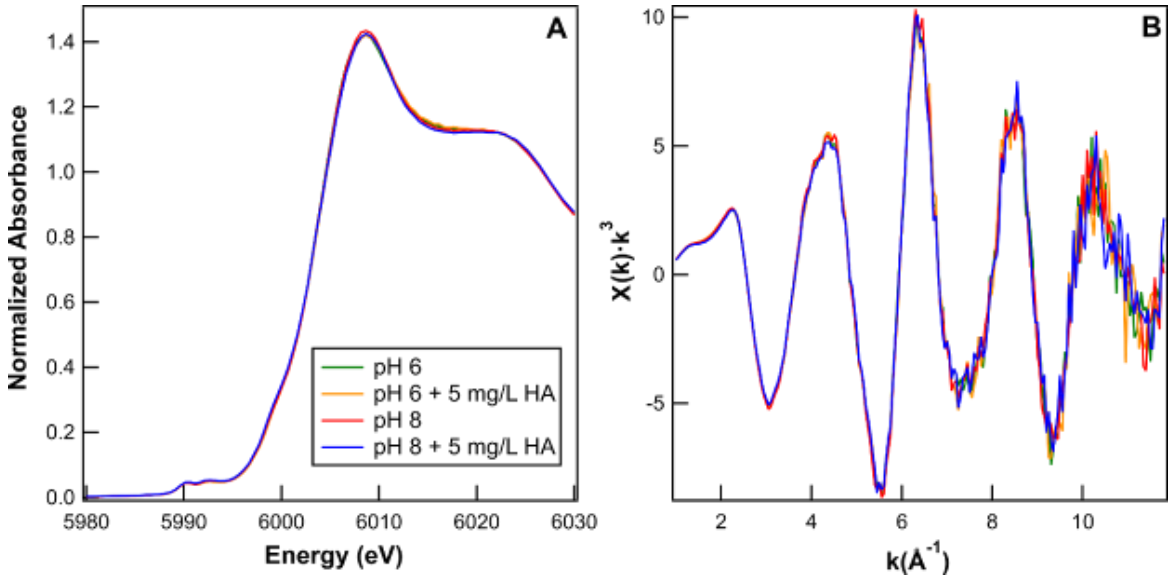

Figure 3.7. Cr K-edge (a) XANES and (b) EXAFS spectra of electrocoagulation products at pH 6 and pH 8 with and without 5 mg/L HA, all with an initial Cr(VI) concentration of 2 mg/L and operated at oxic conditions.

To examine the coordination environment of Cr within the Fe oxide mineral structure, shell-by-shell fitting was performed on Cr K-edge EXAFS spectra of EC products (Figure S3.7). Sample spectra were well-fit with one Cr-O shell at 1.98 Å and one Cr-Fe shell at 3.04 Å (Table

S3.3). A second Cr-Fe shell could be fit at 3.5 Å or at 3.9 Å, but the N values for either fit refined to values within error of zero and increased the reduced chi-squared value making their addition not statistically justified. The lack of a second Cr-Fe shell, which was observed in prior studies of Cr-Fe coprecipitates,[176, 181] may reflect the nanocrystalline nature of the products formed during electrocoagulation and the short reaction times (minutes) which inhibit particle ripening. The increase in ferrihydrite content upon addition of Cr(VI) during electrocoagulation suggests that in the present system Cr(VI) reduction by Fe(II) favors nucleation of ferrihydrite. Fitting also shows that HA does not alter Cr speciation, likely because ferrihydrite formation is also promoted during EC by HA.

3.4 Environmental Implications

Hexavalent chromium is a contaminant of great concern in water supplies, and iron-based electrocoagulation can effectively remove Cr(VI) to a very low concentration. The presence of humic acid in raw water during electrocoagulation leads to slower Cr(VI) removal at high pH, indicating that an electrocoagulation process will need more time to completely remove Cr(VI). The presence of HA also resulted in the formation of solid products with close association of Fe(III), Cr(III), and HA. The colloidal conditions of the electrocoagulation products would greatly influence the mobility of chromium even if all the Cr(VI) was reduced to Cr(III) by Fe(II) in EC. Cr(III), HA and Fe(III) could pass through filtration steps when HA results in stable colloid formation during electrocoagulation at high pH. The passage of Cr(III) and HA through filtration steps as colloids could lead to concerns of Cr(III) reoxidation and DBP production during the later disinfection process in water treatment. Humic acid could be aggregated by optimizing the electrocoagulation operation conditions. (e.g., longer electrocoagulation time or higher dosage rate of Fe(II) from the anode with increasing the currency). All of the Cr in the

solids produced by electrocoagulation was the less toxic Cr(III) form, and the coordination environment of Cr was indicative of Cr(III) incorporation into an iron oxide surface regardless of the presence of HA.

Acknowledgements

This research was supported by the U.S. National Science Foundation (CBET 1335613). C.P. acknowledges financial support from school of Engineering Applied Science in Washington University in St. Louis for a first year Ph.D. fellowship. This research used resources of the Advanced Photon Source, a U.S. Department of Energy (DOE) Office of Science User Facility operated for the DOE Office of Science by Argonne National Laboratory under Contract No. DE-AC02-06CH11357. Walter Schenkeveld graciously provided pure lepidocrocite for XRD and EXAFS measurement and comparison with patterns of experimentally-generated solids.

Chapter 3. Supporting Information

Additional information regarding the Faraday's law, dynamic modeling, zeta potential of solids produced from EC, the concentration of colloidal Cr, HA and Fe in EC, Cr XANES spectra and Cr EXAFS fitting parameters is included.

Faraday's Law:

$$Fe_{total} = \frac{M_{Fe} \cdot I \cdot t}{Z \cdot F} \quad \text{(S3.1)}$$

where M_{Fe} is the atomic weight of iron (55.85 g/mol), I is current (A), t is time (in seconds), z is the number of electrons transferred per iron released (z = 2 for release of Fe(II)), and F is Faraday's constant (96,485 C/mol).

Table S3.1. Rate constants for modeling the dynamics of dissolved Cr(VI) and Fe(II) during electrocoagulation

rate constant	definition	value				unit	methods of determination
		pH 6	pH 7	pH 8	pH 9		
k_{homo}	homogeneous rate constant for reduction of Cr(VI) by Fe(II)	35	811	5.15×10^{4}	4.85×10^{6}	$M^{-1}\,s^{-1}$	Published [182, 183]
k'_{hetero}	Heterogeneous rate constant for Cr(VI) reduction by adsorbed Fe(II)	1.1×10^{7}	0	0	0	$M^{-2}\cdot s^{-1}$	Published [183]
k_2	Fe(II) generation rate in EC	1.92×10^{-7}	1.92×10^{-7}	1.92×10^{-7}	1.92×10^{-7}	$M\cdot s^{-1}$	Faraday's law with I=37 mA
k_{O_2}	Fe(II) oxidation rate by O_2	3.85×10^{-6}	1.65×10^{-4}	1.05×10^{-2}	0.20	s^{-1}	Published [184]

Table S3.2. Enhancing factor (f) of Fe(II) oxidation by dissolved oxygen in the presence of HA

	pH 6	pH 7	pH 8	pH 9
No HA	1	1	1	1
1 mg/L HA	1	-	90	200
5 mg/L HA	1	1	200	350
20 mg/L HA	1	1	360	1000

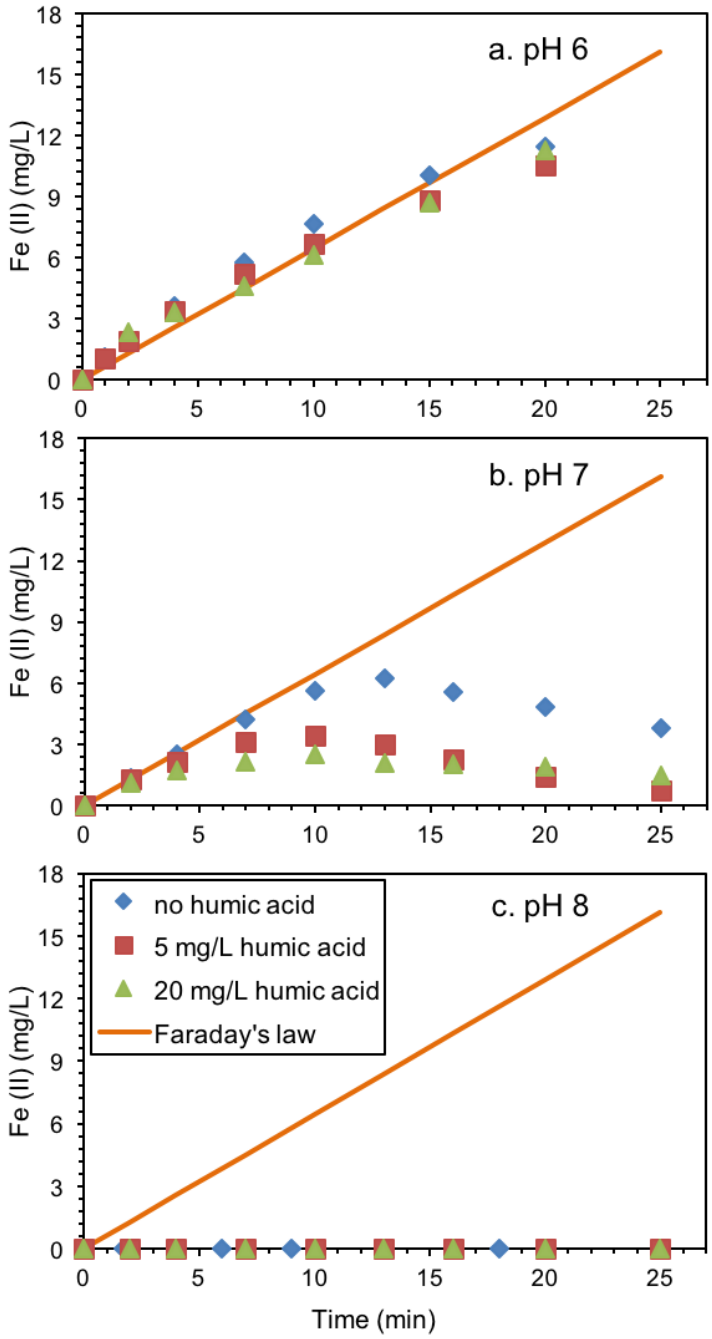

Figure S3.1. Evolution of dissolved Fe(II) during electrocoagulation in the presence of dissolved oxygen and humic acid at (a) pH 6, (b) pH 7, (c) pH 8. Conditions: no chromium, U = 4V, I = 0.037 A, 2 mM MES for pH 6.0, 5 mM HEPES for pH 7.0 and pH 8.0, and conductivity = 460 µS/cm.

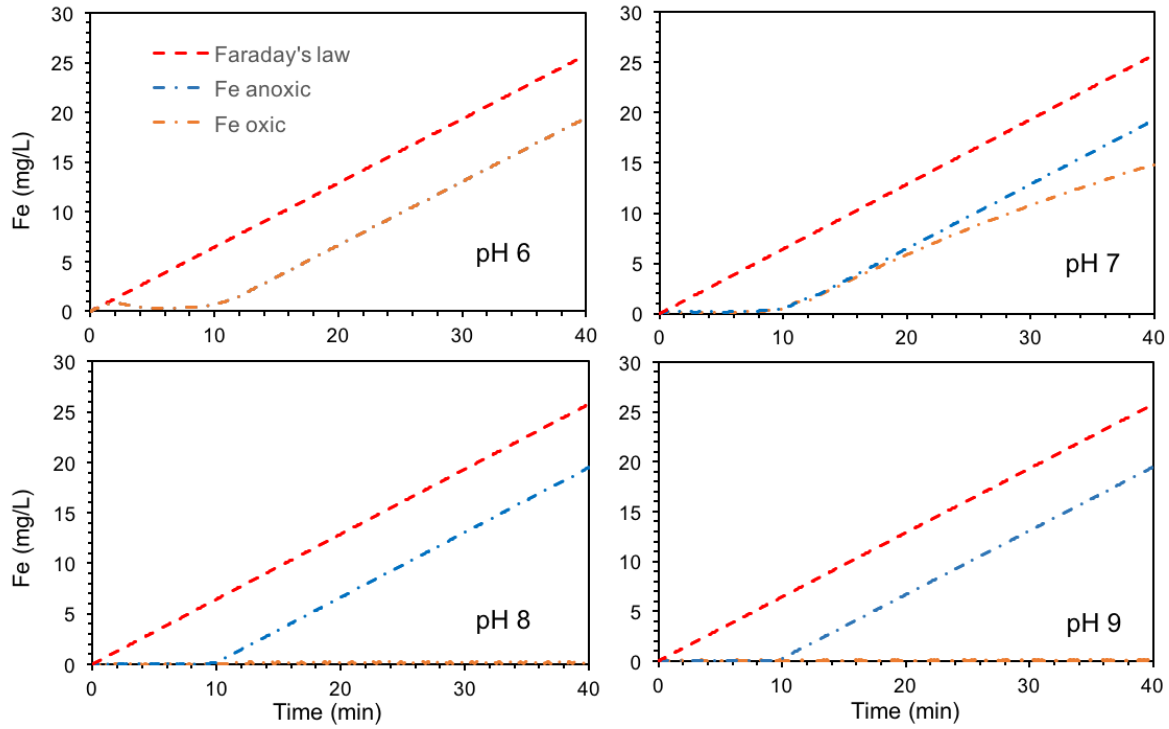

Figure S3.2. Modeled Fe(II) concentration during the Cr(VI) removal in electrocoagulation at both oxic and anoxic conditions. The effect of HA is not shown because the Fe(II) concentrations are almost identical with and without HA at each pH presented.

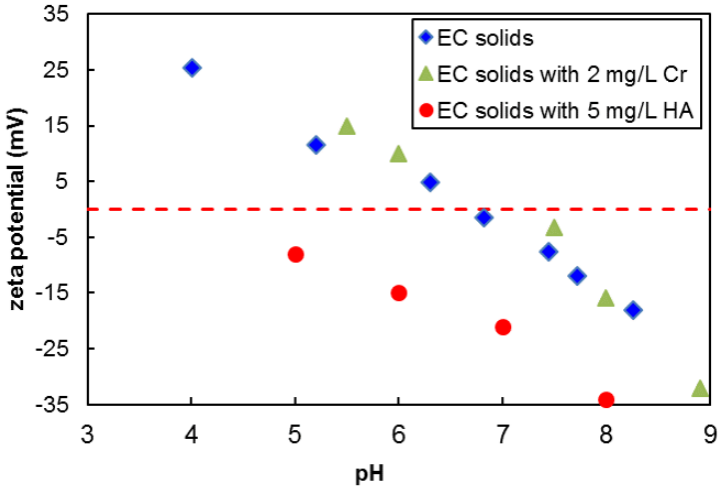

Figure S3.3. Effect of pH on zeta potential of the solids generated by 30 minutes electrocoagulation with or without chromium and HA. U = 4 V, I = 37 mA, conductivity = 460 µS/cm.

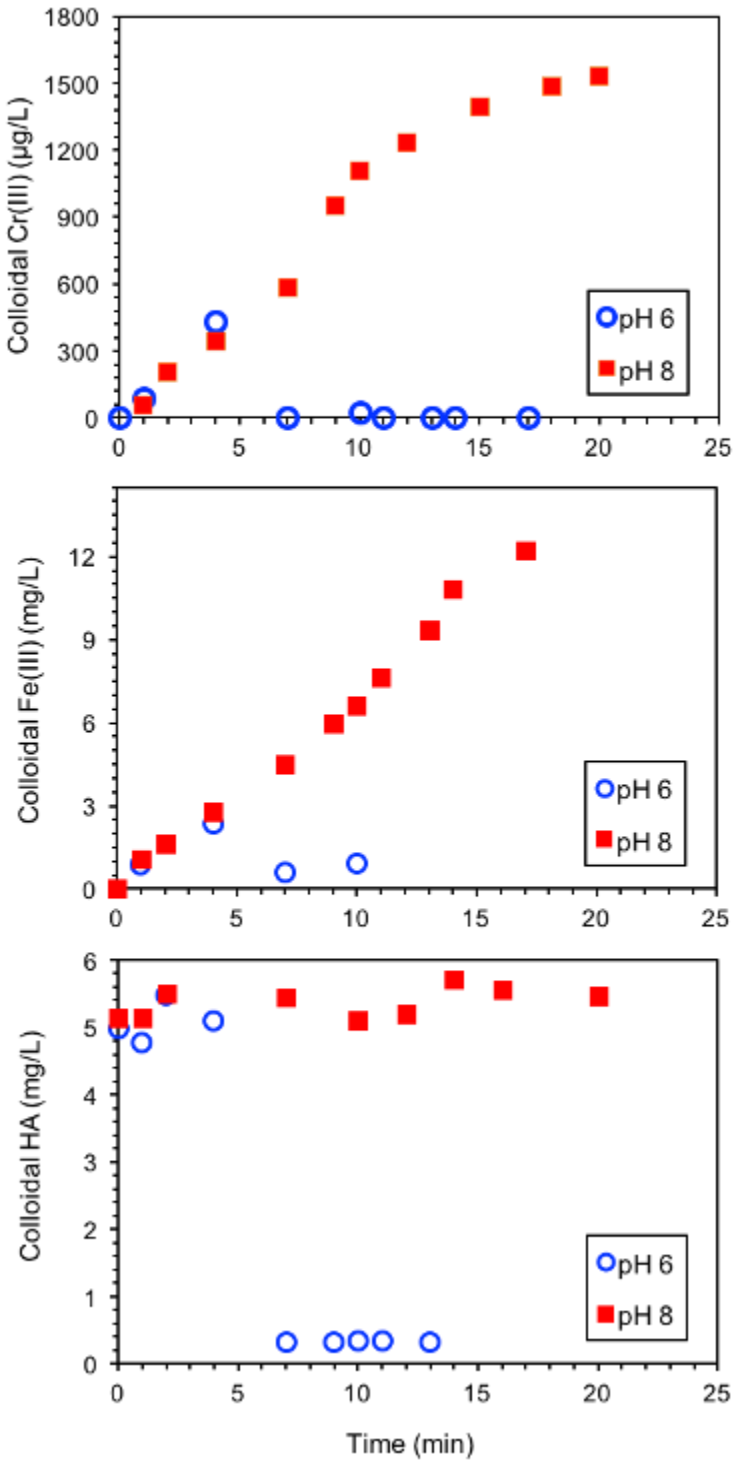

Figure S3.4. The concentration of colloidal chromium(III), humic acid and iron during electrocoagulation at two conditions. Conditions: $[Cr(VI)]_0$ = 2 mg/L, U = 4 V, I = 37 mA, 2 mM MES for pH 6.0, 5 mM HEPES for pH 8.0, and conductivity = 460 µS/cm.

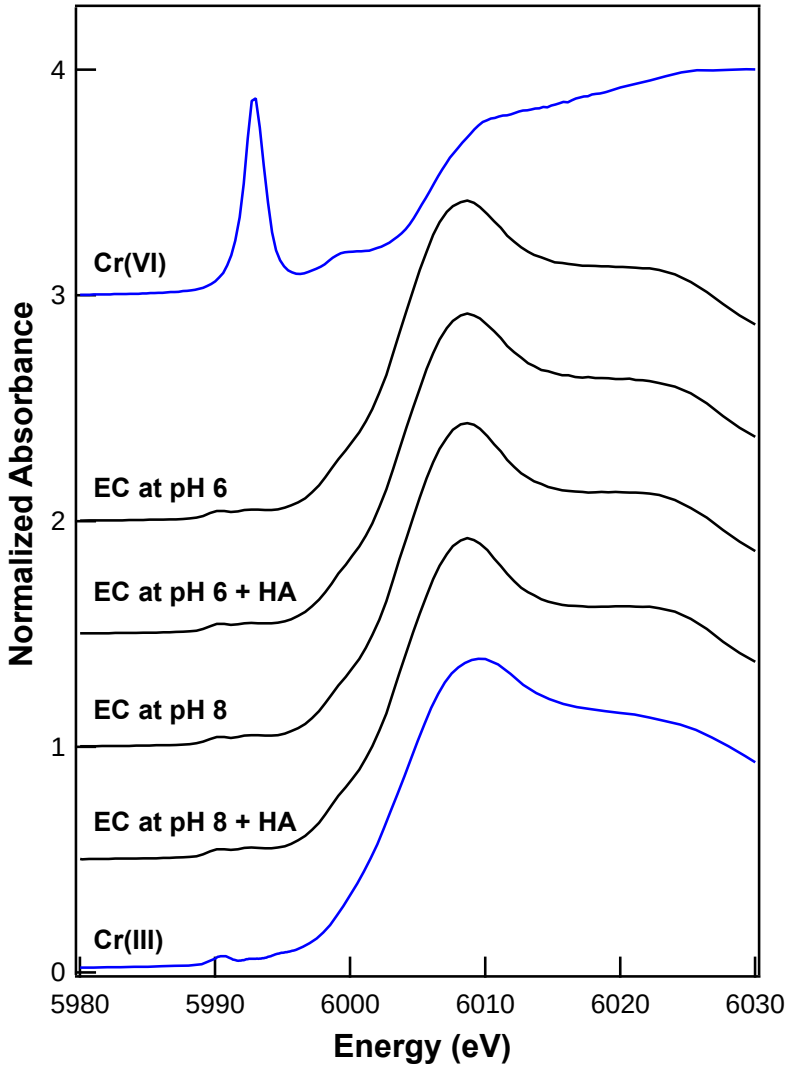

Figure S3.5. Cr K-edge XANES spectra of electrocoagulation products at pH 6 and pH 8 with and without 5 mg/L HA, all with an initial Cr(VI) concentration of 2 mg/L and operated under oxic conditions. Cr K-edge XANES spectra of $Cr(OH)_3$ and Na_2CrO_4 reference standards are plotted for comparison.

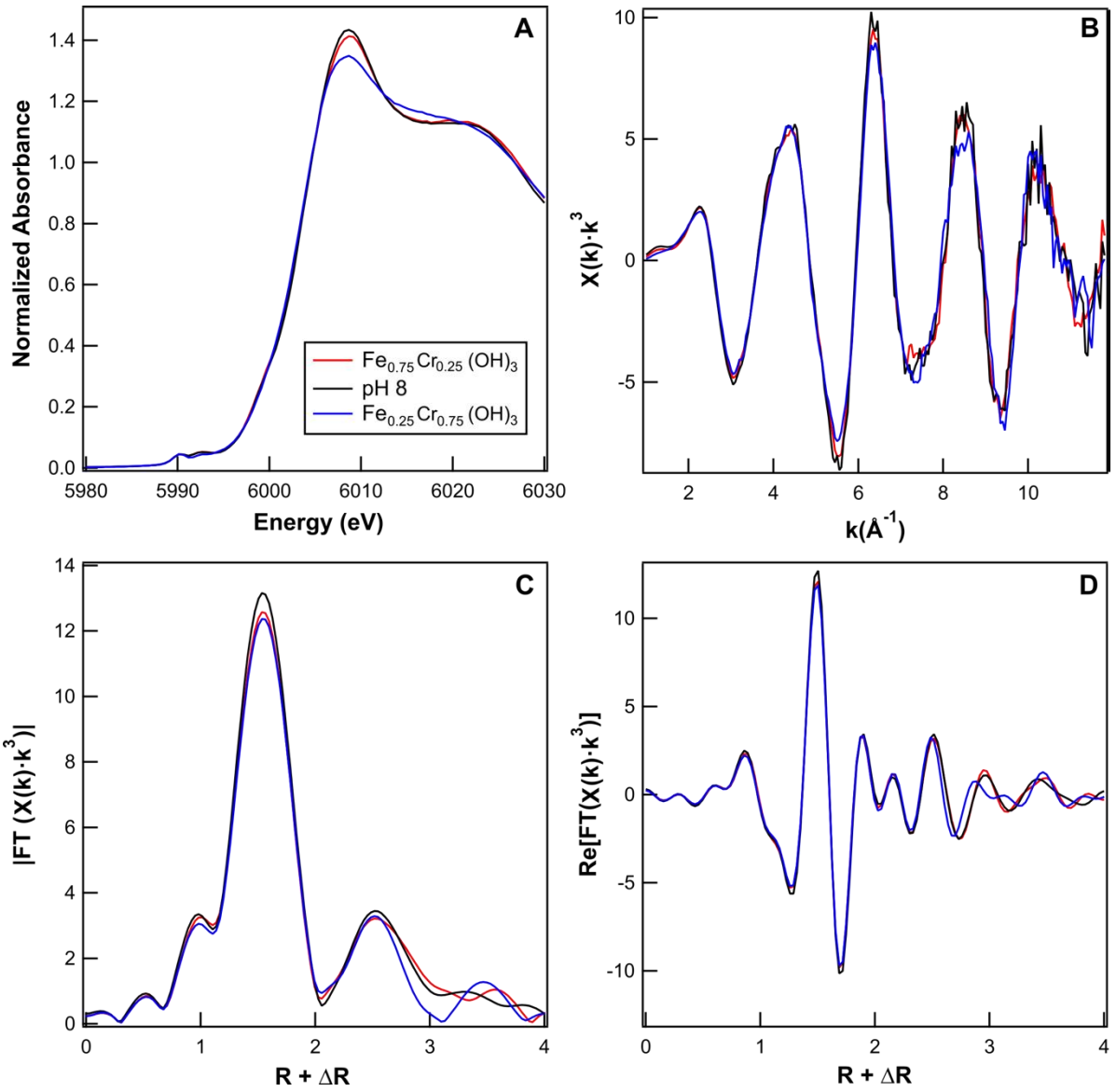

Figure S3.6. Cr K-edge (a) XANES spectra, (b) EXAFS spectra, (c) Fourier transform magnitudes, and (d) real components of the Fourier transforms of the electrocoagulation product at pH 8 with 2 mg/L initial Cr(VI) plotted against 3:1 and 1:3 Fe:Cr hydroxide co-precipitates prepared by pH adjustment to 7. Fe(III)-Cr(III) co-precipitates reference were synthesized by combining Fe(III) chloride and Cr(III) chloride stock solutions in varying ratios with a total concentration of 60 μM Fe and Cr with 10 mM NaCl as a background electrolyte without the presence of humic acid.

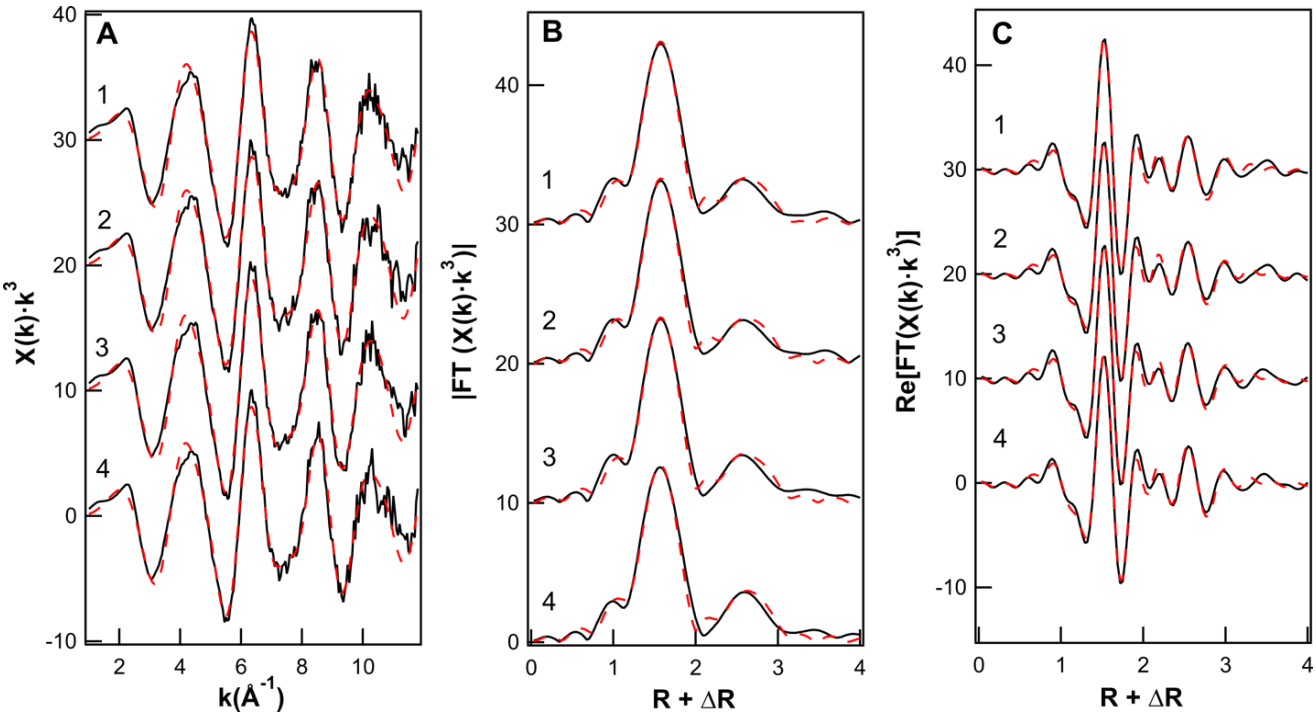

Figure S3.7. Data (black solid) and structural fits (red dashed) to the Cr K-edge EXAFS spectra (a), Fourier transform magnitudes (b), and real components of the Fourier transforms (c) of a set of electrocoagulation reactor solids. Electrocoagulation reactors contained 2 mg/L initial Cr(VI) at pH 8 with (1) and without (2) 5 mg/L humic acid and at pH 6 with (3) and without (4) 5 mg/L humic acid.

Table S3.3. Cr K-edge EXAFS fitting parameters

Sample		Cr-O	Cr-Fe	ΔE_0 (eV)[d]	χ_v^{2e}
pH 8	N[a]	5.4(6)	4(2)	-4(1)	35.2
	R (Å) [b]	1.984(7)[f]	3.04(2)		
	σ^2 (Å^2) [c]	0.0032(9)	0.012(4)		
pH 8 + HA	N	5.4(6)	3(1)	-4(2)	18.1
	R (Å)	1.980(7)	3.04(2)		
	σ^2 (Å^2)	0.0035(9)	0.010(4)		
pH 6	N	5.3(5)	3(1)	-4(1)	19.9
	R (Å)	1.983(6)	3.04(1)		
	σ^2 (Å^2)	0.0031(8)	0.010(4)		
pH 6 + HA	N	5.2(5)	3(1)	-3(1)	22.1
	R (Å)	1.983(7)	3.04(2)		
	σ^2 (Å^2)	0.0030(9)	0.010(4)		

[a] Coordination number. [b] Interatomic distance. [c] Debye-Waller factor. [d] Difference in the threshold Fermi level between the data and theory. [e] Goodness of fit parameter [185]. [f] Value in parentheses represent the 1σ uncertainty in the last digit; parameters without specified uncertainties were held constant during fitting.

Chapter 4. Rates of Cr(VI) Generation from $Cr_xFe_{1-x}(OH)_3$ Solids upon Reaction with Manganese Oxide

This chapter was published in Pan, C.; Liu, H.; Catalano, J. G.; Qian, A.; Wang, Z.; Giammar, D. E., Rates of Cr(VI) generation from CrxFe1-x(OH)$_3$ solids upon reaction with manganese oxide. Environ Sci Technol. 2017. As soon as possible.

Abstract

The reaction of manganese oxides with Cr(III)-bearing solids in soils and sediments can lead to the natural production of Cr(VI) in groundwater. Building on previous knowledge of MnO_2 as an oxidant for Cr(III)-containing solids, this study systematically evaluated the rates and mechanisms of the oxidation of Cr(III) in iron oxides by δ-MnO_2. The Fe/Cr ratio (x = 0.055-0.23 in $Cr_xFe_{1-x}(OH)_3$) and pH (5-9) greatly influenced the Cr(VI) production rates by controlling the solubility of Cr(III) in iron oxides. We established a quantitative relationship between Cr(VI) production rates and Cr(III) solubility of $Cr_xFe_{1-x}(OH)_3$, which can help predict Cr(VI) production rates at different conditions. The adsorption of Cr(VI) and Mn(II) on solids shows a typical pH dependence for anions and cations. A multichamber reactor was used to assess the role of solid-solid contact in $Cr_xFe_{1-x}(OH)_3$-MnO_2 interactions, which eliminates the contact of the two solids while still allowing aqueous species transport by a permeable membrane. Cr(VI) production rates were much lower in multichamber than in completely mixed batch experiments, indicating that the redox interaction is accelerated by mixing of the solids. Our results suggest that soluble Cr(III) released from $Cr_xFe_{1-x}(OH)_3$ solids to aqueous solution can migrate to MnO_2 surfaces where it is oxidized.

4.1 Introduction

Hexavalent chromium [Cr(VI)] is a known carcinogen often found in water supplies both from human activities (e.g. electroplating and wood treatment, leather tanning, and chromite ore processing)[186-188] and from the oxidation of Cr(III) by natural processes. Cr(III) is much less toxic and less mobile than Cr(VI). Common techniques for Cr(VI) removal from solution involve Cr(VI) reduction to Cr(III) by iron-based compounds (e.g. Fe(II), Fe(0) or FeS_2) and the subsequent association of Cr(III) with the produced Fe(III) (oxy)hydroxide solids.[189-191] In addition, iron-reducing bacteria in the environment can drive Cr(VI) reduction under anaerobic conditions by producing Fe^{2+} that then reduces Cr(VI) to Cr(III).[192, 193] For these anthropogenic or natural iron-based Cr(VI) reduction processes, the solid product is often a Cr(III)-Fe(III)-coprecipitate, with a general molecular formula of $Cr_xFe_{1-x}(OH)_3$.[62, 189, 194-197] $Cr_xFe_{1-x}(OH)_3$ can occur as a solid solution, such that the chromium solubility depends on ratio of Fe/Cr in the solid and on the pH of the solution.[194, 198] In this case the dissolved Cr(III) in equilibrium with $Cr_xFe_{1-x}(OH)_3$ is much lower than with pure $Cr(OH)_3$. E.g., compared with $Cr(OH)_3$, dissolved Cr(III) in equilibrium with $Cr_xFe_{1-x}(OH)_3$ is an order of magnitude lower when x=0.69 and five orders of magnitude lower when x=0.01 at the same pH.

Manganese oxides are strong oxidants that provide a major geochemical pathway for Cr(VI) occurrence from Cr(III) in groundwater, soils or subseafloor environments.[52-54] Field-scale studies showed that Mn(III)/Mn(IV) mineral concentration was a good predictor of an aquifer's capacity to form and solubilize Cr(VI). In a study of serpentine soils of the California coast range, McClain et al. detected Cr(VI) in the same horizons where mineral-bound Cr(III) was collocated with biogenic Mn(III/IV) oxides that were similar to birnessite, and they quantified in situ Cr(VI) production rates in the presence of biogenic Mn(III/IV)-oxides.[199]

Similarly, Gonzalez et al. suggested that the significant amounts of Cr(VI) in the drinking water of Santa Cruz County, California were due to Cr(III) mineral deposits being oxidized by manganese oxides in the Aromas Red Sands aquifer.[200]

The oxidation of Cr(III) in real or simulated soils and sediments by manganese oxides has received recent attention. For example, rates and extents of Cr(III) oxidation from chromite ($FeCr_2O_4$), Cr(III)-bearing silicates and $Cr_xFe_{1-x}(OH)_3$ by manganese oxides were compared with that from $Cr(OH)_3$ in previous studies.[52, 53, 199, 201-203] The rate of Cr(VI) generation from solid-associated Cr(III) oxidation by manganese oxides is often proportional to the Cr(III) solubility. Oze et al. demonstrated that Cr(III) from chromite is oxidized in the presence of MnO_2.[204] Even though Cr(III)-bearing silicates have less Cr(III) than chromite, Cr(III)-bearing silicates actually have a higher Cr(VI) production rate upon reaction with manganese oxides because of their higher solubility.[202] Hausladen and Fendorf compared the Cr(VI) genesis in column experiments with sands coated with either $Cr_xFe_{1-x}(OH)_3$ or $Cr(OH)_3$ in the presence of MnO_2 and found that Cr(VI) concentrations were correlated with the Cr(III)-mineral solubility.[201] Most of these studies focused on the dissolved Cr(VI) that was released into water and did not consider the Cr(VI) that was produced but readsorbed onto the solid phases. The undetermined dynamics of Cr(VI) release from solid phase may prevent the establishment of quantitative relationship between Cr solubility and the total oxidation rate of Cr(III). In addition, several studies reported passivation of Mn oxides towards Cr(III) oxidation by reaction with $Cr(OH)_3$, which may have been due to the precipitation of Cr(III) hydroxide on the manganese oxide surface.[205] However, it is not clear whether there is a similar inhibitory effect for oxidation of Cr(III)-bearing Fe(III) oxide or hydroxide minerals by manganese oxides.

The objectives of this study were to (1) determine the rates of total Cr(VI) production from $Cr_xFe_{1-x}(OH)_3$ oxidation by δ-MnO_2 in terms of pH and Fe/Cr ratio and (2) test the role of proximity between $Cr_xFe_{1-x}(OH)_3$ and MnO_2 in Cr(VI) production and identify the products of MnO_2 reaction with $Cr_xFe_{1-x}(OH)_3$. Cr(VI) production rates were correlated with dissolved Cr(III) concentrations in equilibrium with $Cr_xFe_{1-x}(OH)_3$. Completely mixed batch experiments and multichamber experiments were operated to test the role of proximity of these two poorly soluble solids in Cr(VI) production. Initial and reacted manganese oxide phases were characterized by X-ray powder diffraction (XRD), X-ray photoelectron spectroscopy (XPS) and high-resolution transmission electron microscopy (HR-TEM).

4.2 Materials and Methods

4.2.1 Materials

Ultrapure water (resistivity > 18.2 MΩ-cm) was used for all the experiments. At pH 5 and pH 6, no buffer was added to the reactors and the pH values of the solutions were maintained by NaOH/HCl. At pH 7 and pH 8, the pH values of suspensions were buffered by 5 mM 3-(N-morpholino) propanesulfonic acid (MOPS, pK_a=7.2). At pH 9, 5 mM N-cyclohexyl-2-aminoethanesulfonic acid (CHES, pK_a=9.3) was used for buffering the suspension. The pH buffers and their concentrations were chosen to minimize their complexes with Cr(III)/Fe(III) and their stability against oxidation by MnO_2.[62, 108, 206, 207] MOPS and CHES were widely used for their minimal influence on metal complexation.[108, 208-210] The presence of MOPS and CHES did not appear to cause any MnO_2 dissolution in control experiments (Figure S4.1). A NaCl solution was used as the background electrolyte in all experiments since Na^+ and Cl^- do not interfere with the chemistry of Cr(III) oxidation and only affect the ionic strength. The amount of

NaCl was added dependent on pH to provide a total 5 mM ionic strength including contribution from the buffers.

4.2.2 Mineral synthesis

Synthetic δ-MnO_2 was prepared by reacting $KMnO_4$ with $MnCl_2$ at basic pH following the method described by Villalobos, et al. [50] The δ-MnO_2 prepared in this method was previously determined to be a close synthetic analog to naturally-occurring biogenic manganese oxide.[206] X-ray powder diffraction (XRD) confirmed that the solid was δ-MnO_2 (Figure S4.2a). Transmission electron microscopy (TEM) provided evidence of δ-MnO_2 morphology and sizes (Figure S4.3) similar to what was reported previously.[50] The XPS results show that the initial δ-MnO_2 surface is 94.9% Mn(VI) and 5.1% Mn(III). The average oxidation state of Mn is 3.95, consistent with the reported Mn average oxidation state of being close to 4 and Mn(II) under the detection limit in δ-MnO_2.[50, 211] $Cr_xFe_{1-x}(OH)_3$ was synthesized by titrating mixed solutions of $FeCl_3$ and $CrCl_3$ at different Fe:Cr molar ratios with 1 M and 0.1 M NaOH to pH 7 and maintaining the pH for 24 hours. This was similar to the procedure described by Hansel et al.[176, 212, 213] The suspension was then washed five times with ultrapure water, and the supernatant was discarded after centrifugation. Amorphous $Cr(OH)_3$(s) was synthesized with the same method but with no $FeCl_3$ present (i.e., x = 1). Portions of suspension were dissolved in nitric acid to determine the exact Cr and Fe concentrations in the solids produced by inductively coupled plasma-mass spectroscopy (ICP-MS). $Cr_xFe_{1-x}(OH)_3$ solids with three different Fe/Cr ratios were prepared with x being 0.23, 0.11 and 0.055, respectively. XRD patterns of the $Cr_xFe_{1-x}(OH)_3$ appeared similar to that of 2-line ferrihydrite (broad peaks at 35 ° and 63 ° 2θ for Cu Kα) and without characteristic peaks of $Cr(OH)_3$ at 2θ = 19.1 ° (Figure S4.2a). $Cr_xFe_{1-x}(OH)_3$ solids prepared by this co-precipitation method have been suggested as a solid solution based on

chromium solubility and FT-IR evidence.[198, 214] More recent work discovered that Cr(III) substitution in Cr(III)-Fe(III) hydroxide solids was limited to octahedral sites, while Fe(III) can be in both octahedral and tetrahedral sites.[213]

4.2.3 Mixed batch and multichamber reactor

As opposed to multichamber experiments with separated $Cr_xFe_{1-x}(OH)_3$ and MnO_2 suspensions, completely mixed batch experiments were conducted in a glass beaker filled with ultrapure water, NaCl, pH buffer, MnO_2 suspension, and $Cr_xFe_{1-x}(OH)_3$ suspensions with 40 mg/L initial Cr(III) concentration to a total volume of 1 L. Multichamber experiments were used to assess the role of solid-solid contact in $Cr_xFe_{1-x}(OH)_3$-MnO_2 interactions. The multichamber reactor was the same as we used previously in studying UO_2-MnO_2 interactions.[206] Briefly, a dialysis membrane with a molecular weight cut off (MWCO) of 3500 (approximately 2.1nm diameter) divided the reactor into two-110 mL chambers, eliminating the direct contact of the $Cr_xFe_{1-x}(OH)_3$ and MnO_2 solids but allowing the individual chambers to be completely mixed by a magnetic stir bar and dissolved species to diffuse across the membrane. The background solution in $Cr_xFe_{1-x}(OH)_3||MnO_2$ experiment was the same as that used in completely mixed batch experiments. "||" notes the separation of solids by a dialysis membrane. MnO_2||water control experiments were conducted with the multichamber reactor to account for the dissolution of MnO_2. For both completely mixed batch experiments and multichamber experiments, samples were periodically collected and a portion of them were filtered with 0.02 μm polyethersulfone (PES) syringe filters (Tisch Environmental, OH) for analysis of dissolved chromium, dissolved Cr(VI) and dissolved manganese. The remaining portions of the samples were used for total Cr(VI) and total Mn(II) analysis. Experiments were performed under atmosphere for both completely mixed and multichamber experiments.

4.2.4 Aqueous and solid phase analysis

Total and dissolved Cr, Fe and Mn concentrations were measured by ICP-MS (PerkinElmer ELAN DRC II). The instrument detection limits for Cr, Fe and Mn were 0.2 μg/L (0.0039 μM), 0.1 mg/L (1.8 μM), and 0.5 μg/L (0.009 μM), respectively. Dissolved Cr(VI) and dissolved Mn(II) were determined by the diphenylcarbazide method and ICP-MS, respectively. Cr(VI) concentrations in the samples were determined spectrophotometrically (PerkinElmer-Lambda XLS) after reaction with diphenylcarbazide.[215] The detection limit for Cr(VI) by this method was 5 μg/L (0.096 μM). Dissolved Mn(II) concentrations were assumed to equal the total dissolved Mn concentration because both Mn(IV) and Mn(III) are sparingly soluble.[216] Concentrations of total Cr(VI) and total Mn(II), which include adsorbed as well as dissolved species, were measured after extracting the surface-associated species into solution. For total Cr(VI) measurements, adsorbed Cr(VI) was extracted by adding a sodium phosphate solution pre-adjusted to have the same pH as the sample suspension to provide a 10 mM phosphate concentration in the suspension.[210, 217] The efficiency of this extraction procedure was above 90% ± 5% based on control experiments. The control experiments were operated with Cr(VI) adsorption onto Cr(III)-Fe(III) hydroxide solids followed by phosphate addition to induce Cr(VI) desorption. After Cr(VI) was desorbed from solid phases, the suspension was filtered and measured by the diphenylcarbzide method. Other portions of suspensions were treated with 10 mM $CuSO_4$ for 1 hour to extract adsorbed Mn(II). In this method Cu(II) preferentially adsorbs to MnO_2 and induces Mn(II) desorption.[218-220] This method was shown to remove >90% of the adsorbed Mn(II) from a biologically reduced δ-MnO_2.[221] The method only extracts adsorbed Mn(II) and should not mobilize structurally incorporated Mn(II) or Mn(III).

TEM samples were prepared by dropping approximately 30 μL of suspension onto 200 mesh carbon-coated copper grids (Ted Pella, Inc.) followed by immediate evaporation of the remaining water at room temperature under vacuum. TEM micrographs were taken with a transmission electron microscope under 120 kV (FEI Spirit G2). The solid samples for XRD, XPS and HR-TEM were prepared by centrifugation and freeze-drying. XRD patterns were collected using Cu Kα radiation (Bruker d8 Advance X-ray diffractometer). XPS analyses were conducted using a Physical Electronics 5000 Versa Probe II Scanning ESCA Microprobe with an Al Kα X-ray source at 23.5 eV pass energy at a 100 μm X-ray spot size. The binding energy was calibrated using C 1s at 284.6 eV and the XPS spectra were processed by using CasaXPS software (Version 2.3.15)[222] with the Gaussian-Lorentzian function (70% G-30% L), and Shirley background was used for peak fitting. The quantification of Mn valence state was made following a method in which the Mn $2p_{3/2}$ spectrum is divided into five multiplet peaks (total of 15 binding energies) of Mn(IV), Mn(III) and Mn(II).[223] A value of 1.5 for the full width of the peak at half the maximum peak height (FWHM) was assigned to fit the Mn $2p_{3/2}$ spectrum for all of the multiplet binding energy spectra.[224] In this study, the standard deviation of constituents fitted by CasaXPS is around 5%. HR-TEM observation was carried out using an FEI TF electron microscope operated at 200 kV and energy dispersive X-ray (EDX) analysis was used to confirm the particle compositions, and selected area electron diffraction (SAED) patterns were collected to determine the extent of crystallinity of the Mn oxides and Cr(III)-Fe(III) hydroxides as well as to identify the mineral phases.

4.3 Results and Discussion

4.3.1 $Cr_xFe_{1-x}(OH)_3$ oxidation by δ-MnO_2

Cr(VI) and Mn(II) concentrations from $Cr_xFe_{1-x}(OH)_3$ oxidation were experimentally determined at ambient conditions as a function of pH (5-9) and Fe/Cr ratio(x= 0.23,0.11,0.055) (Figure 4.1).

In the $Cr_xFe_{1-x}(OH)_3$ and MnO_2 reaction system, the Cr(VI) concentrations increased linearly with time, indicating a constant Cr(VI) production rate. With a fixed Fe/Cr ratio, Cr(VI) production rates decreased when the pH increased from 5 to 9. For more iron-rich solids (lower x), Cr(VI) production rates are lower at a constant pH. It should be noted that all of the experiments contained the same total amount of initial Cr(III). Cr(VI) production from $Cr_xFe_{1-x}(OH)_3$ reaction with MnO_2 was not inhibited by the sparing solubility of Cr(III)-Fe(III) hydroxides. In addition, Cr(VI) was fully adsorbed onto the solid phases at a low pH while most was released into solution at higher pH, which is the expected adsorption behavior of an anion (Figure 4.2a).

The initial rate of Cr(VI) production at pH 5 is higher for MnO_2 reaction with $Cr(OH)_3$ than with $Cr_{0.23}Fe_{0.77}(OH)_3$, but the total amount of Cr(VI) generated after 200 hours is actually higher for $Cr_{0.23}Fe_{0.77}(OH)_3$ (Figure S4.4). The predicted dissolved Cr(III) in equilibrium with $Cr_{0.23}Fe_{0.77}(OH)_3$ is much lower than in equilibrium with $Cr(OH)_3$, so the lower cumulative Cr(VI) production from $Cr(OH)_3$ may be caused by precipitation of $Cr(OH)_3$ on the surface of MnO_2.[205] In contrast, the dissolved Cr(III) concentration in the $Cr_{0.23}Fe_{0.77}(OH)_3$ system is not high enough for nucleation and formation $Cr(OH)_3$ precipitates on the MnO_2 surface. The concentration of dissolved Cr(III) in equilibrium with $Cr_xFe_{1-x}(OH)_3$ at different pH was shown in Figure 4.3a.

The predicted dissolved Cr(III) concentration was based on empirical equations for the $CrOH^{2+}$ concentration (eq. 4.1)[198] and consideration of other Cr(III) complexes with hydroxide.[225] The $Cr_xFe_{1-x}(OH)_3$ solids for the Cr(III) solubility prediction by Sass et al (1987) were prepared by neutralizing acidic solutions containing Cr(III) and Fe(III) at room temperatures,[14] which is the same approach used in our study. Detailed calculation of Cr(III) solubility are provided in the supporting information (Table S4.1) .

$$\text{Log } (CrOH^{2+}) = -2\ pH + 4.18 + 0.28(1-x)^2 - 1.79(1-x)^3 + \log x \qquad (4.1)$$

The ratio of total Mn(II)/Cr(VI) produced in the solution gives clues to the oxidation state of reduced Mn after MnO_2 reaction with $Cr_xFe_{1-x}(OH)_3$ solids. Different stoichiometric ratios of Cr(VI) to Mn(II) will occur depending on whether the Mn(IV) is reduced to Mn(III) (Mn(II)/Cr(VI) = 0 in eq. 4.2) or to Mn(II) (Mn(II)/Cr(VI) = 1.5 in eq. 4.3). Elementary reactions between Mn(IV) and Cr(III) proceed through one-electron transfer steps, although dissolution of MnO_2 involves a net transfer of two electrons from Mn(IV) to aqueous Mn(II), while three electrons are necessary to fully oxidize Cr(III) to Cr(VI).[226] At pH 5 the ratio of total Mn(II) to total Cr(VI) was very close to 1.5 (Figure 4.1), which indicates that the Mn(IV) was reduced to Mn(II) at this condition. In contrast, at pH 9 the average value of total Mn(II) divided by total Cr(VI) was only around 0.3, which suggests that solid-associated Mn(III) is the dominant final product of the redox reaction at this higher pH.

$$Cr(OH)_{3(s)} + 3MnO_2 + H_2O = HCrO_4^- + 3MnOOH + H^+ \qquad (4.2)$$

$$2Cr(OH)_{3(s)} + 3MnO_2 + 4H^+ = 2HCrO_4^- + 3Mn^{2+} + 4H_2O \qquad (4.3)$$

$$Mn^{2+} + MnO_2 + 2H_2O = 2H^+ + 2MnOOH \qquad (4.4)$$

A possible explanation for this pH effect is more favorable Mn(II) adsorption onto the MnO_2 surface at high pH (Figure 4.2b), a step critical for initiation of interfacial Mn(II)-Mn(IV) comproportionation that produces Mn(III) (eq 4.4).[227] More than 90% of Mn(II) was adsorbed onto the solid phases when the pH is above 7. The observed pH-dependence of Mn(II) adsorption is typical of what would be expected for adsorption of a cation to an iron oxide surface (Figure 4.2b and Figure S4.5).[228] In eq. 4.2 and eq. 4.4, Mn(III)OOH is shown as just one possible Mn(III)-containing solid product.

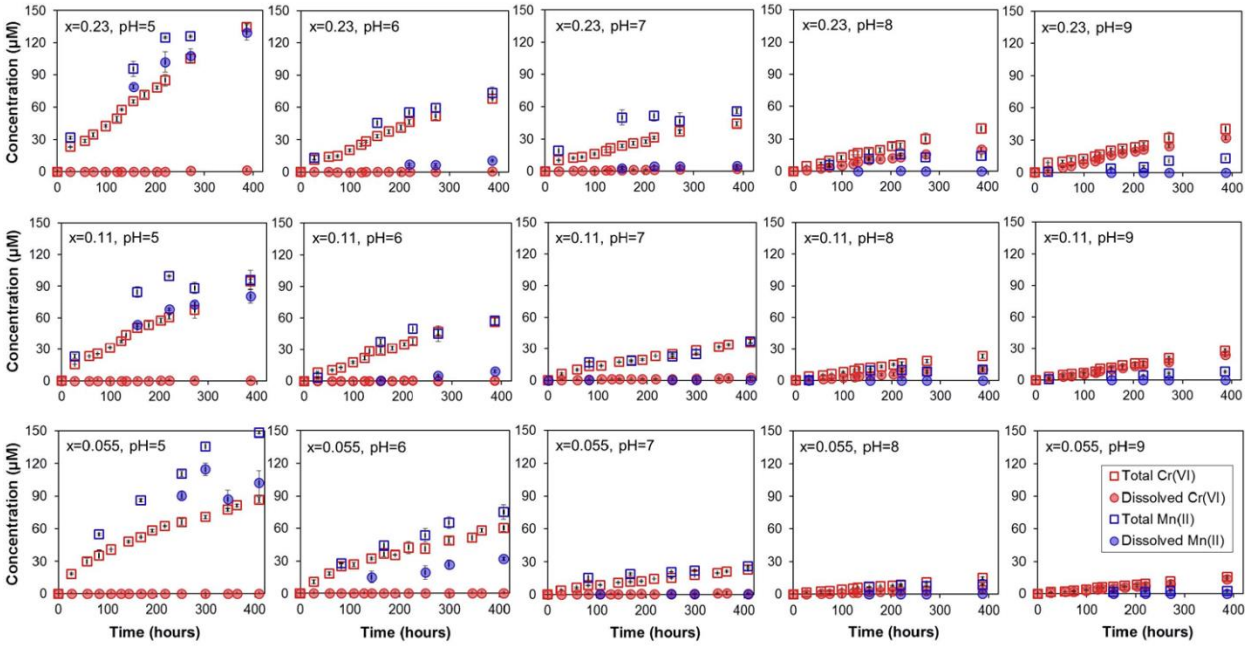

Figure 4.1. Cr(III) oxidation from $Cr_xFe_{1-x}(OH)_3$ oxidation by manganese oxide at pH values from 5 to 9 with 770 μM initial Cr(III) (40 mg/L) and 436 μM of initial MnO_2 (40 mg/L MnO_2) in the mixed suspension. In almost all cases the uncertainty estimates are smaller than the size of symbols.

At pH 9 the total Cr(VI) concentration generated from $Cr_{0.23}Fe_{0.77}(OH)_3$ can be as high as 200 μM, which would have required 600 μM MnO_2 if we assume that Mn(III) is the product of MnO_2 reduction. As there was only 436 μM MnO_2 in the initial solution, reduced Mn(II) might

have been reoxidized to Mn oxides by dissolved oxygen, which can be a fast reaction at high pH.[216, 229] Mn oxides formed in this way can continue oxidizing Cr(III).

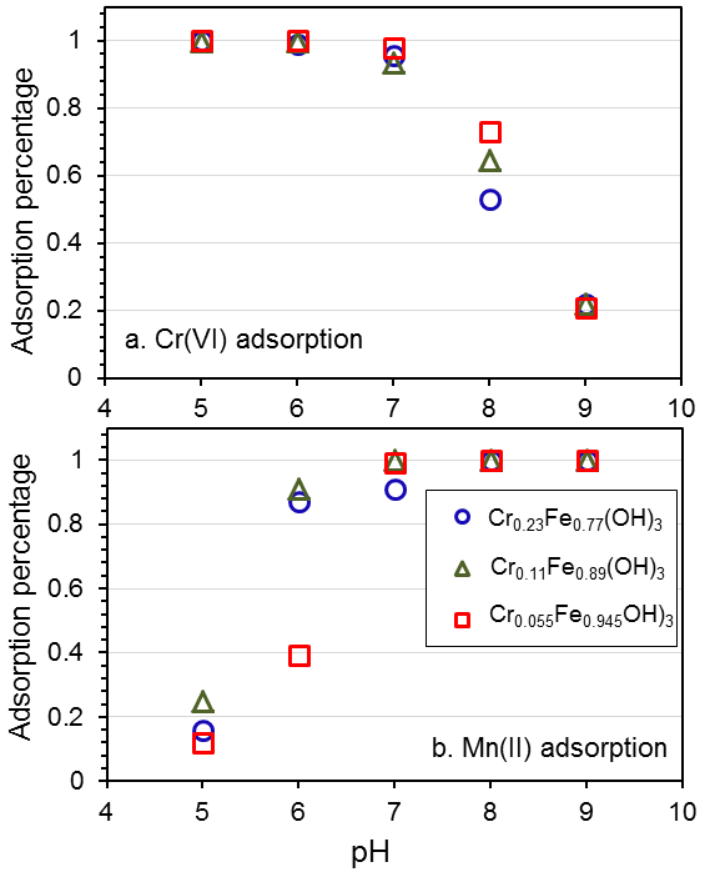

Figure 4.2. The pH dependence of adsorption of (a) Mn(II) and (b) Cr(VI) onto the solid phases in $Cr_xFe_{1-x}(OH)_3$-MnO_2 completely mixed suspensions. The percent adsorbed is calculated from measurements at each sampling event for an experiment with a mixed suspensions of 770 μM initial Cr(III) (40 mg/L) and 436 μM initial MnO_2 (40 mg/L MnO_2). Each point represents the average value of the adsorbed portion to the mixture of $Cr_xFe_{1-x}(OH)_3$ and MnO_2 at each sampling event at a determined pH and Fe/Cr value.

The interaction between δ-MnO_2 and generated Mn(II) can lead to substantial changes in MnO_2 structure, and bulk transformations are promoted by higher pH values.[211, 230, 231] In XRD patterns, the reacted solids from the $Cr_{0.23}Fe_{0.77}(OH)_3$ and MnO_2 completely mixed batch

experiments for 400 hours exhibit new characteristic peaks at 2θ values of 12.44° (d= ~7.2 Å) and 24.85 °(d= ~3.6 Å) at pH 9, which can be attributed to the (001) and (002) lattice spacings of triclinic birnessite.[232] These new diffraction peaks reflect the transformation of δ-MnO_2 layer symmetry from hexagonal to orthogonal at pH 9, consistent with prior work.[232] No observable changes in the pattern are observed at pH 5. HR-TEM images and EDS analysis of the reacted products shows that most of the solids remain poorly crystalline and aggregated at pH 5 while more crystalline MnO_2 particles appear at pH 9 (Figures S4.6 and S4.7), corresponding to the triclinic birnessite identified via XRD. The valence of Mn on the solid surface was determined directly by analyzing the solid products using XPS with a focus on Mn $2p_{3/2}$ peaks (Figure S4.8). Table S4.2 gives the relative portion of each multiplet for the surface species from the fitting in Figure S4.8 and the relative percentage of Mn(IV): Mn(III): Mn(II) at the solid surfaces are listed in Table 4.1. Mn(IV) is reduced to Mn(III) and Mn(II) during reaction with Cr(III) in iron oxides (Table 4.1). For each $Cr_xFe_{1-x}(OH)_3$, the Mn(II) percentage is higher at pH 9 than at pH 5, which is probably because of greater Mn(II) adsorption onto solid phases at pH 9.

Table 4.1. Summary of Mn oxidation state percent at the surface of the solids determined using XPS Mn $2p_{3/2}$.

Sample	Mn(IV) (%)	Mn(III) (%)	Mn(II) (%)
MnO_2 initial solids	94.9	5.1	
$Cr_{0.23}Fe_{0.77}(OH)_3$ + MnO_2, pH 5	17.8	47.3	34.9
$Cr_{0.23}Fe_{0.77}(OH)_3$ + MnO_2, pH 9	11.9	42.0	46.1
$Cr_{0.11}Fe_{0.89}(OH)_3$ + MnO_2, pH 5	23.8	48.5	27.7
$Cr_{0.11}Fe_{0.89}(OH)_3$ + MnO_2, pH 9	15.0	42.4	42.6

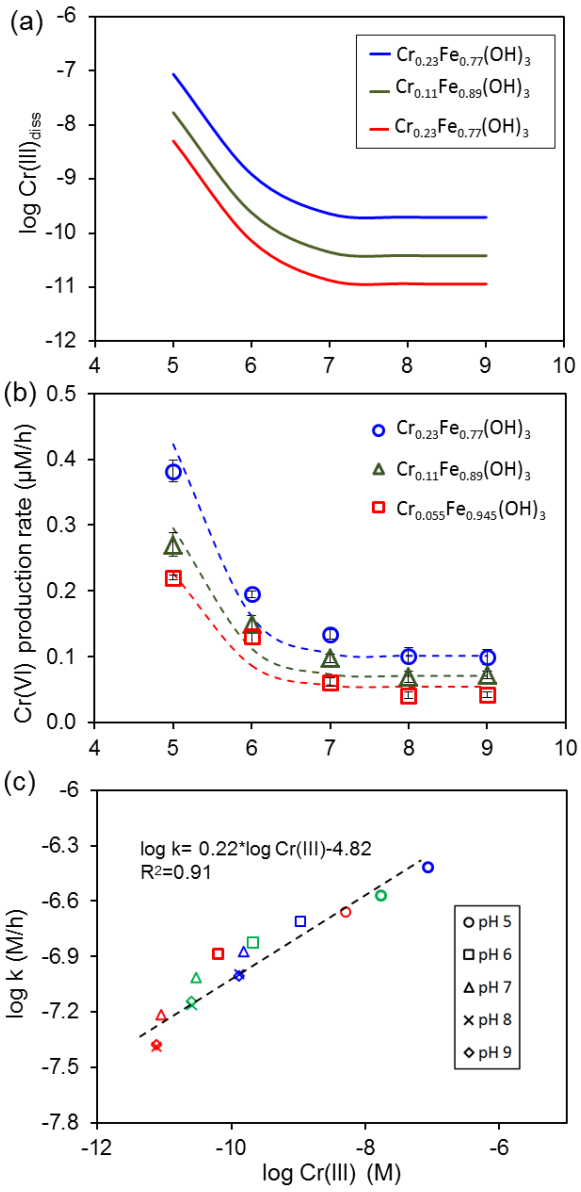

Figure 4.3. (a) Calculated Cr(III) solubility in equilibrium with $Cr_xFe_{1-x}(OH)_3$ solids as a function of pH and Fe/Cr; (b) Cr(VI) production rates calculated from Figure 4.1, the dashed lines are the predicted Cr(VI) production rates dependent on pH and Fe/Cr (equation 4.5); (c) The correlation between Cr(VI) production rates and the calculated Cr(III) solubility of different $Cr_xFe_{1-x}(OH)_3$ solids with the color of the symbols representing solids with different Fe/Cr ratios (blue, green and red symbols represent x=0.23, x=0.11 and x=0.055, respectively). $Cr(III)_0$ =770 μM (40 mg/L), MnO_2 = 436 μM (40 mg/L MnO_2)

Information about the processes controlling Cr(VI) production rates can be gained from examining the results for all three $Cr_xFe_{1-x}(OH)_3$ solids at different pH levels (Figure 4.3b). The rates of Cr(VI) production were determined from the relationship between the total Cr(VI) concentration and time (Figure 4.1). The rates were calculated by linear regression of all the data points with a least squares approach. The error bars in Figure 4.3b show the standard deviation of the rates determined from the duplicate experiments (Figure 4.1). The lower production rates of total Cr(VI) with increasing pH and increasing Fe/Cr are consistent with the chromium solubility of $Cr_xFe_{1-x}(OH)_3$ solids being lower at higher pH and when Cr(III) is more dilute within the solid phase. When the MnO_2 concentration is fixed, the rate of the Cr(VI) production exhibits a log-linear relationship to the predicted equilibrium Cr(III) concentration in the aqueous phase. As shown in Figure 4.3c, suspensions of $Cr_xFe_{1-x}(OH)_3$ and δ-MnO_2 produce Cr(VI) at a rate that can be described by

$$\frac{dCr(VI)}{dt} = k' Cr(III)_{eq,diss}^{\ n} \tag{4.5}$$

where the rate constant k′ is $1.51 \times 10^{-5}\ M^{0.78}\ h^{-1}$, the order of the reaction n is 0.22, and $Cr(III)_{eq,diss}$ is the calculated equilibrium dissolved Cr(III) concentration of $Cr_xFe_{1-x}(OH)_3$ solids (Figure 4.3a). In their study of chromite oxidation by MnO_2, Oze et al. also found that Cr(III) oxidation rates were proportional to the dissolved concentration of Cr(III) predicted from estimated Cr(III) solubility of chromite and exhibited a log-linear relationship with reaction order n close to 0.25.[204] The reaction order is similar to that determined in our study. The effect of pH and Fe/Cr ratio were fully accounted for by the calculated equilibrium dissolved Cr(III) concentration, which was directly correlated to the Cr(VI) generation rates. The model successfully predicted Cr(VI) production rates of $Cr_xFe_{1-x}(OH)_3$ solids at different pH (dash line in Figure 4.3b) based on estimated dissolved Cr(III) concentration in equilibrium with Cr_xFe_{1-}

$_x(OH)_3$. A universal correlation between Cr(VI) production rates and Cr(III) solubility suggests that Cr(III) dissolution plays an important role in Cr(VI) production from oxidation of $Cr_xFe_{1-x}(OH)_3$ solids by manganese oxides. The possibility of specific surface area (SSA) of different $Cr_xFe_{1-x}(OH)_3$ exerting an influence on the rate can be ruled out as the SSA values are similar for the Cr(III)-Fe(III) hydroxides of different Fe/Cr ratios that we used.[212] Cr(III) first dissolves from $Cr_xFe_{1-x}(OH)_3$ and then migrates to the surface of MnO_2, where it is oxidized to Cr(VI). This is consistent with the process interpreted in the previous study that Cr(III) is oxidized through a multistep process to Cr(VI) upon adsorbing to MnO_2.[204] Cr(VI) is then released to the solution and a portion of Cr(VI) can be readsorbed to the solid surfaces.

4.3.2 Role of solid-solid proximity in Cr(III) oxidation

As Cr(VI) production is not limited by the sparing solubility of Cr(III)-Fe(III) hydroxides and MnO_2, the proximity between the two minerals might play an important role in the overall reaction process. Figure 4.4 compares $Cr_{0.23}Fe_{0.77}(OH)_3$ oxidation by MnO_2 at pH 8 in the completely mixed batch with multichamber experiments at the same condition. The rate of Cr(VI) production in the multichamber experiment was much lower than in the completely mixed batch experiment. The difference demonstrates the importance of solid-solid contact or proximity on $Cr_xFe_{1-x}(OH)_3$-MnO_2 interactions. In mixed batch experiments, Cr(VI) production rate was high and not limited by the sparing Cr(III) solubility of $Cr_{0.23}Fe_{0.77}(OH)_3$ and Mn(III)/Mn(IV) of MnO_2. In contrast, the concentration of the total Cr(VI) produced in the multichamber experiment was measureable but below 1 μM even after 400 hours (Figure 4.4 and Figure S4.9). The average Cr(VI) production rate in multichamber reactor is only 1.1×10^{-3} μM/h, 90 times lower than the 0.10 μM/h in well mixed batch experiment. Similarly, for another poorly soluble mineral UO_2 which is a reductive remediation product of uranium, Wang et al. used

multichamber reactor experiments to show that the effective redox interaction between UO_2 and MnO_2 requires proximity of the two dissimilar solids.[206] Plathe et al. found that UO_2 oxidation by MnO_2 needed proximity between the two solids phases as U(IV) oxidation by O_2 was not enhanced by manganese oxides in a porous medium with spatially separated UO_2 and MnO_2 solids in contrast to significant enhancement in completely mixed experiments.[233]

In the multichamber experiments, Cr(III) dissolved from $Cr_{0.23}Fe_{0.77}(OH)_3$, diffused across the membrane and was oxidized in the MnO_2 chamber. Mn(III, IV) intermediates could not persist at an appreciable concentration without the presence of ligands and thus could not transport oxidized forms of Mn to the $Cr_xFe_{1-x}(OH)_3$ chamber. The dissolved Mn concentration in the water chamber of a MnO_2||water control experiment was extremely low and oxidized Mn species were not the soluble intermediate involved in the redox reaction between the two solids. After the Cr(III) was oxidized by the MnO_2 in the MnO_2 chamber, the released Cr(VI) could then diffuse back to the $Cr_xFe_{1-x}(OH)_3$ chamber and adsorb onto the surface of $Cr_{0.23}Fe_{0.77}(OH)_3$ solids. Consistent with a flux of Cr(VI) from the MnO_2 chamber to the $Cr_xFe_{1-x}(OH)_3$ chamber, the dissolved Cr(VI) concentration in the MnO_2 chamber was higher than that in the $Cr_{0.23}Fe_{0.77}(OH)_3$ chamber (Figure S4.9). Because of the low Cr(III) solubility of $Cr_{0.23}Fe_{0.77}(OH)_3$, the driving force for Cr(III) transport across the membrane was small. As a result, $Cr_xFe_{1-x}(OH)_3$ dissolution and Cr(III) transport were the rate-limiting steps for Cr(III) oxidation in the multichamber experiment. In contrast, Cr(III) transport did not limit the oxidation process in completely mixed suspensions since Cr(III) released from solids can move very quickly to the surface of a MnO_2 particle by advection in the completely-mixed suspensions.

Based on the observations that Cr(III) oxidation rates were proportional to the expected Cr(III) solubility of Fe-Cr solids and that proximity of $Cr_xFe_{1-x}(OH)_3$ and MnO_2 is important for

Cr(VI) genesis, we deduce that the overall reaction proceeds as follows. First, Cr(III) dissolves from the solid and transports to the surface of $Cr_xFe_{1-x}(OH)_3$ particles by advection or diffusion. Because Cr(III) can be consumed by oxidation to Cr(VI) when MnO_2 is present, a driving force for Cr(III) transport from the surface and continuing $Cr_xFe_{1-x}(OH)_3$ dissolution is maintained. Second, there were no diffusive transport limitation for soluble Cr(III) to reach the MnO_2 surface when mixing of solid particles. Third, upon adsorbing to MnO_2, Cr(III) is oxidized through a multistep process to Cr(VI). Finally, the Cr(VI) is released to the aqueous phase with some readsorbing to the $Cr_xFe_{1-x}(OH)_3$ solids depending on the particular pH.

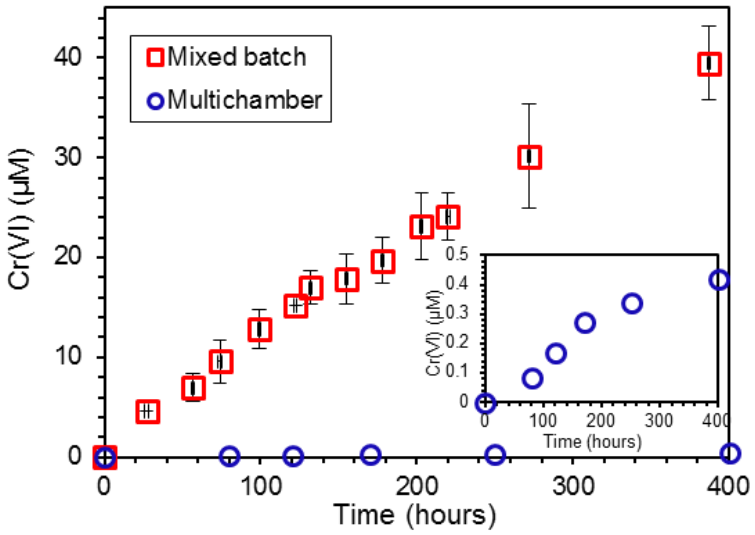

Figure 4.4. Cr(VI) production from $Cr_{0.23}Fe_{0.77}(OH)_3$-MnO_2 reaction in a multichamber or completely mixed batch experiment. For multichamber experiments, $Cr(III)_0$ = 1440 μM (80 mg/L) in the chromium chamber and MnO_2 = 872 μM (80 mg/L MnO_2) in the MnO_2 chamber. These concentrations are twice as high as in the completely mixed experiments so that the overall the Mn and Cr concentration are the same for multichamber and completely mixed experiments. Inset shows the Cr(VI) concentrations in the multichamber experiment in a narrower y-axis range.

4.4 Environmental Implication

In this study we established a quantitative relationship between Cr(VI) production rates and Cr(III) solubility of $Cr_xFe_{1-x}(OH)_3$ upon reaction of $Cr_xFe_{1-x}(OH)_3$ with δ-MnO_2 in well-mixed systems. This relationship enables predictions of Cr(VI) production rates at different pH and Fe/Cr ratios. Cr(III) dissolves from $Cr_xFe_{1-x}(OH)_3$ and transfers to the surface of MnO_2 where it is oxidized to Cr(VI) and is subsequently released to solution or adsorbed onto the $Cr_xFe_{1-x}(OH)_3$. Dissolved Cr(VI) at pH 9 is much higher than at pH 5 after reaction of $Cr_xFe_{1-x}(OH)_3$ with MnO_2 because less Cr(VI) adsorbs at higher pH. However, the desorption of Cr(VI) in the presence of natural water with competing adsorbates (e.g. phosphate) might lead to overall higher Cr(VI) release at lower pH. Thus it is important to study both dissolved Cr(VI) and total Cr(VI) in $Cr_xFe_{1-x}(OH)_3$ and MnO_2 systems, which could improve predictions of the concentration of Cr(VI) released into water. The systematic study of dissolved and total Cr(VI) generation at different pH and Fe/Cr ratios is helpful for predicting Cr(VI) release in natural environments when Cr(III)-containing solids are disposed above ground in waste piles or below ground.[234, 235] As $Cr_xFe_{1-x}(OH)_3$ solids with higher Fe/Cr ratio are less susceptible to oxidation by MnO_2, higher iron dosages in coagulation-based Cr treatments would yield more stable products.

Our findings clarify the important role of proximity between $Cr_xFe_{1-x}(OH)_3$ and MnO_2 in the rate of Cr(VI) generation. In subsurface environments, if the two solids are physically separated, then $Cr_xFe_{1-x}(OH)_3$ dissolution rates will be quite slow and Cr(VI) genesis rates are far less than when the two solids are mixed. Thus, Cr(VI) release rate predictions need to consider whether there is proximity between the $Cr_xFe_{1-x}(OH)_3$ and MnO_2, especially with respect to whether particle-associated chromium could be transported to enable contact with MnO_2. MnO_2 might also be formed in close proximity with Cr(III)-containing solid surfaces through biotic or

abiotic Mn(II) oxidation by dissolved oxygen. The resulting MnO_2 would be a more potent oxidant of the Cr(III) in the solid than would be the dissolved oxygen. Therefore, when we consider options for Cr(III)-containing waste disposal we should avoid soils or groundwater that contain substantial manganese oxides.

Acknowledgements

This research was supported by the U.S. National Science Foundation (CBET 1335613). C.P. acknowledges financial support from school of Engineering Applied Science in Washington University in St. Louis for a first year Ph.D. fellowship. We thank Dr. Wenlu Li for the help with TEM analysis for solid samples. We appreciate the comments of four anonymous reviewers whose perspectives helped us improve the presentation and interpretation of our study.

Chapter 4. Supporting Information

Additional information regarding the δ-MnO_2 dissolution, XRD patterns and TEM images of initial solids, $Cr_{0.11}Fe_{0.89}(OH)_3$ and $Cr_{0.055}Fe_{0.945}(OH)_3$ oxidation by manganese oxide, comparison of $Cr(OH)_3$ and $Cr_{0.23}Fe_{0.77}(OH)_3$ oxidation by MnO_2, pH-dependence of Cr(VI) and Mn(II) adsorption, zeta potential of initial solids, calculated Cr(III) solubility of Cr_xFe_{1-x} $(OH)_3$, Cr(VI) and Mn concentrations in $Cr_{0.23}Fe_{0.77}(OH)_3$-MnO_2 multichamber experiments, HR-TEM images of the solid product and their EDS results, and XPS results of reacted solid products are provided in the supplementary documents.

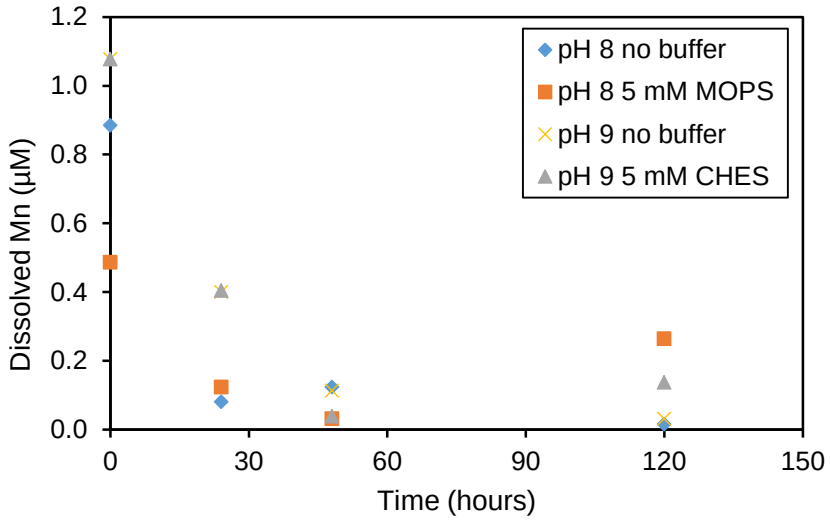

Figure S4.1. *δ*-MnO_2 dissolution at pH 8 and pH 9 with or without buffer. MnO_2 = 436 μM, I = 5 mM with NaCl as background electrolyte.

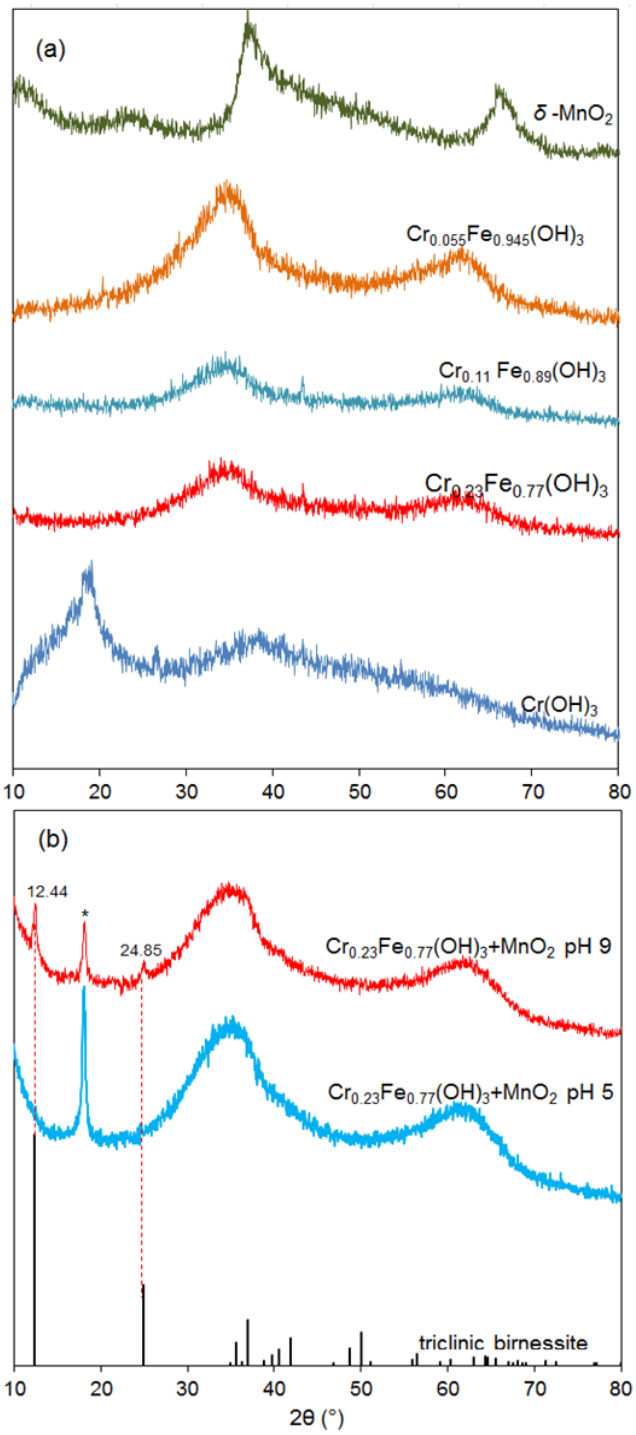

Figure S4.2. X-ray diffraction patterns of (a) initial MnO_2 and $Cr_xFe_{1-x}(OH)_3$ solids (b) reaction products of MnO_2 and $Cr_{0.23}Fe_{0.77}(OH)_3$ after 400 hours at pH 5 and pH 9. The reference pattern for triclinic birnessite[236] is included for comparison. The asterisk (*) indicates the diffraction features from PTFE abraded from the stir bar.[237]

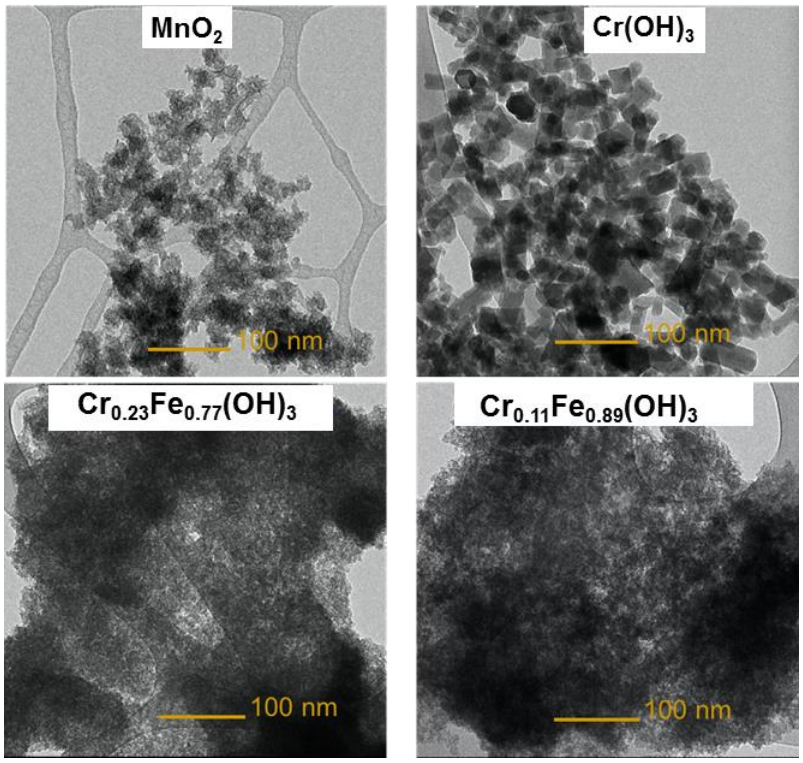

Figure S4.3. Transmission electron microscographs of initial solids

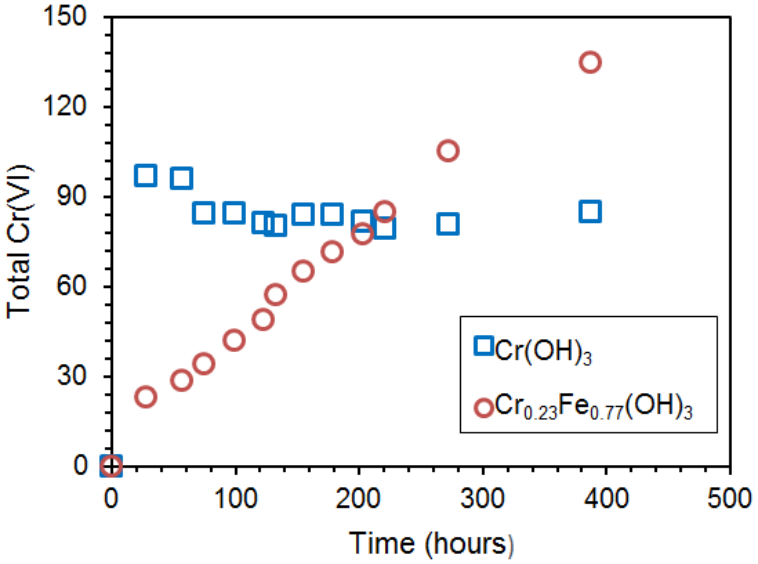

Figure S4.4. Total Cr(VI) concentration from $Cr(OH)_3$ and $Cr_{0.23}Fe_{0.77}(OH)_3$ oxidation by MnO_2 at pH 5 with 770 μM initial Cr(III) (40 mg/L) and 436 μM of initial MnO_2 (40 mg/L MnO_2) in the mixed suspension for both experiments.

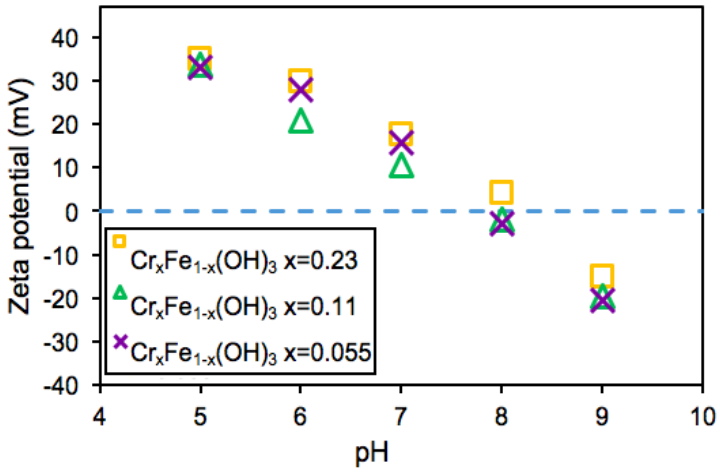

Figure S4.5. Zeta potential of $Cr_xFe_{1-x}(OH)_3$ initial solids. For comparison with the zeta potential of the Cr-containing solids, the zeta potential of the MnO_2 is -54 mV at pH 8.

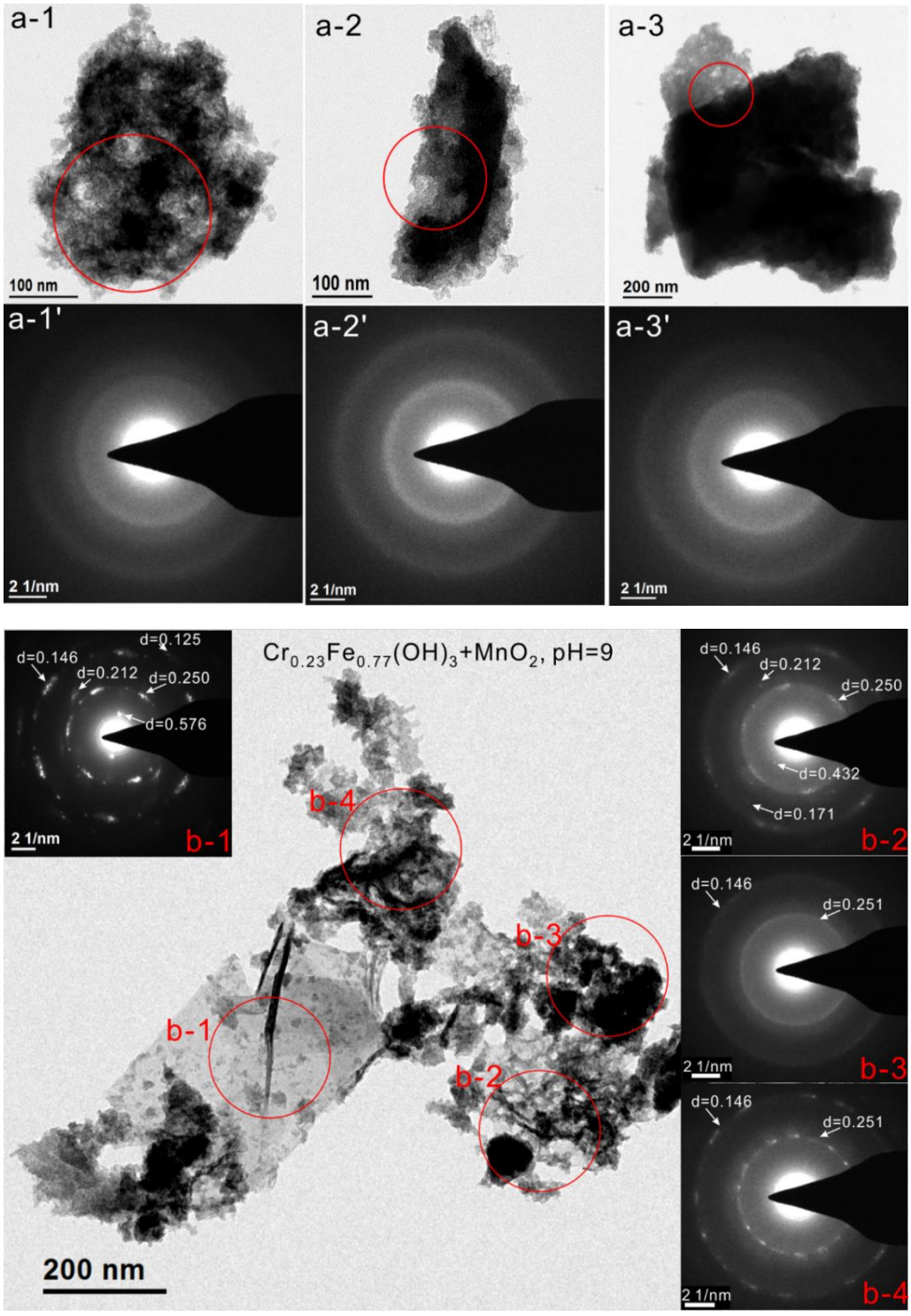

Figure S4.6. TEM images and SAED patterns of the solid products of MnO_2 and $Cr_{0.23}Fe_{0.77}(OH)_3$ reacted for 400 hours at pH 5 (a) and pH 9 (b). The red circles refer to the areas for SAED patterns.

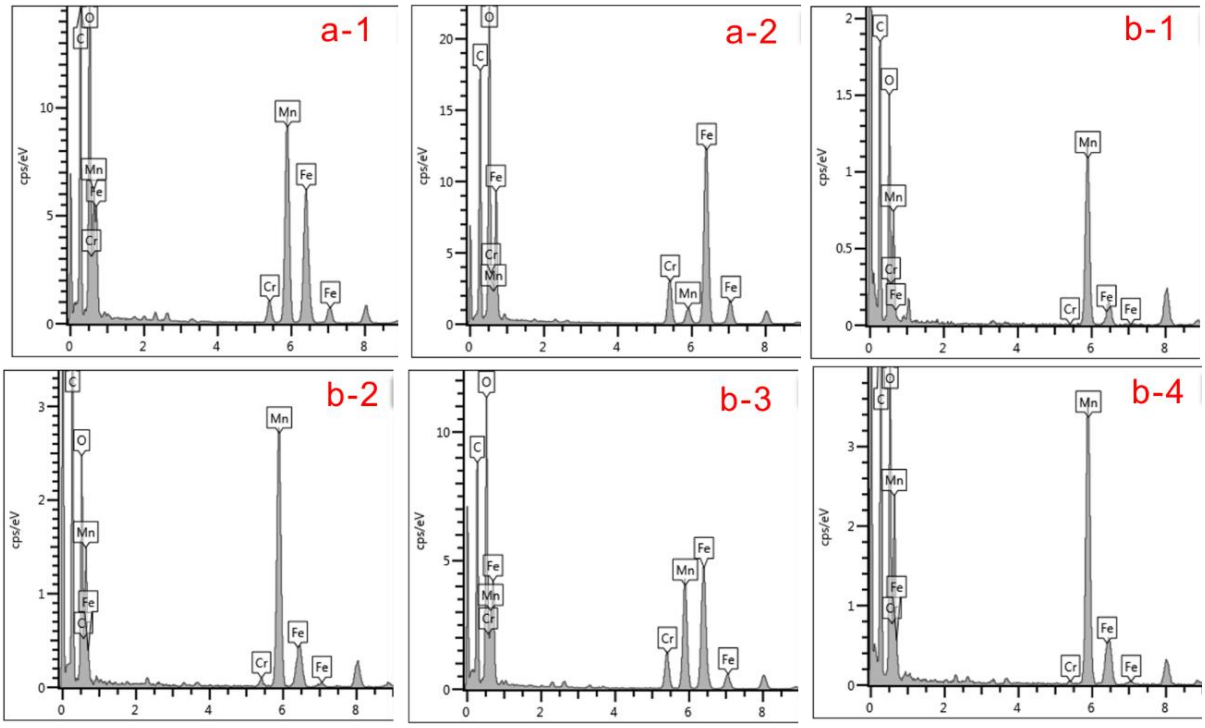

Figure S4.7. EDS results of reacted solid products. The analyzed areas are the same as the labeled circles in Figure S4.6.

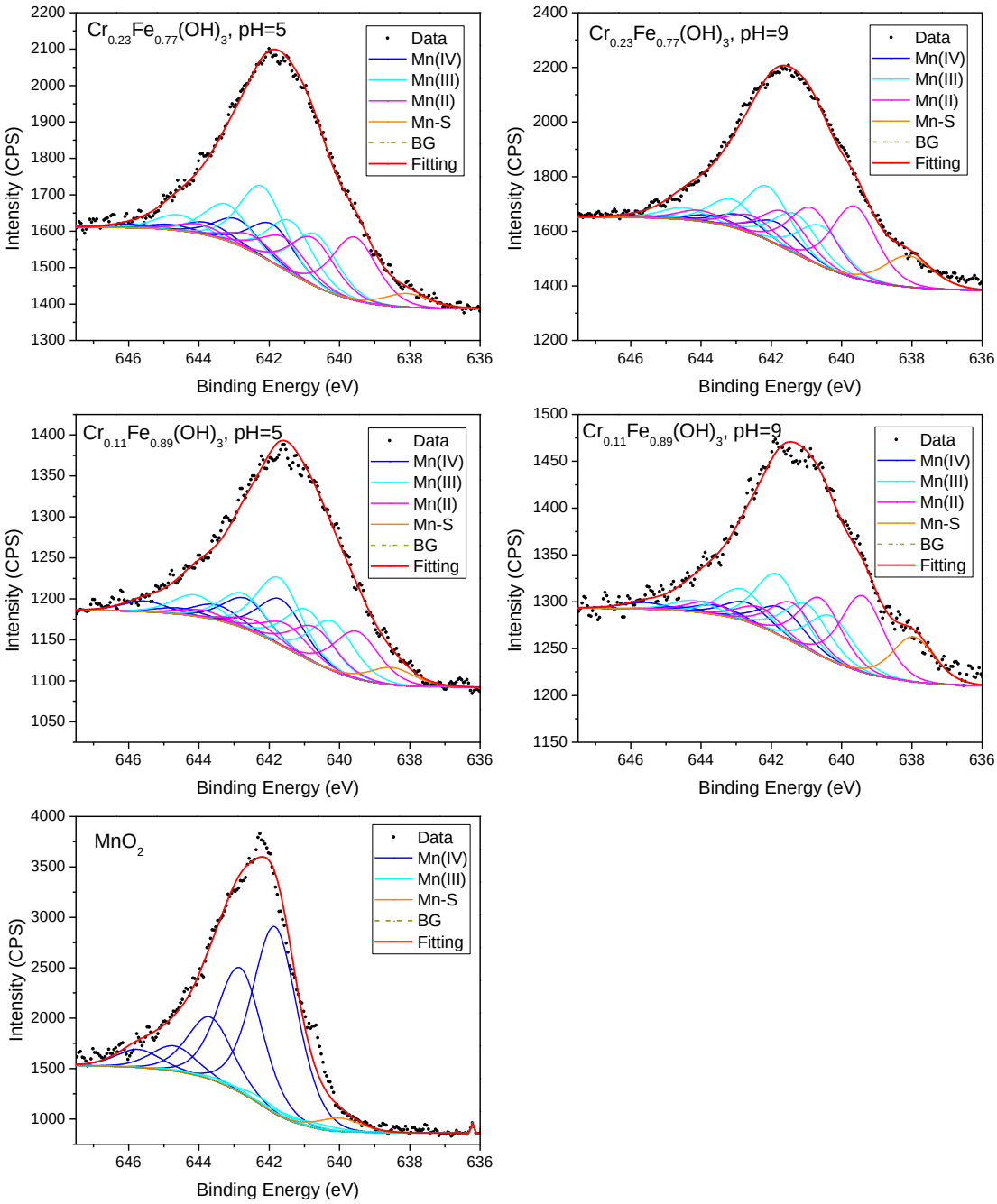

Figure S4.8. XPS spectra of Mn $2p_{3/2}$ photoelectron lines for the solid product and initial MnO_2

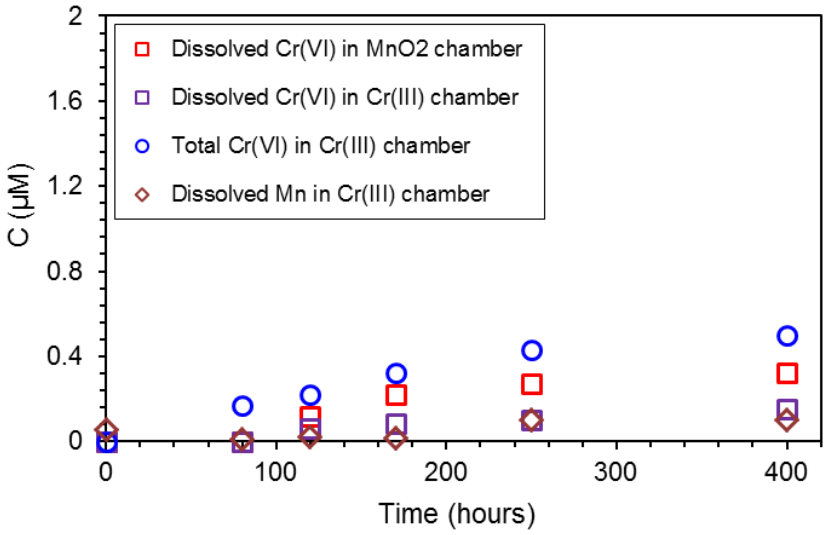

Figure S4.9. Cr(VI) and Mn(II) concentrations in $Cr_{0.23}Fe_{0.77}(OH)_3||MnO_2$ multichamber experiments. $Cr(III)_0$ = 1440 μM (80 mg/L) in the chromium chamber and MnO_2 = 872 μM (80 mg/L MnO_2) in the MnO_2 chamber, pH=8 with 5mM MOPS as buffers and NaCl as background electrolyte.

A general relationship [log ($CrOH^{2+}$) = -2pH + 4.18 + $0.28(1-x)^2$-$1.79(1-x)^3$ + log x] was used to calculate the Cr concentrations in solution between pH 2 and pH 6 that are in equilibrium with CrxFe1-x(OH)3 ($x \leq 0.69$).[198] As CrOH2+ is the dominant species at pH ≤ 6, total dissolved Cr(III) concentrations including CrOH2+, Cr(OH)2+, Cr(OH)3(aq) and Cr(OH)4- in equilibrium with CrxFe1-x(OH)3 were calculated to cover dissolved Cr(III) concentrations from pH 5 to pH 9 by accounting for these additional dissolved Cr(III) species above pH 6. The concentrations of Cr(OH)2+, Cr(OH)3(aq) and Cr(OH)4- were calculated according to equilibrium constants from Rai et al.[225]

Table S4.1. Dissolved Cr(III) speciation and concentration in equilibrium with $Cr_xFe_{1-x}(OH)_3$ solids

Cr(III) species (M)	pH 5	pH 6	pH 7	pH 8	pH 9
log $CrOH^{2+}$ in $Cr_{0.23}Fe_{0.77}(OH)_3$ [a]	-7.11	-9.11	-11.11	-13.11	-15.11
log $CrOH^{2+}$ in $Cr_{0.11}Fe_{0.89}(OH)_3$	-7.82	-9.82	-11.82	-13.82	-15.82
log $CrOH^{2+}$ in $Cr_{0.055}Fe_{0.945}(OH)_3$	-8.34	-10.34	-12.34	-14.34	-16.34
log $Cr(III)_{diss}$ in $Cr_{0.23}Fe_{0.77}(OH)_3$ [b]	-7.07	-8.91	-9.64	-9.70	-9.71
log $Cr(III)_{diss}$ in $Cr_{0.11}Fe_{0.89}(OH)_3$	-7.77	-9.62	-10.35	-10.41	-10.42
log $Cr(III)_{diss}$ in $Cr_{0.055}Fe_{0.945}(OH)_3$	-8.30	-10.14	-10.87	-10.93	-10.94
dominant species	$CrOH^{2+}$	$CrOH^{2+}$	$Cr(OH)_{3(aq)}$	$Cr(OH)_{3(aq)}$	$Cr(OH)_{3(aq)}$

a. The calculated logarithm of the $CrOH^{2+}$ concentration (M) in equilibrium with $Cr_xFe_{1-x}(OH)_3$

b. The calculated logarithm of the total dissolved Cr(III) concentration (M) in equilibrium with $Cr_xFe_{1-x}(OH)_3$

Table S4.2. Binding energies (BE) of surface Mn species for fitting the $Mn_{2p3/2}$peak of the solid product and the relative area of each multiplet for the surface species (All peaks were modeled as 50% Gaussian-50% Lorentzian)

Initial MnO_2

surface species	BE (eV)	FWHM (eV)	Percent (%)
Mn(IV)-O multiplet 1	641.83	1.5	42.5
Mn(IV)-O multiplet 2	642.83	1.5	28.4
Mn(IV)-O multiplet 3	643.68	1.5	14.2
Mn(IV)-O multiplet 4	644.71	1.5	5.7
Mn(IV)-O multiplet 5	645.73	1.5	4.1
Mn(IV)-O overall: 94.9 (%)			
Mn(III)-O multiplet 1	640.70	1.5	1.2
Mn(III)-O multiplet 2	641.40	1.5	1.2
Mn(III)-O multiplet 3	642.21	1.5	1.6
Mn(III)-O multiplet 4	643.23	1.5	0.8
Mn(III)-O multiplet 5	644.60	1.5	0.3
Mn(III)-O overall: 5.1 (%)			

$Cr_{0.23}Fe_{0.77}(OH)_3$ +MnO_2 pH=5

surface species	BE(eV)	FWHM(eV)	Percent (%)
Mn(IV)-O multiplet 1	641.90	1.5	8.0
Mn(IV)-O multiplet 2	642.90	1.5	5.3
Mn(IV)-O multiplet 3	643.75	1.5	2.7
Mn(IV)-O multiplet 4	644.78	1.5	1.1
Mn(IV)-O multiplet 5	645.80	1.5	0.8
Mn(IV)-O overall: 17.8 (%)			
Mn(III)-O multiplet 1	640.68	1.5	10.9
Mn(III)-O multiplet 2	641.38	1.5	10.9
Mn(III)-O multiplet 3	642.19	1.5	14.7
Mn(III)-O multiplet 4	643.21	1.5	7.6
Mn(III)-O multiplet 5	644.58	1.5	3.3
Mn(III)-O overall: 47.3 (%)			
Mn(II)-O multiplet 1	639.57	1.5	13.1
Mn(II)-O multiplet 2	640.77	1.5	9.9
Mn(II)-O multiplet 3	641.57	1.5	6.7
Mn(II)-O multiplet 4	642.47	1.5	3.3
Mn(II)-O multiplet 5	643.97	1.5	2.0
Mn(II)-O overall: 34.9 (%)			

$Cr_{0.23}Fe_{0.77}(OH)_3 + MnO_2 + MnO_2$ pH=9

surface species	BE (eV)	FWHM (eV)	Percent (%)
Mn(IV)-O multiplet 1	641.85	1.5	5.3
Mn(IV)-O multiplet 2	642.85	1.5	3.6
Mn(IV)-O multiplet 3	643.70	1.5	1.8
Mn(IV)-O multiplet 4	644.73	1.5	0.7
Mn(IV)-O multiplet 5	645.75	1.5	0.5
Mn(IV)-O overall: 11.9 (%)			
Mn(III)-O multiplet 1	640.59	1.5	9.7
Mn(III)-O multiplet 2	641.29	1.5	9.6
Mn(III)-O multiplet 3	642.10	1.5	13.0
Mn(III)-O multiplet 4	643.12	1.5	6.8
Mn(III)-O multiplet 5	644.49	1.5	2.9
Mn(III)-O overall: 42.0 (%)			
Mn(II)-O multiplet 1	639.63	1.5	17.3
Mn(II)-O multiplet 2	640.83	1.5	13.0
Mn(II)-O multiplet 3	641.63	1.5	8.8
Mn(II)-O multiplet 4	642.53	1.5	4.4
Mn(II)-O multiplet 5	644.03	1.5	2.6
Mn(II)-O overall: 46.1 (%)			

$Cr_{0.11}Fe_{0.89}(OH)_3 + MnO_2$ pH=5

surface species	BE (eV)	FWHM (eV)	Percent (%)
Mn(IV)-O multiplet 1	641.66	1.5	10.1
Mn(IV)-O multiplet 2	642.66	1.5	6.7
Mn(IV)-O multiplet 3	643.51	1.5	3.4
Mn(IV)-O multiplet 4	644.54	1.5	1.4
Mn(IV)-O multiplet 5	645.56	1.5	2.3
Mn(IV)-O overall: 23.8 (%)			
Mn(III)-O multiplet 1	640.21	1.5	10.8
Mn(III)-O multiplet 2	640.91	1.5	10.8
Mn(III)-O multiplet 3	641.72	1.5	14.6
Mn(III)-O multiplet 4	642.74	1.5	7.6
Mn(III)-O multiplet 5	644.11	1.5	4.7
Mn(III)-O overall: 48.5 (%)			
Mn(II)-O multiplet 1	639.51	1.5	10.4
Mn(II)-O multiplet 2	640.71	1.5	7.8
Mn(II)-O multiplet 3	641.51	1.5	5.3
Mn(II)-O multiplet 4	642.41	1.5	2.6
Mn(II)-O multiplet 5	643.91	1.5	1.6
Mn(II)-O overall: 27.7 (%)			

$Cr_{0.11}Fe_{0.89}(OH)_3 + MnO_2$ pH=9

surface species	BE (eV)	FWHM (eV)	Percent (%)
Mn(IV)-O multiplet 1	641.70	1.5	6.3
Mn(IV)-O multiplet 2	642.70	1.5	4.2
Mn(IV)-O multiplet 3	643.55	1.5	2.1
Mn(IV)-O multiplet 4	644.58	1.5	0.9
Mn(IV)-O multiplet 5	645.60	1.5	1.5
Mn(IV)-O overall: 15.0 (%)			
Mn(III)-O multiplet 1	640.30	1.5	9.9
Mn(III)-O multiplet 2	641.00	1.5	9.9
Mn(III)-O multiplet 3	641.81	1.5	13.3
Mn(III)-O multiplet 4	642.83	1.5	6.9
Mn(III)-O multiplet 5	644.20	1.5	2.5
Mn(III)-O overall: 42.4 (%)			
Mn(II)-O multiplet 1	639.40	1.5	16.0
Mn(II)-O multiplet 2	640.60	1.5	12.0
Mn(II)-O multiplet 3	641.40	1.5	8.1
Mn(II)-O multiplet 4	642.30	1.5	4.0
Mn(II)-O multiplet 5	643.80	1.5	2.4
Mn(II)-O overall: 42.6 (%)			

Chapter 5. Understanding the Role of Dissolution and Diffusion in $Cr(OH)_3$ Oxidation by δ-MnO_2

This chapter was a manuscript in preparation for submission to ACS Earth and Space Chemistry.

Abstract

Manganese oxides are the major oxidants of Cr(III) to Cr(VI) in natural environments. This study evaluated the rate and extent of Cr(III) oxidation from $Cr(OH)_3$ by δ-MnO_2 from pH 5 to pH 9, with a particular focus on quantify the rate constant of Cr(III) oxidation on MnO_2 surface at pH 5. Cr(III) oxidation was initially fast, but it then slowed and ceased for pH 5 to pH 7, which agrees with previously reported inhibition of the redox reaction above pH 4 by precipitation of Cr(III) on MnO_2 surface. Above pH 7, Cr(VI) production was higher than at lower pH even though the dissolved Cr(III) concentration in equilibrium with $Cr(OH)_3$ decreased with increasing pH, probably due to the generated Mn(II) being reoxidized by dissolved oxygen. Manganese oxides are finally reduced to feitknechtite at high pH. Multichamber experiments were used to assess the role of solid-solid proximity in $Cr(OH)_3$-MnO_2 interactions. At pH 5, the rates of aqueous Cr(III) oxidation by manganese oxides were calculated by optimizing the fit of data on Cr(VI) concentrations to a model for the multichamber experiments. The model could also predict Cr(VI) release in completely mixed batch experiments. The Cr(VI) production conditions in multichamber reactor and completely mixed batch reactor at different pH suggests that mixing of $Cr(OH)_3$ and MnO_2 solids play a more important role for Cr(VI) generation when dissolved Cr(III) concentration is low, as the transport of Cr(III) through solution would not be

limited by diffusion in completely mixed batch experiments due to either close approaches of the two solutes or convective transport of soluble Cr(III) to MnO_2 surfaces.

5.1 Introduction

Chromium (Cr) is widespread in soils, sediments and water from natural and anthropogenic sources. The predominant species of Cr in aquatic and soil environments are Cr(III) and Cr(VI), with Cr(III) being less mobile and less toxic.[238] The chromium content of natural solids varies widely with the type and nature of rocks or sediments, with highest chromium contents associated with finest particles in soils and sediments.[11] Cr is generally present in the +III oxidation state in these solids.[239, 240] In natural waters, the range of chromium concentration is large and dissolved chromium concentration has been observed as high as 4 μmol/L, around twice of maximum contaminant level goals in drinking water set by EPA, which is 100 μg/L (1.92 μM). These high chromium concentration in natural waters are mostly Cr(VI), which are more soluble than Cr(III) species.[11] Much higher Cr(VI) concentrations are found in groundwater that has been contaminated by human activities.[240]

Manganese oxides, which are ubiquitous in soils, can rapidly oxidize Cr(III) to Cr(VI).[241-243] They provide the major geochemical pathway for Cr(VI) occurrence from Cr(III) in groundwater, soils or subseafloor environments.[52, 53] Manganese oxides are believed to form primarily by Mn(II) oxidation via either direct or indirect microbial activity.[47] The predominant type of biogenic manganese oxides formed at circumneutral pH are highly disordered and nanocrystalline phases, similar to hexagonal birnessite (its synthetic analogue is δ-MnO_2).[47, 50, 244-246] Several studies have investigated the kinetics of Cr(III) oxidation by various manganese oxides.[199, 201, 204, 247, 248] X-ray absorption spectroscopy (XAS) and X-ray photoelectron

spectroscopy (XPS) have indicated that Cr(III) aqueous ions first diffuse towards Mn(IV) vacancies in the sheet of MnO_6 octahedra; the coupled Cr(III) oxidation/ Mn(IV) reduction occurs through one-electron-transfer reactions and the Cr(VI) produced is then released into solution.[226, 249] However, a sharp rate decline and cessation of the reaction followed the initially fast Cr(VI) generation from $Cr(OH)_3$ oxidation by manganese oxides, and this decline is due to the formation of a $Cr(OH)_3$ precipitate on δ-MnO_2.[203, 205] The initial rates of Cr(III) oxidation on the MnO_2 surface notably depend on pH, temperature, and Cr(III) and manganese concentrations.[203, 250-253] However, most studies have focused on the Cr(III) oxidation kinetics at low pH and total Cr(VI) concentrations were not usually measured during the reaction processes.

The objectives of this study were to investigate the rates and mechanism of Cr(VI) production from $Cr(OH)_3$ oxidation by δ-MnO_2 as a function of pH and to identify the final Mn-containing oxide products. Total Cr(VI) concentration including adsorbed Cr(VI) on solid surface and dissolved Cr(VI) in solution were both measured. Multichamber experiments were operated to test the role of mixing of $Cr(OH)_3$ and MnO_2 solids in the Cr(VI) production. The reaction products were characterized by high-resolution transmission electron microscopy (HRTEM), X-ray diffraction (XRD) and X-ray photoelectron spectroscopy (XPS).

5.2 Materials and Methods

5.2.1 Materials

Ultrapure water (resistivity > 18.2 MΩ-cm) was used for the experiments, and the chemicals used were analytical reagents of high purity. At pH 5 and pH 6, no buffer was added to the reactors and the pH was maintained by NaOH or HCl additions. At pH 7 and pH 8, the pH of the suspensions was buffered by 5 mM 3-(N-morpholino) propanesulfonic acid (MOPS,

pKa=7.2). At pH 9, 5 mM N-cyclohexyl-2-aminoethanesulfonic acid (CHES, pKa=9.3) was used. The pH buffers and their concentrations were chosen because of their minimal formation of complexes with Cr(III) and their stability against oxidation by MnO_2.[62, 206, 207] NaCl was added to provide 5 mM ionic strength as the background electrolyte because Na^+ and Cl^- do not interfere with the chemistry of Cr(III) oxidation.

5.2.2 Mineral synthesis

Synthetic δ-MnO_2 was prepared by reacting $KMnO_4$ with $MnCl_2$ at a basic pH following the method described by Villalobos et al.[50] XRD confirmed that the solid was δ-MnO_2, and TEM provided evidence of δ-MnO_2 morphology and sizes as we have presented previously.[247] $Cr(OH)_3$(s) was synthesized by titrating $CrCl_3$ solutions with NaOH solution to pH 7 and maintaining the pH for 24 hours.[229, 247] The suspension was then washed five times with ultrapure water, and the supernatant was discarded after centrifugation. The final chromium concentration of $Cr(OH)_3$(s) suspension was measured by inductively coupled plasma-mass spectroscopy (ICP-MS, PerkinElmer ELAN DRC II) after nitric acid digestion. $Cr(OH)_3$ exist as crystalline solid ($Cr(OH)_3$ $3H_2O$) in suspension and it almost entirely converted to amorphous $Cr(OH)_3$ upon drying,[197] which explains the broad humps in XRD pattern in Figure 5.5. The solubility of crystalline solid $Cr(OH)_3$ is actually greater than its amorphous form.[225] The $Cr(OH)_3$ stock solution was sonicated for 5 minutes before use in experiments to disperse the particles before they were added to the reactors.

5.2.3 Mixed batch experiments and multichamber reactor

Completely mixed batch experiments were conducted in glass beakers filled with ultrapure water, 5 mM NaCl, a pH buffer, MnO_2 suspension, and $Cr(OH)_3$ suspensions with 40

mg/L (770 μM) initial Cr(III) concentration to a total volume of 1 L. Multichamber experiments were used to assess the role of mixing and solid-solid contact in $Cr(OH)_3$-MnO_2 interactions. The reactor was the same as described in our group's previous work (Figure S5.1).[206, 247] Briefly, a dialysis membrane with a molecular weight cut off (MWCO) of 3500 divided the reactor into two 110-mL chambers, eliminating the direct contact of the $Cr(OH)_3$ and MnO_2 solids but allowing dissolved species to diffuse across the membrane with a flux due to concentration difference. The suspensions were completely mixed in each chamber. For both completely mixed batch experiments and multichamber experiments, samples were periodically collected and a portion of them were filtered with 0.05 μm polyethersulfone (PES) syringe filters (Tisch Environmental, OH) for dissolved chromium, dissolved Cr(VI), and dissolved manganese analysis. The remaining portions of the unfiltered samples were used for total Cr(VI) and total Mn(II) analysis. Experiments were performed under the ambient laboratory atmosphere for both completely mixed batch experiments and multichamber experiments.

5.2.4 Aqueous and solid phase analysis

Total and dissolved Cr, Fe and Mn concentrations were measured by ICP-MS (PerkinElmer ELAN DRC II). The instrument detection limits for Cr, Fe and Mn were 0.2 μg/L (0.0039 μM), 0.1 mg/L (1.8 μM) and 0.5 μg/L (0.009 μM), respectively. The samples for measuring dissolved Cr(VI) and dissolved Mn(II) were filtered and then measured by the diphenylcarbazide method and ICP-MS, respectively. Dissolved Mn(II) concentrations were assumed to equal the total dissolved Mn concentration because both Mn(IV) and Mn(III) are sparingly soluble.[216] Cr(VI) concentrations in the samples were determined spectrophotometrically (PerkinElmer-Lambda XLS) after reacting with diphenylcarbazide.[215] The detection limit for Cr(VI) by this method was 5 μg/L (0.096 μM). Total Cr(VI) and total

Mn(II), including adsorbed species, were measured the same way as dissolved Cr(VI) and Mn(II) after extracting the surface-associated species into the solution. For total Cr(VI) concentration, adsorbed Cr(VI) was extracted by providing a 10 mM phosphate concentration in the suspension to displace adsorbed Cr(VI); the Cr(VI) was then measured by the diphenylcarbzide method. The efficiency of this extraction method was above 90% ± 5% based on control experiments. The control experiments were operated with Cr(VI) adsorption onto Cr(III)–Fe(III) hydroxide solids followed by phosphate addition to induce Cr(VI) desorption. Other portion of selected sample suspensions were treated with 10 mM $CuSO_4$ to extract adsorbed Mn(II). In this method Cu(II) preferentially adsorbs to MnO_2, and induce Mn(II) desorption.[206, 247] This method has been shown to remove >90% of the adsorbed Mn(II) from a biologically reduced δ-MnO_2.[221] The method only extracts adsorbed Mn(II) and would not mobilize any structurally incorporated Mn(II) or Mn(III).

TEM samples were prepared by dropping approximately 30 μL of suspension onto 200 mesh carbon-coated copper grids (Ted Pella, Inc.) followed by immediate evaporation of the remaining water at room temperature under vacuum. TEM micrographs were taken with a transmission electron microscope under 120 kV (FEI Spirit G2). The solid samples for XRD, XPS and HR-TEM were prepared by centrifugation and freeze-drying. XRD patterns were collected using Cu Kα radiation (Bruker d8 Advance X-ray diffractometer). XPS analyses were conducted using a Physical Electronics 5000 Versa Probe II Scanning ESCA Microprobe with an Al Kα X-ray source at 23.5 eV pass energy at a 100 μm X-ray spot size. The binding energy was calibrated using C 1s at 284.6 eV, and the XPS spectra were processed by using CasaXPS software (Version 2.3.15)[222] with the Gaussian-Lorentzian function (70% G-30% L), and a Shirley background for peak fitting. The quantification of Mn valence state was made following

a method in which the Mn $2p_{3/2}$ spectrum is divided into five multiplet peaks (total of 15 binding energies) of Mn(IV), Mn(III) and Mn(II).[223] A value of 1.5 for the full width of the peak at half the maximum peak height (fwhm) was assigned to fit the $Mn2p_{3/2}$ spectrum for all of the multiplet binding energy spectra.[224] TEM observation was carried out using an FEI TF electron microscope operated at 200 kV and energy dispersive X-ray (EDX) analysis was used to confirm the particle compositions, and selected area electron diffraction (SAED) patterns were collected to determine the extent of crystallinity of the Mn oxides and $Cr(OH)_3$ as well as to identify the mineral phases.

5.2.5 Model for dynamics of Cr(VI) production

A quantitative model for the dynamics of $Cr(OH)_3$ oxidation by δ-MnO_2 in multichamber experiments was developed based on the dissolution rate of $Cr(OH)_{3(s)}$, the rates of aqueous Cr(III) and Cr(VI) transport across the membrane, rate of dissolved Cr(III) oxidation by δ-MnO_2, and Cr(VI) adsorption on $Cr(OH)_3$ solids. The rate of aqueous Cr(III) oxidation on the surface of MnO_2 was calculated by determining the parameters that provided the best fit of the model output to the experimental data.

For the $Cr(OH)_3$||MnO_2 system, where "||" notes the separation of solids by a dialysis membrane, the governing equations are

$$V\frac{d[Cr(III)]_{Mn}}{dt} = -V \cdot k \cdot [Cr(III)]_{Mn} \cdot [MnO_2] + \nu_{Cr(III)} \cdot A \cdot ([Cr(III)]_{Cr} - [Cr(III)]_{Mn}) \quad (5.1)$$

$$V\frac{d[Cr(III)]_{Cr}}{dt} = V \cdot k' \cdot (1 - \frac{[Cr(III)]_{Cr}}{[Cr(III)]_{eq}}) - \nu_{Cr(III)} \cdot A \cdot ([Cr(III)]_{Cr} - [Cr(III)]_{Mn}) \quad (5.2)$$

$$V\frac{d[Cr(VI)]_{Mn}}{dt} = V \cdot k \cdot [Cr(III)]_{Mn} \cdot [MnO_2] - \nu_{Cr(VI)} \cdot A \cdot ([Cr(VI)]_{Mn} - [Cr(VI)_{diss}]_{Cr}) \quad (5.3)$$

$$V\frac{d[Cr(VI)_{tot}]_{Cr}}{dt} = \nu_{Cr(VI)} \cdot A \cdot ([Cr(VI)]_{Mn} - [Cr(VI)_{diss}]_{Cr}) \quad (5.4)$$

$$[MnO_2] = [MnO_2]_0 - 1.5 \cdot [Cr(VI)]_{Mn} - 1.5 \cdot [Cr(VI)_{tot}]_{Cr} \quad (5.5)$$

The transmembrane mass transfer coefficient was estimated from the Cr(VI) tracer experiment (Figure S5.4 in Supporting Information) and the aqueous Cr(III) transmembrane mass transfer coefficient was calculated based on a semi-empirical equation relating the molecular weight and mass transfer coefficients of Cr(VI) and Cr(III) (eq S5.3 in Supporting Information). The flux (mol m^{-2} s^{-1}) of an aqueous species is proportional to its concentration gradient across the membrane. The relationship between $[Cr(VI)_{diss}]_{Cr}$ and $[Cr(VI)_{tot}]_{Cr}$ was estimated by adsorption experiments of Cr(VI) onto $Cr(OH)_3$ solids (eq S5.12, S5.13 and Figure S5.7 in Supporting Information). The rate constant for $Cr(OH)_3$ dissolution is k' (5.5×10^{-10} mol L^{-1} s^{-1}), which was obtained from fitting the data from $Cr(OH)_3$||water experiments (Figure S5.4 in Supporting Information). The rate constant of dissolved Cr(III) oxidation by MnO_2 was k (3.6 L mol^{-1} s^{-1}), which was estimated by fitting the $[Cr(VI)]_{Mn}$, $[Cr(VI)_{tot}]_{Cr}$ and $[Cr(VI)_{diss}]_{Cr}$ experimental data with modeling output in from eq 5.1 to eq 5.5. The ordinary differential equations (ODEs) from eq 5.1 to eq 5.5 in the model were solved by the ode45 solver in Matlab 7.0. More detailed model derivation can be found in the Supporting Information.

5.3 Results and Discussion

5.3.1 $Cr(OH)_3$ oxidation by MnO_2

From pH 5 to pH 7, Cr(III) oxidation rates were initially rapid, followed by a cessation of the reaction (Figure 5.1). The Cr(VI) concentration was nearly constant after increasing to around 100 μM within the first ten hours. Both dissolved Cr(III) and MnO_2 are in excess amount

even after cessation of the reactions. At pH 5, the Cr(VI) produced was lower than the dissolved Cr(III) concentration of 240 μM, which was measured before MnO_2 was added to the $Cr(OH)_3$ suspension. The stoichiometry of Cr(VI) and Mn(II) produced was around 1.5 times, indicating that Mn(II) was the reduction product of MnO_2 at pH 5 (eq 5.6). The Mn(II) generated was lower than the total amount of Mn(II) that could have been generated if the reaction had gone to completion, so Cr(III) oxidation had stopped even though there was sufficient MnO_2 for further oxidation. This inhibitory effect of $Cr(OH)_3$ oxidation by Mn-oxides has also been previously observed at pH values greater than 4 and with higher Cr(III) loadings than those in our study.[203, 205, 251] Those previous studies attributed the inhibition to the formation of a $Cr(OH)_3$ precipitate on δ-MnO_2.[205] As a result, the amount of Cr(III) oxidized may be governed by the surface area of MnO_2 when Cr(III) is in excess.

$$2Cr(OH)_{3(s)} + 3MnO_2 = 2CrO_4^{2-} + 3Mn^{2+} + 2OH^- + 2H_2O \quad (5.6)$$

$$Cr(OH)_{3(s)} + 3MnO_2 + H_2O = CrO_4^{2-} + 3MnOOH \quad (5.7)$$

From pH 8 to pH 9 when $Cr(OH)_3$ solubility is much lower than at pH 5-7(Table 5.1), the Cr(VI) concentrations increased more gradually, and they ultimately increased to a higher levels and without any observable inhibition. At pH 8, the oxidation reaction proceeds until MnO_2 was limiting as Mn(III) is the dominant reaction products according to the stoichiometry of the reaction (Figure 5.1 and eq 5.7). At pH 9, Cr(VI) can be as high as 200 μM, which would require 600 μM MnO_2. As there was only 436 μM MnO_2 in the initial suspension, Mn(II) might be oxidized by dissolved oxygen to MnO_2, which could continue oxidizing Cr(III) at this high pH.[229]

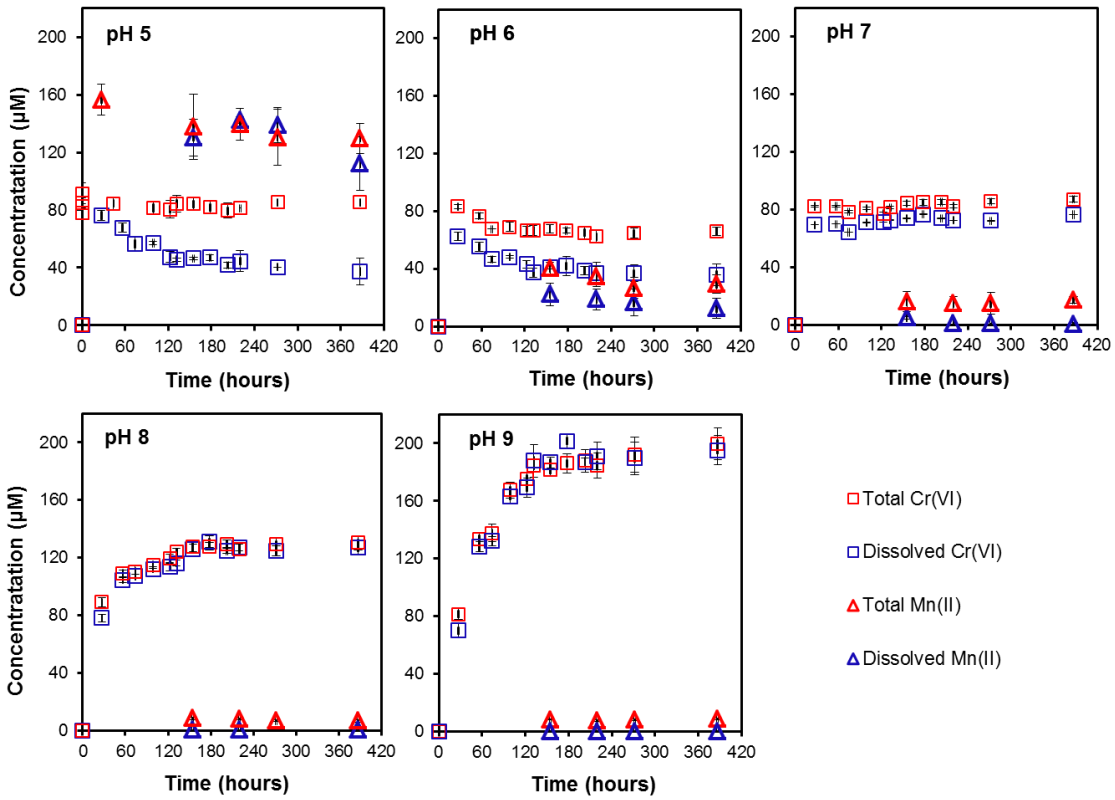

Figure 5.1. $Cr(OH)_3$ oxidation by manganese oxide from pH 5 to pH 9 with 770μM initial Cr(III) (40 mg/L) and 436 μM initial MnO_2 (40 mg/L MnO_2) in completely mixed batch experiments.

Table 5.1 Comparison of $Cr(OH)_3$ solubility with oxidation extent in the presence of MnO_2

pH value	5	6	7	8	9
Amorphous $Cr(OH)_3$ solubility[1] (μM)	17.0	0.3	0.02	0.0025	0.1
Measured Cr solubility[2] (μM)	240.0	1.0	0.8	0.2	0.9
$Cr(VI)_{total}$ produced at 400 hours (μM)	95	80	80	130	200
$Mn(II)_{total}$ produced at 400 hours (μM)	156.1	40.2	16.1	8.3	8.2
$Mn(II)_{total}/Cr(VI)_{total}$	1.64	0.50	0.20	0.06	0.04

1. Cr(III) solubility was calculated with MINEQL+[254]

2. Cr(III) concentration was measured after equilibrating with 40 mg/L Cr(III) at different pH for 24 hours before adding 436 μM MnO_2 to the completely mixed reactor.

To better understand the inhibitory mechanism of $Cr(OH)_3$ oxidation by manganese oxides at low pH, different amounts of MnO_2 were dosed to $Cr(OH)_3$ suspension at pH 5. As shown in Figure 5.2a, with different amounts of MnO_2 initial concentration, Cr(VI) production rates were high in the initial stage, followed by the cessation of the reaction. When the reaction ceased, both Cr(III) and MnO_2 were still present at amounts that theoretically could react with one another. Even though neither reactant was completely consumed, with higher MnO_2 dosage, the higher total Cr(VI) were generated.

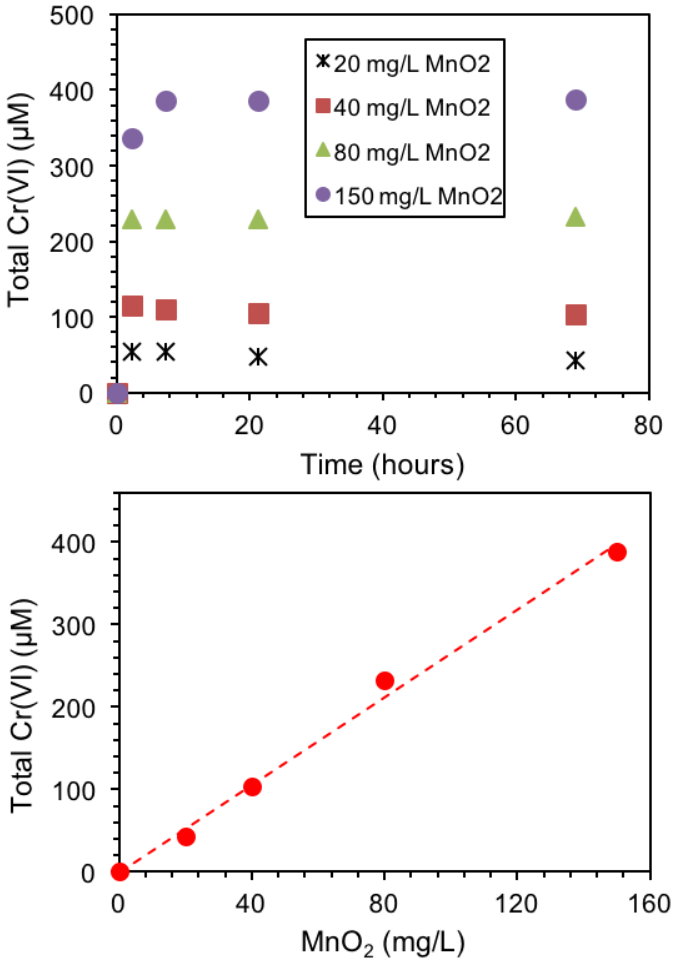

Figure 5.2. $Cr(OH)_3$ (770 μM/ 40 mg/L) oxidation by different concentrations of MnO_2 at pH 5. (a) total Cr(VI) production along the reaction time (b) total Cr(VI) produced after reaching equilibrium at 8 hours correlated with MnO_2 added.

Total Cr(VI) concentration after reaching equilibrium were proportional to the MnO_2 dosed (Figure 5.2b), indicating that the MnO_2 concentration was the limiting factor for Cr(III) oxidation. Manceau and Charlet proposed that mononuclear Cr(III) diffuses to the lattice vacancies in the Mn-oxide structure and is complexed in these sites subsequent to the electron transfer with Mn(IV) during Cr(III) oxidation by manganese oxides.[249] As a result, the number of vacancies in the MnO_2 lattice structure determines the extent of Cr(III) oxidation and the amount of Cr(III) oxidized is dependent on MnO_2 concentration. This provides another explanation of the Cr(III) oxidation cessation, which might be due to vacancies in MnO_2 lattice structure are occupied.

5.3.2 Kinetic modeling of Cr(III) oxidation in multichamber experiments

Cr(VI) occurs through chromium(III) dissolution from $Cr(OH)_3$ and its oxidation on the MnO_2 surface. At pH 5 when the initial dissolved Cr(III) concentration was as high as 240 μM, the aqueous Cr(III) ions could quickly reach the MnO_2 surface by diffusing through the membrane in the multichamber reactor. The total Cr(VI) concentration in the multichamber reactors (average of Cr(VI) concentrations in the $Cr(OH)_3$ and MnO_2 chambers, Figure 5.3a) is around 110 μM, similar to the 95 μM total Cr(VI) produced in completely mixed batch experiments. At pH 8 when the Cr(III) solubility was much lower than at pH 5, very little Cr(VI) was generated in multichamber experiment while much more was produced when the $Cr(OH)_3$ and MnO_2 were mixed in the same suspension. The Cr(III) arrives at the MnO_2 surface efficiently only when there was no diffusive transport limitation for dissolved Cr(III) to contact an MnO_2 surface from advective transport of the Cr(III) to MnO_2 (Figure 5.3c).

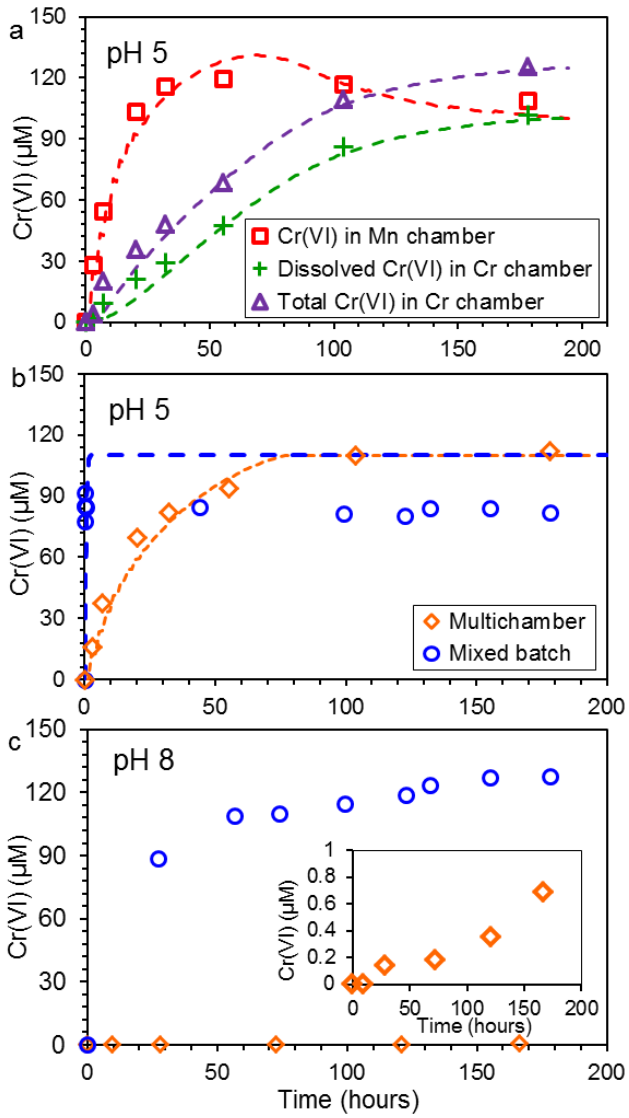

Figure 5.3. Concentration of Cr(VI) from $Cr(OH)_3$-MnO_2 reaction in (a) multichamber experiments at pH 5, (b) multichamber and completely mixed experiments at pH 5, (c) multichamber and completely mixed experiments at pH 8. Sufficient data for control experiments was available to parameterize a model to simulate the reactions at pH 5 but not at pH 8. For all multi-chamber experiments, $Cr(III)_0$ = 1440μM (80 mg/L) in chromium chamber, MnO_2 = 872 μM (80 mg/L MnO_2) in MnO_2 chamber, which are twice as high as in the completely mixed experiments. Then overall Mn and Cr concentrations are the same for multichamber experiments and the completely mixed experiments.

The rates of aqueous Cr(III) oxidation by MnO_2 at pH 5 can be evaluated from the multichamber experiments (Figure 5.3a). The chromium mass transfer coefficients ($\nu_{Cr(III)}$ and $\nu_{Cr(VI)}$) and the rate constant of $Cr(OH)_{3(s)}$ dissolution (k') were determined independently in control experiments and then included in the model for examination of Cr(VI) release in multichamber experiments. For control experiments, chromium concentrations were measured in Cr(VI)||water and $Cr(OH)_3$||water multichamber experiments. The Cr(VI)||water experiment was only affected by Cr(VI) diffusion across the membrane, so it was used to determine the mass transfer coefficient. The $Cr(OH)_3$||water multichamber experiment had Cr(III) concentrations that were only affected by dissolution and by mass transfer across the membrane, so this experiment was used to estimate the dissolution rate constant of $Cr(OH)_{3(s)}$. Detailed discussions of parameter determination are included in the Supporting Information. By fitting the rate constant of aqueous Cr(III) oxidation by manganese oxides, Cr(VI) concentrations in the MnO_2 chamber, and dissolved and total Cr(VI) concentrations in the $Cr(OH)_3$ chamber could be successfully modeled at pH 5 (Figure 5.3a). The rate constant of Cr(III) oxidation was then applied to the completely mixed batch experiments, and the model fit the experimental data well with respect to the rate of initial Cr(III) oxidation and the extent of oxidation (Figure 5.3b).

5.3.3 Mn-containing products of the reaction

The reaction products of $Cr(OH)_3$ and MnO_2 lead to more feitknechtite at higher pH as shown from XRD pattern (Figure 5.4). Recent work has shown that hexagonal birnessite is subject to structural and mineralogical changes during reaction with aqueous Mn(II), and solution pH could affect this interaction as Mn(II) adsorption depends on pH.[211, 231, 255, 256] Our work shows that Mn(II) strongly adsorbed onto the solid phases at high pH (Figure S5.3) , which could lead to bulk transformation of the birnessite into feitknechtite and even a more stable

manganite phase through a reductive transformation process.[33] The XRD pattern at pH 8 and pH 9 indicated that feitknechtite was the dominant product and that no manganite formed within the reaction time in this study. This is because some remnant δ-MnO_2 has taken up Mn(II), forming Mn(III) in the mineral distorting the sheet structure. The feitknechtite formation is consistent with results in Figure 5.1 that Mn(III) was the dominant reduction products of δ-MnO_2 at high pH. At pH 5, MnO_2 reduction by $Cr(OH)_3$ did not introduce new manganese oxides phases (Figure 5.5), as Mn(II) was generated and then released to the solution (Figure 5.1a).

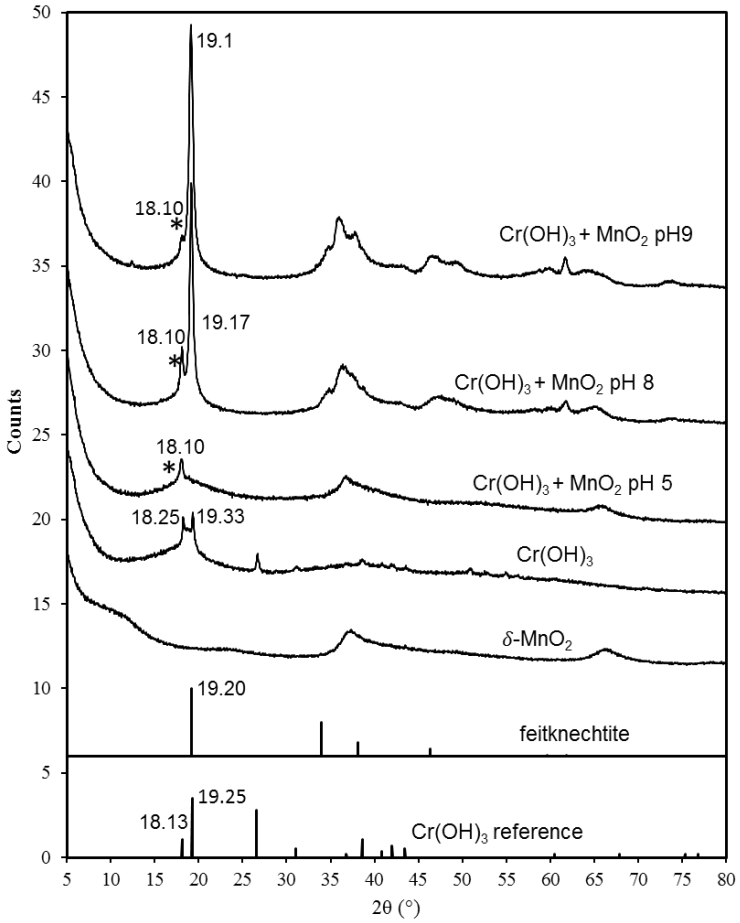

Figure 5.4. X-ray diffraction patterns of MnO_2 and $Cr(OH)_3$ reaction products after 200 hours at pH 5, pH 8, and pH 9. The reference patterns for feitknechtite (044-1445 from the International Crystal Diffraction Database) and $Cr(OH)_3$ is included for comparison. The asterisk (*) indicates the diffraction features from PTFE abraded from the stir bar.[237]

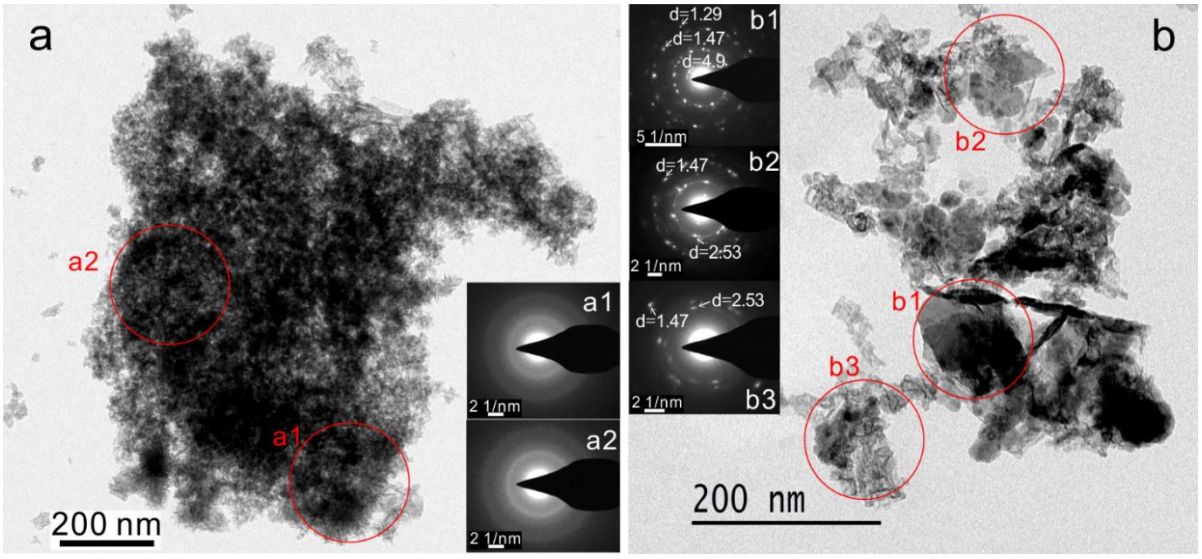

Figure 5.5. HR-TEM images of the reaction products of $Cr(OH)_3$ and MnO_2 at pH 5 (a) and pH 9 (b). The inset figures are the SAED patterns obtained from the area of the red circle.

The products formed at pH 5 and pH 9 in the oxidation of $Cr(OH)_3$ by MnO_2 were also investigated by TEM (Figure 5.4). At pH 5, the reaction products did not show any strong diffraction, revealing that there was not much change in the crystallinity of the primary solids of MnO_2 and $Cr(OH)_3$ but aggregated after reaction, which is consistent with the results from XRD. While at pH 9, the change of the morphology of the particles indicated that a mineral phase transformation occurred and the formed minerals were identified by SAED pattern. Surprisingly, feitknechtite is not observed in TEM despite it being a dominant reaction product identified by XRD. Instead, the SAED patterns at pH 9 are most consistent with the formation of triclinic birnessite. We hypothesize that this is a result of sampling bias associated with the small area analyzed by TEM as XRD clearly shows triclinic birnessite is not abundant. However, revaluation of the XRD pattern for the pH 9 sample (Figure 5.4) reveals a small peak at ~12^o 2θ, consistent with the (001) diffraction peak for birnessites with excellent layer stacking, including the triclinic form. Triclinic birnessite is a known product of the reaction of δ-MnO_2 with

dissolved Mn(II) at alkaline pH conditions and results from Mn(II) adsorption and comproportionation with structural Mn(IV), forming Mn(III) in the manganese oxide sheet.[255]

The valence of Mn on the solid surface was determined directly by analyzing the solid product with $Mn2p_{3/2}$ and Mn3s splitting energy intervals using XPS (Figure 5.6 and Figure S5.4). Table 5.2 summarizes the Mn oxidation state percentage in all the solids as determined by XPS 2p3/2, and percentages determined by Mn3s splitting energy intervals gave similar results (Figure S5.2 and Table S5.2). For the initial δ-MnO_2, Mn(IV) and Mn(III) were present in the near-surface of 94.9% and 5.1%, respectively (Table 5.2) and the average oxidation state of Mn is 3.95. For manganese oxides after reacting with $Cr(OH)_3$, the Mn(IV) had almost entirely been reduced to Mn(II) and Mn(III) on the solid surface at both pH 5 and pH 9. At pH 9, Mn(II) reduced from Mn(IV) is more likely to adsorb on the surface of the solids, which can lead to phase transformation of δ-MnO_2. At pH 5 even though XPS results show that a large portion of the surface Mn are Mn(II), most of the Mn(II) is in solution.

Table 5.2. Summary of Mn oxidation state percent in solids determined using XPS Mn $2p_{3/2}$

Sample	Mn(IV)	Mn(III)	Mn(II)
MnO_2 initial solids	94.9%	5.1%	
$Cr(OH)_3$+MnO_2 pH 5	3.9%	46.7%	49.4%
$Cr(OH)_3$+MnO_2 pH 9	4.4%	42.9%	52.7%

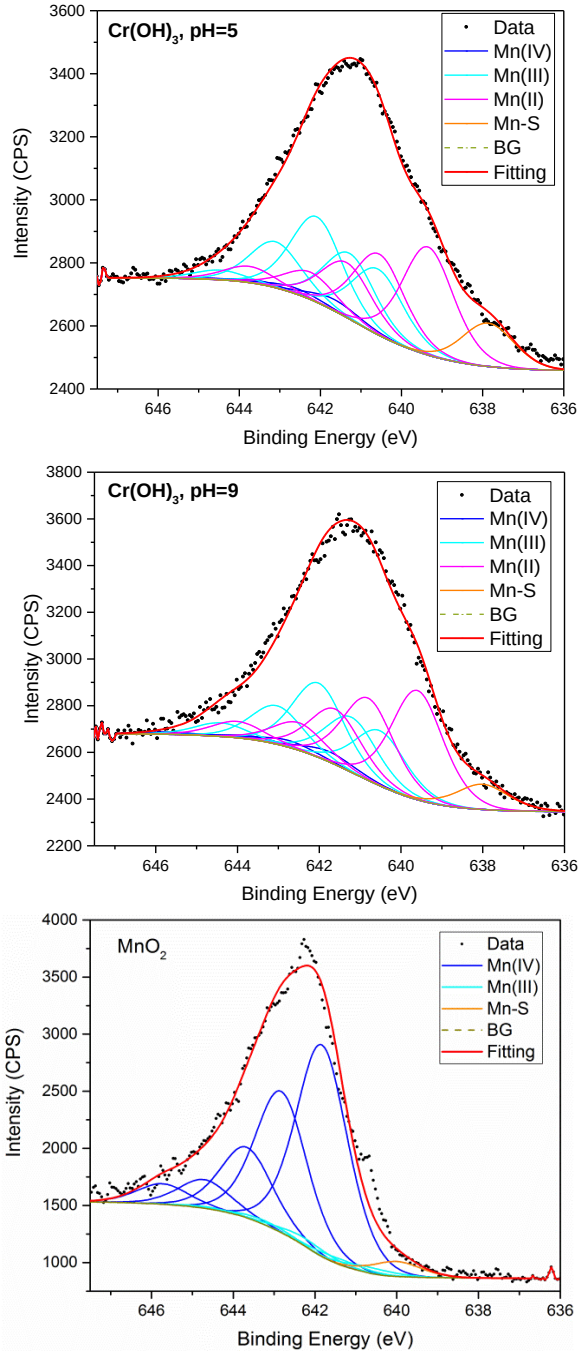

Figure 5.6. XPS spectra of Mn $2p_{3/2}$ photoelectron lines for the solid product and initial MnO_2.

5.4 Conclusion

Collectively, our results demonstrate that oxidation of $Cr(OH)_3$ by manganese oxides was highly dependent on pH even in a relative narrow range of circumneutral pH. In a completely

mixed system, Cr(III) oxidation was inhibited after an initially rapid stage at pH 5-7. When pH increased to pH 8 or 9, then Cr(VI) production was higher. At pH 5 Cr(VI) generated in equilibrium was proportional to the amount of MnO_2 added. Multichamber reactors were used to test the role of mixing of $Cr(OH)_3$ and MnO_2 on Cr(III) oxidation, which could simulate the presence of a contact barrier. At pH 5 when the dissolved Cr(III) concentration was high, Cr(VI) concentrations in multichamber reactor reached a similar level to that in completely mixed batch reactor within 50 hours. While at pH 8 when dissolved Cr(III) concentration is low, the Cr(VI) concentration in multichamber reactor is almost negligible compared with that in completely mixed batch reactor even after 400 hours. Our modeling work could successfully fit the Cr(VI) production rates at pH 5 in completely mixed batch experiments based on parameters determined from multichamber experiments. This work could help us predict the rate and extent of Cr(III) oxidation in natural environments at different conditions. The Cr(VI) production rates were determined by the transport of dissolved Cr(III) in equilibrium with Cr(III)-containing solids upon reaction with δ-MnO_2 when there is no direct contact of the solids, e.g in porous media environments. Furthermore, δ-MnO_2 was reduced to feitknechtite at high pH in the presence of $Cr(OH)_3$, which would affect the further reactivity of manganese oxides and biogeochemical cycling of nutrient elements and trace metals.

Acknowledgements

This research was supported by the U.S. National Science Foundation (CBET 1335613). C.P. acknowledges financial support from school of Engineering Applied Science in Washington University in St. Louis for a first year Ph.D. fellowship.

Chapter 5. Supporting Information

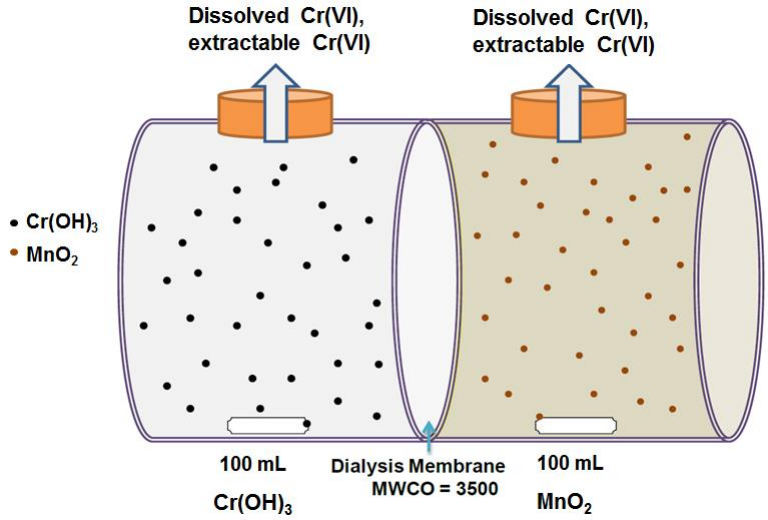

Figure S5.1. Multichamber experimental setup

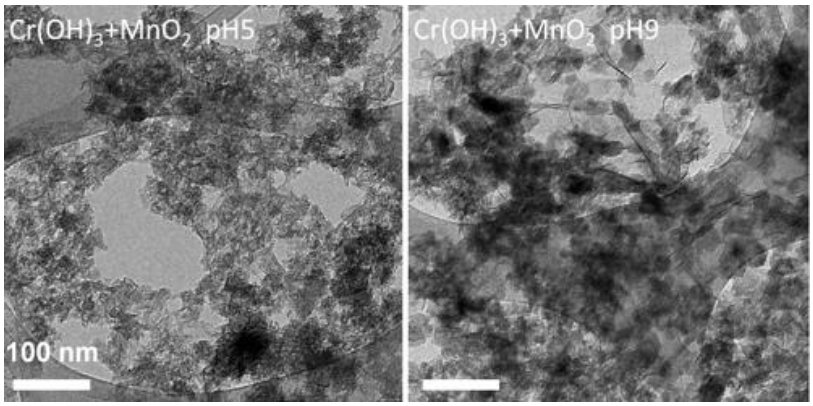

Figure S5.2. TEM images of Cr(III) and MnO_2 reaction products after 400 hours

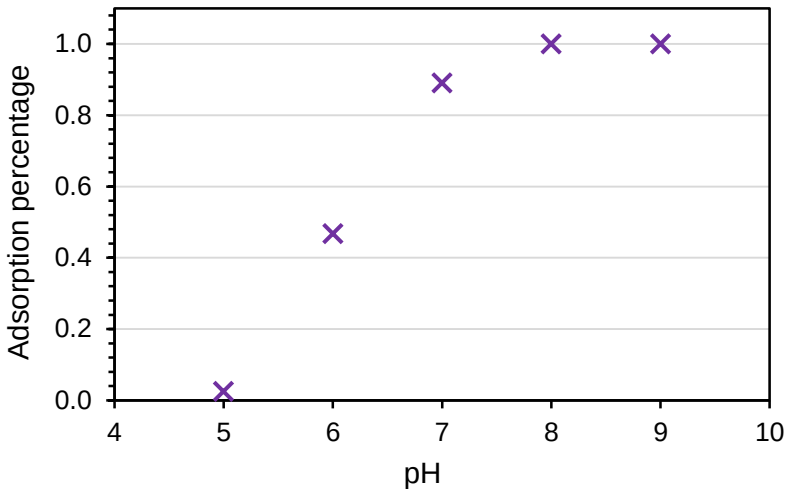

Figure S5.3. pH dependence of Mn(II) adsorption onto the solid phases in $Cr(OH)_3$-MnO_2 completely mixed suspensions. The percent adsorbed is calculated from measurement at each sampling event for an experiment with a mixed suspensions of 770 μM initial Cr(III) (40 mg/L) and 436 μM (40 mg/L MnO_2). Each point represents the average value of the adsorbed portion to the mixture of $Cr(OH)_3$ and MnO_2 at each sampling event at a determined pH.

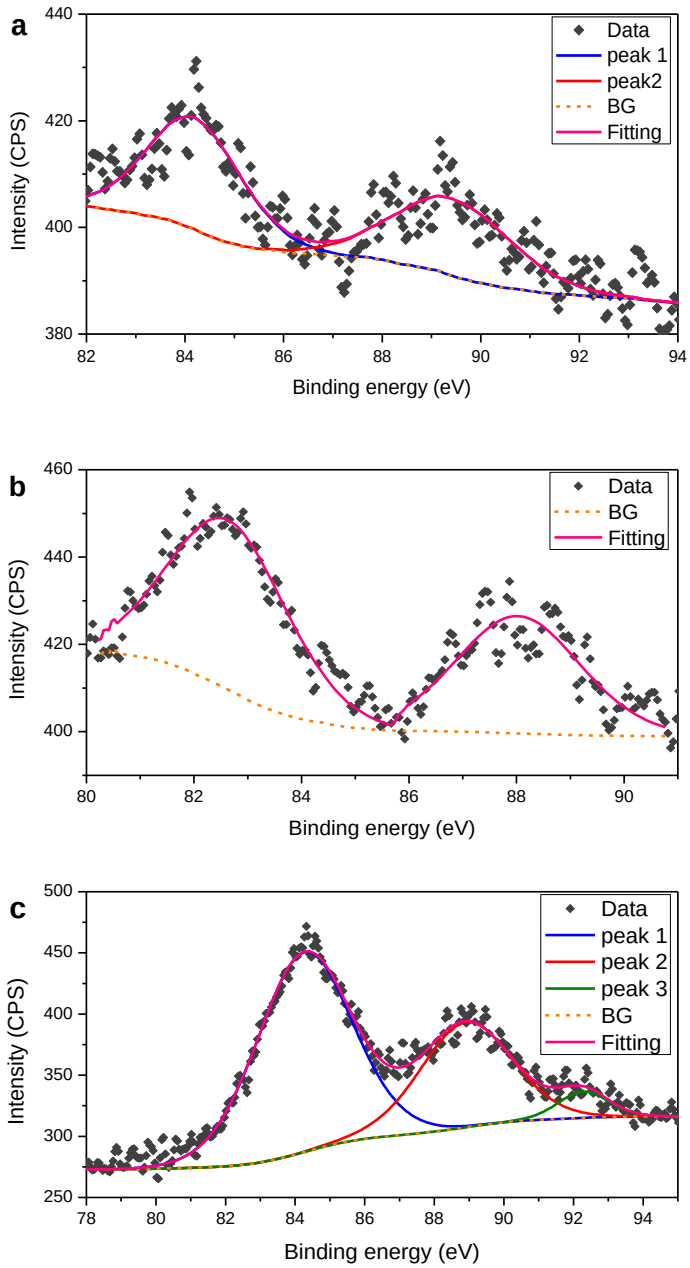

Figure S5.4. XPS spectra of Mn 3s photoelectron lines for the solid product and initial MnO_2. (a) and (b) are the reaction products of $Cr(OH)_3$ with MnO_2 at pH5 and pH 9 respectively; (c) is the initial MnO_2.

Table S5.1. Binding energies (BE) of surface Mn species for fitting the $Mn_{2p3/2}$ peak of the solid product and the relative area of each multiplet for the surface species (All peaks were modeled as 50% Gaussian-50% Lorentzian)

Initial MnO_2

surface species	BE (eV)	FWHM (eV)	Percent (%)
Mn(IV)-O multiplet 1	641.83	1.5	42.52
Mn(IV)-O multiplet 2	642.83	1.5	28.36
Mn(IV)-O multiplet 3	643.68	1.5	14.16
Mn(IV)-O multiplet 4	644.71	1.5	5.73
Mn(IV)-O multiplet 5	645.73	1.5	4.11
Mn(IV)-O overall: 94.9 (%)			
Mn(III)-O multiplet 1	640.70	1.5	1.18
Mn(III)-O multiplet 2	641.40	1.5	1.18
Mn(III)-O multiplet 3	642.21	1.5	1.59
Mn(III)-O multiplet 4	643.23	1.5	0.82
Mn(III)-O multiplet 5	644.60	1.5	0.35
Mn(III)-O overall: 5.1 (%)			

$Cr(OH)_3$+MnO_2 pH=5

surface species	BE (eV)	FWHM (eV)	Percent (%)
Mn(IV)-O multiplet 1	641.65	1.5	1.9
Mn(IV)-O multiplet 2	642.65	1.5	1.0
Mn(IV)-O multiplet 3	643.50	1.5	0.6
Mn(IV)-O multiplet 4	644.53	1.5	0.2
Mn(IV)-O multiplet 5	645.55	1.5	0.2
Mn(IV)-O overall: 3.9 (%)			
Mn(III)-O multiplet 1	640.58	1.5	11.3
Mn(III)-O multiplet 2	641.28	1.5	11.3
Mn(III)-O multiplet 3	642.09	1.5	14.7
Mn(III)-O multiplet 4	643.11	1.5	7.9
Mn(III)-O multiplet 5	644.48	1.5	1.7
Mn(III)-O overall: 46.9 (%)			
Mn(II)-O multiplet 1	639.4	1.5	18.5
Mn(II)-O multiplet 2	640.6	1.5	13.9
Mn(II)-O multiplet 3	641.4	1.5	9.4
Mn(II)-O multiplet 4	642.3	1.5	4.7
Mn(II)-O multiplet 5	643.8	1.5	2.8
Mn(II)-O overall: 49.4 (%)			

$Cr(OH)_3$+MnO_2 pH=9			
surface species	BE(eV)	FWHM(eV)	Percent(%)
Mn(IV)-O multiplet 1	641.75	1.5	1.9
Mn(IV)-O multiplet 2	642.75	1.5	1.2
Mn(IV)-O multiplet 3	643.60	1.5	0.6
Mn(IV)-O multiplet 4	644.63	1.5	0.3
Mn(IV)-O multiplet 5	645.65	1.5	0.4
Mn(IV)-O overall: 4.4 (%)			
Mn(III)-O multiplet 1	640.51	1.5	10.0
Mn(III)-O multiplet 2	641.21	1.5	10.0
Mn(III)-O multiplet 3	642.02	1.5	13.5
Mn(III)-O multiplet 4	643.04	1.5	7.0
Mn(III)-O multiplet 5	644.41	1.5	2.5
Mn(III)-O overall: 42.9 (%)			
Mn(II)-O multiplet 1	639.60	1.5	19.8
Mn(II)-O multiplet 2	640.80	1.5	14.9
Mn(II)-O multiplet 3	641.60	1.5	10.1
Mn(II)-O multiplet 4	642.50	1.5	5.0
Mn(II)-O multiplet 5	644.00	1.5	3.0
Mn(II)-O overall: 52.7 (%)			

Table S5.2. Summary of Mn3s splitting energy intervals for manganese oxides determined using XPS

Compounds	Splitting energy interval (eV)	Reference
Mn(II)-O	5.8	216, 257
	5.7	[224]
Mn(III)-O	5.4	[224, 258]
	5.5	[259]
Mn(IV)-O	4.6	[216, 258]
MnO_2 initial solids	4.65	
$Cr(OH)_3$+MnO_2 pH 5	5.23	
$Cr(OH)_3$+MnO_2 pH 9	5.41	

Derivation of multi-chamber model for $Cr(OH)_3$ oxidation by MnO_2

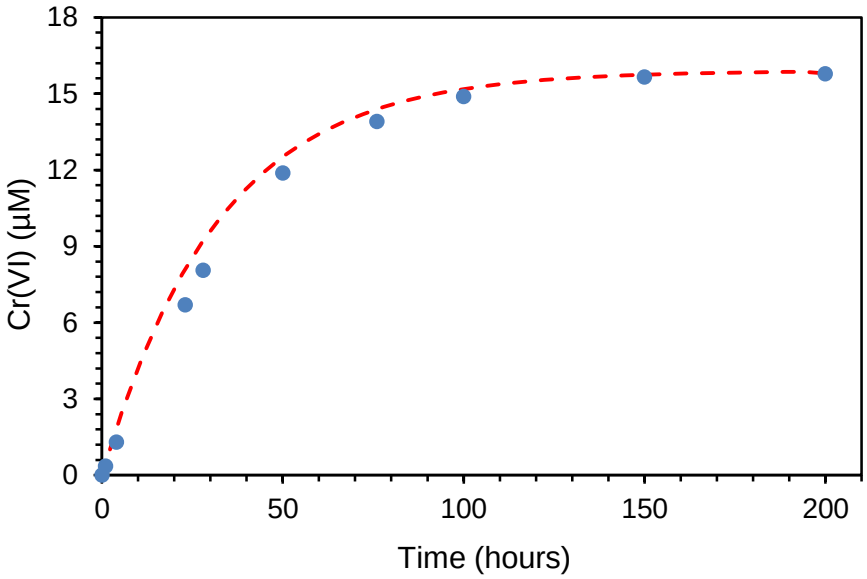

Figure S5.5. Cr(VI) tracer experiment results (symbols) in water chamber of the Cr(VI)||water multichamber reactor and the simulated concentrations (dash line) using the calculated transmembrane mass transfer coefficient ($\upsilon_{CrO_4^{2-}} = 2.3 \times 10^{-7}$ m/s). $[Cr(VI)]_0$ =31.4 μM in Cr(VI) chamber, pH = 5 and V = 100 mL for both chamber.

The multichamber Cr(VI)||water, $Cr(OH)_3$||water, $Cr(OH)_3$||MnO_2 and $Cr_xFe_{1-x}(OH)_3$||MnO_2 experiments were operated to test the mechanism of Cr(III) oxidation by MnO_2.In the Cr(VI) tracer experiment, 100 mL of 31.4 μM Cr(VI) (from $K_2Cr_2O_7$) solution of pH 5 was added to one side of the multichamber reactor with 100 mL water in the other chamber. The samples of the water chamber were collected periodically and measured by ICP-MS for chromium concentration. Both chambers were completely mixed during the experiment. The transmembrane mass transfer coefficient of Cr(VI) ($\nu_{Cr(VI)} = 2.3\times 10^{-7}$ m/s) was obtained by optimizing the simulated concentration (eq S5-1 and eq S5-2) to the measured chromium concentration (Figure S5.3).

$$V\frac{d[Cr(VI)]_{Cr}}{dt} = -\nu_{Cr(VI)} \cdot A \cdot ([Cr(VI)]_{Cr} - [Cr(VI)]_{w}) \quad \text{(S5-1)}$$

$$V\frac{d[Cr(VI)]_{w}}{dt} = \nu_{Cr(VI)} \cdot A \cdot ([Cr(VI)]_{Cr} - [Cr(VI)]_{w}) \quad \text{(S5-2)}$$

where V (100 mL or 10^{-4} m^3) is the volume of each chamber, A (20 cm^2 or 0.002 m^2) is the interfacial area of the dialysis membrane, ν is the transmembrane mass transfer coefficient of Cr(VI). The flux (mol m^{-2} s^{-1}) of an aqueous species is proportional to its concentration gradient across the membrane. As both sides of the membrane were well-mixed, we assume that the mass transfer resistance is entirely that of the membrane and not that of the boundary layer on each side of the membrane.

The mass transfer coefficient of $CrOH^{2+}$ species ($\nu_{CrOH^{2+}}$) was estimated to be 3.0×10^{-7} m/s using the following empirical equation[260]

$$\frac{\nu_{CrO_4^{2-}}}{\nu_{Cr(OH)^{2+}}} = \left(\frac{MW_{CrO_4^{2-}}}{MW_{Cr(OH)^{2+}}}\right)^{-\frac{1}{2}} \quad \text{(S5-3)}$$

where MW is the molecular weight for the dissolved species. At the experimental conditions, the dissolved Cr(VI) species ($HCrO_4^-$ at pH 5) has a molecular weight of 117 and the dominant dissolved Cr(III) species ($Cr(OH)^{2+}$) has a molecular weight of 69.

The $Cr(OH)_3$||water multichamber experiment was operated to determine the $Cr(OH)_{3(s)}$ dissolution rate constant. Although we could also get the dissolution rate constant of $Cr(OH)_{3(s)}$ from a batch or flow-through experiments, the multichamber experiment of $Cr(OH)_3$||water is more comparable to the $Cr(OH)_3$||MnO_2 experiment which will be discussed later.

For the $Cr(OH)_3$||water system, the governing equations are

$$V\frac{d[Cr(III)]_{Cr}}{dt} = V \cdot k'\left(1 - \frac{[Cr(III)]_{Cr}}{[Cr(III)]_{eq}}\right) - \nu_{Cr(III)} \cdot A \cdot ([Cr(III)]_{Cr} - [Cr(III)]_{w}) \quad \text{(S5-4)}$$

$$V\frac{d[Cr(III)]_w}{dt} = \nu_{Cr(III)} \cdot A \cdot ([Cr(III)]_{Cr} - [Cr(III)]_w) \quad \text{(S5-5)}$$

$[Cr(III)]_{eq}$ is the observed final concentration of dissolved Cr in equilibrium with $Cr(OH)_3$. The experimentally observed final Cr concentration of 240 µM was higher than calculated solubility of amorphous $Cr(OH)_{3(s)}$ (21.6 µM) based on the thermodynamic equilibrium constants from MINEQL+ 5.0, which is reasonable that the solubility of crystalline $Cr(OH)_3$ is higher than amorphous $Cr(OH)_3$. The rate constant k' (5.5×10^{-10} mol L^{-1} s^{-1}) for $Cr(OH)_3$ dissolution was obtained by optimizing the fit of the output of equation 4-5 to the data from the $Cr(OH)_3$||water experiments (Figure S5.5).

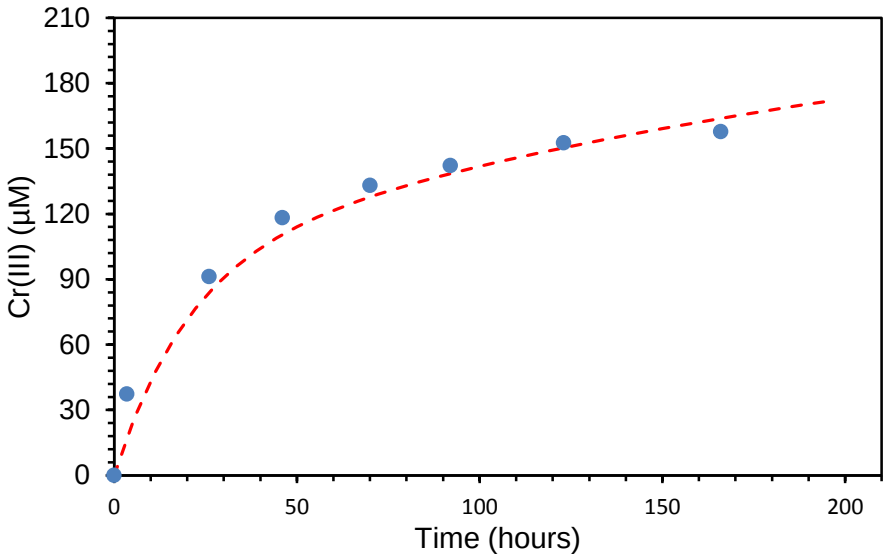

Figure S5.6. Cr(III) release from $Cr(OH)_3$ in $Cr(OH)_3$||water multichamber experiments. $Cr(III)_0$ = 1.54 mM (80 mg/L) in $Cr(OH)_3$ chamber. For both chambers pH=5 and 5mM NaCl was present. Model simulations are shown in dash lines.

For the $Cr(OH)_3$||MnO_2 system the governing equations are

$$V\frac{d[Cr(III)]_{Mn}}{dt} = -V \cdot k \cdot [Cr(III)]_{Mn} \cdot [MnO_2] + \nu_{Cr(III)} \cdot A \cdot ([Cr(III)]_{Cr} - [Cr(III)]_{Mn}) \quad \text{(S5-6)}$$

$$V\frac{d[Cr(III)]_{Cr}}{dt} = V \cdot k' \cdot \left(1 - \frac{[Cr(III)]_{Cr}}{[Cr(III)]_{eq}}\right) - \nu_{Cr(III)} \cdot A \cdot ([Cr(III)]_{Cr} - [Cr(III)]_{Mn}) \quad \text{(S5-7)}$$

$$V\frac{d[Cr(VI)]_{Mn}}{dt} = V \cdot k \cdot [Cr(III)]_{Mn} \cdot [MnO_2] - \nu_{Cr(VI)} \cdot A \cdot ([Cr(VI)]_{Mn} - [Cr(VI)_{diss}]_{Cr}) \quad \text{(S5-8)}$$

$$V\frac{d[Cr(VI)_{tot}]_{Cr}}{dt} = \nu_{Cr(VI)} \cdot A \cdot ([Cr(VI)]_{Mn} - [Cr(VI)_{diss}]_{Cr}) \quad \text{(S5-9)}$$

$$[Cr(VI)_{tot}]_{Cr} = [Cr(VI)_{diss}]_{Cr} \cdot \frac{k_L \cdot [Cr(VI)_{diss}]_{Cr} + Q_M \cdot k_L + M}{k_L \cdot [Cr(VI)_{diss}]_{Cr} + M} \quad \text{(S5-10)}$$

$$[MnO_2] = [MnO_2]_0 - 1.5 \cdot [Cr(VI)]_{Mn} - 1.5 \cdot [Cr(VI)_{tot}]_{Cr} \quad \text{(S5-11)}$$

where t is reaction time (s), $[Cr(III)]_{Mn}$ (M) is the dissolved Cr(III) concentration in the MnO_2 chamber, $[Cr(III)]_{Cr}$ (M) is the dissolved Cr(III) concentration in the $Cr(OH)_3$ chamber, $[Cr(VI)]_{Mn}$ (M) is the Cr(VI) concentration in the MnO_2 chamber, $[Cr(VI)_{diss}]_{Cr}$ (M) is the dissolved Cr(VI) concentration in the $Cr(OH)_3$ chamber, $[Cr(VI)_{tot}]_{Cr}$ (M) is the total Cr(VI) concentration in the $Cr(OH)_3$ chamber including adsorbed Cr(VI) onto $Cr(OH)_3$ solids, $[MnO_2]$ (M) is the concentration of MnO_2 sites available for Cr(III) oxidation, and k' (5.5×10^{-10} mol L^{-1} s^{-1}) is the $Cr(OH)_3$ dissolution rate constant derived in Figure S4. According to Figure 5.2, Cr(VI) produced during $Cr(OH)_3$ oxidation by MnO_2 is proportional to the amount of MnO_2 added into solution. Based on this, we assume that MnO_2 reactive sites were consumed during the reaction, and the amount of sites consumed is proportional to the amount of Cr(VI) produced. The total MnO_2 sites available for Cr(III) oxidation ($[MnO_2]_0$) is 230 μM when MnO_2= 80 mg/L (determined from Figure S5.4a). The reaction between aqueous Cr(III) and MnO_2 was a second order reaction.[261] k (L mol^{-1} s^{-1}) is the rate constant of dissolved Cr(III) oxidation by MnO_2, which is estimated by fitting the $[Cr(VI)]_{Mn}$, $[Cr(VI)_{tot}]_{Cr}$ and $[Cr(VI)_{diss}]_{Cr}$ experimental data with modeling output (k= 3.6 L mol^{-1} s^{-1}). The models gave generally good fits of the experimental data and supports the proposed pathway of truly dissolved Cr(III) oxidation by MnO_2 in the process of $Cr(OH)_3$ oxidation by MnO_2 at pH 5 (Figure 5.3a). The k value of 3.6 L mol^{-1} s^{-1} is then applied in mixed batch experiments to predict Cr(VI) production (Figure 5.3b).

The relationship between $[Cr(VI)_{tot}]_{Cr}$ and $[Cr(VI)_{diss}]_{Cr}$ (eq S5-10) is determined by the Langmuir adsorption model. As the Langmuir model can be derived to the following equation[262]:

$$q = \frac{Q_M \cdot k_L \cdot C}{1 + k_L \cdot C} \quad \text{(S5-12)}$$

$$C_{Total} = C_A + C_{ads} = C_A\left(\frac{C_A Q_M + M + k_L Q_M}{M + k_L C_A}\right) \quad \text{(S5-13)}$$

where q is concentration of Cr(VI) on adsorbent (mg adsorbate/g adsorbent), C is the concentration of Cr(VI) in solution (mg/L), K_L is the Langmuir adsorption constant (L/mg), and Q_M is the maximum adsorption capacity (mg/g). Based on this we could conclude that $Cr(VI)_{diss}/Cr(VI)_{ads}$ correlated linearly with $Cr(VI)_{diss}$ (Figure 5-4) and get eq S5-10.

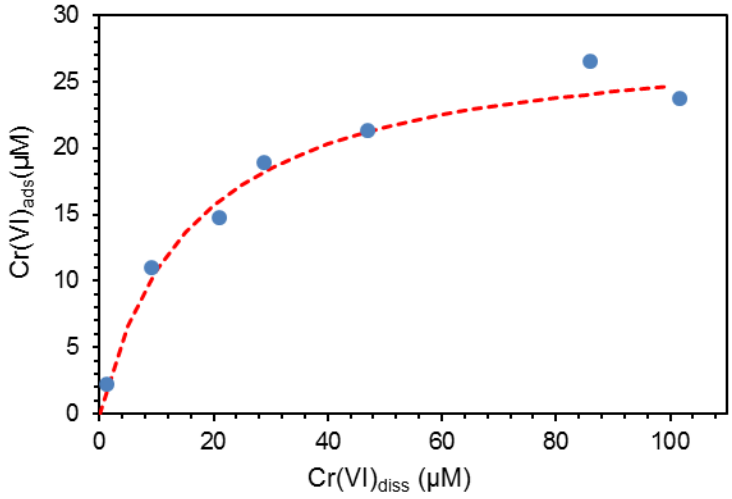

Figure S5-7. Correlation between $Cr(VI)_{diss}/Cr(VI)_{ads}$ and $Cr(VI)_{diss}$ in the $Cr(OH)_3$ chamber of $Cr(OH)_3||MnO_2$ multichamber system at pH 5. $Cr(III)_0$= 1.54 mM (80 mg/L) in $Cr(OH)_3$ chamber, MnO_2 = 80 mg/L in MnO_2 chamber. Both chambers are at pH 5 and have 5mM NaCl. The dash line was based on equation: $Cr(VI)_{diss}/Cr(VI)_{ads} = 0.037Cr(VI)_{diss} + 0.58$

Chapter 6. Cr(VI) formation from $Cr_xFe_{1-x}(OH)_3$ induced by surface catalyzed Mn(II)

This chapter was a manuscript in preparation for submission to Environmental Science& Technology Letters

Abstract

Cr(III)-Fe(III) hydroxide ($Cr_xFe_{1-x}(OH)_3$) is a common product of Cr(VI) reduction by Fe(II) that decreases the solubility and mobility of chromium. Reoxidation of Cr(III) in subsurface environments can generate Cr(VI) and impair groundwater quality. Here we investigate the feasibility of $Cr_xFe_{1-x}(OH)_3$ oxidation in the presence of Mn(II) at neutral pH as a potential pathway of Cr(VI) formation. Although homogenous Mn(II) oxidation by dissolved oxygen is slow, $Cr_xFe_{1-x}(OH)_3$ surfaces can catalyze Mn(II) oxidation by dissolved oxygen to form manganese oxide rapidly that then oxidizes the Cr(III) in $Cr_xFe_{1-x}(OH)_3$. The redox cycling of manganese can keep driving Cr(VI) generation from $Cr_xFe_{1-x}(OH)_3$. The rate of Mn(II) oxidation increased with increasing pH and Fe/Cr ratios in solids. The rates of both the Mn(II) oxidation to manganese oxide and subsequent Cr(III) oxidation from $Cr_xFe_{1-x}(OH)_3$ govern the overall Cr(VI) production rates. Our findings demonstrate that Cr(VI) can be naturally produced from $Cr_xFe_{1-x}(OH)_3$ mediated by surface catalyzed Mn(II) oxidation in ambient environments.

6.1 Introduction

Geogenic Cr(III) is widespread in natural solids such as rocks and sediments.[11, 263] Weathering of the Cr(III)-bearing minerals within soils and sediments commonly results in Cr(III) hydroxide precipitates, often coprecipitated with Fe(III) hydroxides.[238, 264] The higher oxidation

state Cr(VI), which is rarely found in primary minerals,[265] is more mobile and toxic. Cr(VI) can be reduced to Cr(III) by Fe(II) through biotic[196, 266] or abiotic pathways.[62, 182, 267] The reduction products are mixed Cr(III)-Fe(III) (oxy)hydroxides with Cr(III) substitution for Fe(III) to form a solid solution. Compared with $Cr(OH)_3$, $Cr_xFe_{1-x}(OH)_3$ has much lower Cr(III) solubility and the iron contents could significantly affect their stability, structure, size and phase transformation.[197, 198, 268, 269]

Manganese (Mn) is the second most abundant transition metal after iron in the earth's crust.[270] Manganese oxides are ubiquitous in aquatic and terrestrial environments[271, 272] and can control the fate and transport of chromium by adsorption, coprecipitation, and redox reactions.[273, 274] Mn oxides are likely to be responsible for most Cr(III) oxidation in natural environments.[53, 202, 204] For Cr(III) oxidation from $Cr_xFe_{1-x}(OH)_3$ by δ-MnO_2, Cr(III) oxidation rates are proportional to the dissolved concentration of Cr(III) predicted from estimated mineral solubility.[201, 204, 247] In addition, the two solids must be in proximity for Cr(III) oxidation, indicating that the reaction proceeds through Cr(III) dissolution from $Cr_xFe_{1-x}(OH)_3$ and subsequent transport to manganese oxide surface.[204, 247] In this reaction process, δ-MnO_2 transformed from hexagonal to orthogonal at high pH.[232, 247] In contrast, δ-MnO_2 transformed to feitknechtite when oxidizing $Cr(OH)_3$.

Although Mn(IV) or Mn(III) oxides are stable at oxic environments, Mn(II) is still found there[275, 276] because of the reduction of Mn oxides by natural organic matter[277, 278] and the slow Mn(II) oxidation kinetics.[279] Homogeneous Mn(II) oxidation by dissolved oxygen is on the order of days or years at neutral pH environments, and the oxygenation kinetics are autocatalytic.[280-282] However Mn(II) oxidation by dissolved oxygen can be catalyzed by metal oxide surfaces, especially those of iron oxides.[229, 282, 283] The primary product of Mn(II) oxidation on mineral

surfaces such as hematite, goethite and albite surfaces in aerated solutions at neutral pH was feitknechtite (β-MnOOH). Mn(II) oxidation to Mn(IV) occurs as a two-step process in which solid phase Mn(III)-bearing oxides (Mn_3O_4) or oxyhydroxides (β-MnOOH) are initially formed and then undergo slower disproportionation, ultimately forming Mn(IV) oxides.[47, 216, 284]

A recent study found that Cr(VI) was produced from oxidation of Cr(III) in $Cr(OH)_3$ by a newly formed Mn oxide via Mn(II) oxidation by dissolved oxygen that was catalyzed by the $Cr(OH)_{3(s)}$ surface.[229] $Cr_xFe_{1-x}(OH)_3$ is much more common than $Cr(OH)_3$ in natural aquatic environments.[93, 110, 191] However, no studies have examined the Cr(VI) genesis from $Cr_xFe_{1-x}(OH)_3$ in the presence of Mn(II). The objectives of this study were to investigate the influence of $Cr_xFe_{1-x}(OH)_3$ on Mn oxides formation from Mn(II) oxidation, determine the likelihood of Cr(VI) occurrence in this process, and identify the corresponding factors and underlying mechanisms. The understanding of the reaction pathway and kinetics were approached by controlled bench-scale experiments and the analysis of solutions and solids.

6.2 Material and Methods

6.2.1 $Cr_xFe_{1-x}(OH)_3$ synthesis and characterization

$Cr_xFe_{1-x}(OH)_3$ was synthesized by titrating mixed solutions of $FeCl_3$ and $CrCl_3$ at different Fe:Cr molar ratios with NaOH to pH 7 and maintaining the pH for 24 hours. The suspension was then washed with ultrapure water. More information about the synthesis and the resulting solids is provided in our previous work.[247] $Cr(OH)_3$ was synthesized by the same method but with no $FeCl_3$ present. XRD patterns of the $Cr_xFe_{1-x}(OH)_3$ are similar to those of 2-line ferrihydrite (broad peaks at 35 ° and 63 ° 2θ for Cu Kα) and without characteristic peaks of $Cr(OH)_3$ at 2θ of 19.1 °(Figure S6.1).

6.2.2 Batch experiments

Experiments were conducted in a glass beaker filled with ultrapure water, NaCl, pH buffers, Mn(II), and $Cr_xFe_{1-x}(OH)_3$ suspensions to a total volume of 1 L under the ambient laboratory atmosphere. At pH 7 and pH 8, the pH values of suspensions were buffered by 5 mM-3-(N-morpholino) propanesulfonic acid (MOPS, pK_a=7.2). At pH 9, 5 mM N-cyclohexyl-2-aminoethanesulfonic acid (CHES, pK_a=9.3) was used for buffering the suspension. The pH buffers and their concentrations were chosen due to their stability against oxidation by MnO_2 and to minimize their formation of complexes with Cr(III) and Fe(III). A NaCl stock solution was added to provide a total of 5 mM ionic strength, including the contribution from the buffer. Samples were periodically collected and portions of them were filtered with 0.02 μm polyethersulfone (PES) for analysis of dissolved Cr(VI) and dissolved manganese. The remaining unfiltered portions were used for total Cr(VI) and total Mn(II) analysis.

6.2.3 Aqueous and solid phase analysis

The dissolved Cr(VI) concentration was determined by the diphenylcarbazide method.[215] Briefly, the absorbances of the samples were measured at 540 nm using a UV-vis spectrophotometer with 1 cm path length cuvettes after reaction with diphenylcarbazide. The detection limit for Cr(VI) by this method was 5 μg/L (0.096 μM). Concentrations of total Cr(VI) and total Mn(II), which include adsorbed as well as dissolved species, were measured after extracting the surface-associated species into solution. For total Cr(VI) measurements, adsorbed Cr(VI) was extracted by adding a sodium phosphate solution pre-adjusted to pH 8 to provide a 10 mM phosphate concentration in the suspension.[210, 217] After Cr(VI) was desorbed from solid phases, the suspension was filtered and measured by the diphenylcarbazide method. Other

portions of suspensions were treated with 10 mM $CuSO_4$ for 1 hour to extract adsorbed Mn(II). In this method Cu(II) preferentially adsorbs to MnO_2 and induces Mn(II) desorption.[206, 247, 285] Total and dissolved Mn concentrations were measured by ICP-MS (PerkinElmer ELAN DRC II) and the detection limit was 0.5 μg/L (0.009 μM). Dissolved Mn(II) concentrations were assumed to equal the total dissolved Mn concentration because both Mn(IV) and Mn(III) are essentially insoluble.[216]

6.3 Results and Discussion

6.3.1 Cr(VI) formation from $Cr_xFe_{1-x}(OH)_3$ in the presence of Mn(II)

$Cr_xFe_{1-x}(OH)_3$ could catalyze Mn(II) oxidation to Mn oxides in the presence of oxygen at pH 8 and higher, which is relevant to environmental conditions (Figure 6.1a and Figure S6.2). At pH 7, almost no Mn(II) was consumed because even surface-catalyzed abiotic Mn(II) oxidation was negligible at pH < 8.0.[229, 283] A higher consumption rate of total Mn(II) at pH 9 than pH 8 was observed in our experiments, consistent with previous studies that found that the rate of Mn(II) oxidation usually increased two orders of magnitude for each increase of one pH unit for both homogeneous and heterogeneous reactions.[283] To further confirm the catalytic role of $Cr_xFe_{1-x}(OH)_3$ in Mn(II) oxidation, control experiments were operated at pH 9 for measuring total Mn(II) consumption under the ambient atmosphere without $Cr_xFe_{1-x}(OH)_3$ (Figure S6.1a). Mn(II) oxidation was much slower without the presence of $Cr_xFe_{1-x}(OH)_3$. When at anoxic conditions, $Cr_xFe_{1-x}(OH)_3$ could not oxidize Mn(II) (Figure S6.1b), indicating that dissolved oxygen was the oxidant in oxic experiments and that the $Cr_xFe_{1-x}(OH)_3$ surface was catalyzing Mn(II) oxidation.

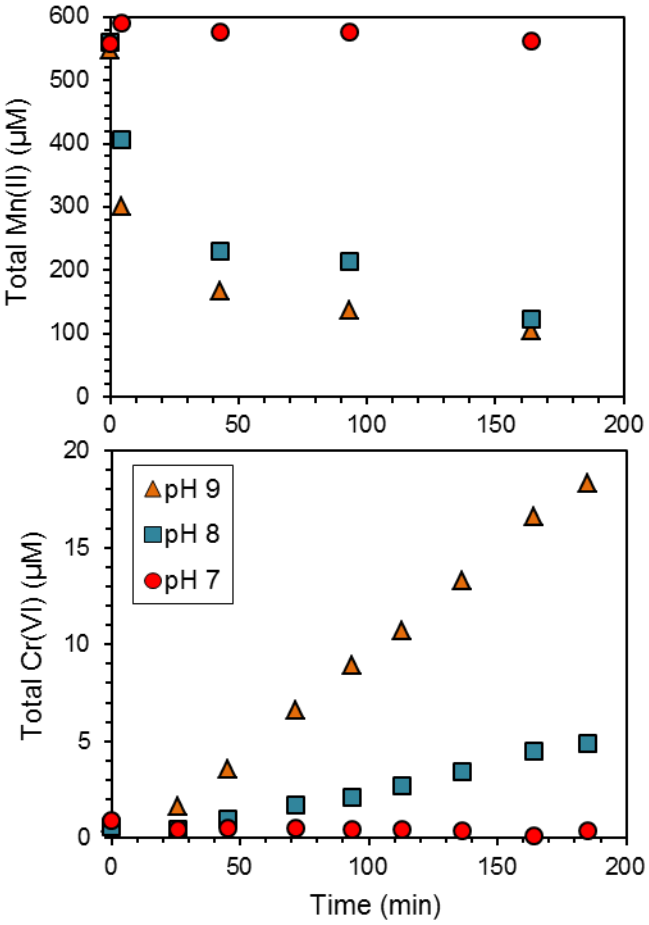

Figure 6.1. $Cr_xFe_{1-x}(OH)_3$ (Fe/Cr=4.1) associated with manganese oxide formation for oxidation systems with initial Mn(II) present under the atmosphere from pH 7 to pH 9. The reaction can be tracked by following (a) the decrease in Mn(II) concentration and (b) the increase in Cr(VI) concentration. $Cr(III)_0$=3.85 mM (200 mg/L), Mn(II)=545 μM (30 mg/L).

Manganese oxide formed from Mn(II) oxidation on the $Cr_xFe_{1-x}(OH)_3$ surface could in turn oxidize $Cr_xFe_{1-x}(OH)_3$, with significant Cr(VI) generation above pH 8 (Figure 6.1b). At pH 7 no Cr(VI) production was observed because no manganese oxide generation occurred (Figure 6.1a). Cr(VI) generation at pH 9 was much higher than at pH 8, consistent with higher manganese oxide generation. In our previous work, we showed that the rates of Cr(III) oxidation from $Cr_xFe_{1-x}(OH)_3$ by MnO_2 decreased with increasing pH from pH 5 to pH 9.[247] As a result,

the generation of manganese oxide plays the most important role in Cr(VI) generation. At the same time, the rate of Cr(III) oxidation from $Cr_xFe_{1-x}(OH)_3$ by dissolved oxygen is negligible compared with that oxidation by manganese oxide (Figure 6.1b and Figure S6.2). Similarly, Mn(II) could promote $Cr(OH)_3$ oxidation as well as UO_2 dissolution under oxic conditions through Mn redox cycling.[146, 229] Oxidation of Mn(II) by O_2 on $Cr(OH)_3$ or UO_2 produced reactive Mn species that oxidize dissolved Cr(III) from $Cr(OH)_3$ or U(IV) from UO_2 more rapidly than could the O_2 alone. Not only we measured the total Cr(VI) generation from $Cr_xFe_{1-x}(OH)_3$ /Mn(II) system, the dissolved Cr(VI) production, which directly regulates chromium contamination in groundwater, was also measured in the study (Figure S6.3). The dissolved Cr(VI) concentration was lower than the total Cr(VI) concentration due to partial Cr(VI) adsorption onto solid surfaces. The portion of adsorbed Cr(VI) at pH 8 is higher than at pH 9 as Cr(VI) adsorption is pH-dependent.

6.3.2 The influence of Fe/Cr in $Cr_xFe_{1-x}(OH)_3$ on Cr(VI) production

Both manganese oxide formation and subsequent Cr(III) oxidation from $Cr_xFe_{1-x}(OH)_3$ by manganese oxide play an important role in overall Cr(VI) occurrence rates at pH 8 and higher. Mn(II) oxidation rates increased with increasing Fe/Cr ratio in $Cr_xFe_{1-x}(OH)_3$ at pH 8 and pH 9 (Figure 6.2a and 6.2c), possibly because $Cr_xFe_{1-x}(OH)_3$ with higher Fe/Cr ratio has higher catalytic capacity for Mn(II) oxidation by dissolved oxygen. Our previous study shows that $Cr_xFe_{1-x}(OH)_3$ with higher Fe/Cr ratio with the same initial Cr(III) concentration has lower Cr(VI) occurrence rates.[247] As a result, the effects of Fe/Cr on the rates of manganese oxide formation and on Cr(III) oxidation from $Cr_xFe_{1-x}(OH)_3$ are offsetting and the Cr(VI) production rates in the presence of Mn(II) and dissolved oxygen are similar for all Fe/Cr ratios studied at pH 8. At pH 9 the dependence of Mn(II) oxidation rates on Fe/Cr ratio has the same trend as at pH 8. Cr_xFe_{1-}

$_x(OH)_3$ with Fe/Cr of 1.2 and 4.1 have similar Cr(VI) generation rates, higher than that of $Cr_xFe_{1-x}(OH)_3$ solids of Fe/Cr with 7.6 and 17.1.

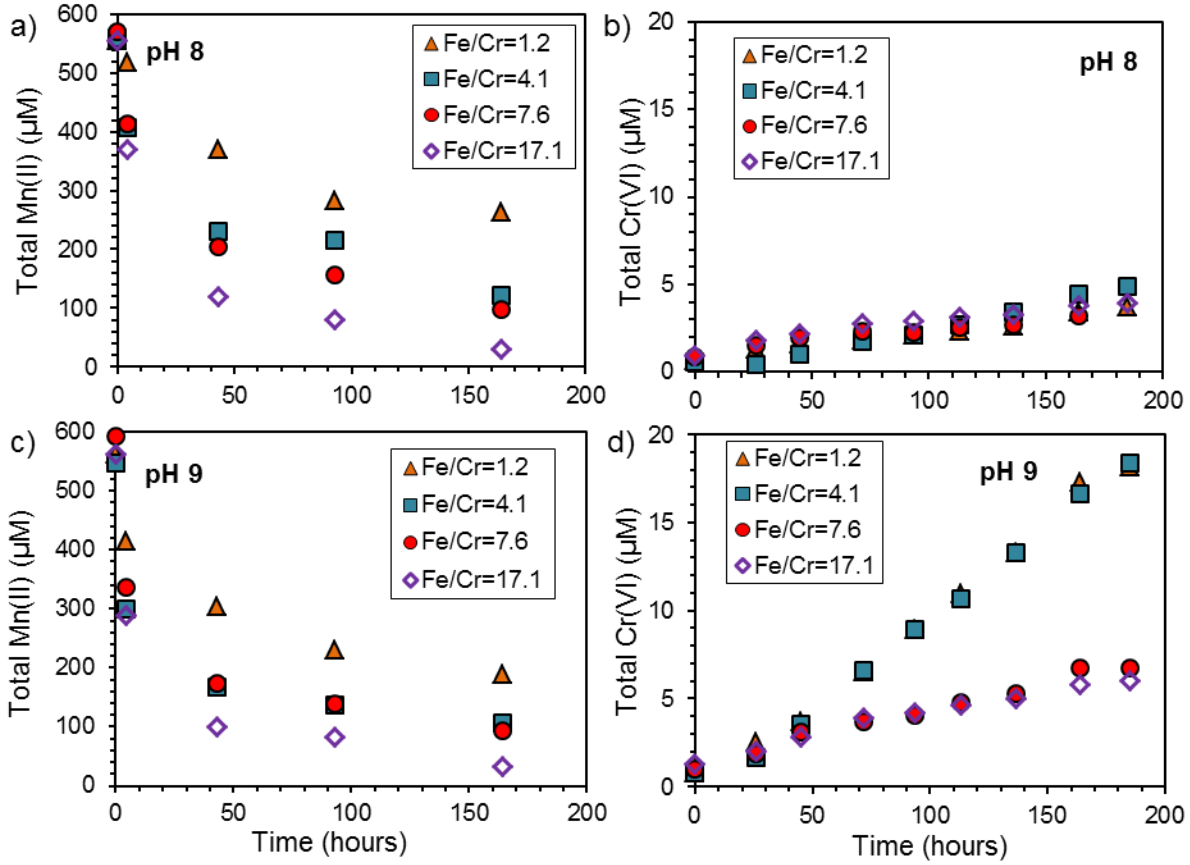

Figure 6.2. The effect of Fe/Cr ratio on $Cr_xFe_{1-x}(OH)_3$ oxidation with Mn(II) present under the ambient atmosphere. $Cr(III)_0$=3.85 mM, Mn(II)=545 μM. The reaction progress can be tracked by following Mn(II) consumption at (a) pH 8 and (c) pH 9 and the Cr(VI) generation at (b) pH 8 and (d) pH 9.

The Cr(VI) production rates at pH 8 and pH 9 are constant along with reaction time, indicating the constant MnO_2 amount in solution. The amount of MnO_2 in solution was determined both by the rate of manganese oxide formation as well as the rate of manganese oxide consumption for Cr(III) oxidation. The rate of Mn(II) oxidation is fast in the initial five hours and then gradually slows down even reaching constant value, consistent with the constant

Cr(VI) production rates. Thus, the rapid cycling between Mn(II) and Mn(III)/Mn(IV) could keep driving Cr(III) oxidation from $Cr_xFe_{1-x}(OH)_3$.

6.3.3 The effect of Fe concentration on Cr(VI) production

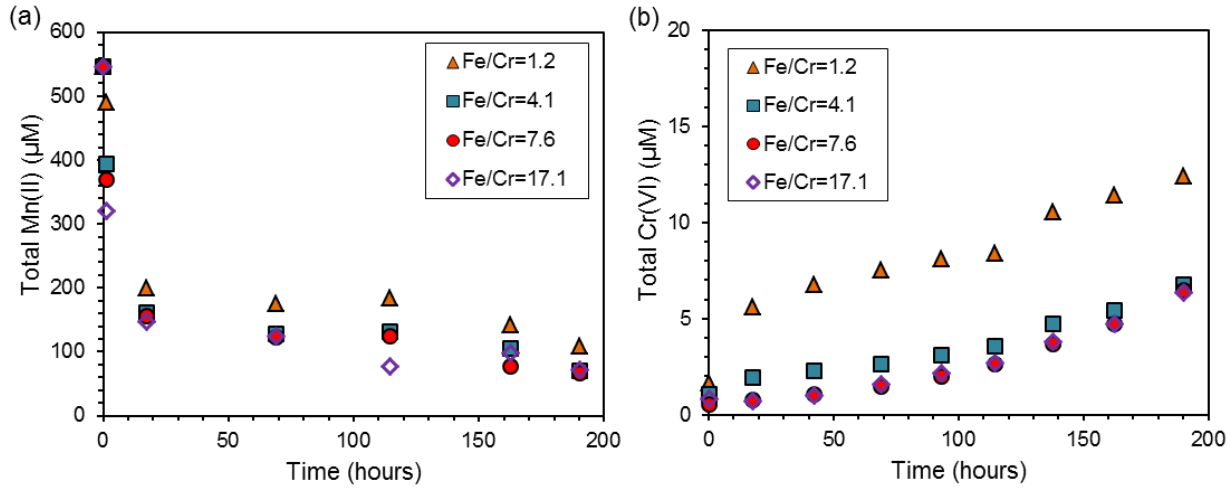

Figure 6.3. Oxidation of Cr(III) in $Cr_xFe_{1-x}(OH)_3$ for a series of experiments with a fixed iron concentration (8.9 mM or 500 mg/L) and varying Fe/Cr ratios at pH 9. The reaction can be followed by observing (a) the consumption of Mn(II) and (b) the production of Cr(VI). Experiments were performed under the ambient atmosphere with an initial Mn(II) concentration of 545 μM (30 mg/L).

The role of iron reactive sites in $Cr_xFe_{1-x}(OH)_3$ surface catalytic Mn(II) oxidation was assessed by holding the Fe concentration in experiments constant for solids with different Fe/Cr ratios. For $Cr_xFe_{1-x}(OH)_3$ solids with Fe/Cr ratios of 4.1, 7.6, and 17.1, the rates of Mn(II) oxidation were almost the same, while the solid with Fe/Cr of 1.2 had a notably lower Mn(II) oxidation rate (Figure 6.3a). Higher Cr contents in $Cr_xFe_{1-x}(OH)_3$ could lead to lower catalytic effects of Mn(II) oxidation, which was also confirmed in Cr(III) oxidation from $Cr_xFe_{1-x}(OH)_3$ with Fe/Cr of 4.1 (Figure S6.5a). The lowest initial Cr(III) of 25 mg/L in $Cr_xFe_{1-x}(OH)_3$ leads to

the highest Mn(II) oxidation rate. For $Cr_xFe_{1-x}(OH)_3$ solids with Fe/Cr ratios from 1.2 to 17.1, Mn(II) concentrations stayed around 100 μM after rapid decreasing from 545 μM within 20 hours, indicating that the manganese redox cycling reached equilibrium after initial stage. For Cr(VI) occurrence, the Cr(VI) concentration in the experiment with a $Cr_xFe_{1-x}(OH)_3$ solid with Fe/Cr of 1.2 increased much faster in the first twenty hours than it did in experiments with solids of other ratios (Figure 6.3b). After the first twenty hours, the rate of Cr(VI) occurrence for the $Cr_xFe_{1-x}(OH)_3$ with Fe/Cr of 1.2 was the same as for the other Fe/Cr ratios. This is probably because higher initial equilibrium Cr(III) concentration with $Cr_xFe_{1-x}(OH)_3$ with Fe/Cr of 1.2 get rapidly oxidized once MnO_2 got generated.

6.4 Conclusion

In summary, our findings demonstrate that sparingly soluble $Cr_xFe_{1-x}(OH)_3$ solids were readily oxidized in the presence of dissolved Mn(II) above pH 8 under oxic conditions. For Cr(III) oxidation from iron oxides by manganese oxide, which is a reaction between two sparingly soluble solids, the reaction must proceed through soluble Cr(III) intermediates and the rates are controlled by the transport of aqueous Cr(III).[247] In contrast, this work shows that for Mn(II)-promoted Cr(III) oxidation from iron oxide, manganese oxide can be formed on the surface of the $Cr_xFe_{1-x}(OH)_3$ that are to be oxidized, which removes any barriers of Cr(III) transport to MnO_2 surface. Dissolved Mn(II) could rapidly transport to the surface of $Cr_xFe_{1-x}(OH)_3$ solids even in porous media. $Cr_xFe_{1-x}(OH)_3$ catalyzed Mn(II) oxidation coupled with the oxidation of $Cr_xFe_{1-x}(OH)_3$ could release substantial amounts of toxic Cr(VI). Even ambient Mn concentrations could lead to significant Cr(VI) release. This study evokes another potential pathway for Mn oxide formation and Cr(VI) contamination from sparingly soluble $Cr_xFe_{1-x}(OH)_3$

in natural aquatic systems. Both Mn(II) oxidation by dissolved oxygen catalyzed by the $Cr_xFe_{1-x}(OH)_3$ surface and subsequent Cr(III) oxidation from $Cr_xFe_{1-x}(OH)_3$ by manganese oxide are crucial for Cr(VI) genesis dynamics. This dynamics of Cr(VI) generation is affected by pH, Fe/Cr ratio, and total iron content. Future studies should investigate the influence of more parameters influencing Cr(VI) production and build a comprehensive kinetic model based on Mn(II) oxidation and subsequent Cr(III) oxidation from $Cr_xFe_{1-x}(OH)_3$.

6.5 Acknowledgements

This research was supported by the U.S. National Science Foundation (CBET 1335613). C.P. acknowledges financial support from school of Engineering Applied Science in Washington University in St. Louis for a first year Ph.D. fellowship.

Chapter 6. Supporting Information

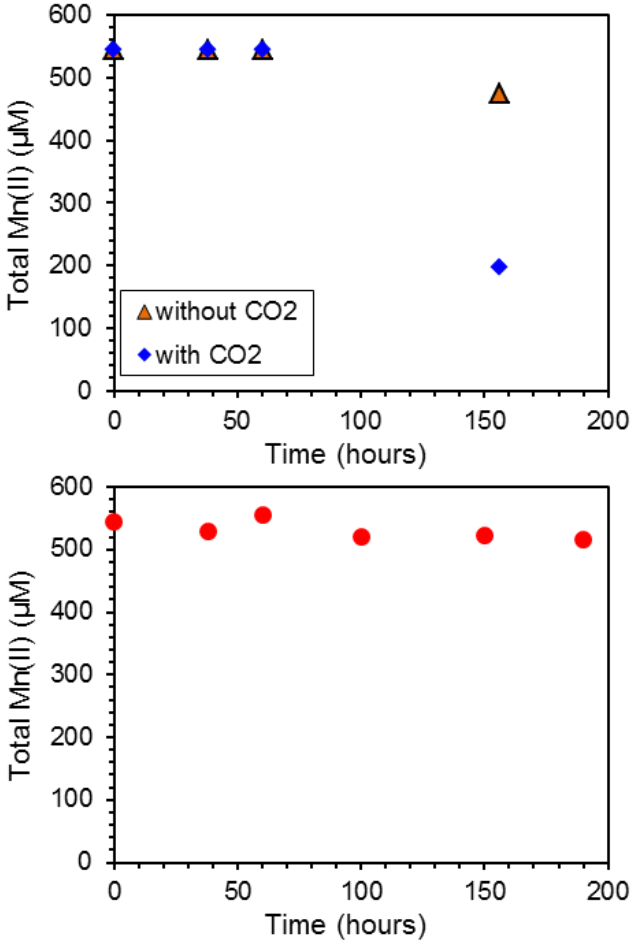

Figure S6.1. a) Mn(II) oxidation by DO without the presence of $Cr_xFe_{1-x}(OH)_3$ at pH 9. b) Total Mn(II) concentration with $Cr_xFe_{1-x}(OH)_3$ present at anoxic conditions at pH 9.

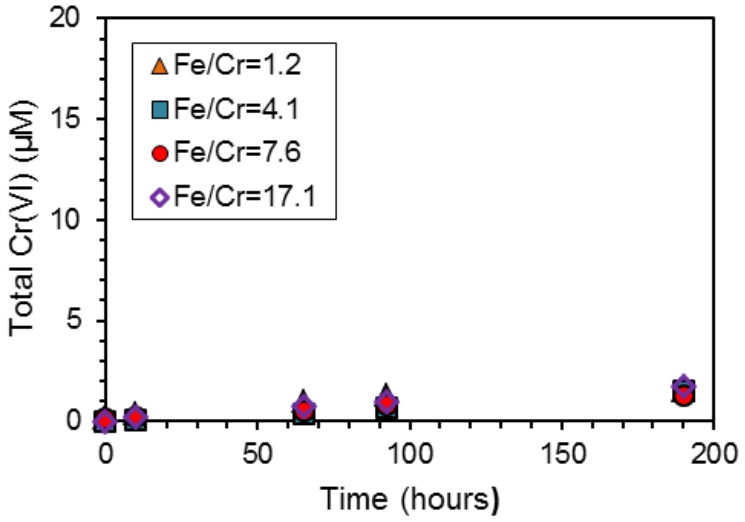

Figure S6.2. $Cr_xFe_{1-x}(OH)_3$ oxidation by dissolved oxygen under the atmosphere without the presence of manganese at pH 9. $Cr(III)_0$=3.85 mM, Mn(II)=545 µM.

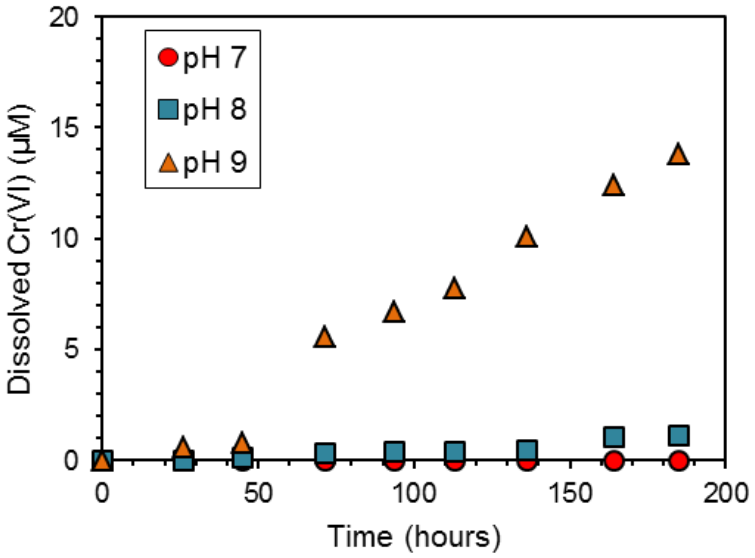

Figure S6.3. Dissolved Cr(VI) concentration from $Cr_xFe_{1-x}(OH)_3$ oxidation with Mn(II) present under the atmosphere. $Cr(III)_0$=3.85 mM (200 mg/L), Mn(II)=545 µM (30 mg/L).

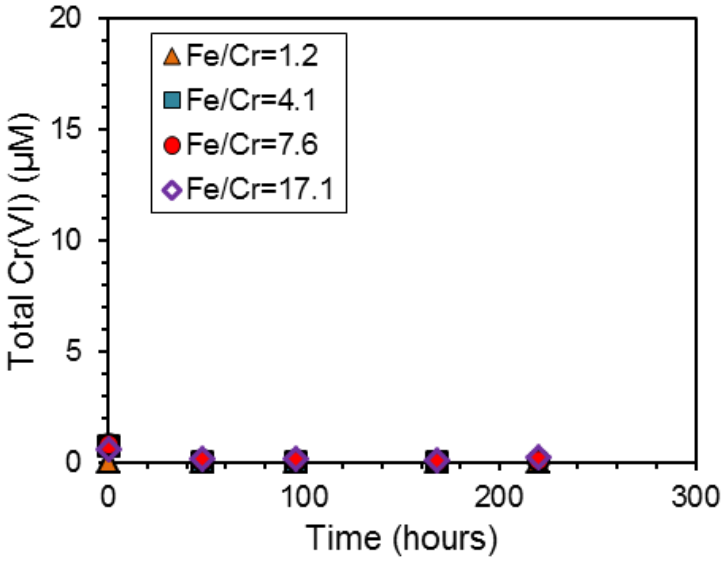

Figure S6.4. Cr(VI) generation from $Cr_xFe_{1-x}(OH)_3$ (Fe/Cr=4.1) with Mn(II) present at anoxic conditions. $Cr(III)_0$=3.85 mM (200 mg/L), Mn(II)=545 µM (30 mg/L), pH= 9.

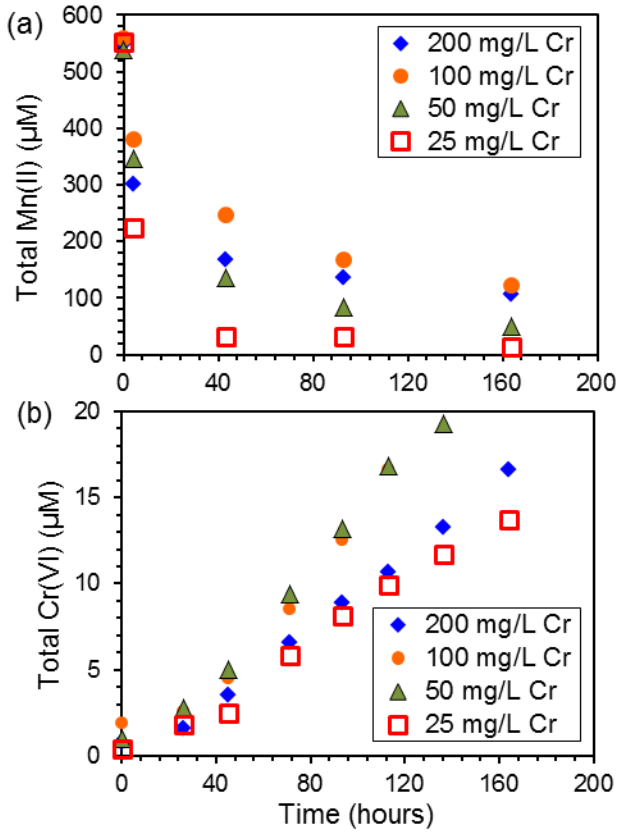

Figure S6.5. Cr(VI) generation from $Cr_xFe_{1-x}(OH)_3$ (Fe/Cr=4.1) with Mn(II) present under the atmosphere. Mn(II)=545 µM (30 mg/L), pH= 9. The reaction can be followed by observing (a) the consumption of Mn(II) and (b) the production of Cr(VI).

Chapter 7. Conclusions and Recommendations

7.1 Conclusions

The doctoral thesis research investigated the coupling of the geochemical cycles of chromium, iron, and manganese and its implication for chromium fate and transport in both water treatment and subsurface environments. It contributed to the still-growing literature of chromium environmental chemistry, especially regarding the previously underappreciated role of sparingly soluble Cr(III)-Fe(III) hydroxide and Mn redox cycles on chromium fate. This project provided fundamental information about various interaction pathways between chromium, iron and manganese that involve redox reactions, adsorption, and precipitation. As the redox reaction of Fe and Mn impacts the fate of other reductively remediated contaminants, the conclusions from this project are expected to extend beyond chromium and to provide valuable insights for these other contaminants. Specific conclusions of each task are described below.

Task 1: Study the rate and extent of Cr(VI) removal from iron electrocoagulation and establish a model to predict Cr(VI) removal

The effect of water chemistry including humic acid on Cr(VI) removal from electrocoagulation were investigated. A comprehensive understanding of Cr(VI) reduction by iron electrocoagulation was provided with batch experiments, spectroscopy and modelling approaches.

The dynamics of Cr(VI) in electrocoagulation were evaluated. Cr(VI) and dissolved Cr concentrations could decrease rapidly to below current and likely future drinking water limits over a wide range of conditions. Even in the presence of common groundwater solutes, Cr(VI)

concentrations could be lowered far below drinking water regulations. The reduction-precipitation mechanism of EC was confirmed by Cr species measurement, XANES spectra and the modeling work. The dynamics of Cr(VI) removal in electrocoagulation at pH 6 and pH 8 at both oxic and anoxic conditions can be described by a new model that incorporates Fe(II) release from the iron electrode and heterogeneous and homogeneous reduction of Cr(VI) by Fe(II).

The presence of humic acid inhibited the Cr(VI) removal rate in electrocoagulation, with the greatest inhibition at higher pH. The inhibition was due to the formation of Fe(II) complexes with HA that are more rapidly oxidized than uncomplexed Fe(II) by dissolved oxygen, making less Fe(II) available for Cr(VI) reduction in EC. The formation of colloids with Cr(III), Fe(III) and HA confirmed the close association of the three in the solid products formed in EC. At pH 8 the solid products were colloids while at pH 6 they form large particles due to aggregation.

Task 2: Examine the Cr(VI) production rates coupled with Mn redox cycling and establish a model to describe the process

The effects of Mn(II) and Mn(IV) oxide on Cr(III)-containing solids were investigated in well-controlled laboratory experiments. Experimental conditions were designed to study the kinetics and pathway of various interactions involving Cr(III)-containing solids and Mn(II)/Mn(IV).

The kinetics of Cr(VI) generation from $Cr_xFe_{1-x}(OH)_3$ oxidation by δ-MnO_2 were investigated using both well mixed batch experiments and multichamber experiments. In well mixed batch experiments, the rates of Cr(VI) generation were controlled by the dissolved Cr(III) concentration in equilibrium with $Cr_xFe_{1-x}(OH)_3$. We established a quantitative relationship between Cr(VI) production rates and Cr(III) solubility of $Cr_xFe_{1-x}(OH)_3$, which can help predict Cr(VI) production rates at different conditions. The multichamber reactor was used to assess the

role of solid-solid contact in $Cr_xFe_{1-x}(OH)_3$-MnO_2 interactions, confirming that the mixing of suspensions of the solids could accelerate the oxidation. Cr(III) dissolves from $Cr_xFe_{1-x}(OH)_3$ and transport to the surface of MnO_2 particles. Cr(III) gets oxidized once upon adsorbing to the surface of MnO2 particles, followed by subsequently releasing into solution.

The multichamber reactor was further used to evaluate the interaction between $Cr(OH)_3$ and MnO_2 at different pH. The rates of aqueous Cr(III) oxidation by manganese oxides at pH 5 were calculated by modeling the Cr(VI) dynamics in multichamber experiments. The Cr(VI) production conditions in the multichamber reactor and completely mixed batch reactors at different pH values suggests that the transport of aqueous Cr(III) to the surface of MnO_2 was a limiting step in the overall kinetics of Cr(VI) generation in multichamber experiments, and the dissolved Cr(III) concentrations in equilibrium with Cr(III)-containing solids directly drive the rate of Cr(III) transport through permeable membrane in multichamber reactors.

The role of Mn(II) on $Cr_xFe_{1-x}(OH)_3$ oxidation by dissolved oxygen was also examined in batch experiments. $Cr_xFe_{1-x}(OH)_3$ could catalyze Mn(II) oxidation by dissolved oxygen to form manganese oxides and the rate increased with increasing pH and Fe/Cr in solids. The formed manganese oxides could in turn oxidize Cr(III) in low-solubility $Cr_xFe_{1-x}(OH)_3$ to significant Cr(VI) concentrations. Both the Mn(II) oxidation to manganese oxides and subsequent $Cr_xFe_{1-x}(OH)_3$ oxidation play an important role in Cr(VI) production rates. Our findings demonstrate that Cr(VI) can be naturally produced from $Cr_xFe_{1-x}(OH)_3$ mediated by surface catalyzed Mn(II) oxidation.

7.2 Recommendations for Future Work

Recommended future work includes but is not limited to (1) performing electrocoagulation experiments in flow through reactor for Cr(VI) removal; (2) evaluating the influence of natural organic matter on Cr(III) oxidation associated with manganese redox cycling; (3) investigating the Cr(VI) generation from $Cr_xFe_{1-x}(OH)_3$ oxidation by MnO_2 in porous media and field sediments; (4) comparing the Cr(VI) generation from $Cr_xFe_{1-x}(OH)_3$ driven by microbial Mn oxidation with that from abiotic pathway.

We have proved that Cr(VI) could be rapidly removed from iron-electrocoagulation relevant to drinking water level in well mixed batch experiments. However, the Cr(VI) removal by electrocoagulation in flow through reactors is not clear. The performance of electrocoagulation in flow-through reactors can be studied to be able to better predict the application of EC in real water treatment systems, which will be continuous-flow operations. The experiments will include determining the amount of power needed for a given amount of coagulation, and the specification of the transport properties. These transport properties must ensure the appropriate residence time, voltage, and electrode characteristics.

Natural organic matter is ubiquitous in aquatic environments and it can associate with manganese, dissolved iron and iron oxides, affecting the iron and manganese redox chemistry. In future studies it will be valuable to investigate the influence of different types of natural organic matter on $Cr_xFe_{1-x}(OH)_3$ oxidation by MnO_2 from both aquatic chemistry and colloidal aspects. It would be particular interesting to test some strong organic complexing ligands which form complexes with Mn(III) as natural organic matter that may cause reductive dissolution of MnO_2

and subsequent complexation with Mn(III). The presence of Mn(III)-ligands may affect the oxidation rate and extent of Cr(III) oxidation from $Cr_xFe_{1-x}(OH)_3$.

The present results highlight the role of solid-solid mixing in Cr(VI) generation from Cr(III)-containing solids oxidation by MnO_2. We compared the multichamber experiments and well mixed batch experiments and established a model to predict Cr(VI) generation in two experiments. However, it is unknown of Cr(VI) generation rates in a porous medium (such as subsurface sediments), which is more common in field conditions. There is no mixing of Cr(III) and Mn(IV) in a porous matrix in which the two solids are immobilized, and solute transport can be limited to that which occurs by diffusion. The aqueous Cr(III) would take more time to transfer to the surface of MnO_2 particles in porous medium, where the model of predicting Cr(VI) generation needs to consider reactive transport model.

Although the present results involve biogenic materials, the processes investigated in our laboratory experiments were primarily abiotic. Given that manganese oxide formation in natural environments is largely driven by manganese oxidizing bacteria, it would be valuable to integrate more biologically active processes in future studies. It would be particularly interesting to test whether Mn oxidizing bacteria could accelerate $Cr_xFe_{1-x}(OH)_3$ oxidation by dissolved oxygen in the presence of Mn(II).

References

1. Venitt, S.; Levy, L., Mutagenicity of chromates in bacteria and its relevance to chromate carcinogenesis. *Nature* **1974**, *250*, 493-495.

2. Kimbrough, D. E.; Cohen, Y.; Winer, A. M.; Creelman, L.; Mabuni, C., A critical assessment of chromium in the environment. *Critical Reviews in Environmental Science and Technology* **1999**, *29*, 1-46.

3. U.S.EPA, Revisions to the unregulated contaminant monitoring rule (UCMR 3) for public water systems. *Federal Register* **2012**, *77*, 26072.

4. U.S.EPA, National Primary Drinking Water Regulations. 40 CFR Part 141. **2010**.

5. Zachara, J. M.; Girvin, D. C.; Schmidt, R. L.; Resch, C. T., Chromate adsorption on amorphous iron oxyhydroxide in the presence of major groundwater ions. *Environmental Science & Technology* **1987**, *21*, 589-594.

6. Mesuere, K.; Fish, W., Chromate and oxalate adsorption on goethite. 1. Calibration of surface complexation models. *Environmental Science & Technology* **1992**, *26*, 2357-2364.

7. Ajouyed, O.; Hurel, C.; Ammari, M.; Allal, L. B.; Marmier, N., Sorption of Cr(VI) onto natural iron and aluminum (oxy)hydroxides: effects of pH, ionic strength and initial concentration. *Journal of Hazardous Materials* **2010**, *174*, 616-622.

8. Johnston, C. P.; Chrysochoou, M., Investigation of chromate coordination on ferrihydrite by in situ ATR-FTIR spectroscopy and theoretical frequency calculations. *Environmental Science & Technology* **2012**, *46*, 5851-5858.

9. Bailey, R.; Bennett, T.; Benjamin, M., Sorption onto and recovery of Cr(VI) using iron-oxide-coated sand. *Water Science & Technology* **1992**, *26*, 1239-1244.

10. Rai, D.; Eary, L.; Zachara, J., Environmental chemistry of chromium. *Science of the Total Environment* **1989**, *86*, 15-23.

11. Richard, F. C.; Bourg, A. C., Aqueous geochemistry of chromium: A review. *Water Research* **1991**, *25*, 807-816.

12. Villalobos, M.; Trotz, M. A.; Leckie, J. O., Surface complexation modeling of carbonate effects on the adsorption of Cr(VI), Pb(II), and U(VI) on goethite. *Environmental Science & Technology* **2001**, *35*, 3849-3856.

13. Davis, J. A., Adsorption of natural dissolved organic matter at the oxide/water interface. *Geochimica et cosmochimica acta* **1982**, *46*, 2381-2393.

14. Davis, C. C.; Knocke, W. R.; Edwards, M., Implications of aqueous silica sorption to iron hydroxide: mobilization of iron colloids and interference with sorption of arsenate and humic substances. *Environmental Science & Technology* **2001**, *35*, 3158-3162.

15. Lee, G.; Hering, J., Removal of chromium(VI) from drinking water by redox-assisted coagulation with iron(II). *Aqua* **2003**, *52*, 319-332.

16. Blowes, D. W.; Ptacek, C. J.; Jambor, J. L., In-situ remediation of Cr(VI)-contaminated groundwater using permeable reactive walls: laboratory studies. *Environmental Science & Technology* **1997**, *31*, 3348-3357.

17. Fuller, S. J.; Stewart, D. I.; Burke, I. T., Chromate reduction in highly alkaline groundwater by zerovalent iron: implications for its use in a permeable reactive barrier. *Industrial & Engineering Chemistry Research* **2013**, *52*, 4704-4714.

18. Wilkin, R. T.; Su, C.; Ford, R. G.; Paul, C. J., Chromium-removal processes during groundwater remediation by a zerovalent iron permeable reactive barrier. *Environmental Science & Technology* **2005**, *39*, 4599-4605.

19. Mackay, D. M.; Cherry, J. A., Groundwater contamination: Pump-and-treat remediation. *Environmental Science & Technology* **1989**, *23*, 630-636.

20. Haight Jr, G.; Perchonock, E.; Emmenegger, F.; Gordon, G., The mechanism of the oxidation of sulfur(IV) by chromium(VI) in acid solution1. *Journal of the American Chemical Society* **1965**, *87*, 3835-3840.

21. Wittbrodt, P. R.; Palmer, C. D., Reduction of Cr(VI) in the presence of excess soil fulvic acid. *Environmental Science & Technology* **1995**, *29*, 255-263.

22. WITTBRODT, P. R.; PALMER, C. D., Reduction of Cr(VI) by soil humic acids. *European Journal of Soil Science* **1997**, *48*, 151-162.

23. McGuire, M. J.; Blute, N. K.; Seidel, C.; Qin, G.; Fong, L., Pilot-scale studies of hexavalent chromium removal from drinking water. *American Water Works Association* **2006**, 134-143.

24. Qin, G.; McGuire, M. J.; Blute, N. K.; Seidel, C.; Fong, L., Hexavalent chromium removal by reduction with ferrous sulfate, coagulation, and filtration: A pilot-scale study. *Environmental Science & Technology* **2005**, *39*, 6321-6327.

25. Guan, X.; Dong, H.; Ma, J.; Lo, I., Simultaneous removal of chromium and arsenate from contaminated groundwater by ferrous sulfate: Batch uptake behavior. *Journal of Environmental Sciences* **2011**, *23*, 372-380.

26. Pettine, M.; D'ottone, L.; Campanella, L.; Millero, F. J.; Passino, R., The reduction of chromium(VI) by iron(II) in aqueous solutions. *Geochimica et cosmochimica acta* **1998**, *62*, 1509-1519.

27. Eary, L.; Rai, D., Chromate removal from aqueous wastes by reduction with ferrous ion. *Environmental Science & Technology* **1988**, *22*, 972-977.

28. Lakshmanan, D.; Clifford, D. A.; Samanta, G., Ferrous and ferric ion generation during iron electrocoagulation. *Environmental Science & Technology* **2009**, *43*, 3853-3859.

29. Harif, T.; Khai, M.; Adin, A., Electrocoagulation versus chemical coagulation: coagulation/flocculation mechanisms and resulting floc characteristics. *Water Research* **2012**, *46*, 3177-3188.

30. Holt, P. K.; Barton, G. W.; Mitchell, C. A., The future for electrocoagulation as a localised water treatment technology. *Chemosphere* **2005**, *59*, 355-367.

31. Chen, G., Electrochemical technologies in wastewater treatment. *Separation and Purification Technology* **2004**, *38*, 11-41.

32. Wang, J. W.; Bejan, D.; Bunce, N. J., Removal of arsenic from synthetic acid mine drainage by electrochemical pH adjustment and coprecipitation with iron hydroxide. *Environmental Science & Technology* **2003**, *37*, 4500-4506.

33. Wan, W.; Pepping, T. J.; Banerji, T.; Chaudhari, S.; Giammar, D. E., Effects of water chemistry on arsenic removal from drinking water by electrocoagulation. *Water Research* **2011**, *45*, 384-392.

34. Ratna Kumar, P.; Chaudhari, S.; Khilar, K. C.; Mahajan, S., Removal of arsenic from water by electrocoagulation. *Chemosphere* **2004**, *55*, 1245-1252.

35. Li, L.; van Genuchten, C. M.; Addy, S. E.; Yao, J.; Gao, N.; Gadgil, A. J., Modeling As(III) oxidation and removal with iron electrocoagulation in groundwater. *Environmental Science & Technology* **2012**, *46*, 12038-12045.

36. Kongsricharoern, N.; Polprasert, C., Electrochemical precipitation of chromium (Cr^{6+}) from an electroplating wastewater. *Water science and technology* **1995**, *31*, 109-117.

37. Martnez, S.; Rodrguez, M.; Aguilar, R.; Soto, G., Removal of chromium hexavalent from rinsing chromating waters electrochemical reduction in a laboratory pilot plant. *Water Science & Technology* **2004**, *49*, 115-122.

38. Ma, H.; Allen, H. E.; Yin, Y., Characterization of isolated fractions of dissolved organic matter from natural waters and a wastewater effluent. *Water Research* **2001**, *35*, 985-996.

39. Stevenson, F. J., *Humus chemistry: genesis, composition, reactions*. John Wiley & Sons: 1994.

40. Aiken, G. R.; Hsu-Kim, H.; Ryan, J. N., Influence of dissolved organic matter on the environmental fate of metals, nanoparticles, and colloids. In ACS Publications: 2011.

41. Buffle, J., Complexation reactions in aquatic systems. An analytical approach. **1988**.

42. Tessier, A.; Turner, D. R., *Metal speciation and bioavailability in aquatic systems*. Wiley Chichester: 1995; Vol. 3.

43. Christensen, J. B.; Jensen, D. L.; Christensen, T. H., Effect of dissolved organic carbon on the mobility of cadmium, nickel and zinc in leachate polluted groundwater. *Water Research* **1996**, *30*, 3037-3049.

44. MacLeod, K. C.; Patrick, B. O.; Smith, K. M., Reactivity of Cr(III) μ-oxo compounds: Catalyst regeneration and atom transfer processes. *Inorganic Chemistry* **2012**, *51*, 688-700.

45. Schwertmann, U., The influence of simple organic anions on the formation of goethite and haematite from amorphous ferric hydroxide. *Geoderma* **1970**, 207-214.

46. Schwertmann, U., Inhibitory effect of soil organic matter on the crystallization of amorphous ferric hydroxide. *Nature* **1966**, *212*, 645-646.

47. Tebo, B. M.; Bargar, J. R.; Clement, B. G.; Dick, G. J.; Murray, K. J.; Parker, D.; Verity, R.; Webb, S. M., Biogenic manganese oxides: Properties and mechanisms of formation. *Annu. Rev. Earth Planet. Sci.* **2004**, *32*, 287-328.

48. Friedl, G.; Wehrli, B.; Manceau, A., Solid phases in the cycling of manganese in eutrophic lakes: New insights from EXAFS spectroscopy. *Geochimica et Cosmochimica Acta* **1997**, *61*, 275-290.

49. Learman, D. R.; Wankel, S. D.; Webb, S. M.; Martinez, N.; Madden, A. S.; Hansel, C. M., Coupled biotic-abiotic Mn(II) oxidation pathway mediates the formation and structural evolution of biogenic Mn oxides. *Geochimica et Cosmochimica Acta* **2011**, *75*, 6048-6063.

50. Villalobos, M.; Toner, B.; Bargar, J.; Sposito, G., Characterization of the manganese oxide produced by *Pseudomonas putida* strain MnB1. *Geochimica et Cosmochimica Acta* **2003**, *67*, 2649-2662.

51. Lucht, K. P.; Mendoza-Cortes, J. L., Birnessite: a layered manganese oxide to capture sunlight for water-splitting catalysis. *Journal of Physical Chemistry C* **2015**, *119*, 22838-22846.

52. Butler, E. C.; Chen, L.; Hansel, C. M.; Krumholz, L. R.; Madden, A. S. E.; Lan, Y., Biological versus mineralogical chromium reduction: Potential for reoxidation by manganese oxide. *Environmental Science: Processes & Impacts* **2015**, *17*, 1930-1940.

53. Fandeur, D.; Juillot, F.; Morin, G.; Olivi, L.; Cognigni, A.; Webb, S. M.; Ambrosi, J.-P.; Fritsch, E.; Guyot, F. o.; Brown, J. G. E., XANES evidence for oxidation of Cr(III) to Cr(VI) by Mn-oxides in a lateritic regolith developed on serpentinized ultramafic rocks of New Caledonia. *Environmental Science & Technology* **2009**, *43*, 7384-7390.

54. Ivarsson, M.; Broman, C.; Holm, N. G., Chromite oxidation by manganese oxides in subseafloor basalts and the presence of putative fossilized microorganisms. *Geochemical Transactions* **2011**, *12*, 5.

55. Hausladen, D. M.; Fendorf, S., Hexavalent chromium generation within naturally structured soils and sediments. *Environmental Science & Technology* **2017**, *51*, 2058-2067.

56. Eary, L. E.; Rai, D., Kinetics of chromium(III) oxidation to chromium(VI) by reaction with manganese dioxide. *Environmental Science & Technology* **1987**, *21*, 1187-1193.

57. Schroeder, D. C.; Lee, G. F., Potential transformations of chromium in natural waters. *Water Air & Soil Pollution* **1975**, *4*, 355-365.

58. Varadharajan, C.; Beller, H. R.; Bill, M.; Brodie, E. L.; Conrad, M. E.; Han, R.; Irwin, C.; Larsen, J. T.; Lim, H.-C.; Molins, S., Re-oxidation of chromium(III) products formed under different biogeochemical regimes. *Environmental Science & Technology* **2017**, *51*, 4918-4927.

59. Amacher, M. C.; Baker, D. E., Redox reactions involving chromium, plutonium, and manganese in soils. *Radiation Chemistry Radiochemistry & Nuclear Chemistry* **1982**.

60. Fendorf, S. E.; Zasoski, R. J.; Burau, R. G., Competing metal ion influences on chromium(III) oxidation by birnessite. *Soilence Society of America Journal* **1993**, 1508-1515.

61. Fendorf, S. E.; Fendorf, M.; Sparks, D. L.; Gronsky, R., Inhibitory mechanisms of Cr(III) oxidation by δ-MnO_2. *Journal of Colloid & Interface Science* **1992**, *153*, 37-54.

62. Pan, C.; Troyer, L. D.; Catalano, J. G.; Giammar, D. E., Dynamics of chromium(VI) removal from drinking water by iron electrocoagulation. *Environmental Science & Technology* **2016**, *50*, 13502-13510.

63. Kaprara, E.; Kazakis, N.; Simeonidis, K.; Coles, S.; Zouboulis, A.; Samaras, P.; Mitrakas, M., Occurrence of Cr (VI) in drinking water of Greece and relation to the geological background. *Journal of Hazardous materials* **2015**, *281*, 2-11.

64. Brandhuber, P., Frey, M.M., McGuire, M.j., Chao, P.-F., Seidel, C., Amy, G., Yoon, J., McNeill, L.S.&Banerjee,K., Low-level hexavalent chromium treatment options: Bench-scale evaluation. *American Water Works Association* **2005**.

65. McNeill, L. S.; McLean, J. E.; Parks, J. L.; Edwards, M. A., Hexavalent Chromium Review, Part 2: Chemistry, Occurrence, and Treatment. *American Water Works Association* **2012**, *104*, E395-E405.

66. Dermatas, D.; Mpouras, T.; Chrysochoou, M.; Panagiotakis, I.; Vatseris, C.; Linardos, N.; Theologou, E.; Boboti, N.; Xenidis, A.; Papassiopi, N., Origin and concentration profile of chromium in a Greek aquifer. *Journal of Hazardous materials* **2015**, *281*, 35-46.

67. U.S.EPA, National Primary Drinking Water Regulations. *40 CFR Part 141* **2010**.

68. Health, C. D. o. P., California Regulations Related to Drinking Water. In 2014.

69. Seidel, C. J.; Najm, I. N.; Blute, N. K.; Corwin, C. J.; Wu, X., National and California treatment costs to comply with potential hexavalent chromium MCLs. *Journal: American Water Works Association* **2013**, *105*.

70. Seidel, C. J.; Corwin, C. J., Total chromium and hexavalent chromium occurrence analysis. *Journal-American Water Works Association* **2013**, *105*, E310-E319.

71. Mouedhen, G.; Feki, M.; De Petris-Wery, M.; Ayedi, H., Electrochemical removal of Cr(VI) from aqueous media using iron and aluminum as electrode materials: Towards a better understanding of the involved phenomena. *Journal of Hazardous materials* **2009**, *168*, 983-991.

72. van Genuchten, C. M.; Peña, J.; Amrose, S. E.; Gadgil, A. J., Structure of Fe(III) precipitates generated by the electrolytic dissolution of Fe(0) in the presence of groundwater ions. *Geochimica et Cosmochimica Acta* **2014**, *127*, 285-304.

73. Buerge, I. J.; Hug, S. J., Influence of mineral surfaces on chromium(VI) reduction by iron(II). *Environmental Science & Technology* **1999**, *33*, 4285-4291.

74. Tong, M.; Yuan, S.; Wang, Z.; Luo, M.; Wang, Y., Electrochemically induced oxidative removal of As(III) from groundwater in a dual-anode sand column. *Journal of Hazardous materials* **2016**, *305*, 41-50.

75. Zongo, I.; Leclerc, J.-P.; Maïga, H. A.; Wéthé, J.; Lapicque, F., Removal of hexavalent chromium from industrial wastewater by electrocoagulation: A comprehensive comparison of aluminium and iron electrodes. *Separation and Purification Technology* **2009**, *66*, 159-166.

76. Heidmann, I.; Calmano, W., Removal of Cr(VI) from model wastewaters by electrocoagulation with Fe electrodes. *Separation and Purification Technology* **2008**, *61*, 15-21.

77. Malakootian, M.; Mansoorian, H.; Moosazadeh, M., Performance evaluation of electrocoagulation process using iron-rod electrodes for removing hardness from drinking water. *Desalination* **2010**, *255*, 67-71.

78. Jeon, B.-H.; Dempsey, B. A.; Royer, R. A.; Burgos, W. D., Low-temperature oxygen trap for maintaining strict anoxic conditions. *Journal of Environmental Engineering* **2004**, *130*, 1407-1410.

79. U.S.EPA *SW-846, ,Method 7196A, Chromium, Hexavalent (Colorimetric).*

80. Viollier, E.; Inglett, P.; Hunter, K.; Roychoudhury, A.; Van Cappellen, P., The ferrozine method revisited: Fe(II)/Fe(III) determination in natural waters. *Applied Geochemistry* **2000**, *15*, 785-790.

81. Ravel, B.; Newville, M., ATHENA , ARTEMIS , HEPHAESTUS : data analysis for X-ray absorption spectroscopy using IFEFFIT. *Journal of synchrotron radiation* **2005**, *12*, 537–541.

82. Newville, M., IFEFFIT : interactive XAFS analysis and FEFF fitting. *Journal of synchrotron radiation* **2001**, *8*, 322–324.

83. van Genuchten, C. M.; Addy, S. E.; Peña, J.; Gadgil, A. J., Removing arsenic from synthetic groundwater with iron electrocoagulation: An Fe and As K-edge EXAFS study. *Environmental Science & Technology* **2012**, *46*, 986-994.

84. Dubrawski, K. L.; van Genuchten, C. M.; Delaire, C.; Amrose, S. E.; Gadgil, A. J.; Mohseni, M., Production and transformation of mixed valent nanoparticles generated by Fe (0) electrocoagulation. *Environmental Science & Technology* **2015**.

85. Benjamin, M. M., *Water chemistry*. McGraw-Hill New York: 2002.

86. Sass, B. M.; Rai, D., Solubility of amorphous chromium(III)-iron(III) hydroxide solid solutions. *Inorganic Chemistry* **1987**, *26*, 2228-2232.

87. Schlautman, M. A.; Han, I., Effects of pH and dissolved oxygen on the reduction of hexavalent chromium by dissolved ferrous iron in poorly buffered aqueous systems. *Water Research* **2001**, *35*, 1534-1546.

88. Stumm, W., Catalysis of redox processes by hydrous oxide surfaces. *Croatica Chemica Acta* **1997**, *70*, 71-93.

89. Williams, A. G.; Scherer, M. M., Spectroscopic evidence for Fe(II)-Fe(III) electron transfer at the iron oxide-water interface. *Environmental Science & Technology* **2004**, *38*, 4782-4790.

90. Urrutia, M. M.; Roden, E. E.; Zachara, J. M., Influence of aqueous and solid-phase Fe(II) complexants on microbial reduction of crystalline iron(III) oxides. *Environmental Science & Technology* **1999**, *33*, 4022-4028.

91. Singer, P. C.; Stumm, W., Oxygenation of ferrous iron. *Water Poll. Cont. Res. Ser* **1970**, 14010-06169.

92. Morgan, B.; Lahav, O., The effect of pH on the kinetics of spontaneous Fe(II) oxidation by O_2 in aqueous solution–basic principles and a simple heuristic description. *Chemosphere* **2007**, *68*, 2080-2084.

93. Sedlak, D. L.; Chan, P. G., Reduction of hexavalent chromium by ferrous iron. *Geochimica et Cosmochimica Acta* **1997**, *61*, 2185-2192.

94. Buerge, I. J.; Hug, S. J., Kinetics and pH dependence of chromium(VI) reduction by iron (II). *Environmental Science & Technology* **1997**, *31*, 1426-1432.

95. Ölmez, T., The optimization of Cr(VI) reduction and removal by electrocoagulation using response surface methodology. *Journal of Hazardous materials* **2009**, *162*, 1371-1378.

96. Aber, S.; Amani-Ghadim, A.; Mirzajani, V., Removal of Cr(VI) from polluted solutions by electrocoagulation: Modeling of experimental results using artificial neural network. *Journal of Hazardous materials* **2009**, *171*, 484-490.

97. Lai, H.; McNeill, L. S., Chromium redox chemistry in drinking water systems. *Journal of Environmental Engineering* **2006**, *132*, 842-851.

98. Chebeir, M.; Liu, H., Kinetics and mechanisms of Cr(VI) formation via the oxidation of Cr(III) solid phases by chlorine in drinking water. *Environmental Science & Technology* **2015**, *50*, 701-710.

99. Golder, A.; Samanta, A.; Ray, S., Removal of trivalent chromium by electrocoagulation. *Separation and Purification Technology* **2007**, *53*, 33-41.

100. Appelo, C. A. J.; Postma, D., *Geochemistry, groundwater and pollution*. CRC Press: 2005.

101. James, B. R.; Bartlett, R. J., Behavior of chromium in soils: VII. Adsorption and reduction of hexavalent forms. *Journal of Environmental Quality* **1983**, *12*, 177-181.

102. Gu, C.; Wang, Z.; Kubicki, J. D.; Wang, X.; Zhu, M., X-ray absorption spectroscopic quantification and speciation modeling of sulfate adsorption on ferrihydrite surfaces. *Environmental Science & Technology* **2016**, *50*, 8067-8076.

103. Guan, X.; Dong, H.; Ma, J., Influence of phosphate, humic acid and silicate on the transformation of chromate by Fe(II) under suboxic conditions. *Separation and Purification Technology* **2011**, *78*, 253-260.

104. Hochella, M. F.; White, A. F., Mineral-water interface geochemistry: An overview. *Reviews in mineralogy and geochemistry* **1990**, *23*, 1-16.

105. Dzombak, D. A.; Morel, F. M., *Surface complexation modeling: Hydrous ferric oxide*. John Wiley & Sons: 1990.

106. Rai, D.; Sass, B. M.; Moore, D. A., Chromium(III) hydrolysis constants and solubility of chromium (III) hydroxide. *Inorganic Chemistry* **1987**, *26*, 345-349.

107. Schecher, W. D. M., D. C, MINEQL+: A Chemical Equilibrium Modeling System, version 4.6. *Environmental Research Software: Hallowell, ME* **2007**.

108. Pan, C.; Troyer, L. D.; Liao, P.; Catalano, J. G.; Li, W.; Giammar, D. E., Effect of humic acid on the removal of chromium(VI) and the production of solids in iron electrocoagulation. *Environmental Science & Technology* **2017**, *51*, 6308-6318.

109. Brandhuber, P.; Frey, M.; McGuire, M., *Low-level hexavalent chromium treatment options: bench-scale evaluation*. American Water Works Association: 2005.

110. Eary, L. E.; Rai, D., Chromate removal from aqueous wastes by reduction with ferrous ion. *Environmental Science & Technology* **1988**, *22*, 972-977.

111. Kuokkanen, V.; Kuokkanen, T.; Rämö, J.; Lassi, U., Electrocoagulation treatment of peat bog drainage water containing humic substances. *Water Research* **2015**, *79*, 79-87.

112. Dubrawski, K. L.; Mohseni, M., In-situ identification of iron electrocoagulation speciation and application for natural organic matter (NOM) removal. *Water Research* **2013**, *47*, 5371-5380.

113. Aiken, G.; McKnight, D.; Wershaw, R.; MacCarthy, P., *Humic substances in soil, sediment, and water: geochemistry, isolation and characterization*. 1985.

114. Thurman, E. M.; Wershaw, R. L.; Malcolm, R. L.; Pinckney, D. J., Molecular size of aquatic humic substances. *Organic Geochemistry* **1982**, *4*, 27-35.

115. Tipping, E., Cation binding by humic substances. *Geochimica et Cosmochimica Acta* **2002**, *56*, 3627–3641.

116. Wang, Y. G.; Michel, F. M.; Choi, Y.; Eng, P. J.; Levard, C.; Siebner, H.; Gu, B. H.; Bargar, J. R.; Brown, G. E., Pb, Cu, and Zn distributions at humic acid-coated metal-oxide surfaces. *Geochimica et Cosmochimica Acta* **2016**, *188*, 407-423.

117. Gledhill, M.; Buck, K. N., The organic complexation of iron in the marine environment: a review. *Frontiers in Microbiology* **2012**, *3*, 1-17.

118. Tipping, E., Modeling ion-binding by humic acids. *Colloids and Surfaces A: Physicochemical and Engineering Aspects* **1993**, *73*, 117-131.

119. Lalonde, K.; Mucci, A.; Ouellet, A.; Gélinas, Y., Preservation of organic matter in sediments promoted by iron. *Nature* **2012**, *483*, 198-200.

120. Tombácz, E.; Libor, Z.; Illés, E.; Majzik, A.; Klumpp, E., The role of reactive surface sites and complexation by humic acids in the interaction of clay mineral and iron oxide particles. *Organic Geochemistry* **2004**, *35*, 257-267.

121. Gu, B.; Schmitt, J.; Chen, Z.; Liang, L.; Mccarthy, J. F., Adsorption and desorption of natural organic matter on iron oxide: mechanisms and models. *Environmental Science & Technology* **1994**, *28*, 38-46.

122. Illés, E.; Tombácz, E., The effect of humic acid adsorption on pH-dependent surface charging and aggregation of magnetite nanoparticles. *Journal of Colloid and Interface Science* **2006**, *295*, 115-123.

123. Chen, C.; Dynes, J. J.; Wang, J.; Sparks, D. L., Properties of Fe-organic matter associations via coprecipitation versus adsorption. *Environmental Science & Technology* **2014**, *48*, 13751-13759.

124. Mikutta, R.; Schaumann, G. E.; Gildemeister, D.; Bonneville, S.; Kramer, M. G.; Chorover, J.; Chadwick, O. A.; Guggenberger, G., Biogeochemistry of mineral–organic associations across a long-term mineralogical soil gradient (0.3–4100kyr), Hawaiian Islands. *Geochimica et Cosmochimica Acta* **2009**, *73*, 2034-2060.

125. Wagai, R.; Mayer, L. M., Sorptive stabilization of organic matter in soils by hydrous iron oxides. *Geochimica et Cosmochimica Acta* **2007**, *71*, 25–35.

126. Eusterhues, K.; Wagner, F. E.; Häusler, W.; Hanzlik, M.; Knicker, H.; Totsche, K. U.; Kögel-Knabner, I.; Schwertmann, U., Characterization of ferrihydrite-soil organic matter coprecipitates by X-ray diffraction and Mössbauer spectroscopy. *Environmental Science & Technology* **2008**, *42*, 7891-7897.

127. Karlsson, T.; Persson, P., Coordination chemistry and hydrolysis of Fe(III) in a peat humic acid studied by X-ray absorption spectroscopy. *Geochimica et Cosmochimica Acta* **2010**, *74*, 30-40.

128. Benedetti, M. F.; Riemsdijk, W. H. V.; Koopal, L. K.; Kinniburgh, D. G.; Gooddy, D. C.; Milne, C. J., Metal ion binding by natural organic matter: From the model to the field. *Geochimica et Cosmochimica Acta* **1996**, *60*, 2503-2513.

129. Gustafsson, J. P.; Persson, I.; Oromieh, A. G.; Schaik, J. W. J. V.; Sjöstedt, C.; Dan, B. K., Chromium(III) complexation to natural organic matter: mechanisms and modeling. *Environmental Science & Technology* **2014**, *48*, 1753-1761.

130. Westall, J. C.; Jones, J. D.; Turner, G. D.; Zachara, J. M., Models for association of metal ions with heterogeneous environmental sorbents. 1. complexation of Co(II) by leonardite humic

acid as a function of pH and $NaClO_4$ concentration. *Environmental Science & Technology* **1995**, *29*, 951-959.

131. Mak, M. S. H.; Lo, I. M. C., Influences of redox transformation, metal complexation and aggregation of fulvic acid and humic acid on Cr(VI) and As(V) removal by zero-valent iron. *Chemosphere* **2011**, *84*, 234-240.

132. Liu, T.; Tsang, D. C.; Lo, I. M., Chromium(VI) reduction kinetics by zero-valent iron in moderately hard water with humic acid: iron dissolution and humic acid adsorption. *Environmental Science & Technology* **2008**, *42*, 2092-2098.

133. Theis, T. L.; Singer, P. C., Complexation of iron(II) by organic matter and its effect on iron(II) oxygenation. *Environmental Science & Technology* **1974**, *8*, 569-573.

134. Miles, C. J.; Brezonik, P. L., Oxygen consumption in humic-colored waters by a photochemical ferrous-ferric catalytic cycle. *Environmental Science & Technology* **1981**, *15*, 1089-1095.

135. Rose, A. L.; Waite, T. D., Kinetic model for Fe(II) oxidation in seawater in the absence and presence of natural organic matter. *Environmental Science & Technology* **2002**, *36*, 433-444.

136. Rose, A. L.; Waite, T. D., Effect of dissolved natural organic matter on the kinetics of ferrous iron oxygenation in seawater. *Environmental Science & Technology* **2003**, *37*, 4877-4886.

137. Stumm, W.; Morgan, J., *Aquatic Chemistry, 780 pp*. 1981.

138. Liang, L.; Mcnabb, J. A.; Paulk, J. M.; Gu, B.; Mccarthy, J. F., Kinetics of iron(II) oxygenation at low partial pressure of oxygen in the presence of natural organic matter. *Environmental Science & Technology* **1993**, *27*, 1864-1870.

139. Emmenegger, L.; King, D. W.; Sigg, L.; Sulzberger, B., Oxidation kinetics of Fe(II) in a eutrophic Swiss lake. *Environmental Science & Technology* **1998**, *32*, 2990-2996.

140. Guan, X.; Dong, H.; Ma, J., Influence of phosphate, humic acid and silicate on the transformation of chromate by Fe(II) under suboxic conditions. *Separation and Purification Technology* **2011**, *78*, 253-260.

141. Buerge, I. J.; Hug, S. J., Influence of organic ligands on chromium(VI) reduction by iron(II). *Environmental Science & Technology* **1998**, *32*, 2092-2099.

142. Agrawal, S. G.; Fimmen, R. L.; Chin, Y.-P., Reduction of Cr(VI) to Cr(III) by Fe(II) in the presence of fulvic acids and in lacustrine pore water. *Chemical Geology* **2009**, *262*, 328-335.

143. Good, N. E.; Winget, G. D.; Winter, W.; Connolly, T. N.; Izawa, S.; Singh, R. M., Hydrogen ion buffers for biological research. *Biochemistry* **1966**, *5*, 467-477.

144. Ferguson, W. J.; Braunschweiger, K.; Braunschweiger, W.; Smith, J. R.; McCormick, J. J.; Wasmann, C. C.; Jarvis, N. P.; Bell, D. H.; Good, N. E., Hydrogen ion buffers for biological research. *Analytical Biochemistry* **1980**, *104*, 300-310.

145. Hinkle, M. A.; Wang, Z.; Giammar, D. E.; Catalano, J. G., Interaction of Fe(II) with phosphate and sulfate on iron oxide surfaces. *Geochimica et Cosmochimica Acta* **2015**, *158*, 130-146.

146. Wang, Z.; Tebo, B. M.; Giammar, D. E., Effects of Mn(II) on UO_2 dissolution under anoxic and oxic conditions. *Environmental Science & Technology* **2014**, *48*, 5546-5554.

147. Kim, C.; Zhou, Q.; Deng, B.; Thornton, E. C.; Xu, H., Chromium (VI) reduction by hydrogen sulfide in aqueous media: stoichiometry and kinetics. *Environmental Science & Technology* **2001**, *35*, 2219-2225.

148. Carbonaro, R. F.; Gray, B. N.; Whitehead, C. F.; Stone, A. T., Carboxylate-containing chelating agent interactions with amorphous chromium hydroxide: adsorption and dissolution. *Geochimica et Cosmochimica Acta* **2008**, *72*, 3241-3257.

149. Lipson, D. A.; Raab, T. K.; Goria, D.; Zlamal, J., The contribution of Fe(III) and humic acid reduction to ecosystem respiration in drained thaw lake basins of the Arctic Coastal Plain. *Global Biogeochemical Cycles* **2013**, *27*, 399-409.

150. Li, T.; Jiang, Y.; An, X.; Liu, H.; Hu, C.; Qu, J., Transformation of humic acid and halogenated byproduct formation in UV-chlorine processes. *Water Research* **2016**, *102*, 421-427.

151. Dries, J.; Bastiaens, L.; Springael, D.; Kuypers, S.; Agathos, S. N.; Diels, L., Effect of humic acids on heavy metal removal by zero-valent iron in batch and continuous flow column systems. *Water Research* **2005**, *39*, 3531-40.

152. Jeon, B. H.; Burgos, W. D.; Royer, R. A.; Dempsey, B. A., Low-temperature oxygen trap for maintaining strict anoxic conditions. *Journal of Environmental Engineering* **2004**, *130*, 1407-1410.

153. SW-846, U. S. E., Method 7196A, Chromium, Hexavalent (Colorimetric).

154. Viollier, E.; Inglett, P. W.; Hunter, K.; Roychoudhury, A. N.; Cappellen, P. V., The ferrozine method revisited: Fe(II)/Fe(III) determination in natural waters. *Applied Geochemistry* **2000**, *15*, 785-790.

155. Doane, T. A.; Horwáth, W. R., Eliminating interference from iron(III) for ultraviolet absorbance measurements of dissolved organic matter. *Chemosphere* **2010**, *78*, 1409-15.

156. Luo, Y.; Giammar, D. E.; Huhmann, B. L.; Catalano, J. G., Speciation of selenium, arsenic, and zinc in class C fly ash. *Energy & fuels* **2011**, *25*, 2980-2987.

157. Catalano, J. G.; Huhmann, B. L.; Luo, Y.; Mitnick, E. H.; Slavney, A.; Giammar, D. E., Metal release and speciation changes during wet aging of coal fly ashes. *Environmental Science & Technology* **2012**, *46*, 11804-11812.

158. Schwertmann, U.; Cornell, R. M., *Iron oxides in the laboratory: preparation and characterization*. John Wiley & Sons: 2008.

159. Ravel, B.; Newville, M., ATHENA, ARTEMIS, HEPHAESTUS: data analysis for X-ray absorption spectroscopy using IFEFFIT. *Journal of Synchrotron Radiation* **2005**, *12*, 537-541.

160. Newville, M., IFEFFIT : interactive XAFS analysis and FEFF fitting. *Journal of Synchrotron Radiation* **2001**, *8*, 322-324.

161. Webb, S. M., SIXPack: A graphical user interface for XAS analysis using IFEFFIT. *Physica Scipta* **2005**, *T115*, 1011-1014.

162. Ankudinov, A. L.; Rehr, J. J., Relativistic calculations of spin-dependent x-ray-absorption spectra. *Physical Review B* **1997**, *56*, R1712-R1715.

163. Nagai, T.; Kagi, H.; Yamanaka, T., Variation of hydrogen bonded O··O distances in goethite at high pressure. *American Mineralogist* **2003**, *88*, 1423-1427.

164. Voelker, B. M.; Sulzberger, B., Effects of fulvic acid on Fe(II) oxidation by hydrogen peroxide. *Environmental Science & Technology* **1996**, *30*, 1106-1114.

165. Wang, Z.; Schenkeveld, W. D.; Kraemer, S. M.; Giammar, D. E., Synergistic effect of reductive and ligand-promoted dissolution of goethite. *Environmental Science & Technology* **2015**, *49*, 7236-7244.

166. Kim, D.; Duckworth, O. W.; Strathmann, T. J., Reactions of aqueous iron–DFOB (desferrioxamine B) complexes with flavin mononucleotide in the absence of strong iron (II) chelators. *Geochimica et Cosmochimica Acta* **2010**, *74*, 1513-1529.

167. Liao, P.; Li, W.; Wang, D.; Jiang, Y.; Pan, C.; Fortner, J. D.; Yuan, S., Effect of reduced humic acid on the transport of ferrihydrite nanoparticles under anoxic conditions. *Water Research* **2017**, *109*, 347-357.

168. Yan, S. C.; Ouyang, S. X.; Gao, J.; Yang, M.; Feng, J. Y.; Fan, X. X.; Wan, L. J.; Li, Z. S.; Ye, J. H.; Zhou, Y., A room-temperature reactive-template route to mesoporous $ZnGa_2O_4$ with improved photocatalytic activity in reduction of CO_2. *Angewandte Chemie* **2010**, *122*, 6544-6548.

169. Xie, Y., *Disinfection byproducts in drinking water: Formation, analysis, and control*. CRC press: 2016.

170. Diemert, S.; Wang, W.; Andrews, R. C.; Li, X.-F., Removal of halo-benzoquinone (emerging disinfection by-product) precursor material from three surface waters using coagulation. *Water Research* **2013**, *47*, 1773-1782.

171. Watson, K.; Farré, M. J.; Knight, N., Enhanced coagulation with powdered activated carbon or MIEX® secondary treatment: a comparison of disinfection by-product formation and precursor removal. *Water Research* **2015**, *68*, 454-466.

172. Tian, C.; Liu, R.; Liu, H.; Qu, J., Disinfection by-products formation and precursors transformation during chlorination and chloramination of highly-polluted source water: Significance of ammonia. *Water Research* **2013**, *47*, 5901-5910.

173. Dubrawski, K. L.; Mohseni, M., Standardizing electrocoagulation reactor design: Iron electrodes for NOM removal. *Chemosphere* **2013**, *91*, 55-60.

174. Rodrigues, A.; Brito, A.; Janknecht, P.; Proença, M. F.; Nogueira, R., Quantification of humic acids in surface water: effects of divalent cations, pH, and filtration. *Journal of Environmental Monitoring* **2009**, *11*, 377-382.

175. Liu, T. Z.; Rao, P. H.; Lo, I. M. C., Influences of humic acid, bicarbonate and calcium on Cr(VI) reductive removal by zero-valent iron. *Science of the Total Environment* **2009**, *407*, 3407-3414.

176. Hansel, C. M.; Wielinga, B. W.; Fendorf, S., Structural and compositional evolution of Cr/Fe solids after indirect chromate reduction by dissimilatory iron-reducing bacteria. *Geochimica et Cosmochimica Acta* **2003**, *67*, 401-412.

177. Voegelin, A.; Senn, A. C.; Kaegi, R.; Hug, S. J.; Mangold, S., Dynamic Fe-precipitate formation induced by Fe(II) oxidation in aerated phosphate-containing water. *Geochimica et Cosmochimica Acta* **2013**, *117*, 216-231.

178. Schwertmann, U.; Wagner, F.; Knicker, H., Ferrihydrite–humic associations. *Soil Science Society of America Journal* **2005**, *69*, 1009-1015.

179. Song, J.; Jia, S. Y.; Yu, B.; Wu, S. H.; Han, X., Formation of iron (hydr)oxides during the abiotic oxidation of Fe(II) in the presence of arsenate. *Journal of Hazardous Materials* **2015**, *294*, 70-79.

180. Papassiopi, N.; Pinakidou, F.; Katsikini, M.; Antipas, G. S. E.; Christou, C.; Xenidis, A.; Paloura, E. C., A XAFS study of plain and composite iron(III) and chromium(III) hydroxides. *Chemosphere* **2014**, *111*, 169-176.

181. Charlet, L.; Manceau, A. A., X-ray absorption spectroscopic study of the sorption of Cr(III) at the oxide-water interface: II. Adsorption, coprecipitation, and surface precipitation on hydrous ferric oxide. *Journal of Colloid and Interface Science* **1992**, *148*, 443-458.

182. Buerge, I. J.; Hug, S. J., Kinetics and pH dependence of chromium(VI) reduction by iron(II). *Environmental Science & Technology* **1997**, *31*, 1426-1432.

183. Pan, C.; Troyer, L. D.; Catalano, J. G.; Giammar, D. E., Dynamics of chromium(VI) removal from drinking water by iron electrocoagulation. *Environmental Science & Technology* **2016**.

184. King, D. W., Role of carbonate speciation on the oxidation rate of Fe(II) in aquatic systems. *Environmental Science & Technology* **1998**, *32*, 2997-3003.

185. Kelly, S. D.; Hesterberg, D.; Ravel, B., Analysis of soils and minerals using X-ray absorption spectroscopy. In *Methods of Soil Analysis, Part 5 - Mineralogical Methods*, Ulery, A. L.; Drees, L. R., Eds. Soil Science Society of America: Madison, WI, 2008; pp 367-463.

186. Hillier, S.; Lumsdon, D. G.; Brydson, R.; Paterson, E., Hydrogarnet: A host phase for Cr(VI) in chromite ore processing residue (COPR) and other high pH wastes. *Environmental Science & Technology* **2007**, *41*, 1921-1927.

187. Nriagu, J. O.; Nieboer, E., *Chromium in the natural and human environments*. John Wiley & Sons: 1988; Vol. 20.

188. Iyer, G. V.; Mastorakis, N. E., Assessment of pollution load from unsafe chromium leather tanneries in india. *WSEAS Transactions on Environment and Development* **2006**, *2*, 207-215.

189. Eary, L. E.; Rai, D., Chromate removal from aqueous wastes by reduction with ferrous ion. *Environmental Science & Technology* **1988**, *22*, 972-997.

190. Blowes, D. W.; Ptacek, C. J.; Jambor, J. L., In-situ remediation of Cr(VI)-contaminated groundwater using permeable reactive walls: laboratory studies. *Environmental Science & Technology* **1997**, *31*, 3348-3357.

191. Mullet, M.; Demoisson, F.; Humbert, B.; Michot, L. J.; Vantelon, D., Aqueous Cr(VI) reduction by pyrite: Speciation and characterisation of the solid phases by X-ray photoelectron, Raman and X-ray absorption spectroscopies. *Geochimica et Cosmochimica Acta* **2007**, *71*, 3257-3271.

192. Battaglia-Brunet, F.; Foucher, S.; Morin, D.; Ignatiadis, I., Chromate (CrO_4^{2-}) reduction in groundwaters by using reductive bacteria in fixed-bed bioreactors. *Water, Air, & Soil Pollution: Focus* **2004**, *4*, 127-135.

193. Papassiopi, N.; Kontoyianni, A.; Vaxevanidou, K.; Xenidis, A., Evaluation of Fe(III) reducing microorganisms for the biostabilisation of chromium in contaminated soils. In *GeoCongress 2008: Geotechnics of Waste Management and Remediation*, 2008; pp 535-542.

194. Papassiopi, N.; Pinakidou, F.; Katsikini, M.; Antipas, G. S. E.; Christou, C.; Xenidis, A.; Paloura, E. C., A XAFS study of plain and composite iron(III) and chromium(III) hydroxides. *Chemosphere* **2014**, *111*, 169-176.

195. Puls, R. W.; Paul, C. J.; Powell, R. M., The application of in situ permeable reactive (zero-valent iron) barrier technology for the remediation of chromate-contaminated groundwater: a field test. *Applied Geochemistry* **1999**, *14*, 989-1000.

196. Wielinga, B.; Mizuba, M. M.; Hansel, C. M.; Fendorf, S., Iron promoted reduction of chromate by dissimilatory iron-reducing bacteria. *Environmental Science & Technology* **2001**, *35*, 522-527.

197. Papassiopi, N.; Vaxevanidou, K.; Christou, C.; Karagianni, E.; Antipas, G. S. E., Synthesis, characterization and stability of Cr(III) and Fe(III) hydroxides. *Journal of Hazardous Materials* **2014**, *264*, 490-497.

198. Sass, B. M.; Rai, D., Solubility of amorphous chromium(III)-iron(III) hydroxide solid solutions. *Inorganic Chemistry* **1987**, *26*, 2228-2232.

199. McClain, C. N.; Fendorf, S.; Webb, S. M.; Maher, K., Quantifying Cr(VI) production and export from serpentine soil of the California coast range. *Environmental Science & Technology* **2016**, *51*, 141-149.

200. Gonzalez, A. R.; Ndung'u, K.; Flegal, A., Natural occurrence of hexavalent chromium in the Aromas Red Sands Aquifer, California. *Environmental Science & Technology* **2005**, *39*, 5505-5511.

201. Hausladen, D. M.; Fendorf, S., Hexavalent chromium generation within naturally structured soils and sediments. *Environmental Science & Technology* **2017**, *51*, 2058-2067.

202. Rajapaksha, A. U.; Vithanage, M.; Ok, Y. S.; Oze, C., Cr(VI) formation related to Cr(III)-muscovite and birnessite interactions in ultramafic environments. *Environmental Science & Technology* **2013**, *47*, 9722-9729.

203. Landrot, G.; Ginder-Vogel, M.; Sparks, D. L., Kinetics of chromium(III) oxidation by manganese(IV) oxides using quick scanning X-ray absorption fine structure spectroscopy (Q-XAFS). *Environmental Science & Technology* **2009**, *44*, 143-149.

204. Oze, C.; Bird, D. K.; Fendorf, S., Genesis of hexavalent chromium from natural sources in soil and groundwater. *Proceedings of the National Academy of Sciences* **2007**, *104*, 6544-6549.

205. Fendorf, S. E.; Fendorf, M.; Sparks, D. L.; Gronsky, R., Inhibitory mechanisms of Cr(III) oxidation by δ-MnO_2. *Journal of Colloid and Interface Science* **1992**, *153*, 37-54.

206. Wang, Z.; Lee, S.-W.; Kapoor, P.; Tebo, B. M.; Giammar, D. E., Uraninite oxidation and dissolution induced by manganese oxide: A redox reaction between two insoluble minerals. *Geochimica et Cosmochimica Acta* **2013**, *100*, 24-40.

207. Wadhawan, A. R.; Livi, K. J.; Stone, A. T.; Bouwer, E. J., Influence of oxygenation on chromium redox reactions with manganese sulfide (MnS(s)). *Environmental Science & Technology* **2015**, *49*, 3523-3531.

208. Wang, Z.; Xiong, W.; Tebo, B. M.; Giammar, D. E., Oxidative UO_2 dissolution induced by soluble Mn(III). *Environmental Science & Technology* **2013**, *48*, 289-298.

209. Huangfu, X.; Ma, C.; Ma, J.; He, Q.; Yang, C.; Zhou, J.; Jiang, J.; Wang, Y., Effective removal of trace thallium from surface water by nanosized manganese dioxide enhanced quartz sand filtration. *Chemosphere* **2017**, *189*, 1-9.

210. Wadhawan, A. R.; Stone, A. T.; Bouwer, E. J., Biogeochemical controls on hexavalent chromium formation in estuarine sediments. *Environmental Science & Technology* **2013**, *47*, 8220-8228.

211. Hinkle, M. A. G.; Flynn, E. D.; Catalano, J. G., Structural response of phyllomanganates to wet aging and aqueous Mn(II). *Geochimica et Cosmochimica Acta* **2016**, *192*, 220-234.

212. Saad, E. M.; Sun, J.; Chen, S.; Borkiewicz, O. J.; Zhu, M.; Duckworth, O. W.; Tang, Y., Siderophore and organic acid promoted dissolution and transformation of Cr(III)-Fe(III)-(oxy) hydroxides. *Environmental Science & Technology* **2017**, *51*, 3223-3232.

213. Tang, Y.; Michel, F. M.; Zhang, L.; Harrington, R.; Parise, J. B.; Reeder, R. J., Structural properties of the Cr(III)-Fe(III)(oxy) hydroxide compositional series: insights for a nanomaterial "solid solution". *Chemistry of Materials* **2010**, *22*, 3589-3598.

214. Amonette, J. E.; Rai, D., Identification of noncrystalline (Fe, Cr)$(OH)_3$ by infrared spectroscopy. *Clays and Clay Minerals* **1990**, *38*, 129-136.

215. U.S.EPA, SW-846, Method 7196A, Chromium, Hexavalent (Colorimetric).

216. Murray, J. W.; Dillard, J. G.; Giovanoli, R.; Moers, H.; Stumm, W., Oxidation of Mn(II): Initial mineralogy, oxidation state and ageing. *Geochimica et Cosmochimica Acta* **1985**, *49*, 463-470.

217. James, B. R.; Petura, J. C.; Vitale, R. J.; Mussoline, G. R., Hexavalent chromium extraction from soils: A comparison of five methods. *Environmental Science & Technology* **1995**, *29*, 2377-2381.

218. Fredrickson, J. K.; Zachara, J. M.; Kennedy, D. W.; Liu, C. X.; Duff, M. C.; Hunter, D. B.; Dohnalkova, A., Influence of Mn oxides on the reduction of uranium(VI) by the metal-reducing bacterium Shewanella putrefaciens. *Geochimica et Cosmochimica Acta* **2002**, *66*, 3247-3262.

219. Liu, C. X.; Zachara, J. M.; Fredrickson, J. K.; Kennedy, D. W.; Dohnalkova, A., Modeling the inhibition of the bacterial reduction of U(VI) by β-MnO_2(S)(g). *Environmental Science & Technology* **2002**, *36*, 1452-1459.

220. van der Zee, C.; van Raaphorst, W.; Epping, E., Absorbed Mn^{2+} and Mn redox cycling in Iberian continental margin sediments (northeast Atlantic Ocean). *Journal of Marine Research* **2001**, *59*, 133-166.

221. Burdige, D. J.; Nealson, K. H., Microbial manganese reduction by enrichment cultures from coastal marine sediments. *Applied and Environmental Microbiology* **1985**, *50*, 491-497.

222. Fairley, N.; Carrick, A.; Fairly, N., *The casa cookbook*. Acolyte Science Cheshire: 2005; Vol. 1.

223. Nesbitt, H.; Banerjee, D., Interpretation of XPS Mn(2p) spectra of Mn oxyhydroxides and constraints on the mechanism of MnO_2 precipitation. *American Mineralogist* **1998**, *83*, 305-315.

224. Lee, G.; Song, K.; Bae, J., Permanganate oxidation of arsenic(III): Reaction stoichiometry and the characterization of solid product. *Geochimica et Cosmochimica Acta* **2011**, *75*, 4713-4727.

225. Rai, D.; Sass, B. M.; Moore, D. A., Chromium(III) hydrolysis constants and solubility of chromium(III) hydroxide. *Inorganic Chemistry* **1987**, *26*, 345-349.

226. Banerjee, D.; Nesbitt, H. W., Oxidation of aqueous Cr(III) at birnessite surfaces: Constraints on reaction mechanism. *Geochimica et Cosmochimica Acta* **1999**, *63*, 1671-1687.

227. Elzinga, E. J., 54Mn radiotracers demonstrate continuous dissolution and reprecipitation of vernadite (δ-MnO_2) during interaction with aqueous Mn(II). *Environmental Science & Technology* **2016**, *50*, 8670-8677.

228. Wang, Z.; Ulrich, K.-U.; Pan, C.; Giammar, D. E., Measurement and modeling of U(IV) adsorption to metal oxide minerals. *Environmental Science & Technology Letters* **2015**, *2*, 227-232.

229. Namgung, S.; Kwon, M. J.; Qafoku, N. P.; Lee, G., Cr(OH)3(s) oxidation induced by surface catalyzed Mn(II) oxidation. *Environmental Science & Technology* **2014**, *48*, 10760-10768.

230. Elzinga, E. J., Reductive transformation of birnessite by aqueous Mn(II). *Environmental Science & Technology* **2011**, *45*, 6366-6372.

231. Lefkowitz, J. P.; Rouff, A. A.; Elzinga, E. J., Influence of pH on the reductive transformation of birnessite by aqueous Mn(II). *Environmental Science & Technology* **2013**, *47*, 10364-10371.

232. Lopano, C. L.; Heaney, P. J.; Post, J. E.; Hanson, J.; Komarneni, S., Time-resolved structural analysis of K- and Ba-exchange reactions with synthetic Na-birnessite using synchrotron X-ray diffraction. *American Mineralogist* **2007**, *92*, 380-387.

233. Plathe, K. L.; Lee, S.-W.; Tebo, B. M.; Bargar, J. R.; Bernier-Latmani, R., Impact of microbial Mn oxidation on the remobilization of bioreduced U(IV). *Environmental Science & Technology* **2013**, *47*, 3606-3613.

234. Kent, D.; Davis, J.; Anderson, L.; Rea, B.; Waite, T., Transport of chromium and selenium in the suboxic zone of a shallow aquifer: Influence of redox and adsorption reactions. *Water Resources Research* **1994**, *30*, 1099-1114.

235. Jardine, P.; Fendorf, S.; Mayes, M.; Larsen, I.; Brooks, S.; Bailey, W., Fate and transport of hexavalent chromium in undisturbed heterogeneous soil. *Environmental Science & Technology* **1999**, *33*, 2939-2944.

236. Post, J. E.; Veblen, D. R., Crystal structure determinations of synthetic sodium, magnesium, and potassium birnessite using TEM and the Rietveld method. *American Mineralogist* **1990**, *75*, 477-489.

237. Bouznik, V.; Kirik, S.; Solovyov, L.; Tsvetnikov, A., A crystal structure of ultra-dispersed form of polytetrafluoroethylene based on X-ray powder diffraction data. *Powder Diffraction* **2004**, *19*, 219-224.

238. Fendorf, S. E., Surface reactions of chromium in soils and waters. *Geoderma* **1995**, *67*, 55-71.

239. Kotaś, J.; Stasicka, Z., Chromium occurrence in the environment and methods of its speciation. *Environmental Pollution* **2000**, *107*, 263-283.

240. Krishnamurthy, S.; Wilkens, M. M., Environmental chemistry of chromium. *Northeastern Geology* **1994**, *16*, 14-17.

241. Bartlett, R.; James, B., Behavior of chromium in soils: III. Oxidation. *Journal of Environmental Quality* **1979**, *8*, 31-35.

242. Nico, P. S.; Zasoski, R. J., Importance of Mn(III) availability on the rate of Cr(III) oxidation on δ-MnO_2. *Environmental Science & Technology* **2000**, *34*, 3363-3367.

243. Landrot, G.; Ginder-Vogel, M.; Livi, K.; Fitts, J. P.; Sparks, D. L., Chromium(III) oxidation by three poorly-crystalline manganese(IV) oxides. 1. Chromium(III)-oxidizing capacity. *Environmental Science & Technology* **2012**, *46*, 11594-11600.

244. Villalobos, M.; Lanson, B.; Manceau, A.; Toner, B.; Sposito, G., Structural model for the biogenic Mn oxide produced by Pseudomonas putida. *American Mineralogist* **2006**, *91*, 489-502.

245. Lee, J. Y.; Kim, S. B.; Hong, S. C., Characterization and reactivity of natural manganese ore catalysts in the selective catalytic oxidation of ammonia to nitrogen. *Chemosphere* **2003**, *50*, 1115-1122.

246. Tang, Y.; Webb, S. M.; Estes, E. R.; Hansel, C. M., Chromium(III) oxidation by biogenic manganese oxides with varying structural ripening. *Environmental Science: Processes & Impacts* **2014**, *16*, 2127-2136.

247. Pan, C.; Liu, H.; Catalano, J. G.; Qian, A.; Wang, Z.; Giammar, D. E., Rates of Cr(VI) generation from $Cr_xFe_{1-x}(OH)_3$ solids upon reaction with manganese oxide. *Environmental Science & Technology* **2017**, *51*, 12416-12423.

248. Kim, J. G.; Dixon, J. B.; Chusuei, C. C.; Deng, Y., Oxidation of chromium(III) to (VI) by manganese oxides. *Soil Science Society of America Journal* **2002**, *66*, 306-315.

249. Manceau, A.; Charlet, L., X-ray absorption spectroscopic study of the sorption of Cr(III) at the oxide-water interface: I. Molecular mechanism of Cr(III) oxidation on Mn oxides. *Journal of Colloid and Interface Science* **1992**, *148*, 425-442.

250. Fendorf, S. E.; Zasoski, R. J., Chromium(III) oxidation by δ-manganese oxide (MnO_2). 1. Characterization. *Environmental Science & Technology* **1992**, *26*, 79-85.

251. Kim, J. G.; Moon, H.-S., Oxidation of chromium(III) to chromium(VI) by a series of synthesized birnessites (σ-MnO_2): Kinetics and oxidation capacity. *Clay Science* **1998**, *10*, 363-373.

252. Weaver, R. M.; Hochella, M. F., The reactivity of seven Mn-oxides with Cr^{3+} aq: A comparative analysis of a complex, environmentally important redox reaction. *American Mineralogist* **2003**, *88*, 2016-2027.

253. Johnson, C. A.; Xyla, A. G., The oxidation of chromium(III) to chromium(VI) on the surface of manganite (γ-MnOOH). *Geochimica et Cosmochimica Acta* **1991**, *55*, 2861-2866.

254. Schecher, W.; MINEQL, D. M., A Chemical Equilibrium Modeling System, Version 4.6, 4.5. *Environmental Research Software: Hallowell, ME* **2007**.

255. Zhao, H.; Zhu, M.; Li, W.; Elzinga, E. J.; Villalobos, M.; Liu, F.; Zhang, J.; Feng, X.; Sparks, D. L., Redox reactions between Mn(II) and hexagonal birnessite change its layer symmetry. *Environmental Science & Technology* **2016**, *50*, 1750-1758.

256. Elzinga, E. J.; Kustka, A. B., A Mn-54 radiotracer study of Mn isotope solid-liquid exchange during reductive transformation of vernadite (δ-MnO_2) by aqueous Mn(II). *Environmental Science & Technology* **2015**, *49*, 4310-4316.

257. Junta, J. L.; Hochella, M. F., Manganese(II) oxidation at mineral surfaces: A microscopic and spectroscopic study. *Geochimica et Cosmochimica Acta* **1994**, *58*, 4985-4999.

258. Carver, J.; Schweitzer, G.; Carlson, T. A., Use of X‐Ray photoelectron spectroscopy to study bonding in Cr, Mn, Fe, and Co compounds. *The Journal of Chemical Physics* **1972**, *57*, 973-982.

259. Hüfner, S.; Wertheim, G.; Wernick, J., X-Ray photoelectron spectra of the valence bands of some transition metals and alloys. *Physical Review B* **1973**, *8*, 4511.

260. Bird, R. B.; Stewart, W. E.; Lightfoot, E. N., *Transport phenomena*. John Wiley & Sons: 2007.

261. Landrot, G.; Ginder-Vogel, M.; Sparks, D. L., Kinetics of chromium (III) oxidation by manganese (IV) oxides using quick scanning X-ray absorption fine structure spectroscopy (Q-XAFS). *Environmental Science & Technology* **2009**, *44*, 143-149.

262. Foo, K.; Hameed, B., Insights into the modeling of adsorption isotherm systems. *Chemical Engineering Journal* **2010**, *156*, 2-10.

263. Barnhart, J., Occurrences, uses, and properties of chromium. *Regulatory Toxicology and Pharmacology* **1997**, *26*, S3-S7.

264. Berger, A.; Frei, R., The fate of chromium during tropical weathering: A laterite profile from Central Madagascar. *Geoderma* **2014**, *213*, 521-532.

265. Godgul, G.; Sahu, K., Chromium contamination from chromite mine. *Environmental Geology* **1995**, *25*, 251-257.

266. Fendorf, S.; Wielinga, B. W.; Hansel, C. M., Chromium transformations in natural environments: The role of biological and abiological processes in chromium(VI) reduction. *International Geology Review* **2000**, *42*, 691-701.

267. And, I. J. B.; Hug, S. J., Influence of mineral surfaces on chromium(VI) reduction by iron(II). *Environmental Science & Technology* **1999**, *33*, 4285-4291.

268. Papassiopi, N.; Gaitanarou, Z.; Xenidis, A., Stabilization of chromium in the form of mixed Fe(III)-Cr(III) hydroxides. *Fresenius Environmental Bulletin* **2012**, *21*.

269. Dai, C.; Zuo, X.; Cao, B.; Hu, Y., Homogeneous and Heterogeneous $(Fe_x, Cr_{1-x})(OH)_3$ Precipitation: Implications for Cr Sequestration. *Environmental Science & Technology* **2016**, *50*, 1741-1749.

270. Turekian, K. K.; Wedepohl, K. H., Distribution of the elements in some major units of the earth's crust. *Geological Society of America Bulletin* **1961**, *72*, 175-192.

271. Butterfield, C. N.; Soldatova, A. V.; Lee, S.-W.; Spiro, T. G.; Tebo, B. M., Mn(II, III) oxidation and MnO_2 mineralization by an expressed bacterial multicopper oxidase. *Proceedings of the National Academy of Sciences* **2013**, *110*, 11731-11735.

272. Post, J. E., Manganese oxide minerals: Crystal structures and economic and environmental significance. *Proceedings of the National Academy of Sciences* **1999**, *96*, 3447-3454.

273. Huang, P., Kinetics of redox reactions on manganese oxides and its impact on environmental quality. *Rates of Soil Chemical Processes* **1991**, 191-230.

274. Hansel, C. M.; Zeiner, C. A.; Santelli, C. M.; Webb, S. M., Mn(II) oxidation by an ascomycete fungus is linked to superoxide production during asexual reproduction. *Proceedings of the National Academy of Sciences* **2012**, *109*, 12621-12625.

275. Watmough, S. A.; Eimers, M. C.; Dillon, P. J., Manganese cycling in central Ontario forests: response to soil acidification. *Applied Geochemistry* **2007**, *22*, 1241-1247.

276. Carpenter, R., Quantitative electron spin resonance (ESR) determinations of forms and total amounts of Mn in aqueous environmental samples. *Geochimica et Cosmochimica Acta* **1983**, *47*, 875-885.

277. Stone, A. T.; Morgan, J. J., Reduction and dissolution of manganese(III) and manganese(IV) oxides by organics: 2. Survey of the reactivity of organics. *Environmental Science & Technology* **1984**, *18*, 617-624.

278. Stone, A. T.; Morgan, J. J., Reduction and dissolution of manganese(III) and manganese(IV) oxides by organics. 1. Reaction with hydroquinone. *Environmental Science & Technology* **1984**, *18*, 450-456.

279. Davison, W., Iron and manganese in lakes. *Earth-Science Reviews* **1993**, *34*, 119-163.

280. Wilson, D. E., Surface and complexation effects on the rate of Mn(II) oxidation in natural waters. *Geochimica et Cosmochimica Acta* **1980**, *44*, 1311-1317.

281. Diem, D.; Stumm, W., Is dissolved Mn^{2+} being oxidized by O_2 in absence of Mn-bacteria or surface catalysts? *Geochimica et Cosmochimica Acta* **1984**, *48*, 1571-1573.

282. Davies, S. H. R. Mn(II) oxidation in the presence of metal oxides. California Institute of Technology, 1985.

283. Sung, W.; Morgan, J. J., Oxidative removal of Mn(II) from solution catalysed by the γ-FeOOH (lepidocrocite) surface. *Geochimica et Cosmochimica Acta* **1981**, *45*, 2377-2383.

284. Hem, J. D.; Lind, C. J., Nonequilibrium models for predicting forms of precipitated manganese oxides. *Geochimica et Cosmochimica Acta* **1983**, *47*, 2037-2046.

285. Fredrickson, J. K.; Zachara, J. M.; Kennedy, D. W.; Liu, C.; Duff, M. C.; Hunter, D. B.; Dohnalkova, A., Influence of Mn oxides on the reduction of uranium(VI) by the metal-reducing bacterium Shewanella putrefaciens. *Geochimica et Cosmochimica Acta* **2002**, *66*, 3247-3262.